Detection of optical water quality parameters for eutrophic waters by high resolution remote sensing

Dekker, A.G.

1993

document version
Publisher's PDF, also known as Version of record

Detection of optical water quality parameters for eutrophic waters by high resolution remote sensing

A.G. Dekker

DETECTION OF OPTICAL WATER QUALITY PARAMETERS FOR EUTROPHIC WATERS BY HIGH RESOLUTION REMOTE SENSING

CIP-GEGEVENS KONINKLIJKE BIBLIOTHEEK, DEN HAAG

Dekker, A.G.

Detection of optical water quality parameters for
eutrophic waters by high resolution remote sensing / A.G.
Dekker. - [S.l. : s.n.]
Proefschrift Vrije Universiteit Amsterdam. - Met lit. opg.
ISBN 90-9006234-3
Trefw.: remote sensing.

VRIJE UNIVERSITEIT

DETECTION OF OPTICAL WATER QUALITY PARAMETERS FOR EUTROPHIC WATERS BY HIGH RESOLUTION REMOTE SENSING

ACADEMISCH PROEFSCHRIFT

ter verkrijging van de graad van doctor aan
de Vrije Universiteit te Amsterdam,
op gezag van de rector magnificus
dr. C. Datema,
hoogleraar aan de faculteit der letteren,
in het openbaar te verdedigen
ten overstaan van de promotiecommissie
van de faculteit der aardwetenschappen
op vrijdag 11 juni 1993 te 13.30 uur
in het hoofdgebouw van de universiteit,
De Boelelaan 1105

door

Arnold Graham Dekker

geboren te Den Helder

Promotor	prof.dr. I. Simmers
Copromotor	dr. T.J. Malthus
Referent	prof.dr. P.J. Curran

to

Marchien
&
Rogier

"3 mal 7 ist einundzwanzig: Höchstens zweiundzwanzig"

(Schöne Geschichten: 1. Wissenschaft; Stefan Wolpe, 1927)

The Spectron SE-590 was provided by the University of Nottingham and calibrated by the equipment pool of the National Environmental Research Council, UK. A grant from NERC made it possible for Dr. T.J. Malthus to perform and analyze the measurements. The CASI was made available for research purposes by Aerospace Image Productions, Herrenberg, Germany.

This work was funded by the National Remote Sensing Programme of The Netherlands via the Dutch Remote Sensing Board (BCRS), by the Water Management and Pollution Control Authorities Amstel- en Gooiland (NL) and by the Institute for Inland Water Management and Wastewater Treatment (NL).

LIST OF ABBREVIATIONS AND SYMBOLS

Abbreviations

AGL	=	*above ground level*
ASIP	=	*AeroSpace Image Productions, Heidelberg, FRG.*
AWCA	=	*Water Pollution Control Authority Amstel- en Gooiland*
BRDF	=	*bi-directional reflectance distribution function*
BRF	=	*bi-directional reflectance function*
CAESAR	=	*CCD Airborne Experimental Scanner for Application in Remote sensing*
CASI	=	*Compact Airborne Spectrographic Imager*
CCD	=	*charge coupled device*
CCHD	=	*cosine-corrected hemispherical diffuser*
C-IWM	=	*CAESAR Inland Water Mode*
DN	=	*digital number*
FA	=	*fulvic acids*
FOV	=	*field of view*
HA	=	*humic acids*
INRA	=	*Institut National de la Recherche Agronomique, Avignon, (France)*
LI	=	*Limnological Institute, Nieuwersluis, The Netherlands*
NERC	=	*Natural Environment Research Council (UK)*
$\delta R(0-)$	=	*noise equivalent subsurface irradiance reflectance difference*
δR_{rs}	=	*noise equivalent remote sensing reflectance difference*
NIST	=	*National Institute of Standards and Technology (USA)*
PAR	=	*photosynthetically active radiation from 400-700 nm.*
PTFE	=	*polytetrafluorethylene*
SPOT-HRV	=	*Sensor on board of the SPOT satellite*

Symbols

Optical water quality parameters

DW	=	*seston dry weight (mg l^{-1})*
K_d	=	*vertical attenuation coefficient for E_{wd} over PAR (m^{-1})*
SD	=	*Secchi depth or Secchi disc transparency (cm)*
C	=	*concentration of chlorophyll a ($\mu g\ l^{-1}$)*
C_{pigm}	=	*concentration of a pigment ($\mu g\ l^{-1}$)*
$C_{CP\text{-}cyanin}$	=	*concentration of CP-cyanin ($\mu g\ l^{-1}$)*
C_{est}	=	*estimated concentration of chlorophyll a ($\mu g\ l^{-1}$)*
C_{meas}	=	*measured concentration of chlorophyll a ($\mu g\ l^{-1}$)*
DOC	=	*dissolved organic carbon*

Inherent optical properties and related symbols

Note:
any subscript between 400 and 850 is a wavelength λ
any subscript between 0 and 180 is a degree °

a	=	*absorption coefficient (m^{-1})*
$a(w)$	=	*spectral absorption by water (m^{-1})*
$a(ah)$	=	*spectral absorption by aquatic humus (m^{-1})*
$a(s)$	=	*spectral absorption by seston (m^{-1})*
$a(t)$	=	*spectral absorption by tripton (m^{-1})*
$a(ph)$	=	*spectral absorption by phytoplankton (m^{-1})*
$a(d)$	=	*spectral absorption by detritus (m^{-1})*
$a(p)$	=	*spectral absorption by particulate matter (m^{-1})*
$a(total)$	=	*spectral absorption of all components (m^{-1})*
a'	=	*apparent absorption coefficient (m^{-1})*
a^*_λ	=	*a parameter-specific absorption coefficient at λ ($m^2\ mg^{-1}$)*
a^*_{624}	=	*the CP-cyanin-specific absorption coefficient at 624 nm ($m^2\ mg^{-1}$)*
a^*_{676}	=	*the chlorophyll a-specific absorption coefficient at 676 nm ($m^2\ mg^{-1}$)*
a^{**}_λ	=	*a parameter-correlated absorption coefficient at λ ($m^2\ mg^{-1}$)*
b	=	*scattering coefficient (m^{-1})*
$b(s)$	=	*scattering coefficient by seston (m^{-1})*
$b(t)$	=	*scattering coefficient by tripton (m^{-1})*
$b(ph)$	=	*scattering coefficient by phytoplankton (m^{-1})*
b'	=	*apparent scattering coefficient (b over 40° to 180 °)*
b^*_λ	=	*specific backscattering coefficient at λ ($m^2\ mg^{-1}$)*
b_b	=	*backscattering coefficient (b over 90° - 180°)*
b_b^*	=	*specific backscattering coefficient ($m^2\ mg^{-1}$)*
$b_{b\,\lambda}^*$	=	*specific backscattering coefficient at λ ($m^2\ mg^{-1}$)*
c	=	*beam attenuation coefficient (m^{-1})*
k	=	*b'/b*
ω_o	=	*scattering albedo (= b/c)*
$\beta(\Theta)$	=	*volume scattering function*
S	=	*slope parameter in exponential equation*

Apparent optical properties of the radiance field

μ	=	*average cosine of the radiation field*
μ_0	=	*cosine of the zenith angle of refracted solar photons (direct beam) just beneath the surface*
μ_s	=	*average cosine of scattering*
$C(\mu_0)$	=	*coefficient in expression for reflectance as a function of b_b/a and μ_0*
Q	=	*The angular distribution factor of spectral radiance.*
θ	=	*zenith angle*
ϕ	=	*azimuth angle*
	=	*measured in nadir (or from zenith)*
	=	*denoting: of incident radiance*
	=	*denoting: of reflected radiance*
		all irradiance values in units of (W m^{-2} nm^{-1})
E_{ad}	=	*downwelling irradiance above the water surface (=E_{sun} + E_{dif})*
E_{au}	=	*upwelling irradiance above the water surface*
E_{wd}	=	*subsurface downwelling irradiance*
E_{wu}	=	*subsurface upwelling irradiance*
E_u	=	*inherent surface upwelling irradiance*
E_{sun}	=	*direct downwelling irradiance or solar beam*
E_{dif}	=	*diffuse downwelling irradiance or sky light*
E_{CCHD}	=	*correction factor for CCHD measured E_{ad}*
F	=	*fraction diffuse to total downwelling irradiance (E_{dif}/E_{ad})*
		all radiance values in units of (W m^{-2} nm^{-1} sr^{-1})
$L_{rs}(\theta,\varphi)$	=	*radiance as measured by the remote sensor in the direction of view (θ,φ)*
$L_p(\theta,\varphi)$	=	*path radiance scattered by air molecules and dust particles into direction of view of the remote sensor(θ,φ)*
$L_{p'}$	=	*atmospheric path radiance with an atmospheric transmittance effect included*
$L_a(\theta,\varphi)$	=	*upwelling radiance above the water surface in direction of view (θ,φ)*
L_{az}	=	$L_u + L_{ar} = L_a(0,0))$
L_{ar}	=	*radiance that is reflected against the water surface in nadir view*
L_u	=	*radiance in nadir direction transmitted upward from beneath the water surface ≡ water leaving radiance*
L_{wu}	=	*subsurface upwelling radiance in nadir view for fresh waters: $((n^2/(1-r^0))L_u = (1/0.551)L_u)$*
L_{pxw}	=	*subsurface upwelling radiance in nadir view measured with perspex attachment*
L_o	=	*radiance reflected from a perfectly diffuse reflecting Lambertian panel ($\equiv E_{ad}/\pi$)*
L_{pxo}	=	*L_o measured with the perspex attachment*
L_{rp}	=	*radiance reflected from a reference panel in nadir view*
L_{ad}	=	*downwelling radiance above the water surface*
L_{wd}	=	*subsurface downwelling radiance*
L_{dif}	=	*diffuse component of L_{ad}*
L_{sun}	=	*solar (direct) component of L_{ad}*

R	=	*reflectance*
$R(0)$	=	*the inherent irradiance reflectance* ($=E_{wu}/E_{ad}$)
$R(0+)$	=	*the above surface irradiance reflectance* ($= E_{au}/E_{ad}$)
$R(0-)$	=	*subsurface irradiance reflectance* ($=E_{wu}/E_{wd}$)
R_{az}	=	*the apparent reflectance = bidirectional reflectance factor of a target*
R_{ar}	=	*surface reflectance* ($=L_{ar}/L_o$)
R_p	=	*bi-directional reflectance factor of the reference panel*
T_a	=	*atmospheric transmittance along direction* (θ,φ)
T_{az}	=	*atmospheric transmittance in nadir direction*
Q	=	*The angular distribution factor of spectral radiance for conversion of* L_{wu} *to* E_{wu} *:* $E_{wu} = 5\ L_{wu}$ *i.e.* $Q = 5$.
n	=	*index of refraction (=1.341)*
r^0	=	*Fresnel coefficient for 0° angle of incidence (= 0.021)*
ρ	=	*surface irradiance reflectance* ($\rho_{sun}+\rho_{dif}$)
ρ_{sun}	=	*Fresnel coefficient for the reflectance of the direct solar beam*
ρ_{dif}	=	*reflectance of sky light*
		= *assuming a uniform radiance distribution: 6.6 %*
		= *assuming a cardional distribution of sky radiation: 5.2 %*
ρ_w	=	*internal reflectance of diffuse upwelling radiation: 48 %*
f	=	*a factor accounting for the state of the water surface and solar elevation angle*
r_1	=	*coefficient in equation 4.5 dependent on solar zenith angle, volume scattering function and state of the water surface*

Statistical symbols

Δ	=	*relative error*
σ	=	*standard deviation*
r	=	*correlation coefficient*
r^2	=	*coefficient of determination*
N	=	*number of samples*
$S_{y'}$	=	*standard error of estimate of the dependent variable*
$S_{x'}$	=	*standard error of estimate of the independent variable*

CONTENTS

1 INTRODUCTION

1.1 Introduction to the remote sensing of inland waters

Remote sensing of surface water has been mainly used to investigate the oceans. This has contributed greatly to the discovery, mapping and understanding of large scale marine processes. As compared to applications in research on inland waters this can be understood from an organizational point of view: oceanography as a discipline is much better organized to undertake large scale scientific projects. Most work to develop the optical models to explain and predict the reflected signal from surface water was done in marine waters. Preisendorfer (1976), Jerlov (1976) and Austin (1974) laid a firm physical basis defining the inherent and apparent optical properties of marine waters.

Since inland waters are bordered by land, there is usually no problem to detect their crude structure: it is already given on maps. Most general research in inland water ecology has been concerned in developing zero dimensional models that consider a lake to be a perfectly mixed system; different lakes are compared and single lakes are studied by monitoring over long periods. Only when the internal structure of a lake must be known, or when large numbers of lakes must be compared do remote sensing techniques become useful. Airborne remote sensing even offers the possibility of imaging rivers and canals; the interaction between lakes and rivers or canals can thus be studied by remote sensing (Dekker & Donze, 1992).

The remote sensing of waters is restricted to a relatively narrow range of optical wavelengths compared to remote sensing of terrestrial objects. This is caused by low solar irradiance at wavelengths shorter than approximately 400 nm and by a combination of lower solar energy and the sharply increasing absorption of light by water beyond approximately 850 nm. Therefore the range of 400 to 850 nm is often chosen for research aimed at determining methods for estimation of water quality parameters within the water column from remote sensing data.

The desired radiance component of a remotely sensed signal from a pixel of surface water is the upwelling (ir)radiance just under the water surface, the subsurface upwelling (ir)radiance. Other contributions to the measured signal are, among others, surface reflectance and backscatter from the atmosphere. Correction methods for these effects exist, but residual systematic effects remain, while their contribution to noise is inevitable. The remote sensing signal arises in the top layer of the water column, so information from below the level where light intensity is below, say, one quarter of surface intensity, cannot be obtained (Dekker & Donze, 1992).

Information can be extracted on those components in the water that interact with the natural light field from the incident light intensity and subsurface upwelling irradiance. These components are mainly the presence or absence of surface layers of oil and algal blooms, concentration of suspended algae with some information on their content of

different pigments, suspended matter and aquatic humus. In addition to the above components generalized optical water quality parameters such as vertical attenuation of incident light in the water body, Secchi transparency and optical depth, and in shallow clear water also depth, can be calculated from remotely sensed reflection spectra.

Quantitative images obtained in this way can play a role in calibration and validation of two- and three dimensional hydrodynamic and ecological models. Interactions between waterbodies such as inflow and outflow of polluted water and their mixing processes, can be visualised and in part quantified. Wind-induced resuspension of bottom material may also potentially be observed over whole lakes.

Most freshwater systems in the world are affected by anthropogenetic eutrophication, leading to undesirable increases in biomass of higher plants and/or planktonic algae. These phenomena often show large local differences and interactions with patterns of water flow. The amount and distribution of nuisance-forming cyanobacteria is of primary concern for water management. Remotely sensed images give indications on the patterns of distribution of water colour and associated physical properties. Often even a few images are useful as aids to design or improve point sampling monitoring programmes through highlighting the best locations of sampling points.

Large increases in spatial resolution of satellite-sensor derived images have become available during the last decade and increased spectral resolution is now available through instruments flown in aircraft. High spectral resolution is also planned for new satellites in the near future. These developments will make extensive application of passive optical remote sensing to problems in research and management of inland waters attractive in the near future.

1.2 The study area

1.2.1 *General description of the Vecht Lakes area*

The Loosdrecht lakes and the northern Vecht lakes lie in the central west part of The Netherlands (Fig. 1.1). The Loosdrecht lakes (or southern Vecht lakes) are a system of lakes, separated by dikes and ranging in water quality from a clear water-storage basin (WR: Secchi depth up to 500 cm) to very eutrophic, turbid lakes (Secchi depth 20 - 60 cm: Tables 1.1, 1.3 and 6.3.e). Some lakes are interconnected through narrow, shallow waterways. The lakes are important as a nature reserve, for recreational purposes and as reservoirs for drinking water. For a detailed description of the Loosdrecht lakes and current restoration measures see Gulati *et al.* (1991).

The northern Vecht lakes are not all interconnected or adjacent. The Lakes Spiegel (LSP) and Wijde Blik (LWB) are relatively deep lakes created by the extraction of sand and gravel. Lake Wijde Gat (LWG) is a shallow, very eutrophic lake in connection with

Table 1.1

Names, abbreviations and trophic status of water bodies used in the field research. The bold italic name heading each group of water bodies is the name with which those waters will be designated from here on. The trophic status of the RVE and ARK was determined on the basis of their nutrient loading only. The location of the water bodies is given in Fig. 1.1; WCAG = Water Pollution Control Authority Amstel- en Gooiland; LI = Limnological Institute.

		Trophic status	Water quality measurements by
shallow mesotrophic			
LNG	Lake Naardermeer Groote Meer	oligo- mesotrophic	WCAG
LNS	Lake Naardermeer Spookgat	oligo- mesotrophic	WCAG
LSA	Lake Stichts Ankeveen	meso- eutrophic	WCAG
LHO	Lake 't Hol	oligo- mesotrophic	WCAG
shallow eutrophic			
LNW	Lake Naardermeer Wijde Blik	highly eutrophic	WCAG
LHA	Lake Hollands Ankeveen	highly eutrophic	WCAG
LWG	Lake Wijde Gat	highly eutrophic	WCAG
LWL	Lake Western Loenderveen	eutrophic	LI
LEL	Lake Eastern Loenderveen	highly eutrophic	LI
LNP	Lake Nieuwe Polder	highly eutrophic	LI
LVU	Lake Vuntus	highly eutrophic	LI
LLO	Lake Loosdrecht	highly eutrophic	LI
LBR	Lake Breukeleveen	highly eutrophic	LI
deep lakes			
LSP	Lake Spiegel	mesotrophic	WCAG
LWB	Lake Wijde Blik	meso- eutrophic	WCAG
WR	Water Reservoir	oligo- mesotrophic	LI
river & canal			
HIK	Hilversumsch Kanaal	variable	WCAG
ARK	Amsterdam-Rijn Kanaal	eutrophic	WCAG
RVE	River Vecht	highly eutrophic	WCAG/LI

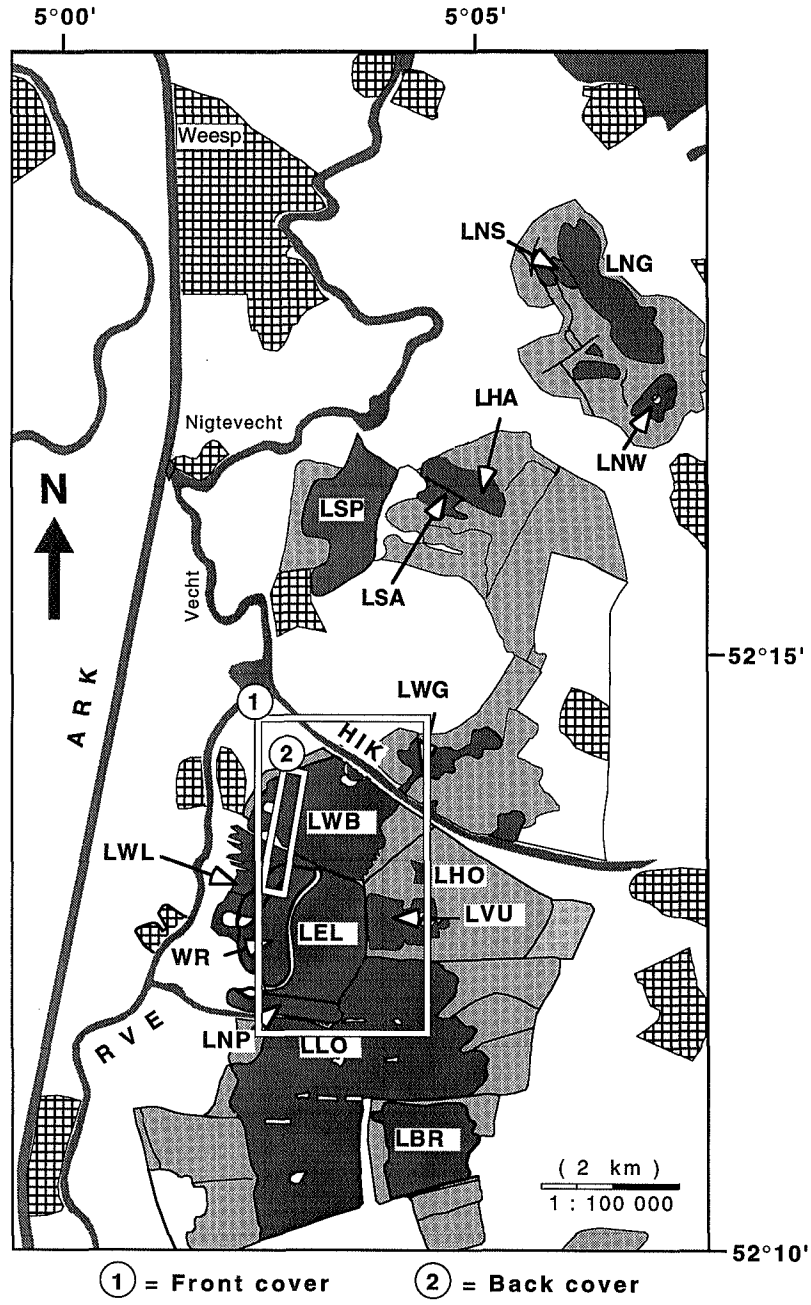

Figure 1.1 *Map of the Vecht lakes area in the central western part of The Netherlands. Names and abbreviations are given in Table 1.1.(Front cover = location of CAESAR chlorophyll a concentration image (see § 6.3.5); Back cover is location of CASI CP-cyanin concentration image (see § 6.2.5).*

the Hilversumsch Kanaal (HIK) which is in turn connected to Lake Wijde Blik. These deep lakes differ in water quality from the other Vecht lakes in their algal composition and they are not prone to wind-induced resuspension of bottom material. Lakes Hollands and Stichts Ankeveen (LHA and LSA respectively) are shallow lakes created by peat excavation. Lake Hollands Ankeveen is eutrophic and turbid with a high algal concentration. Water quality in Lake Stichts Anke-veen is mesotrophic due to water replenishment from groundwater. Lake Naardermeer is a natural lake, consisting of several smaller water bodies, Lakes Groote Meer (LNG), Veertigmorgen and Wijde Blik (LNW). This system was one of the first nature reserves in The Netherlands. In contrast to the lakes Groote Meer and Veertigmorgen, Lake Naardermeer Wijde Blik is highly eutrophic.

The Amsterdam-Rijn Kanaal (ARK) and River Vecht (RVE) are located to the west of the lakes (Fig. 1.1). The Amsterdam-Rijn Kanaal is an approximately 60 km long and 100 m wide canal connecting the River Rhine with Amsterdam. Turbidity is usually high, due to intense mixing of the waters by boats. The River Vecht flows from the south of the city of Utrecht to Lake IJ. It is in open connection with the ARK at several locations. The River Vecht is connected to the Vecht lakes by sluices.

Table 1.2 presents data on the phytoplankton composition of these waters in the summer of 1990. The number of cells per ml varied from less than 50 for the River Vecht, approximately 750 for the Amsterdam-Rijn Kanaal, between 500 and 3,750 for the shallow mesotrophic lakes, 80 to 2,250 for the oligotrophic to mesotrophic deep lakes to 30,000 to 50,000 for the shallow eutrophic lakes. A maximum of 400,000 cells per ml was determined in the shallow eutrophic southern Vecht lakes in 1990 (van Tongeren *et al.*, 1992). Lake Wijde Blik, dominated by *Microcystis aeruginosa*, contained approximately 3,500 cell colonies per ml, where each colony was composed of 300 to 500 individual cells.

Apart from their concentration the algal species also vary with water type: the shallow mesotrophic lakes are dominated by cryptophyceae, the shallow eutrophic lakes by filamentous prokaryotic species *Oscillatoria spp.* and *Prochlorothrix hollandica*. The deep lakes are dominated according to their eutrophic status by cryptophyceae (WR), diatoms (LSP) or gasvacuolate cyanobacteria (LWB). The river and canal algae consisted mainly of diatoms.

1.2.2. *A preliminary division of the water bodies*

The water bodies can generally be divided into four main groups on the basis of their physiography, their optical water quality characteristics and their inherent optical properties. Most of the tables presenting data in this study are structured according to these groups; some of the algorithms required adjustment of parameters to produce correct estimation of optical water quality parameters.

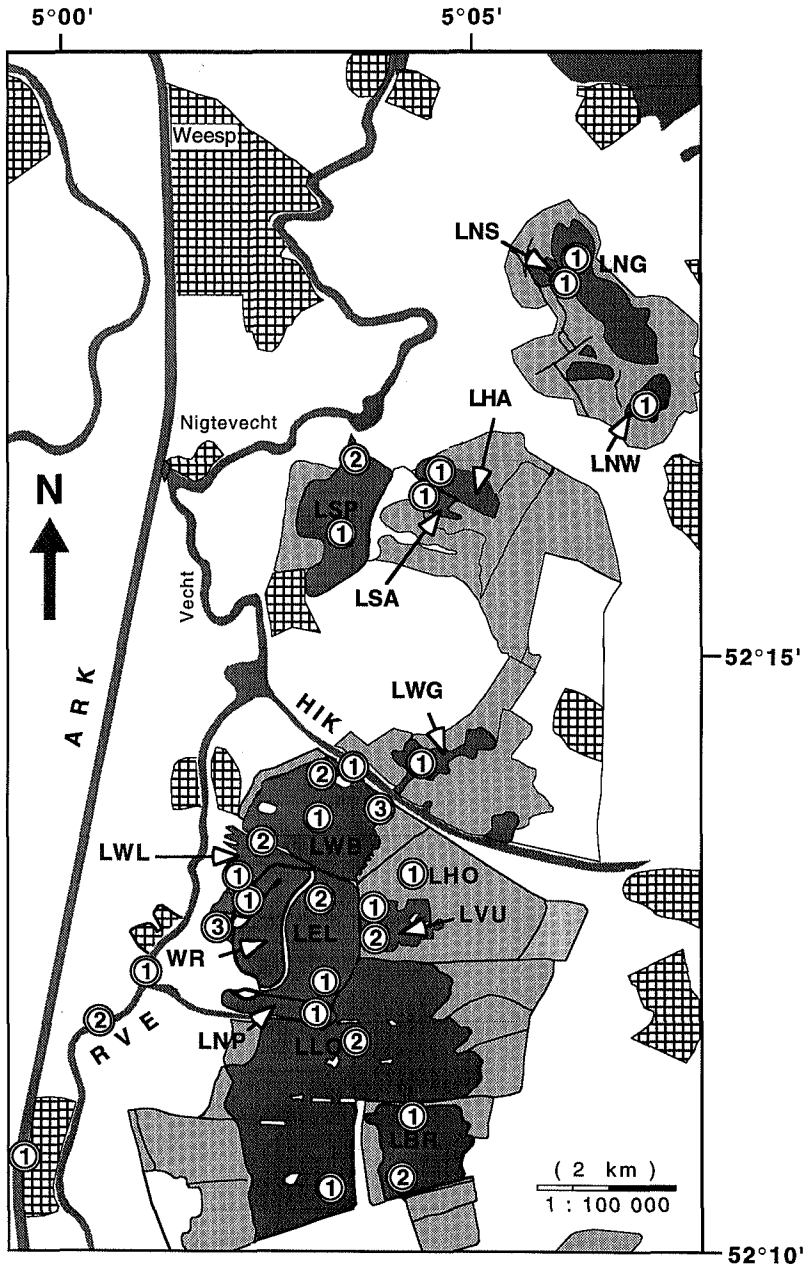

Figure 1.2 *Sampling points for the remote sensing mission in 1990. Water bodies with only one sampling point are not numbered. Tables with water body abbreviations without a number refer to sampling points numbered 1 by default.*

Table 1.2

The phytoplankton composition of waters sampled on 12 September 1990. (%C = % cyanobacteria; %P(B) = % Prochlorothrix hollandica expressed as a percentage of cyanobacteria; %D = % diatoms; %G = % Chlorophyceae; %other = % Cryptophyceae and other algae). The samples for the northern Vecht lake area and the RVE and ARK where analysed by R. Koeleman of the WCAG ; those for the southern Vecht lakes where analysed by N. Boesewinkel-De Bruyn of the LI; the percentage of Prochlorothrix hollandica was determined following the method by Van Liere et al.(1989) and was analysed by L.van Liere and J. Eberts of the LI)

	%C	%P(B)	%D	%G	%Other	main phytoplankton species
shallow mesotrophic						**Cryptophyceae; Chlorophyceae**
LNG	4		4	9	83	*Cryptonomas; Rhodonomas*
LSA	49		10	28	13	*Oscillatoria spp.; Lyngbia*
LHO	0		1	2	97	*Cryptonomas; Trachelomonas*
shallow eutrophic						**Cyanobacteria; Prochlorophyteae**
LNW	53	8	11	31	5	*Oscillatoria limn.; Scenedesmus*
LHA	86	66	0	9	5	*Oscillatoria spp.; Lyngbia limn.*
LWG	89	3	1	5	1	*Oscillatoria redekei & agardii*
LWL	81	43	2	2	15	*Oscillatoria spp.; P. hollandica*
LEL	93	45	1	0	6	*Oscillatoria spp.; P. hollandica*
LVU	91	41	1	0	8	*Oscillatoria spp.; P. hollandica*
LLO	94	42	0	0	6	*Oscillatoria spp.; P. hollandica*
LBR	90	51	0	0	10	*Oscillatoria spp.; P. hollandica*
deep						**Diatoms; Cyanobacteria; Other**
LSP	13		37	11	39	*Ceratium; Asterionella; M. aeruginosa*
LWB	72		1	18	11	*M. aeruginosa; Phormidium*
WR	23	0	1	10	62	Cryptophyceae; *Volvox spp.*
river & canal						**Diatoms; Cyanobacteria**
HIK	5		78	12	5	*Melosira*
ARK	15		60	15	10	*Stephanodiscus; Coscinodiscus*
RVE	0		60	15	25	*Stephanodiscus*

Table 1.3

The range in optical water quality parameters for the Vecht lakes area based on measurements made during the remote sensing campaign : August 28 - September 14 1990 (SD = Secchi disk transparency (cm); K_d = vertical attenuation coefficient; DW = seston dry weight (mg l^{-1}); chlorophyll a = sum of chlorophyll a and phaeopigments (µg l^{-1}); CP-cyanin = cyanophycocyanin (µg l^{-1}). If only one measurement is available only one entry is given. An asterix (*) before a value signifies that the CP-cyanin value was estimated from a(ph) spectra using the CP-cyanin-specific absorption coefficient of 0.0032 m^2 mg^{-1} (see § 2 and 5).

	SD (cm)		K_d (m^{-1})		*DW* (mg)		chlorophyll *a* (µg l^{-1})		CP-cyanin (µg l^{-1})	
shallow mesotrophic										
LNG	80	120		0.82	1	3	4	42		--
LSA	120	135		1.54	4	10	15	27	*7	7
LHO		150		--		4		12		
shallow eutrophic										
LNW	25	30		--	30	37	130	162		130
LHA	35	50		3.08	13	19	112	140	*51	110
LWG	35	40		4.58	31	45	140	212	*67	*96
LWL	50	145	2.02	2.51	3	13	21	70	8	*29
LEL	45	55	2.83	3.31	19	22	69	90	*34	*41
LVU	35	40	3.16	3.49	30	31	87	130		38
LLO	35	40	3.38	4.40	30	37	106	170	49	*53
LBR	30	40	3.49	3.89	32	37	85	128		46
deep										
LSP	290	450	0.72	0.74	1	16	6	17		--
LWB	70	185	1.06	1.52	3	17	11	219	*7	*113
WR	400	490	0.64	0.69	1	1	5	5		--
river & canal										
HIK	60	60		4.07	7	21	93	174		57*
ARK	60	90		2.02	7	28	8	11		--
RVE	60	120		--	1	19	9	37		

The four main groups are (see Table 1.1):

1) The shallow eutrophic to highly eutrophic lakes
2) The shallow oligotrophic to mesotrophic lakes
3) The mesotrophic to eutrophic deep lakes
4) The river and canal waters

In general the shallow eutrophic lakes are characterised by high phytoplankton and tripton concentrations. The tripton consists of detritus and of resuspended bottom material. The phytoplankton is dominated by filamentous prokaryotes dispersed throughout the water column.

The shallow mesotrophic lakes are characterised by low phytoplankton levels. They show high tripton relative to phytoplankton levels, albeit both at low absolute values. The phytoplankton composition is varied.

The deep lakes have phytoplankton levels related to their trophic status (Table 1.2). The tripton is probably dominated by detritus, because wind induced resuspension of bottom material is unlikely. The phytoplankton composition is different from the shallow lakes: instead of filamentous algae there is a dominance of round cyanobacteria such as *Microcystis aeruginosa* and chlorophyceae such as *Volvox spp.* These algae often form colonies consisting of thousands of cells, thus changing the optical properties at micro-scale and possibly at larger scales.

The River Vecht (RVE) and Amsterdam-Rijn Kanaal (ARK) waters are turbid with high tripton but relatively low phytoplankton levels. The ARK sustains heavy shipping traffic all year, the RVE mainly in the summer season. Microscopic analyses showed that most of the organic material in these waters was composed of fragments of algal cells. The Hilversumsch Canal and to some extent the RVE water composition may be strongly influenced by influx of water from adjacent lakes. The ARK may in turn be influenced by the RVE water.

Each of the four water types distinguished has its own characteristic algal type and concentration, contributing to different inherent optical property characteristics. Other parameters also vary along with the four water types (Table 1.3). This large variation of waters in a small geographical area where a few remote sensing flight tracks cover 18 different water bodies, provides an unique opportunity for the development of algorithms valid for a wide range of inland water types. Research results from remote sensing of inland waters are often restricted by the limited number of water bodies studied or by the limited range in water quality parameters.

1.3. Extraction of water quality parameters from remotely sensed spectral data

1.3.1 *General methodology for estimation of water quality parameters from spectral data*

The underwater light field is determined by those optical properties which are independent of the ambient light field (i.e. independent of changes in the angular distribution of radiant flux): the inherent optical properties. These properties for light of a certain wavelength are specified by the absorption coefficient a (m^{-1}), the scattering coefficient b (m^{-1}), and the volume scattering function $\beta(\Theta)$. The last parameter describes the angular distribution of scattered flux resulting from the primary scattering process. The definitions are based on the behaviour of a parallel beam of light incident upon a thin layer of medium (Jerlov, 1976; Kirk, 1981 a & b, Kirk, 1983); direct field measurements of these properties are not yet feasible. A particle-dominated normalized $\beta(\Theta)$ determined by Petzold (1972) for the turbid water of the San Diego Harbour is often used in optical models of the underwater light field for inland waters, for example by Kirk (1980, 1981, 1983, 1984, 1989 & 1991); Dekker *et al.* (1990, 1991, 1992 a-d), Dekker & Donze (1992) and by Dekker & Peters (1993).

Morel & Gordon (1980) pointed out three different approaches by which measurements of spectral (ir)radiance can be used to estimate concentrations of water constituents using remote sensing:

The empirical method
Statistical relationships are sought between measured spectral values and measured water parameters. This is the least scientific method; spurious results may occur, because a causal relationship does not necessarily exist between the parameters studied.

The semi-empirical method
Spectral characteristics of the compounds sought are more or less accurately known. This knowledge can be included in the statistical analysis, which is focused on well chosen spectral areas and appropriate bands or combinations of bands are used as correlates. Reasonable algorithms can be found by common sense and improved by experience. Quantitatively, the coefficients only apply to the data set at hand so each application must be individually calibrated. This method is commonly used.

The analytical method
The inherent and apparent optical properties are used to model the reflectance and vice versa. The water constituents are expressed in their specific (per unit measure) absorption and backscatter coefficients. Subsequently, a suite of analytical methods can be used to optimally retrieve the water constituents or parameters from the remotely sensed upwelling radiance or radiance reflectance signal. This method was applied and further developed for the present study.

1.3.2 *Examples of remote sensing studies that applied the empirical and semi-empirical model*

A review of satellite and airborne remote sensing of inland waters is given in Kirk (1983) and of airborne remote sensing by Hilton (1984). After 1984 remote sensing of inland waters has taken place mainly using data from satellite based sensors such as Landsat Thematic Mapper and SPOT-HRV, and airborne remote sensing using instruments varying from multispectral scanners to line spectrometers and imaging spectrometers.

1.3.2.1 *Satellite remote sensing of inland waters*

As a result of their adequate spatial resolution, the Thematic Mapper (since 1984) and SPOT-HRV (since 1986) sensors are suited for imaging medium sized or smaller inland waters, such as occur in the Vecht lakes area (Dekker & Peters, 1993). Landsat MSS data was the only available source of satellite data until the Landsat Thematic Mapper instrument became operational.

Landsat MSS data for inland water quality analysis was used: for Lake Balaton in Hungary (Shimoda *et al.*, 1986); Mono Lake, California (Almanza & Melack, 1985); Moon Lake (in turbid, mineral matter rich waters), Mississippi (Ritchie *et al.*, 1983 and 1987; Ritchie & Cooper, 1987, 1988 and 1991). Landsat TM data was used: for 16 lakes varying in eutrophic status in The Netherlands (Dekker & Peters, 1993); approximately 100 lakes in Ireland, varying in eutrophic status (McGarrigle, 1989; Reardon & McGarrigle, 1989); 50 inland water bodies in Switzerland and France (Jacquet & Zand, 1989); the Great Lakes area in the USA and Canada (Lathrop & Lillesand, 1986, Lathrop *et al.*, 1991 and Lathrop, 1992), Moon Lake, Mississippi (Ritchie *et al.*, 1990); Lake Constance, Germany (Grunwald *et al.*, 1988). SPOT-HRV data was used in: the Great Lakes area in the USA and Canada (Lathrop & Lillesand, 1988 and 1989).

All research using Landsat MSS and TM and SPOT-HRV data involved statistical techniques to derive correlations between spectral bands or band combinations and the desired water quality parameters, often without analysis of the underlying spectral features taking place within the spectral bands of the remote sensing systems. Only Dekker & Peters (1993) explained and interpreted the results achieved through statistical analysis of TM band radiances and water quality parameters. They also noted that relatively broad spectral band systems could not analytically resolve underlying spectral features and, worse, could not discriminate between chlorophyll *a* and suspended matter. Thus, relatively low spectral resolution satellite data does not allow analytical algorithm development for estimation of spectral features such as high pigment absorption.

1.3.2.3 *High resolution airborne remote sensing of inland waters*

For the development of high spectral resolution remote sensing applications, both imaging and non-imaging (either line or point measurements) data are of interest. Ground-based surface and subsurface spectral measurements may serve as surface calibration and as the link between the remotely sensed signal and the inherent optical properties. Line spectrometric measurements from the air over inland waters were reported from Ireland (McGarrigle *et al.*, 1990), eastern Europe and the former Soviet Union (Gitelson & Keydan, 1990; Gitelson, 1991; Kondratyev & Podzniakov, 1990) and the Netherlands (Dekker *et al.*, 1990). The only published imaging spectrometry results for inland waters are those by Dekker *et al.* (1990, 1991, 1992 a-d) and by Dekker & Donze (1992).

Airborne line spectrometry measurements:

The application of a low altitude remote sensing line spectrometer for water quality analysis was described in McGarrigle *et al.* (1990). Spectra from 49 lakes in Ireland were analysed using principal components and spectral function analysis to estimate water quality parameters. The instrument collected spectra at 10 nm resolution over 400 to 890 nm. Statistically significant correlations were obtained between spectral functions and parameters such as lake chlorophyll levels, suspended solids concentration, water transparency and with humic substances in a subset of the data. The regression equations were highly significant. However, the margins of error were relatively wide. The instrument was intended as a prototype for a national lake water quality surveillance program in Ireland.

Several hundred airborne spectral measurements have also been made in test areas in Hungary, Germany and the former USSR, along with simultaneous ground-based data (reviewed by Gitelson *et al.*, 1991a). The test areas had a very large range in water quality parameters; chlorophyll *a* : 3 - 350 $\mu g\ l^{-1}$; suspended matter: 2 - 43 $mg\ l^{-1}$; dissolved organic matter absorption at 330 nm: 0.1 - 10 m^{-1}. The origins and composition of the suspended matter and dissolved organic matter varied for the different water bodies. The spectral measurements were made with a 10 channel spectroradiometer with 10-12 nm wide bands spaced between 400 and 720 nm. Using spectral band ratioing of reflectances at different wavelengths it was possible to estimate the chlorophyll *a* concentration with a standard error of less than 2.6 $\mu g\ l^{-1}$, mineral suspended matter concentrations at less than 4 $mg\ l^{-1}$ and dissolved organic matter concentrations at less than 0.5 mg C l^{-1}. The spectral bands were chosen on the assumed measured spectral optical properties. Factor analysis was applied to verify the choice of spectral bands. Spectral ratios of the 670 and 700 nm band were selected for chlorophyll *a* analysis, 560 nm and 520 nm for suspended matter analysis and 430 and 620 nm for dissolved organic matter analysis. The correlation coefficients were generally high with $r^2 > 0.94$, and the standard error increased from chlorophyll *a* to suspended matter concentrations to the dissolved organic matter concentrations.

Imaging spectrometry measurements

Imaging spectrometer data from the Programmable Multispectral Imager were analysed for a lake system in the Netherlands by Dekker *et al.* (1990) using the semi-empirical model. Secchi disk transparency, vertical attenuation coefficients and surface and subsurface spectroradiometric measurements were made *in situ*. Seston dry weight, and chlorophyll-a and phaeopigments were determined from water samples. Inherent optical properties were estimated from measured apparent optical properties. The Programmable Multispectral Imager was flown in spectral mode at 1000 m altitude and in spatial mode at 3000 m altitude. In spectral mode 288 spectral channels at 1.3 nm intervals over 430-805 nm wavelength range were acquired. These airborne spectra showed a large similarity with the *in situ* upwelling irradiance spectra from 500 nm to longer wavelengths. In spatial mode an eight channel spectral bandset, developed by Moniteq for chlorophyll *a* analysis, was used. The spatial mode bandsetting was simulated using 25 subsurface upwelling irradiance measurements and 17 airborne spectral mode measurements. The highest correlation was found for the spectral band ratio (673-687 nm)/(708-715 nm) with seston dry weight (r = 0.95; range 3 - 40 mg l^{-1}); chlorophyll *a* (r = 0.96; range 6 - 91 µg l^{-1}); Secchi disk transparency (r = 0.98; range 30 - 225 cm) and the vertical attenuation coefficient over 400-700 nm (r = 0.97; range 0.7 - 5.3 m^{-1}). The linear regression equations used were derived from log-transformed data and the limited amount of spatial mode data was processed using these algorithms. The result was a map showing the spatial distribution of these water quality parameters. Three simultaneously measured in situ samples illustrated the validity of the modelling by comparing closely with parameters estimated from the remotely sensed data.

These spectra were also used to model the performance of other existing multispectral scanning systems such as Landsat Thematic Mapper and SPOT-HRV (Dekker *et al.* 1992c & d; Dekker & Peters, 1993), and were applied to develop an inland water quality spectral bandset for the 9-channel multispectral CAESAR airborne scanner (Dekker *et al.*, 1990). Examples of spectra obtained by CASI in spectral and spatial mode, and spectra and images collected by CAESAR in the Inland Water Mode configuration, were shown in Dekker *et al.* (1992b) as illustrations of the use for this type of data for optimising spectral band location for remote sensing of turbid and/or eutrophic waters. In Dekker *et al.* (1992a), CASI imaging spectrometry data was used to illustrate how imaging spectrometry can be applied to determine the presence and concentration of cyanobacteria in inland waters.

The results presented to date in the literature show that there is a good potential for accurately estimating water quality constituents and properties from high spectral resolution airborne remote sensing systems. However, none of the results presented led to generalised algorithms based on the analytical method. Insufficient evidence was given that the results obtained from these semi-empirical approaches are valid on a multitemporal basis. Therefore a remote sensing campaign was undertaken in 1990 with the aim of developing multitemporally valid algorithms based on knowledge of the underlying inherent optical properties.

1.3.3 *Methodology*

This study aimed to apply the analytical model to turbid, mesotrophic to highly eutrophic inland waters and thereby contribute to increased scientific understanding of the influence of underwater optical properties on the remotely sensed reflectance signal. Much of the underwater optical theory stems from research concerning ocean waters. The main difference for the development of an analytical method for inland waters lies in the variation, range and magnitude of the absorption and scattering quantities; in the spectral distribution of these quantities and in changes in the shape of volume scattering functions due to the different nature of the substances in inland waters.

A comprehensive discussion of the analytical models available for clear ocean waters through to turbid coastal waters was given in Gordon & Morel (1983). Kirk (1983) extended the discussion to inland waters.

In clear oceanic waters the spectral reflectance is a function of:

1. Absorption by algal pigments, detritus and low concentrations of (aquatic) humus at short wavelengths and by pure water at long wavelengths.
2. Scattering by water molecules at short wavelengths and Raman scattering at intermediate wavelengths.
3. Fluorescence caused by humus at shorter and algal pigments at longer optical wavelengths.

In turbid coastal water and in almost all inland waters these effects also occur, but the analysis becomes more complicated due to:

A The importance of three additional components:

4. Backscattering from particles which becomes the dominant scattering factor; up to 1000 times the backscattering of the clearest oceanic waters.
5. Absorption at short visible wavelengths by high concentrations of humus and tripton.
6. Absorption at longer (orange to red) wavelengths of algal pigments (this red pigment absorption cannot be remotely sensed in oceans because the relative contribution of absorption by water is much stronger than the absorption by the low concentration of algal pigments).

B A decrease in the relative contribution of water molecule scattering, Raman scattering and fluorescence by aquatic humus and algal pigments.

These additional effects introduce complex, interacting relations among the constituents. Increase in silt, for example, will make algae less visible, and absorption by humus does the same to the molecular backscattering by water. In nature these variables are often highly correlated, while non-linear relations between concentrations and reflection can occur. As a consequence the statistical approach to data analysis is possible, but not recommended if analytical information is available.

In order to accomplish the aim of developing multitemporally valid algorithms it was necessary to apply a suite of laboratory-based, field-based and airborne spectral radiance and irradiance measurements. These data were used to either model or measure the subsurface irradiance reflectance, *R(0-)*. The *R(0-)* is the most appropriate parameter of the under water lightfield for use as the independent optical parameter in algorithms for remote sensing, because it is independent of light intensities and only slightly dependent on atmospheric conditions, solar elevation angle and the state of the water surface. It is possible to relate *R(0-)* to the inherent optical properties of absorption and scattering, provided the volume scattering function is known. Once the exact nature of the relationship between the inherent optical properties and the optical water quality parameters is known, it is possible to develop an algorithm for extraction of this property from *R(0-)*. The upwelling radiance signal detected by a remote sensor (L_{rs}) may be recalculated to *R(0-)*. Thus it also becomes possible to estimate the optical water quality parameters from L_{rs}.

1.4 The present study: concept and structure

The ordering of chapters in this study follows the method introduced in § 1.3.3: i.e. an analytical approach involving the measurement and analysis of the inherent optical properties, the determination of their relationship with the apparent reflectance properties and the measurement of these reflectance properties by a remote sensor.

Chapter 2 discusses the inherent optical properties of spectral absorption and scattering. Using laboratory-based spectrophotometric measurements of light attenuation in water samples, a method is described and applied to separate the absorption from the scattering within the attenuation measurements. The water samples were first separated into a part containing water and aquatic humus (dissolved organic substances with a yellow colour) and a part containing the seston (particulate matter). The absorption and scattering properties of the seston are determined, after which it was possible to apply a model derived from the literature to separate the absorption signal of seston into a phytoplankton absorption component and a tripton component. In combination with optical water quality parameter measurements, this enabled the determination of the effect of a unit measure of chlorophyll *a*, cyanophycocyanin and seston dry weight on the spectral absorption and scattering coefficients.

Chapter 3 considers the theoretical and practical aspects of the derivation of the subsurface irradiance reflectance (*R(0-)*) from the remotely sensed upwelling radiance using *in situ* spectroradiometric measurements. For this purpose it was necessary to describe and perform the following calculations:

1) Correction of the remotely sensed upwelling radiance to the field-based above-surface upwelling radiance to the subsurface upwelling radiance to the subsurface upwelling irradiance.
2) Correction of the above-surface downwelling irradiance to the subsurface downwelling irradiance.

The ratio of the subsurface upwelling irradiance to the subsurface downwelling irradiance is equal to *R(0-)*.

The nature of the relationship between *R(0-)* and the absorption and the scattering and backscattering coefficients is investigated in chapter 4. Models for coastal waters and one model for turbid river waters were available from the literature. The general model applicable was found to be:

$$R(0-) = r_1 \, b_b \, / \, (a + b_b)$$

where a is the absorption coefficient, b_b the backscattering coefficient describing the proportion of incident light scattered backwards and r_1 is a coefficient dependent on solar zenith angle and volume scattering function. It was therefore also necessary to determine the backscattering coefficient from the scattering coefficient.

The results of chapters 2 to 4 are combined in chapter 5 to derive algorithms for the estimation of concentrations of chlorophyll *a*, cyanophycocyanin and seston dry weight from *R(0-)*. The estimation of vertical attenuation K_d and Secchi depth transparency from *R(0-)* was also investigated. Although the aim was to determine algorithms following the analytical method this was not always possible, in which case a semi-empirical algorithm with as much multitemporal validity as possible was developed.

On 3 September 1990 a flight with a multispectral scanner (CAESAR) equipped with nine spectral bands (the "Inland Water Mode") took place. On the 14 September in the same year a flight with an imaging spectrometer (CASI) took place. It was initially intended to fly the two instruments simultaneously, but this was not possible due to operational reasons. The remote sensing data are discussed in chapter 6. First the remotely sensed upwelling radiance was converted to *R(0-)*. Then the remote sensing algorithms developed in chapter 5 were applied to the remote sensing data. This application took place without further corrections thereby illustrating the multitemporal applicability of the algorithms developed in the course of this study.

General conclusions, recommendations and discussion are presented in chapter 7.

1.5 Measurements of the optical water quality parameters

In this study only those optical water quality parameters that caused a change, or were a function of a change in the inherent optical properties were considered. The parameters causing a change in the absorption properties include aquatic humus and phytoplankton pigments such as the primary light harvesting pigment chlorophyll *a* and the cyanobacterial pigment cyanophycocyanin. The total suspended matter expressed as seston dry weight (including the phytoplankton) to a large extent determines the scattering in these waters. The suspended matter may be further separated into the phytoplankton and the tripton; the tripton is the non-algal particulate matter. Both phytoplankton and

tripton have their own absorption and scattering characteristics. The optical water quality parameters that are a function of the changes in inherent optical properties are the vertical attenuation coefficient of subsurface downwelling irradiance (K_d) and the Secchi depth transparency (*SD*). As soon as one of the inherent optical properties change K_d and *SD* will also change.

Figure 1.2 shows the sampling points in the Vecht lakes area. The laboratory-based analysis of chlorophyll *a* and seston dry weight (*DW*) took place at two institutes: the samples for the northern Vecht lakes were analysed by the Water Pollution Control Authority Amstel- en Gooiland (WCAG: see Table 1.1); those for the southern Vecht lakes were analysed by the Limnological Institute (LI: see Table 1.1); phycocyanin was analysed at the University of Amsterdam. The K_d and *SD* measurements were performed simultaneously with the *in situ* spectroradiometric measurements and at the same time samples were taken for laboratory-based spectrophotometric measurements and for chlorophyll *a* and seston dry weight analyses. Additional sampling was carried out by the above named institutes when required.

Chlorophyll a

Although referred to as chlorophyll *a* in the text, this parameter represents the sum of chlorophyll *a* and pheaophytin that is measured in the laboratory. The method for determination of chlorophyll *a* concentration differed between the WCAG and the LI. The WCAG performed single measurements, whereas the LI performed measurements in triplicate for each sample.

At both institutes chlorophyll *a* and pheaopigments were measured after extraction in hot ethanol. The WCAG followed the method of the Netherlands Normalisation Institute (NEN norm no: 6520 Spectrophotometric determination of chlorophyll *a*). The LI followed the method of Moed & Hallegraeff (1978).

The chlorophyll *a* measurements performed by the LI showed a variation per sample of approximately 10% ; for the WPQA this percentage could not be determined. Although chlorophyll *a* concentrations were used as an independent variable in this study, measurement uncertainty and inter-laboratory errors may be present.

Tables 1.3 and 6.3.a present the chlorophyll *a* values measured during the remote sensing campaign. Table 6.3.a also presents the remotely sensed values for chlorophyll *a* calculated using the remote sensing algorithms developed in § 5, based on the results of § 2, 3 and 4.

Cyanophycocyanin

Cyanophycocyanin (CP-cyanin), a pigment unique to cyanobacteria, was determined in the lake samples (Tables 2.7 and 5.7) following the method by Bennett & Bogorad (1973). The results should be regarded as indicative, for the method used may not be

suited for determining these pigments in lake samples where other pigments may influence the absorption measurements to an unknown extent.

Tables 1.3 and 6.3.b present the CP-cyanin concentration measured during the remote sensing campaign as well as the estimated CP-cyanin concentration calculated from the remote sensing data using the algorithms developed in § 5, based on the results of § 2, 3 and 4.

Seston dry weight

Seston dry weight (*DW*) is defined as the gravimetric concentration of phytoplankton and tripton present in the water column. Tripton is the sum of non-algal organic and inorganic material. For the shallow eutrophic southern Vecht lakes *DW* was composed of that fraction of particles larger than 0.45 μm. According to Gons *et al.* (1992), in shallow lakes approximately 33% of *DW* is living algae, the rest is composed of dead algae and detrital peat. On days suitable for remote sensing with fine, calm weather conditions the fraction of living algae will probably increase due to low wind-induced resuspension of bottom sediments. The ratio of algae to detritus is important for water quality assessment because detritus is a potential source of phosphate following microbial breakdown. Dry weight can also be divided into a part that is continuously in the water column - algae and very fine particles, and a part that is resuspended by wind-induced wave action mainly. The resuspendable sediment consists mainly of large-sized peat fragments. The fine-sized particles, mostly algal decay products, occur in aggregates (Otten *et al.* 1992). Presumably the same applies to the shallow eutrophic northern Vecht lakes and to the shallow mesotrophic lakes. For the deep lakes the *DW* is composed mainly of algal-derived detritus. The Amsterdam-Rijn Kanaal *DW* composition is part silt, part algal-derived detritus and partly other organic material. The Vecht *DW* composition is probably intermediate between the ARK and the eutrophic lakes.

Tables 1.3 and 6.3.c present the *DW* concentrations measured during the remote sensing campaign. Table 6.3.c. also presents the *DW* concentrations estimated from the remote sensing data applying the algorithms developed in § 5, based on the results of § 2, 3 and 4.

Vertical attenuation

The measurement of the vertical attenuation, K_d, of photosynthetically active radiation (PAR, 400-700 nm) has become a standard procedure for determining lake optical condition. Vertical attenuation measurements are useful for determining the amount of radiance available to phytoplankton and submerged macrophytes, for determining the transparency of water for swimming water standards, for primary production studies and as an indication of turbidity. From a depth profile of light measurements K_d may be calculated (Kirk, 1983). K_d forms a useful parameter for the comparison of optical conditions between water bodies.

Tables 1.3 and 6.3.d present the K_d values measured during the remote sensing campaign. Table 6.3.d also presents the values for K_d estimated from the remote sensing data applying the algorithms developed in § 5, based on the results of § 2, 3 and 4.

Secchi disk transparency

Secchi disk transparency (*SD*) is measured by lowering a standard disk with black and white markings into the water until the distinction between the black and white markings is no longer visible. *SD* measurement is often considered to be a crude indicator of water quality; it is, however, an easy, fast and low cost measurement. For these reasons it has been widely employed and has become one of the primary parameters for water quality description. One of the main aims of the lake restoration projects carried out in the study area is to restore transparency from the present 35 cm in the shallow eutrophic lakes to 100 cm.

Tables 1.3 and 6.3.e present the *SD* values measured during the remote sensing campaign. Table 6.3.e also presents the *SD* values estimated from the remote sensing data using the algorithms developed in § 5, based on the results of § 2, 3 and 4.

2. SPECTRAL ABSORPTION AND SCATTERING

2.1 Introduction

The prime objective of remote sensing is to map distributions of optical water quality characteristics. The determination and quantification of optical water quality factors is carried out on the spectral reflectance signature as measured by a remote sensor; the information in the spectral reflectance signature is derived from the influence of the optical water quality parameters on the inherent optical properties of spectral absorption, scattering and backscattering. It is, therefore, essential to obtain information on the inherent optical properties of the various components in the water bodies studied.

For this purpose water samples were taken at locations where *in situ* spectroradiometric, vertical attenuation and Secchi depth transparency measurements were made. In the water samples, the various components were separated physically and optically as far as was possible with the available techniques. Physical separation took place using filtration and optical separation was accomplished by spectrophotometry. Because physical separation of the seston was not possible, a published model was applied to separate the seston into a spectral component for phytoplankton and for tripton.

In ocean related studies of water quality the particulate matter is often composed principally of phytoplankton breakdown products referred to as detritus (Bricaud *et al.*, 1983; Bricaud & Stramsky, 1990; Carder *et al.*, 1991; Maske & Haardt, 1987; Roesler *et al.*, 1989). In inland waters the particulate matter is referred to as tripton, for apart from phytoplankton derived detritus it also contains terrigenous organic and inorganic matter. In the waters studied here the tripton of many of the shallow lakes contains peat fragments, whereas the Amsterdam-Rijn Kanaal tripton consists of 5-25% detritus and 75 - 95% mostly inorganic material (pers. comm. R. Koeleman WCAG).

In this chapter theory, method and measurements of the determination of the inherent optical properties are presented and discussed. All the measurements were performed in the laboratory on water samples. First the theory and measurement techniques required to determine the optical absorption and scattering properties from optical attenuation measurements using a spectrophotometer are considered. Next the inherent optical properties of water, aquatic humus, tripton and phytoplankton are discussed. Inherent optical properties of water are derived from the literature. The absorption coefficient of aquatic humus, the only inherent optical property of significance for aquatic humus, is discussed next. It was further investigated whether the aquatic humus absorption could be described by an exponential equation from the literature. Also, the wavelength range over which aquatic humus still noticeably influenced the combined absorption of all components was determined. The inherent optical properties of the seston were derived. Because the optical properties of the phytoplankton, separated from the tripton optical properties, are required for developing remote sensing algorithms for extraction of phytoplankton pigments, it was necessary to separate phytoplankton absorption from tripton absorption. A model developed for this purpose for ocean waters was applied to

the seston absorption spectra. Where necessary the model was modified to the optical properties of freshwater phytoplankton to prevent spurious results. Once the phytoplankton absorption spectra were available it was possible to calculate the specific absorption of a µg of chlorophyll *a* or cyanophycocyanin. These specific absorption values are important input parameters for the remote sensing algorithms discussed in chapter 5.

Once the absorption and the attenuation of seston were known it was possible to determine the scattering of the seston through subtraction of the absorption coefficient from the attenuation coefficient. From the spectral scattering it was possible to calculate approximate chlorophyll *a*-specific and tripton-specific scattering coefficients. The spectral backscattering, besides absorption, is an essential parameter in the equation relating the subsurface irradiance (*R(0-)* to the inherent optical properties (§4: Eq. 4.5). Backscattering is discussed in chapters 4 and 5, because the determination of the spectral backscattering estimation required information on the volume scattering functions; these were not available and had to be derived from *R(0-)*, calculated from *in situ* spectroradiometric measurements as described in chapters 3 and 4. At the end of this chapter a resumé is given discussing the implications of spectral absorption and scattering on subsurface reflectance, a precursor to chapter 5 where the algorithms for water quality parameter extraction from remotely sensed data, recalculated to *R(0-)*, are developed.

Vertical attenuation K_d and Secchi depth transparency (*SD*) are not discussed in this chapter because they are functions of the influence of water, aquatic humus, tripton and phytoplankton on the underwater light climate expressed through their inherent optical properties. K_d and *SD* will, therefore, be discussed in chapter 5.

All parameters discussed in this chapter are parameters of the underwater light field. Therefore, except if otherwise indicated, the prefix 'underwater' or 'subsurface' relates to all parameters (e.g. inherent optical properties are the underwater inherent optical properties).

2.1.1 *Theory*

Inherent optical properties are those properties that are independent of the ambient light field (i.e. independent of changes in the angular distribution of radiant flux). Apparent optical properties are jointly dependent on the inherent optical properties and on the ambient light field. Examples of apparent optical properties are the diffuse attenuation coefficients for upwelling (K_u) and downwelling irradiance (K_d) and the irradiance reflectance *R*.

The inherent optical properties of water for light of any given wavelength are specified in terms of the absorption coefficient *a* (m^{-1}), the scattering coefficient *b* (m^{-1}) and the volume scattering function $\beta(\Theta)$, which describes the angular distribution of scattered flux resulting from the primary scattering process. These definitions are based on the behaviour of a parallel beam of light incident upon a thin layer of medium (Jerlov,

1976; Kirk, 1981 a & b; Kirk, 1983). The direct measurement of these properties in the field is not yet feasible. An additional inherent optical property is the beam attenuation coefficient c, given by

$$c = a + b \qquad [2.1]$$

The beam attenuation coefficient thus represents the total loss of light due to absorption and scattering combined.

The absorption coefficient of the medium as a whole, at a given wavelength, is equal to the sum of the individual absorption coefficients of the components present (Kirk, 1983). Assuming a linear relationship between concentration and absorption (provided that no changes in molecular state or physical aggregation take place with changes in concentration), the absorption coefficient due to any one component is proportional to the concentration of that component (Beer's Law). Therefore:

$$a(total) = a(w) + a(ah) + a(ph) + a(t) \qquad [2.2]$$

Where $a(w)$ is the absorption by pure water, $a(ah)$ by aquatic humus, $a(ph)$ by phytoplankton and $a(t)$ by tripton.

Scattering is the process by which photons change direction through interactions with matter and causes radiant energy to leave the water. More specifically it is backscattering that causes energy to leave the water (Kirk, 1989 & 1991). Scattering is caused mainly by water $b(w)$, by phytoplankton $b(ph)$ and by tripton $b(t)$:

$$b = b(w) + b(ph) + b(t) \qquad [2.3]$$

Spectral scattering is determined by two types of scattering: density fluctuation scattering and particle scattering. Density fluctuation scattering is caused by molecules. It causes the blue colour of the clearest natural waters (e.g the oceans and some ultra-oligotrophic deep lakes). In all except the clearest inland waters density fluctuation scattering by the water molecules is negligible compared to the scattering caused by the particles in the water. Particle scattering was described theoretically by Mie (1908), who calculated the light scattering behaviour of spherical particles of any size. For particles larger than the wavelength of light Mie theory predicts that most of the scattering is in the forward direction within small angles of the initial direction of the light. In the case of particles several times larger than a few wavelengths of light, diffraction and geometrical optics describe the scattering process well (Kirk, 1983; Morel & Bricaud, 1986). Another process causing changes in direction of photons is anomalous diffraction due to the interference effects between diffracted and transmitted light. These interference effects are caused by phase changes as the photons pass through media of differing refractive indices (Kirk, 1983; Morel & Bricaud, 1986; Morel, 1987).

Photons impinging upon an algal cell may either be transmitted (and thus refracted at each interface of different substances, e.g. cell tissue and water) or scattered, or absorbed. The backscattering to total scattering ratio of light by algae is probably less than for similarly sized mineral particles because the scattering process by the semi-transparent, many refractive surfaces containing algae is different (Bricaud *et al.*, 1983).

The spectral scattering of seston is a function of the size distribution of the scattering particles. In productive and/or turbid inland waters as encountered in the central Netherlands the size distribution will be variable and complex. The apparent optical particle size distribution (a transparent algae with gas vacuoles may not be assumed to behave the same as an identical sized opaque particle) determines the degree of influence of each form of scattering.

Once the spectral absorption and scattering properties have been determined for water samples it is possible to calculate specific absorption and scattering coefficients, defined as the per unit spectral absorption and scattering. Units are usually given in concentration per metre; e.g. a useful measure is the amount of spectral absorption caused by 1 µg of chlorophyll *a*, referred to as the chlorophyll *a*-specific absorption.

2.1.2 *Measurement techniques*

2.1.2.1 *Introduction*

It is possible to estimate inherent optical properties from spectrophotometric measurements. Laboratory spectrophotometric measurements were made on water samples taken at sites where radiance and irradiance measurements were made in the field. The spectral absorption of aquatic humus and the attenuation spectra of seston were measured; the absorption spectrum of pure water is constant and was derived from the literature (Buiteveld & Donze, unpublished results, based on: Smith & Baker, 1981 & Boivin *et al.*, 1986). Henceforth, the term attenuation will be used for spectrophotometric measurements that have not been corrected for scattering. Absorption will be reserved for those measurements that have been corrected for scattering.

In principle the measurements were carried out within hours of the sampling. This was not, however, always feasible. A test was carried out on samples after a few hours, then one day and two days old. For a mesotrophic lake sample (LNG) the difference in attenuation over the wavelength range of 400 to 800 nm was 3.5% with a maximum of 0.01 m^{-1}, well below the precision of the spectrophotometer; for a eutrophic lake (LEL) the differences were 2.8% with a maximum of 0.06 m^{-1}, just above the precision (0.05 m^{-1}) of the spectrophotometer. The measured differences showed no spectral dependence.

2.1.2.2 *Spectral absorption measurements*

To determine the spectral absorption of aquatic humus *a(ah)* the lake water samples were filtered through 0.2 µm (Sartorius membrane) filters. Absorption by the filtrate was measured using a Perkin-Elmer UV-VIS 551S double beam spectrophotometer (slit 2 nm, scan speed 2 nm s^{-1}, photometric repeatability ± 0.002).

a(ah) was determined in 10 cm path length cells; the accuracy of measurements was 0.05 m^{-1} (at 95% confidence level, pers. comm. J. Krijgsman). Measurements were carried out over the range 400 - 800 nm at 1 nm intervals and were made in conjunction with research staff at the Faculty of Civil Engineering at the Technical University of Delft (NL).

Light attenuation of seston was usually measured on unconcentrated water samples, unless the attenuation was insufficient, in which case concentration of the seston was carried out following the method of Kirk (1980). In this technique, seston was collected on 0.2 µm membrane filters and resuspended in a smaller known quantity of distilled water. The spectral attenuation by both the unconcentrated and the concentrated samples were measured in 1 cm path length cuvettes. The cuvettes were first measured in the normal cuvette position (or beam attenuation mode) where the scattered light is collected over a small forward angle of 0° to 5°; the cuvettes were subsequently placed next to the openings of an Ulbricht integrating sphere, enabling forward scattered light at angles of 0° to 40° to be collected. Measurements were made using the same instrument, settings and wavelength range as for aquatic humus.

For the concentration technique Kirk (1980) estimated the loss of particulate material to be ca. 10%. The results from this study were corrected using this percentage. The accuracy of this loss estimate is not known for the samples analysed and therefore introduces an unknown error into the measurements. In addition, the loss of particulate matter remaining on the filter could be biased in terms of particle size or morphology, thereby introducing errors of selection and hence measurement.

Calculation of the apparent absorption coefficient a'_λ

Using a scan adopting the beam attenuation mode of the spectrophotometer (in which the cuvette with the seston sample is placed in the normal position) and a scan using an integrating sphere accessory, which enables most forward scattered light to be captured, it is possible to calculate the true absorption properties of the seston sample.

The method is based on a correction of the apparent absorption coefficient a'_λ, as measured using an integrating sphere accessory, for scattered light not captured by the photomultiplier, which is indicated here as the apparent scattering coefficient b'_λ. The method used was based on that by Davies-Colley *et al.* (1986) for freshwater phyto-

plankton cultures. In this study the measuring equipment had a slightly different geometry and a higher spectral resolution compared to that used by Davies-Colley *et al.* (1986) and more attention has been paid to the apparent scattering to scattering ratio.

In our experiments all the light scattered from the beam with a scattering angle greater than 40° was not measured and thus contributes to b'_λ. The apparent absorption is the total of true absorption a_λ plus apparent scattering (the wavelength dependence of a, a', b, b', c and $\beta(\theta)$ is not expressed in the following formulae for reasons of simplicity):

$$a' = a + 2\pi \int_{40}^{180} \beta(\theta) sin(\theta) d\theta \qquad [2.4]$$

$$a' = a + b_{40\text{-}180} \text{ with } b' \equiv b_{40\text{-}180} \qquad [2.5]$$

and therefore Eq. 2.4 may be written as:

$$a' = a + b' \qquad [2.6]$$

where $\beta(\theta)$ is the volume scattering function and $b_{40\text{-}180}$ and b' represents the scattering greater than 40° not collected with the integrating sphere.

Measurement of the beam attenuation c

The beam attenuation coefficient *(c)* is the sum of true absorption *(a)* and the scattering of light out of the view angle of the photomultiplier (5° for the instrument used in this study).

$$c = a + 2\pi \int_{5}^{180} \beta(\theta) sin(\theta) d\theta \qquad [2.7]$$

$$c = a + b_{5\text{-}180} \qquad [2.8]$$

If $b \equiv b_{5\text{-}180}$, then it follows that $c = a + b$ (= Eq. 2.1)

Calculation of the true absorption a

If it is assumed that no absorption takes place for wavelengths between 750-800 nm, then

$$a'/c = (a + b')/(a + b) = b'/b \qquad [2.9]$$

for λ=750-800 nm. It may be assumed that b'/b is constant over wavelengths in the PAR-region (for validity of this assumption see § 2.1.2.3):

$$k = b'/b \qquad [2.10]$$

where k is a constant. With this relationship b' can therefore be written as $k \cdot b$ and it follows that

$$a = a' - k\,b \qquad [2.11]$$

and thus

$$a = a' - k\,(c - a) \qquad [2.12]$$

and

$$a = (a' - k\,c) / (1 - k) \qquad [2.13]$$

where $k = a'_{750\text{-}800\ nm} / c_{750\text{-}800\ nm}$

Using equation 2.13 the true spectral absorption was calculated from the integrating sphere and beam attenuation measurements.

2.1.2.3 *The ratio (k) of apparent scattering (b') to scattering (b)*

The assumption of b'/b being constant over wavelengths in the PAR-region (see Eq. 2.10) was investigated, since it determines the validity of Eqs. 2.10-2.13. To examine the relationship between the scattering coefficient values b' and b, volume scattering function values $\beta(\theta)$ were used as measured by Whitlock *et al.*, (1981) and by Petzold (1972).

Whitlock *et al.*, (1981) investigated properties of three turbid river waters with chlorophyll *a* concentrations of 10 - 15 µg l^{-1} and total suspended solids concentrations of 14 - 23 mg l^{-1}. For these samples the beam attenuation values ranged from 8.9 to 18.9 m^{-1} at 550 nm. $\beta(\theta)$ is given for scattering angle $\theta = 0.374°$ to 155° for the three different waters (at 3 angles < 1.5° and at 11 angles between 25° - 155°). For this study, $b_{40\text{-}155}$ and $b_{0.37\text{-}155}$, as estimations of b' and b respectively, were computed by summing over the mean values of $\beta(\theta)sin(\theta)$. Values of $\beta(\theta)sin(\theta)$ at angles greater than 155° and up to 180° become very small (Tomohiko Oishi, 1990). The lack of $\beta(\theta)$ values at angles greater than 155° in Whitlock *et al.*'s study does not, therefore, appear to introduce significant errors. The approximation for the integral over the 14 measured angles leads to the same result as the cubic spline integration used by Whitlock *et al.*, (1981) for b_b (at $\lambda = 450$ nm) = 1.5 m^{-1} of sample A2. Considering the estimated deviation of 20% in the calculated scattering coefficients by Whitlock *et al.* (1981), summing over the mean terms is sufficiently accurate for our purposes.

The ratio $b_{40\text{-}155}/b_{0.37\text{-}155}$ was thus determined for the three different waters of the Whitlock *et al.* (1981) study, for wavelengths ranging from 450 to 800 nm (at 50 nm intervals); the ratio had only a small spectral variation but changed significantly with

different water types: 4.3 ± 0.3 %, 7.0 ± 0.3 % and 13 ± 1 % for samples B, A1 and A2 respectively. If the normalized $b_{0\text{-}5}$ is independent of wavelength for scattering angles <5°, $b'/b = k$ appears to be a reliable estimation.

Petzold (1972) published volume scattering functions for ocean and clear freshwater samples. Ratios of $b_{40\text{-}180}/b_{0\text{-}180}$ and $b_{40\text{-}180}/b_{5\text{-}180}$ were calculated from these functions along with their integrals $2\pi \int_0^{\theta} sin(\theta)d\theta$ at λ = 530 nm (Table 2.1.a); these ratios were also calculated for the data set of this study (Table 2.1.b). The results presented in Table 2.1.a show that the $b_{5\text{-}180}/b_{0\text{-}180}$ is between 33% and 47% for the natural water samples and between 60% and 73% for the filtered freshwater with and without absorbing and scattering material added. The $b_{40\text{-}180}/b_{5\text{-}180}$ ratio for the inland waters of this study were within the range of those calculated by Petzold (1972).

For 31 samples of different inland water types b'/b was calculated by dividing the integrating sphere values a' by the transmission values c for wavelengths ranging from 750 to 800 nm. The spectral variation of the values (σ = 0 to 1%), was negligible compared to the variation with changing water type which, varied from 5 to 25 %. The b'/b values for this research are given in Figure 2.1. From the data for b'/b from Whitlock *et al.* (1981), Petzold (1972) and from the Vecht lakes area data presented here, it may be concluded that the assumption of spectral independence of b'/b is correct.

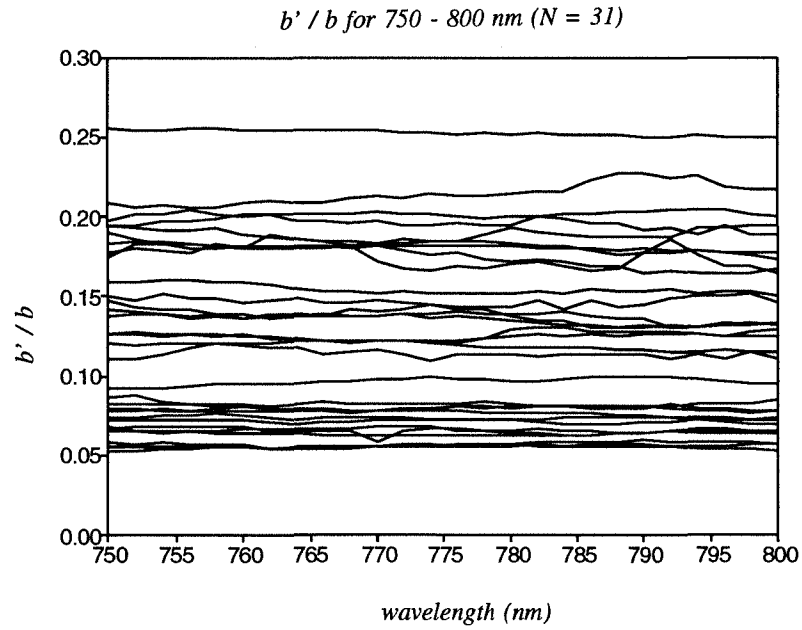

Figure 2.1 *The ratio (k) of apparent scattering (b') to scattering (b): : $k = b/b'(b_{40\text{-}180}/b_{5\text{-}180})$ values over 750 -800 nm for 31 samples from the Vecht Lakes area (see equation 2.10)*

Table 2.1.a *Ratios of $b_{40\text{-}180}/b_{0\text{-}180}$ and $b_{40\text{-}180}/b_{5\text{-}180}$ calculated using the volume scattering functions $\beta(\theta)$ and their integrals $2\pi \int_0^{\theta} \sin(\theta) d\theta$ at λ = 530 nm from Petzold (1972) for ocean and freshwater samples. The scattering over 0° - 5° has a strong influence on the ratios.*

	$b_{40\text{-}180}/b_{0\text{-}180}$ [%]	$b_{40\text{-}180}/b_{5\text{-}180}$ [%]
Tongue of the ocean	9	19
Offshore California	4	12
San Diego Harbour	7	15
Visibility Laboratory freshwater:		
filtered	22	30
+ scattering material	6	10
+ scattering and absorbing material	5.5	9

Table 2.1.b *Ratios of $b_{40\text{-}180}/b_{5\text{-}180}$ calculated for the samples of this study. (N = number of samples; σ = standard deviation). Two samples included in the calculation of all samples could not be placed in any of the water type categories. The shallow eutrophic lakes samples resemble Visibility Laboratory freshwater samples with scattering and absorbing material added. The other water type samples resemble the San Diego Harbour samples.*

	$b_{40\text{-}180}/b_{5\text{-}180}$ [%]	N	σ [%]
All samples	12.3	31	5.4
Shallow eutrophic	9.8	14	2.4
Shallow mesotrophic	15.0	5	2.5
Deep meso-eutrophic	16.8	6	4.6
River & canal	18.1	4	4.3

2.1.2.4 *Spectral scattering*

Once the true absorption was calculated, derivation of the total scattering coefficient b was relatively straightforward. Beam attenuation minus true absorption gives the scattering coefficient over all angles except for the acceptance angle of the photomultiplier tube (5°). The results of these calculations are presented in § 2.2.4.

It should be noted, however, that since more than 50% of the scattering occurs within scattering angles <5° (Tomohiko Oishi, 1990) it is probably not reliable to estimate the total scattering coefficient by $b_{5\text{-}180}$, for the $b_{0\text{-}5}$ could represent a significant part of the total scattering. This is illustrated by calculations using Petzold's (1972) data, as shown in Table 2.1.a. This is of concern when data from the present study are compared with published data of b, b_b and b_b/b, in which generally $b = b_{0\text{-}180}$ and $b_b = b_{90\text{-}180}$. Using $b = b_{0\text{-}180}$ would probably reduce our b'/b by a factor of 2 or slightly less; b would then also become a factor of 2 higher. For remote sensing purposes, however, the backscattering $b_{90\text{-}180}$ is perhaps more important than the scattering at small forward angles.

To confirm the validity of the correction method, the angular distribution of scattering for small scattering angles would be needed to check the assumption that if $b_{40\text{-}180}/b_{0.37\text{-}180}$ is wavelength independent, then $b'/b = b_{40\text{-}180}/b_{5\text{-}180}$ is also wavelength independent. Thus, for the above reasons, scattering functions for angles smaller than 5° should be investigated for light in the range 400 to 850 nm.

2.2 Results

2.2.1 *The spectral properties of water*

Figure 2.2. shows the absorption and scattering spectra for pure water. Water absorbs light only very weakly in the blue and green regions of the spectrum. Absorption increases markedly with wavelength above 550 nm, becoming significant in the red region. At 680 nm a one metre thick layer of pure water will absorb about 35% of the incident light; there are absorption shoulders at 610-620 and 660-670 nm.

Scattering by water is inversely proportional to wavelength and, together with low absorption at short wavelengths, this causes the blue colour of pure water. *In situ* Raman scattering can significantly increase scattering by water in nature (Peacock *et al.* 1990, Stavn & Weidemann, 1988; Stavn, 1990 and 1992) and is a form of inelastic scattering whereby the wavelength of photons change as well as their polarization. However, for the freshwater bodies investigated during this study, molecular and Raman scattering are negligible compared to scattering by particulate matter.

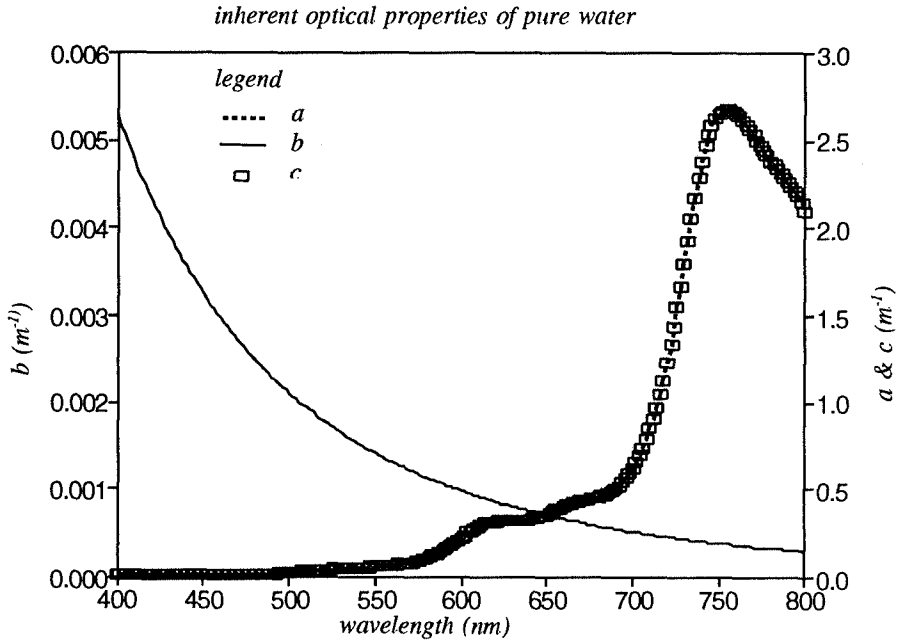

Figure 2.2 *Pure water absorption and scattering spectrum as derived from literature.*

2.2.2 *The spectral properties of aquatic humus*

2.2.2.1 *Introduction*

Aquatic humus can remove blue light efficiently in the top few centimetres of the water column thereby imparting a yellow colour to the water. The practical definition of aquatic humus in this study is based on the sample preparation technique, which usually involves filtration through filters. Aquatic humus mainly consists of dissolved organic carbon in the form of fulvic or humic acids. Table 2.2 lists relevant literature on humus and related matter; also given is the name preferred by the author(s). For ocean and estuarine waters "yellow substance" and "gelbstoff" are preferred names, whereas for inland waters seven names have been used. For this study the term aquatic humus is adopted for it was found to be the least ambiguous. Henceforth humus will indicate aquatic humus and *a(ah)* will indicate aquatic humus absorption.

The sources of humus in lakes can include allochthonous inputs from organic breakdown products on land via soil leaching or autochthonous production within the water body itself (Kirk, 1983). In productive lakes an increase in aquatic humus absorption tends to covary with an increase in lake trophic status. Kirk (1983), Visser (1984) and Davies-Colley & Vant (1987) discuss the possible origins in more detail.

Table 2.2

Relevant literature on the subject of aquatic humus. The name for aquatic humus preferred by the author is also given.

freshwater	**given name:**
Kirk (1980)	gilvin
Zepp & Schlotzhauer (1981)	aquatic humus
De Haan (1982, 1986)	humic substances
Witte *et al.* (1982)	dissolved organic materials/humic substance/gelbstoff
Visser (1984)	aquatic humic matter
Buiteveld *et al.* (1986)	aquatic humus
Davies-Colley & Vant (1987)	yellow substance
Krijgsman *et al.* (in prep.)	aquatic humus
estuarine water	
Ferrari (1991)	yellow substance
ocean water	
Bricaud *et al.* (1981)	yellow substance
Carder *et al.* (1989)	gelbstoff

The number of studies on optical properties, from 400 to 800 nm, of aquatic humus in inland waters is limited. One aim of determining the optical properties of aquatic humus of the waters studied was to increase knowledge about the shape and variability of the curves encountered. Published models for estimating the shape of the aquatic humus spectra were also tested for these waters.

For remote sensing purposes, the aim was to determine the contribution of humus absorption to the background optical signal including the pure water absorption. A knowledge of background absorption would then enable determination of the contribution of particulate matter to absorption, which contains most of the information on the optically active water quality constituents. Alternatively, if the particulate matter absorption is known, the humus spectrum may be determined.

In oceanic applications the absorption of aquatic humus at 440 nm ($a(ah)_{440}$) is often used as an indicator of $a(ah)$ up to 500 or 550 nm. For remote sensing of eutrophic inland waters the 400 to 500 nm area does not appear to be useful because of the low reflectance in this region due to absorption by humus, photosynthetic pigments and tripton. Low sensor sensitivity of remote sensing instrument radiance detectors and the high

atmospheric influence on the measured blue signal also contributes to poor resolution in this region (Dekker *et al.*, 1991). It is, therefore, necessary to know the shape and the extent of *a(ah)* at longer wavelengths, because for inland waters the spectral area between 500 and 800 nm contains the most information; especially the spectral region between 600 and 720 nm (Dekker *et al.*, 1991, 1992c; Gitelson *et al.*, 1990; Gitelson & Kondratyev, 1991a; Kondratyev & Pozdniakov, 1990).

For an analytical approach to the contribution of *a(ah)* to the remote sensing of inland waters the following question need to be answered:

1.a) At which wavelengths can the humus absorption be assumed to be negligible with respect to the increasing pure water absorption at longer wavelengths?
1.b) At which wavelengths can the humus absorption be assumed to be negligible with respect to the seston (phytoplankton and tripton) absorption?
2) Is the shape of the humus spectrum related to the type of water?
3) What are the similarities and differences between humus absorption and detritus or tripton absorption?
4) Does humus absorption prevent the remotely sensed determination of absorption by other water quality parameters at any wavelengths?
5) Can the contribution of humus absorption and hence aquatic humus concentration be retrieved from the remotely sensed signal?

(The answers to questions 1.a and 2 are given in § 2.2.2.2; to question 1.b in § 2.5. The answers to questions 4 and 5 are given in § 5 and further).

2.2.2.2 *Spectral measurements of the aquatic humus absorption*

Absorption spectra of humus exhibit an approximately exponential decrease with increasing wavelength that has been noted in studies on other lakes (Tables 2.2 & 2.4). However, this shape is not identical for all waters. Figure 2.3 shows the aquatic humus spectra for the 31 samples taken in the present study.

As the basis for comparison of absorption of aquatic humus in different waters a reference wavelength of 440 nm was chosen by Kirk (1983), because it corresponded approximately to the mid-point of the first chlorophyll *a* absorption band.

Table 2.3.a presents summarized results of a bi-weekly sampling program of $a(ah)_{440}$ absorption carried out from April to September 1987 in the Loosdrecht lakes area. Dissolved organic carbon was also measured. Data from Frisian lakes (in the northeastern Netherlands) are included to illustrate the range of values possible within a limited geographical area. The correlation between $a(ah)_{440}$ and dissolved organic carbon for the Loosdrecht Lakes is high ($r^2 = 0.96$). The average variation of $a(ah)_{440}$ in any one lake measured during the half year was approximately 0.5 m^{-1} for a range of $a(ah)_{440}$ of 0.83 to 4.70 m^{-1} (Table 2.3.b).

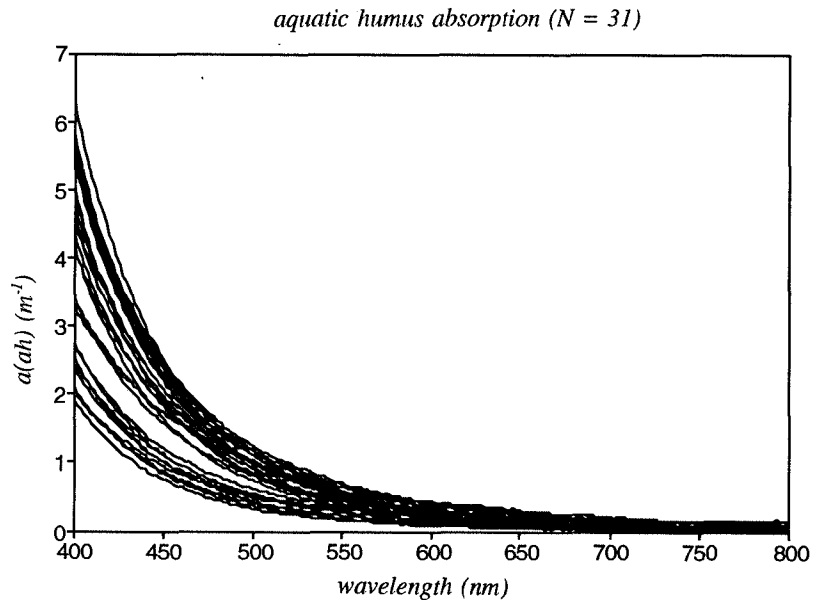

Figure 2.3 *31 aquatic humus spectra for the 1990 remote sensing sampling data set. (As a first approximation these resemble an exponentially decreasing function of wavelength).*

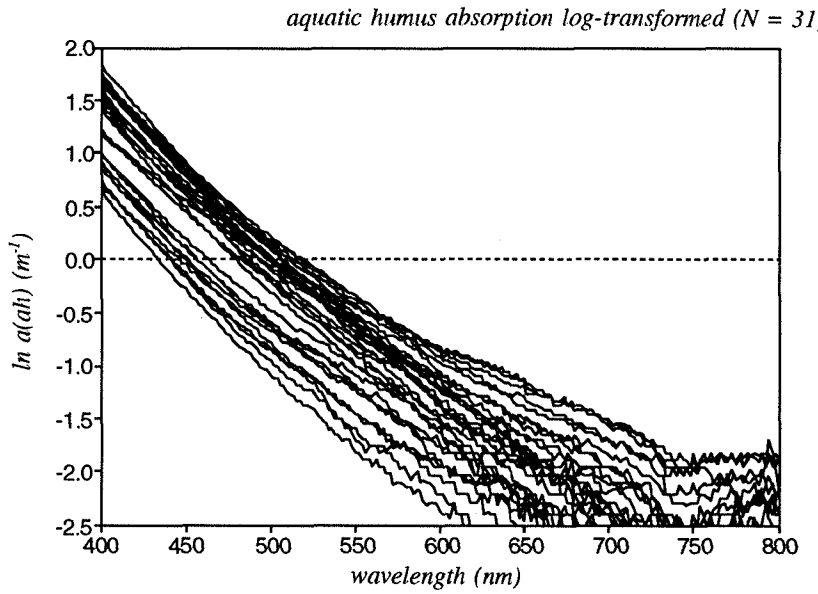

Figure 2.4 *Log-transformed aquatic humus spectra from Fig. 2.3. (Deviations from a straight line in this graph are equivalent to deviations from the exponential model. The varying angles of the aquatic humus spectra correspond to different slopes S).*

Table 2.3.a *Results of a bi-weekly sampling program of $a(ah)_{440}$ absorption carried out from April to September 1987 in the Southern Vecht Lakes area. DOC (Dissolved organic carbon) was also calculated. Data from Frisian lakes (1986) are included to illustrate the range of values possible within a limited geographical area (σ = the standard deviation; N = number of samples); LTJ = Lake Tjeukemeer; LTJO = Lake Tjongemeer; LBA = Lake Beulakkerwijde; LEW = Lake Eernewoude. Frisian lakes data from de Boer et al. (1987 a & b).*

	N	$a(ah)_{440}$ (m^{-1})	σ $a(ah)_{440}$ (m^{-1})	*DOC* ($mg\ l^{-1}$)
Southern Vecht lakes				
WR	17	1.19	0.22	7.33
LWL	16	2.46	0.34	11.23
LEL	15	2.27	0.48	10.33
LBR	14	3.74	0.52	14.55
LVU	17	3.68	0.49	13.94
LLO1	15	2.71	0.35	10.70
LLO2	19	2.78	0.44	11.21

regression equation describing $a(ah)_{440}$ as a function of *DOC*:
$a(ah)_{440}$= -2.042 + 0.423 *DOC* N=13 r^2= 0.96

	N	$a(ah)_{440}$	σ $a(ah)_{440}$	*DOC*
Frisian lakes				
LTJ-1	37	5.62		18.17
LTJ-2	37	4.30		15.30
LTJO	21	6.36		18.05
LBA	21	12.42		33.53
LEW-9	21	14.18		34.81
LEW-5	20	9.22	--	31.77

Published values for the range for $a(ah)_{440}$ are from approximately 0 m^{-1} for the Sargasso Sea (Kirk, 1983) to as high as 22.6 m^{-1} for Frisian lake and ditch water in The Netherlands (Krijgsman, in prep.). Based on these figures an $(ah)_{440}$ value of 0 to 25 m^{-1} should cover most of the variation encountered in surface water bodies.

The wavelengths where *a(ah)* is less than 5% of the absorption by water vary with aquatic humus concentration from 696 nm to beyond 800 nm. For this data set (Fig. 2.3) the *a(ah)* is up to 30 % of the absorption by pure water at 700 nm. This means that for high concentrations of aquatic humus, *a(ah)* is not negligible at longer wavelengths. Davies-Colley & Vant (1987; Fig. 3, p 420) showed absorption spectra from New Zealand lakes where 4 lakes had an *a(ah)* > 0.1 m^{-1} between 600 and 700 nm.

Table 2.3.b *The ranges in $a(ah)_{440}$ (m^{-1}) for inland waters from literature and from this study.*

Year of sampling	N	range $a(ah)_{440}$	water type	reference
----		0.01 - 19.1	Sargasso Sea to lakes	Kirk (1983)
1986		1.60 - 9.83	Netherlands inland	Buiteveld et al. (1986)
1986	157	4.30 - 14.18	Frisian Lakes	De Boer *et al.* (1987)
1987	113	0.83 - 4.70	7 Loosdrecht lakes	Table 2.3
1987	139	0.90 - 4.87	New Zealand lakes	Davies-Colley & Vant (1987)
1988	15	0.78 - 3.51	8 Loosdrecht lakes	this research
1990	32	0.83 - 2.80	15 lakes/5 river&canal	this research
1987	40	0.91 - 22.6	The Netherlands	Krijgsman (in prep.)

A problem in estimating aquatic humus absorption at wavelengths of 600 nm and beyond may be caused by assuming measured attenuation at 700 or 750 nm to be due to residual scattering and correcting for this effect, as is the practice in ocean related studies where the absorption by aquatic humus is very low at longer wavelengths (Bricaud *et al.*, 1983). At high concentrations of aquatic humus, however, this assumption may be incorrect for significant *a(ah)* may still occur and any corrections applied may lead to oversteepening of the *a(ah)* curve at shorter wavelengths (Davies-Colley & Vant, 1987). Krijgsman (in prep.) analyzed 40 samples from different waterbodies in The Netherlands with and without an integrating sphere and found no significant differences from 350 to 550 nm. They concluded that light scattering by aquatic humus could be neglected using this method. Witte *et al.* (1982) investigated the effects of natural aquatic humus and commercial humic acid on reflectance and found a decrease of reflectance even at infrared wavelengths (their filtrate was filtered over 0.45 μm filters), demonstrating the possibility of infrared absorption by humic acid.

These results suggest that because the reflectance and total absorption in a spectral region is a function of the absorbing substances, *a(ah)* will influence the height and locations of reflectance and absorption maxima up to wavelengths of 720 nm and even beyond at high humus concentrations.

2.2.2.3 *Modelling of the a(ah) absorption curve*

It is convenient to model the aquatic humus absorption curve so that the humus absorption at any wavelength may be calculated from the absorption at one specific wavelength. This would be particularly useful in remote sensing applications, where combinations of spectral bands may be used to measure the decrease in radiance reflectance caused by *a(ah)* in order to determine this absorption at another spectral interval.

Another possible application is the estimation of *a(ah)* at a spectral band where the absorption and scattering coefficients of the other water constituents are available. As will be shown below, however, it is recommended to use the actual measurements, if available. If model application is necessary, e.g. in research where only $a(ah)_{440}$ values are known, the exponential model may be used as a rough first order approximation.

2.2.2.4 *The exponential model*

A model to describe spectral aquatic humus absorption was presented by Bricaud & Morel (1981) for ocean waters and by Zepp & Schlotzhauer (1981) for soils and inland, coastal and ocean waters of the form:

$$a(ah)_\lambda = a(ah)_{\lambda_0} exp[-S(\lambda-\lambda_0)]$$

This equation is based on the assumption of a fixed slope, where S is stated to be independent of the choice of reference wavelength λ_0. An analysis of the *a(ah)* values obtained between 400 - 800 nm for water bodies in this study showed a correspondence to an *e*-power function. Fig. 2.4 shows the log-transformed aquatic humus spectra illustrating the variation of slopes from different water bodies and also a degree of curvature that still remained after transformation.

Table 2.4 *List of slopes S for aquatic humus and the measurement technique applied (year = year of publication; FA = fulvic acids; HA = humic acids; F = freshwater ; O = ocean water; C = coastal water; L = lake water; N = number of samples).*

year	author	FA-HA	type of water	λ-range nm	λ zero	N	range in S nm^{-1}	mean S nm^{-1}
1981	Zepp		F	300-500	450	12	0.012-0.018	0.015
		FA				3		0.014
		HA				3		0.010
1981	Bricaud		O/C	375-500	375	105	0.010-0.020	0.014
1987	Davies-Colley		L	280-460	450	12	0.015-0.021	0.019
	Kirk					22		0.016
1988	Hojerslev			240-675	450		0.012-0.017	0.014
1989	Carder	FA	O/C	250-750	450	6	0.017-0.020	0.019
		HA	O/C	250-750	450	3	0.011-0.011	0.011
1993	Krijgsman		F	350-550	380	40	0.013-0.020	0.016
1993	Dekker		F	400-600	440	31	0.011-0.018	0.015

Table 2.4 shows the S values obtained for the current data set along with published values for comparison. For the present study the waters showed a range of values for S, calculated for the range 400 to 600 nm, using a reference wavelength (λ_0) of 440 nm. S ranged from 0.011 for the River Vecht to 0.018 for Lake Naardermeer-Wijde Blik, with an overall average value of 0.015 (N = 31; σ = 0.0015). The lowest values for S were found for river, canal or groundwater-fed water bodies, perhaps reflecting a greater influence from allochthonous sources. Lake Western Loenderveen showed variations in S from 0.014 to 0.016, probably due to variations in lake physiography. The highest values were found in narrow (2 m wide) channels lying between narrow strips of peaty land; Lake Wijde Blik had S values of 0.015 to 0.016. To test the relationship between S and $a(ah)_{440}$ and eutrophic status a linear regression analysis was performed using chlorophyll a concentration as the index of trophic status; there was no apparent relation between slope or $a(ah)_{440}$ and trophic status ($r^2 < 0.1$).

Assuming a fixed slope and using the exponential model with 440 nm as the reference wavelength, an error of up to 54%, for predicting $a(ah)$ at 700 nm, results for those samples with an $a(ah)$ absorption value of 0.1 m^{-1} or higher (N = 13, range of error in $a(ah)_{700}$ is 28 - 54% with an average of 48% and a σ of 7%).

The curvature shown in the log-transformed aquatic humus spectra may be attributed to differences in concentrations of fulvic and humic acids between the lake water samples and to the influence of pH on the slope S. Fulvic and humic acids show different absorption characteristics. According to Carder *et al.* (1989) fulvic acids (FA) have a steeper slope with increasing wavelength and a much lower absorption than humic acids (HA). Freshwater aquatic humus consists mainly of fulvic acids (Visser, 1984; Zepp & Schlotzhauer, 1981; Ghassemi & Christman, 1968). Most aquatic humus in the shallow eutrophic Lake Tjeukemeer, similar to the shallow eutrophic lakes analysed here, consists of fulvic acids (de Haan & de Boer, 1986).

For a marine environment Carder *et al.* (1989) found S = 0.0194 for predominantly fulvic acids in the Mississippi plume and a value of S = 0.0110 for humic acids in a Mexican Gulf loop inclusion (Table 2.4). He also illustrated the influence of differing ratios of fulvic to humic acids on the absorption spectra: the main effect was an increase in slope towards shorter wavelengths with an increasing fulvic acid component. Applying this to these measurements implies a higher FA/HA ratio with increasing slope. It is recommended to carry out research on this ratio for inland waters.

Another factor of influence on the slope S is the effect of pH on the FA and HA absorption. An increase in absorbance at 375 nm with increasing pH by fulvic acids was measured by de Haan *et al.* (1982) in shallow eutrophic lakes similar to those in this study; pH levels in the waters in this study varied from 7.8 to 9.2. The ARC and River Vecht had low pH values, whereas the very eutrophic lakes had the highest pH values. The lowest values for S found for river, canal or groundwater-fed water bodies may imply a lower FA/HA ratio possibly augmented by a pH dependent slope change.

Krijgsman (in prep.) presents an improved model to describe the shape and variability of the absorption spectrum of aquatic humus. Based on the assumption that the variability in shape in the *a(ah)* spectrum is caused by varying linear contributions of constituent components, vectors are used to describe components with arbitrary spectral shape. Abstract factor analysis was applied to determine the number and the abstract shape of the components present in the *a(ah)* spectrum. Three components were identified to accurately describe the data in the range 350-550 nm. Most of the variance in their data set was described by the first component. The second and third components each allowed a gain of one order of magnitude in accuracy expressed by the number of misfits. Due to the similarity between the waters studied by Krijgsman (in prep.) and those of this study, the abstract factor model is probably also appropriate for the data set presented here. Further investigation is required in order to apply this method within a comprehensive algorithm for applications in remote sensing.

2.2.3 *The spectral properties of seston*

2.2.3.1 *Introduction*

Seston is the collective name for all particulate matter suspended in water which does not pass through a 0.45 μm filter. Seston is the major determinant of optical water quality. The seston consists of live organic material (mainly phytoplankton) and dead organic (detritus) and inorganic material. Tripton refers to the sum of the dead organic and the inorganic seston components, also referred to as the non-algal fraction of the seston. It is likely that each of these materials has its own distinctive absorption ($a(s) = a(ph) + a(t)$) and scattering properties ($b(s) = b(ph) + b(t)$).

Most of the seston within the lakes investigated in this study can be considered to be derived from autochthonous sources, namely phytoplankton production and its degradation products combined with organic debris from the breakdown of macrophytes and resuspended peat. The seston in the Amsterdam-Rijn Kanaal (ARK) and the River Vecht (RVE) probably comes from inputs by lakes and rivers, as suggested by the large amounts of algal remains in samples analysed microscopically (Koeleman, pers. comm.). Another seston source in these water bodies is autochthonous production, which is probably lower compared to the lakes studied due to the high turbidity caused by heavy shipping traffic.

The phytoplankton composition is strongly influenced by the water quality in the individual water bodies. The species composition and abundance of phytoplankton is mainly determined by the underwater light climate and by nutrient loading. Phytoplanktonic light harvesting pigments have a major influence on the spectral signature in eutrophic inland waters, through their wavelength specific absorption features (Davies-Colley *et al.*, 1986; Dekker *et al.* 1991, 1992 a-d; Dekker & Donze, 1992; Dekker & Peters, 1993). Phytoplankton may also scatter light in a variety of manners causing another

strong influence on the spectral signature of waters (Davies-Colley *et al.*, 1986; Dubelaar *et al.*, 1987; Ganf *et al.*, 1989).

Little is known about the optical characteristics of tripton and its detrital fractions in freshwaters (Kirk, 1983). Detritus has absorption properties which are probably similar to those of aquatic humus (Yentsch, 1962; Kirk, 1980; Davies-Colley, 1983, Bricaud & Stramsky, 1990). Gons *et al.*(1991) published attenuation values of epipelon for Lake Loosdrecht which showed an exponential increase with decreasing wavelength (epipelon is defined as the sum of micro-organisms and detritus on the bottom of a lake). Klepper *et al.* (1984) published a tripton absorption spectrum for the deep (80 m) Lake Maarsseveen, close to the study area. This tripton absorption spectrum had a (weak) exponentially decreasing slope with increasing wavelength. Kirk (1983) published tripton absorption spectra for Australian freshwater bodies. The spectral absorption shape was similar to that of aquatic humus. The inorganic part of the tripton fraction will probably also have similar absorption features due to the strong colouring of these waters by aquatic humus (Kirk, 1980; Davies-Colley, 1983). It must be kept in mind, however, that inorganc fractions in high concentrations will have their own distinctive colour and hence will have absorption characteristics which are independent of the water in which they are suspended. In the central western part of The Netherlands, however, this does not appear to occur.

Scattering by tripton will most likely differ from scattering by intact phytoplankton because of differences in particle size and breakdown products. Peat fragments and aggregations of detritus could be much larger, also causing the scattering to be different from that produced by phytoplankton.

2.2.3.2 *Seston spectral absorption measurements*

Equation 2.13 was applied to the spectrophotometric measurements of the seston samples measured without (Fig. 2.5.a) and with (Fig. 2.5.b) the integrating sphere accessory to calculate the true seston absorption spectra (Fig. 2.5.c).

General spectral features evident in the seston absorption spectra include: from 400 to 438 nm an almost flat or slightly decreasing slope in the samples with low absorption. For the samples with a higher absorption this slope increases to 438 nm. The peak at 438 is the blue or first chlorophyll *a* absorption maximum $a(ph)_{438}$. Beyond the peak at 438 nm a strong decrease occurs until a shoulder at 480 nm becomes visible. This absorption feature is probably due to β-carotene, a light-harvesting pigment present in all algae. Beyond 480 nm absorption decreases to a minimum at 550 nm, after which it increases to a relatively small peak at 624 nm. This peak is probably caused by cyanophycocyanin (CP-cyanin) absorption, indicating the presence or the dominance of cyanobacteria in these waters (referred to as $a(ph)_{624}$).

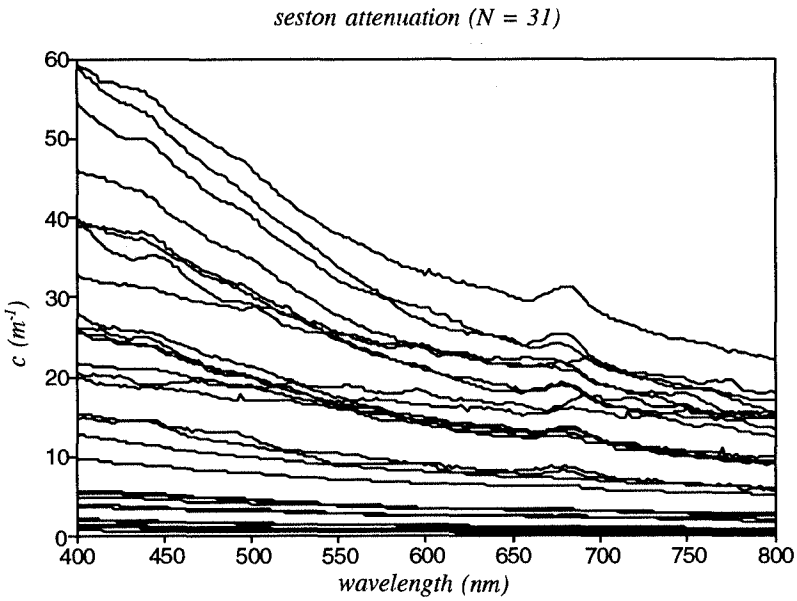

Figure 2.5.a *31 seston attenuation spectra for the 1990 remote sensing sampling data set.*

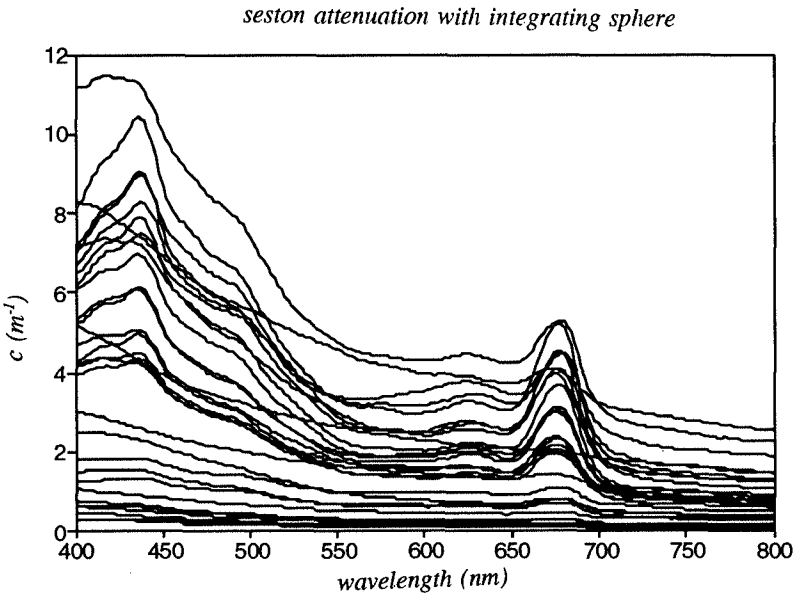

Figure 2.5.b *Seston attenuation spectra for the samples of Fig. 2.5.a measured with an integrating sphere accessory capturing the forward scattered light from 5°- 40° (note different scale y-axis).*

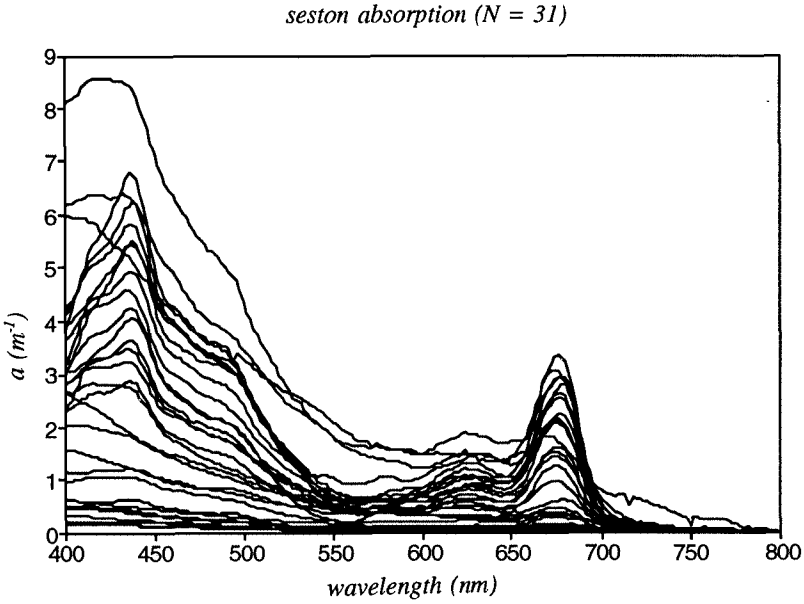

Figure 2.5.c *31 seston absorption spectra for the 1990 remote sensing sampling data set (note different scale y-axis).*

Absorption decreases from 624 nm to a relative low at 650 nm followed by a clear increase in absorption to a maximum at 676 nm: this is the red, or second, chlorophyll *a* absorption peak ($a(ph)_{676}$). Beyond 676 nm the absorption decreases to almost zero at 720 nm.

Although phytoplankton pigments cause the most prominent features in the absorption spectra, especially those from eutrophic waters, tripton, which is present in considerable quantities in these lakes, also absorbs light. As mentioned previously the spectrum of tripton or detritus absorption is probably similar to that for aquatic humus. Seston absorption spectra without a significant absorption feature at 438 nm are probably dominated by tripton absorption.

One of the aims of this study was to develop algorithms for extraction of algal pigment concentrations (i.e. chlorophyll *a* and CP-cyanin) from remotely sensed data. The physical separation of algae and tripton from the seston was not feasible. Therefore, in order to separate the spectral absorption of algae from that of tripton a spectral method is required. In the following section a model by Bricaud & Stramsky (1990) is presented that was developed to separate detritus spectral absorption from phytoplankton spectral absorption, based on spectral indices. This Bricaud & Stramsky model was based on spectral absorption characteristics of algae and detritus in ocean waters. A partial modification to fit the requirements of this study: i.e. spectral separation of freshwater phytoplankton absorption and tripton absorption (instead of detritus absorption), was therefore required.

2.2.3.3 *The Bricaud & Stramsky model for determining the detrital part of the seston absorption spectrum.*

Bricaud & Stramsky (1990) reviewed the literature on methods for the determination of the fractions of living pigmented algal cells and weakly pigmented or unpigmented particles (detritus) mainly derived from phytoplankton and bacteria for ocean waters.

From the literature they distinguished several approaches to determining the absorption of particulate matter. The first method involved the determination of the absorption coefficient of the particulate material from the attenuation spectrum. Indirectly the particulate matter absorption could be determined from the measured apparent optical properties. Another widely used method involves the filterpad method originally developed by Yentsch (1962), but which has the disadvantage of the path length amplification factor due to multiple scattering effects being unknown. The remaining method distinguished was the method of concentration (Kirk, 1980) as was applied in this research. This method has the disadvantages outlined in § 2.1. However, none of these methods allow algal and non-algal fractions to be discriminated.

Once the true particulate matter or seston absorption was known three approaches were identified by Bricaud & Stramsky (1990) to discriminate the particulate matter absorption into algal and non-algal fractions. These approaches were a statistical approach, an experimental approach and a new approach using spectral criteria.

The statistical approach used empirical information such as

- a relationship between detritus concentration and phaeopigment concentration;
  the absence of fluorescence in detrital matter;
  published values of *in vivo* absorption coefficients for the main pigments with appropriate corrections to represent algal suspensions;
  microphotometric determination of the efficiency factors for absorption of individual living or detrital particles.

The experimental approach utilized algal pigment extraction, either via maintaining the integrity of the algal cells through UV radiation or through organic solvent extraction of the material collected on a filterpad. However, ambiguities remained in the interpretation of these results.

Because each of the above methods have methodological difficulties and require experimental determination of parameters, Bricaud & Stramsky (1990) developed method for evaluating the algal and non-algal contributions to absorption based on spectral criteria.

The essence of this method is the recognition that pure phytoplankton absorption spectra have spectral ratios close to 1 for $a(ph)_{380} : a(ph)_{505}$ (the $a(ph)$ at 380 nm : $a(ph)$ at 505 nm) and for $a(ph)_{580} : a(ph)_{692.5}$ and that the particulate matter absorption spectra show an increase towards short wavelengths due to the influence of absorption by non-algal material, similar to the spectral absorption of aquatic humus. The wavelengths

where the ratio is close to 1 were selected on the criteria that the absorption by accessory pigments must be minimal and that the chosen wavelengths are sufficiently spaced to accurately determine a detrital matter slope. Another reason for choosing a ratio close to 1 is that the ratio must not be affected by the package effect. The package effect is a "flattening of absorption spectra" effect that can be induced by an increase of either cell size or of intracellular pigment concentration (Kirk, 1975a; Morel & Bricaud, 1981). The presence of phycobilin pigments may modify both ratios, specifically cyanophycoerythrin with an absorption maximum at 565 nm.

Equations 2.14 to 2.20 represent the essence of the Bricaud & Stramsky (1990) model for determining the detrital part of the particulate matter absorption spectra for ocean waters. The spectral absorption by detritus, *a(d)*, is therefore introduced. In the next section a modification of the model is presented where *a(d)* is replaced by the tripton absorption *a(t)*, and *a(p)* is replaced by *a(s)*. For freshwaters the detrital and inorganic fraction of the tripton cannot yet be distinguished optically.

For ocean waters the spectral dependency of the absorption by detrital material appears to be similar to that found for aquatic humus (see § 2.2.2.4): i.e.

$$a(d) = Y\, exp(-S\, \lambda) \qquad [2.14]$$

where Y and S are both variable and Y is the constant and S the slope. It has already been discussed in § 2.2.2. what errors are introduced when assuming a fixed slope for aquatic humus. Similar types of error may occur when estimating *a(d)* or *a(t)* based on equation 2.14. Without using this assumption, however, there is no possibility at this stage of the research to determine the tripton part of the seston absorption, and thereby obtaining through subtraction: $a(s) - a(t) = a(ph)$, the phytoplankton component of the seston absorption spectrum.

Bricaud & Stramsky (1990) used absorption coefficients of total particulate matter and of living phytoplankton measured in the Sargasso Sea surface mixed layer in their analysis. They used the methanol extraction filterpad method for the determination of the *a(d)*. *a(d)* was subsequently subtracted from *a(p)*, which is equivalent to the *a(s)* used in this study, to give *a(ph)*:

$$a(d)_\lambda = a(p)_\lambda - a(ph)_\lambda \qquad [2.15]$$

An approximation of the path length amplification method was made using the concentration method of Kirk (1980). This concentration method is similar to that used in this research for seston absorption determination for samples that were not turbid enough for direct measurement (see § 2.1.2.2).

For 31 samples from the Sargasso Sea Bricaud & Stramsky found that the best ratios were

$$a(ph)_{505} : a(ph)_{380} = 0.99 \quad [2.16a]$$

and

$$a(ph)_{580} : a(ph)_{692.5} = 0.92 \quad [2.16b]$$

Combining equations 2.14 to 2.16.b the following equations were obtained:

$$Y\ exp(-380\ S) - Y\ exp(-505\ S) = a(p)_{380} - a(p)_{505} - 0.01\ a(ph)_{380} \quad [2.17a]$$

and

$$Y\ exp(-580\ S) - Y\ exp(-692.5\ S) = a(p)_{580} - a(p)_{692.5} - 0.08\ a(ph)_{692.5} \quad [2.17b]$$

If Y and S vary independently, the contributions of algal and non-algal materials to overall absorption can be estimated by solving the system of equations for Y and S:

$$0.99\ Y\ exp\ (-380\ S) - Y\ exp(-505\ S) = 0.99\ a(p)_{380} - a(p)_{500} \quad [2.18a]$$

and

$$Y\ exp\ (-580\ S) - 0.92\ Y\ exp(-692.5\ S) = a(p)_{580} - 0.92\ a(p)_{692.5} \quad [2.18b]$$

and computing for each wavelength

$$a(d) = Y\ exp(-S\lambda) + a(p)_{750} - Y\ exp(-750\ S) \quad [2.19]$$

and the result of equation 2.15 for each wavelength interval.

The term $[a(p)_{750} - Y\ exp(-750\ S)]$ in Eq. 2.19 means that the computed values of $a(d)$ are shifted at all wavelengths in such a way that $a(d)$ equals $a(p)$ (Bricaud & Stramsky, 1990). A wavelength of 750 nm is chosen for $a(p)$ under the assumption that the optical density of pigments can be assumed to be zero.

2.2.3.4 *Application and partial modification of the Bricaud & Stramsky model for absorption spectra of inland waters*

The Bricaud & Stramsky (1990) spectral criteria method was used to distinguish phytoplankton and tripton absorption in the seston spectra measured in this study. For the data presented here spectrophotometric measurements were limited to the 400 - 800 nm range because this was the range assumed to be useful for remote sensing purposes. The Bricaud & Stramsky (1990) model was therefore modified to overcome the problem of missing spectral data at 380 nm. To compensate for the lack of measurements the data from the Bricaud & Stramsky publication were used to determine the 400 to 505 nm ratio instead of the 380 to 505 nm ratio:

$$a(ph)_{400} : a(ph)_{505} = 0.74 \qquad [2.20]$$

This leads to modification of Eq. 2.17.a into:

$$Y\ exp(-400\ S) - Y\ exp(-505\ S) = a(s)_{400} - a(s)_{505} - 0.26\ a(ph)_{400} \qquad [2.21]$$

and subsequently to modification of Eq. 2.18.a to:

$$0.74\ Y\ exp\ (-400\ S) - Y\ exp(-505\ S) = 0.74\ a(s)_{400} - a(s)_{500} \qquad [2.22]$$

Errors introduced this way are caused by transgression of the criterion for preventing the package effect to be of influence, i.e. a ratio of 1 instead of 0.74, and by a larger role of accessory pigments at 400 nm. Bricaud & Stramsky determined the influence of variations in the ratios of $a(ph)_{380} : a(ph)_{505}$ and $a(ph)_{580} : a(ph)_{692.5}$ on the model. For variations in the $a(ph)_{380} : a(ph)_{505}$ ratio of 0.8 to 1.4 they calculated insignificant variations in estimated chlorophyll *a*-specific absorption $a(ph)^*$ in the green and red parts of the spectrum and less than 15% variation in $a(ph)_{440}^*$. A decrease in the $a(ph)_{580} : a(ph)_{692.5}$ ratio from 0.92 to 0.5 modified $a(ph)^*$ by only a few percent throughout the spectrum.

Of the 27 spectral scans to which the calculations were applied only LWG produced anomalous values, because the rightside part of Eq. 2.22: $[0.74\ a(s)_{400} - a(s)_{505}]$ gave negative values. A value of 0.81 for the ratio of $a(ph)_{400} : a(ph)_{505}$ instead of 0.74 was required to give positive results for this part of the equation. The results showed that the method gave results indicative of a correct partitioning of the absorption signal into tripton and phytoplankton fractions for all types of water encountered here except for shallow eutrophic lakes dominated by *Oscillatoria spp.* and by *Prochlorothrix hollandica.* Calculated *a(t)* values for these prokaryotic filamentous species dominated samples were negative, indicating a different ratio of spectral absorption for this type of phytoplankton compared to those ratios derived from ocean algae.

The calculated negative $a(t)$ values obtained for the eutrophic lake samples were caused by the seston absorption spectra having a ratio $a(s)_{580} : a(s)_{692.5}$ of less than 1. This implies that this ratio was even smaller for the phytoplankton signal only, for it is assumed that tripton absorption increases with decreasing wavelength. Thus a combined tripton and phytoplankton absorption, i.e. the seston absorption, must be larger than 1 (under the condition that the $a(ph)_{580} : a(ph)_{692.5}$ ratio for phytoplankton is 1). Gons *et al.*, (1992) calculated a phytoplankton to detritus ratio, expressed in seston dry weight, of 0.3 for the shallow eutrophic Lake Loosdrecht (LLO). If this value also applies to the other shallow eutrophic lake samples used here either the per unit absorption of the detritus is very low or the main phytoplankton species have quite different $a(ph)_{580} : a(ph)_{692.5}$ ratios than found by Bricaud & Stramsky (1990) for ocean algae.

From the shallow eutrophic lakes in this study the lowest value of the ratio $a(s)_{580} : a(s)_{692.5}$ was determined to be 0.67. Such a low ratio seems indicative for a low contribution of tripton absorption (the ratio would otherwise be higher). Data of attenuation spectra partially corrected for scattering of *Prochlorothrix hollandica* cultures (H. Matthijsen, pers. comm.) showed good correspondence with the spectral ratios assumed in the *P. hollandica* dominated seston samples. An *in vivo* absorption spectrum for a laboratory grown *P. hollandica* culture gave spectral ratios $a(ph)_{400} : a(ph)_{505}$ of 0.68 and $a(ph)_{580} : a(ph)_{692.5}$ of 0.67 (calculated from data by Burger-Wiersma *et al.* 1989). It was not clear how the data were corrected for (residual) scattering since a baseline attenuation at 750 nm was evident. Additional absorption measurements are required to test the suitability of the Bricaud & Stramsky model to lakes dominated by filamentous algae such as *Oscillatoria spp.* and *P. hollandica.*

Assuming the ratio of 0.67 for $a(ph)_{580} : a(ph)_{692.5}$ to be representative of a high phytoplankton and low tripton spectrum a ratio value of 0.67 is considered to be a minimum until *in vivo* absorption spectra, fully corrected for scattering, of *Oscillatoria spp.* and *Prochlorothrix hollandica* become available. Equation 2.16b thus became:

$$a(ph)_{580} : a(ph)_{692.5} = 0.67 \qquad [2.23]$$

and equation 2.17b then becomes:

$$Y\ exp(-580\ S) - Y\ exp(-692.5\ S) = a(s)_{580} - a(s)_{692.5} - 0.33\ a(ph)_{692.5} \qquad [2.24]$$

which in turn leads to equation 2.18b being replaced by:

$$Y\ exp\ (-580\ S) - 0.67\ Y\ exp(-692.5\ S) = a(s)_{580} - 0.67\ a(s)_{692.5} \qquad [2.25]$$

Combining these with equations 2.21 and 2.22, the tripton absorption fraction of the shallow eutrophic lakes could also be estimated. The calculated values of tripton absorption are presented in Figure 2.6 and the algal absorption spectra in Figure 2.7.

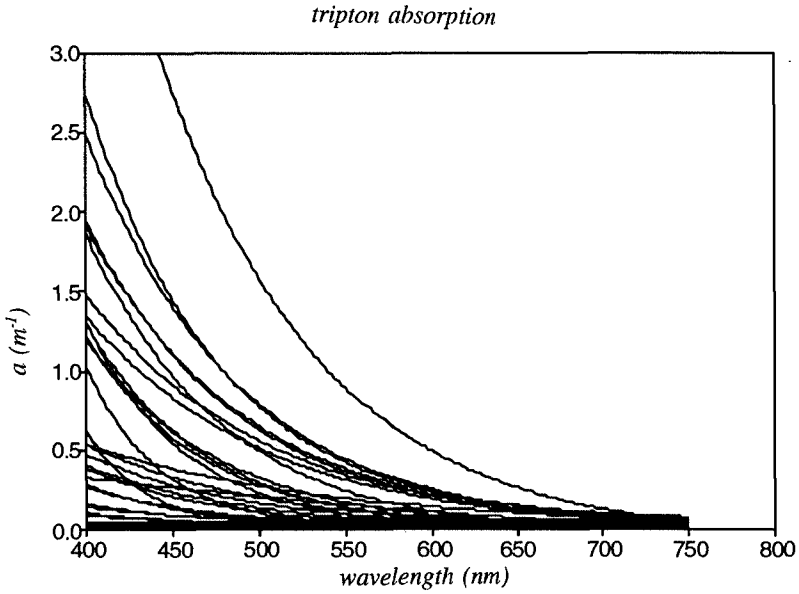

Figure 2.6 *Calculated values of tripton absorption spectra for the 1990 remote sensing sampling data set using the Bricaud & Stramsky (1990) model. The values for the shallow eutrophic lakes were calculated using the modified Bricaud & Stramsky (1990) model (see § 2.2.3.4).*

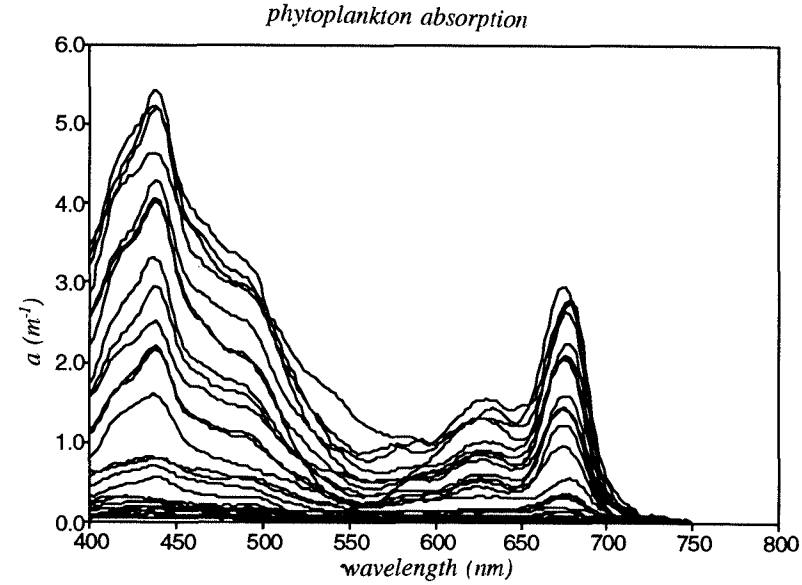

Figure 2.7.a *31 phytoplankton absorption spectra for the 1990 remote sensing sampling data set calculated by subtracting the tripton spectra (Fig. 2.6) from the seston absorption spectra (Fig. 2.5.c).*

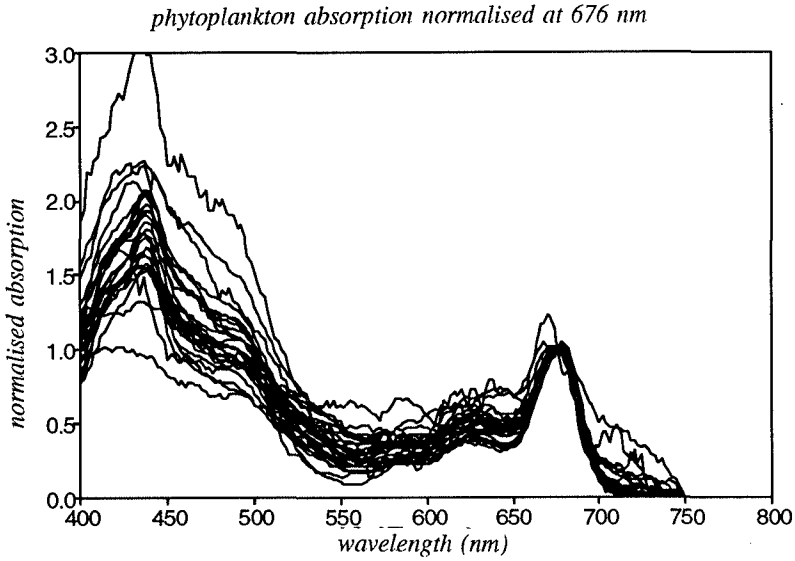

Figure 2.7.b *The log-normalised phytoplankton absorption spectra from Figure 2.7.b*

It appeared that the phytoplankton absorption was several factors higher than the tripton absorption over most of the spectral range for the samples of the shallow eutrophic lakes. Errors introduced by the assumptions adopted for the calculations are that the $a(ph)_{580}$: $a(ph)_{692.5}$ ratio has not been tested on pure phytoplankton cultures of *Oscillatoria spp.*, *Prochlorothrix h.* or other freshwater phytoplankton. Additional errors may be introduced when forcing the shape of phytoplankton absorption spectra to comply with the ratios $a(ph)_{400}$: $a(ph)_{505}$ and $a(ph)_{580}$: $a(ph)_{692.5}$ calculated for other species. Further measurements on the species encountered in these waters should therefore be carried out for a more confident application of the Bricaud & Stramsky model to inland waters.

The ratio $a(ph)_{438}$: $a(ph)_{676}$ (the two chlorophyll *a* absorption maxima; see Fig. 2.7.a & b) can be used to check whether the calculated phytoplankton absorption spectra have been fully corrected for tripton absorption. Published values for the chlorophyll *a* $a(ph)_{438}$: $a(ph)_{676}$ ratio gave values between 1 and 1.5 (Maske & Haardt, 1987). Burger-Wiersma & Post (1989) gave absorption scans of thylakoid preparations of *Prochlorothrix hollandica* cells grown under light limiting conditions from which a 438 to 676 nm ratio of 1.5 was estimated. Burger-Wiersma *et al.* (1989) present an *in vivo* absorption spectrum of *P. hollandica* for which the ratio is 1.66 (with subtraction of baseline scattering the ratio becomes: 1.76). Roesler *et al.* (1989) calculated $a(ph)_{436}$: $a(ph)_{676}$ ratios varying from 1.35 to 1.80 for 25 samples from four different coastal waters. Based on these results values for the $a(ph)_{438}$: $a(ph)_{676}$ ratio greater than 2 may probably be assumed to be due to a residual tripton absorption remaining in the phytoplankton absorption spectrum. Table 2.5 gives the values for this ratio for $a(ph)$ calculated from $a(s)$ for the samples of the Vecht lakes. Only three samples have $a(ph)_{438}$: $a(ph)_{676}$ ratios significantly higher than 2: two Lake Naardermeer samples (LNG and LNS) and

Table 2.5 *Values for the ratio of $a(s)_{438}$:$a(s)_{676}$ and $a(ph)_{438}$:$a(ph)_{676}$ after application of the modified Bricaud & Stramsky model for the samples of the Vecht lakes. A high ratio in $a(s)_{438}$:$a(s)_{676}$ is indicative of a large tripton influence; a ratio > 2 in the column $a(ph)_{438}$:$a(ph)_{676}$ may be indicative of a rest absorption by tripton.*

	$a(s)_{438}$:$a(s)_{676}$	$a(ph)_{438}$:$a(ph)_{676}$
shallow lakes		
eutrophic		
LNW	2.860	1.903
LHA	2.126	1.625
LWG	1.942	1.938
LWL1	2.744	1.633
LWL2	2.243	1.755
LWL3	4.007	2.230
LEL1	2.237	1.858
LEL2	2.276	1.550
LEL3	2.282	1.757
LVU	2.055	1.969
LLO	2.213	2.096
LBR	2.341	2.039
shallow lakes		
mesotrophic		
LNG1	4.760	2.181
LNG2	6.521	2.978
LNS	3.010	1.557
LSA	2.856	2.057
LHO	2.647	1.763
deep lakes		
meso-eutrophic		
LSP1	2.124	1.924
LSP2	2.467	1.684
LWB1	1.987	1.532
LWB2	1.942	1.685
LWB3	1.832	1.807
WR	2.435	2.021
river & canal		
ARC	6.382	1.395
RVE1	3.146	0.935
RVE2	2.917	1.301

one Lake Western Loenderveen (LWL) sample. These samples had the lowest seston dry weight and chlorophyll *a* levels for the shallow lakes and may therefore be more sensitive to errors in the calculations.

The results show, nevertheless, that the approach is robust enough to yield data which are in accordance with expected values, after modification of the parameters to spectral regions for which it was not developed. Because this is the only method published to date for investigating spectral data, the method may be important in the further development of algorithms to decompose spectra obtained over inland waters by imaging spectrometers.

2.2.3.5 *The phytoplankton absorption spectra*

Fig. 2.7.a shows 27 phytoplankton absorption spectra for the water bodies sampled. Normalising these spectra at the chlorophyll *a* red wavelength absorption maximum of 676 nm, enables a comparison of the absorption spectra for the algal species in these waters. The wavelength of 676 nm is appropriate because possible errors introduced by both the correction for scattering and subtraction of the estimated tripton absorption will be relatively low. Both these sources of error have lower absolute values at the red wavelength region as compared to shorter wavelengths. Additionally, the 676 nm absorption maximum is the largest single spectral absorption feature. The same spectral features are evident as were shown in the seston absorption spectra in Fig. 2.5.c; only the features are more pronounced. The shape of the *a(ph)* spectra are similar in general; however, between 500 and 600 nm several crossovers of spectra occur. No differences in wavelength location for the chlorophyll *a* absorption maximum were found between the apparent absorption, the scattering-corrected seston absorption and the phytoplankton absorption spectra. The red chlorophyll *a* maximum is at 676 nm with a standard deviation of 2 nm. For the phycocyanin absorption maximum around 624 nm there is an apparent wavelength shift from 625 nm (σ = 3 nm, N = 24, Fig. 2.5.b & c) for the seston spectra to 628 nm (σ = 3 nm, N = 25, Fig. 2.7.a & b) for the phytoplankton absorption spectra.

2.2.3.6 *Specific absorption of chlorophyll a*

The chlorophyll *a*-specific absorption is defined as the value of *a(ph)* when the chlorophyll *a* concentration in the medium is 1 $\mu g\ l^{-1}$. Using the calculated phytoplankton absorption spectra, specific absorption (a^*) of the light harvesting pigments chlorophyll *a* and CP-cyanin were calculated.

Bricaud *et al.* (1988) summarised the major sources causing variability in a^* calculations as pigment composition and the packaging effect (Kirk, 1975 a & b; Morel & Bricaud, 1981). This latter effect is equivalently ruled by the size and the intracellular

pigment concentration of the cells, and results in a flattening of the *in vivo* absorption spectrum compared to that for the same substance dispersed in solution.

The specific absorption for chlorophyll *a* at 676 nm (a^*_{676}) was determined by dividing the value of $a(ph)_{676}$ by the measured chlorophyll *a* concentrations (in fact the sum of chlorophyll *a* and pheaophytin). a^*_{676} is 0.0153 m^2 mg^{-1} (σ = 0.0041 m^2 mg^{-1}) with the values ranging from 0.0055 to 0.0218; table 2.6 presents the values for the Vecht lakes. The higher values for the shallow eutrophic lakes may be attributed to the package effect having a reduced effect in these lakes due to the diameter of the filaments being in the order of 0.5 µm to 1.5 µm, which is representative for optically small cells. For six freshwater phytoplanktonic species Davies-Colley *et al.* (1986) calculated a^*_{676} to be 0.0098 to 0.0165 m^2 mg^{-1}.

Haardt & Maske (1987) calculated a^*_{675} for healthy marine phytoplankton cultures to be between 0.007 and 0.013 m^2 mg^{-1}. Natural samples from Kiel harbour, in the same study, gave a^*_{675} values of 0.009 to 0.017 m^2 mg^{-1}. Maske & Haardt (1987) were able to measure at close to naturally occurring concentrations. They also reviewed published a^*_{675} values for saltwater organisms: 15 references gave values between 0.004 to 0.034 m^2 mg^{-1}.

Table 2.6 *Values of chlorophyll a-specific absorption and the chlorophyll a and dry weight-specific scattering for the Vecht lakes area samples (N = number of samples; a^*_{676} Chl-a = chlorophyll a-specific absorption at 676 nm (m^2 mg^{-1}); b^*_{550} DW = seston dry weight-specific scattering at 550 nm (m^2 g^{-1}); b^*_{550} Chl-a = chlorophyll a-specific scattering at 550 nm (m^2 mg^{-1}); σ = standard deviation).*

	N	a^*_{676} Chl-a	σ	b^*_{550} DW	σ	b^*_{550} Chl-a	σ
All samples	26	0.0153	0.0041	0.62	0.28	0.173	0.122
Lakes:							
Deep meso-eutrophic	5	0.0136	0.0020	0.52	0.24	0.123	0.017
Shallow eutrophic	11	0.0180	0.0022	0.79	0.15	0.179	0.036
Shallow mesotrophic	4	0.0102	0.0028	0.23	0.09	0.119	0.015
Canal/River	3	0.0146	0.0063	0.47	0.13	0.465	0.338

According to Haardt & Maske (1987) chlorophyll *a* absorption at 675 is negligibly influenced by the accessory pigments chlorophyll *b* and *c*. Burger-Wiersma *et al.* (1989) found negligible absorption by chlorophyll *b* in an *in vivo* absorption spectrum for *P. hollandica* (*P. hollandica* does not contain chlorophyll *c*). In contrast, the 438 nm chlorophyll *a* absorption band is strongly influenced by absorption by accessory pigments. This suggests that the best indices for chlorophyll *a* derived from remotely sensed reflectance data will be derived from wavelengths at the red end of the spectrum around 676 nm as opposed to those at the blue end (see Figs. 2.7. a & b).

2.2.3.7 *Specific absorption of CP-cyanin*

For the calculation of the specific absorption of CP-cyanin it was necessary to determine the contribution of CP-cyanin absorption to the total phytoplankton absorption around 625-624 nm. It is clear from Fig. 2.7 that water samples with little or no CP-cyanin concentrations still show a significant amount of absorption (albeit without a peak between 600 and 648 nm) at 625-628 nm, probably attributable to absorption by chlorophyll *a'*, *c*, *b* and other accessory pigments. A shoulder of the main chlorophyll *a* absorption feature at 676 nm may also influence the absorption at 625-628 nm. A baseline was therefore established from 600 to 648 nm (the two spectral points where the CP-cyanin feature disappears). After subtraction of this baseline from the total *a(ph)* measurement the remaining *a(ph)* was due to CP-cyanin absorption. The wavelength with maximum absorption by CP-cyanin now appeared to be located at 624 nm (Fig. 6.1). Thus 624 nm is taken as the correct *in vivo* absorption maximum of CP-cyanin.

CP-cyanin concentration was measured on samples taken on 12 September 1990 (see Table 2.7) using the method described in § 1. Six of the samples for the spectrophotometric measurements of *a(ph)* were taken 2 to 15 days before the samples taken for the CP-cyanin concentration measurements. Three of the measurements of CP-cyanin concentration and CP-cyanin absorption were performed on the same samples (Table 6.1). The values for CP-cyanin absorption were then divided by the measured CP-cyanin concentrations to determine the specific CP-cyanin absorption at 624 nm, a^*_{624}. For CP-cyanin the specific absorption a^*_{624} is 0.0032 $m^2\ mg^{-1}$ ($N = 8$, $\sigma = 0.0012\ m^2\ mg^{-1}$). The CP-cyanin-specific absorption is approximately 5 times lower than the chlorophyll *a*-specific absorption.

Dekker *et al.* (1992a) calculated values of the specific absorption a^*_{624} to be 0.0035 $m^2\ mg^{-1}$ ($N = 8$, $\sigma = 0.0013\ m^2\ mg^{-1}$) for the same samples using the seston absorption spectra and 624 nm as the maximum CP-cyanin absorption wavelength. It appears that the baseline subtraction method corrected the data for tripton absorption and that the method is not too sensitive regarding the exact location of the absorption maximum.

Table 2.7 *The cyanophycocyanin-specific absorption coefficient for 8 samples from the Vecht lakes area (a^*_{624} = CP-cyanin-specific absorption coefficient (m^2 mg^{-1}). One sample of Lake Western Loenderveen (LWL) was excluded: see text). Also see Fig. 5.13 and Table 5.7.*

	N	a^*_{624}	σ
All samples	8	0.0032	0.0012
LNW		0.0022	
LLO		0.0035	
LVU		0.0058	
LBR		0.0035	
LHA		0.0014	
LSA		0.0033	
LWG		0.0032	
LWB		0.0031	

2.2.4 *Scattering spectra of inland waters*

Before considering spectral reflectance, the inherent optical property that causes the upward change in direction of downwelling light, spectral scattering, will be discussed.

In general algal cells scatter light more strongly than they absorb light (Privoznik *et al.* 1978; Bricaud *et al.*, 1983). Morel & Bricaud (1986) calculated specific absorption and scattering values for 22 saltwater species; their data showed ratios of chlorophyll-specific spectral scattering to absorption of 4 to 22.

The spectral scattering of tripton has been measured by Klepper *et al.* (1984) for the deep Lake Maarsseveen in the central Netherlands; and appears to be a linear decreasing function with increasing wavelength. Information on the sample preparation and measurement is, however, lacking. Bale & Morris (1987) studied particles in estuarine waters and found that the aggregation of particles is an important feature, changing the size of fragments measured *in situ* as compared to measuring them after application of some form of mechanical stress. Thus, in this research, the concentration method used may have altered the aggregation of particles leading to errors in the estimation of the scattering. One sample from Lake Wijde Blik containing *Microcystis aeruginosa* in colonies of up to 5 mm diameter was probably influenced by the colony dispersing into its separate cells: the specific absorption and scattering values were more than two standard deviations out of range of all the other samples; this sample was therefore discarded for further use. Ganf *et al.* (1989) estimated spectral chlorophyll *a*-specific scattering for *Microcystis* cells and colonies at 0.14 and 0.11 m^2 mg^{-1} respectively; indicating that the errors in the Lake Wijde Blik measurements are presumably augmented by another unknown error source. It is, for example, conceivable that the results of measurements on samples are dependent on the number of colonies sampled *in situ*.

Few spectral scattering spectra for inland waters have been published. Davies-Colley *et al.* (1986) determined spectral scattering spectra for six freshwater phytoplankton cultures. Qualitative differences in scattering spectra were explained in terms of optical size of the particles comprising the cultures. The green algal and diatom cultures displayed a complex shaped but non-trending scattering spectrum. The cyanobacterial cultures behaved as optically small particles and displayed a pattern of decreasing scattering with increasing wavelength. According to Davies-Colley *et al.* (1986) as a first approximation, the assumption of constancy at any given wavelength (Bukata *et al.*, 1981), or for visible waveband average values (Vant & Davies-Colley, 1984), may be permissible where account cannot be taken of the factors affecting chlorophyll *a*-specific scattering: such as optical size of cells, surface area to pigment ratios and cell aggregation. Morel & Bricaud (1986) present a scattering spectrum for an unidentified cyanobacterial species with a clearly exponentially decreasing scattering efficiency with increasing wavelength.

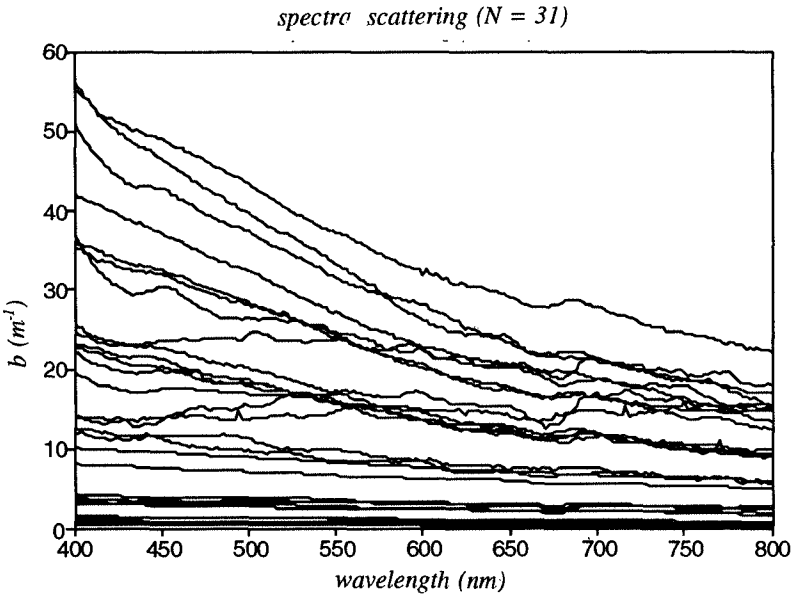

Figure 2.8 *Spectral scattering for the same samples as shown in Figs. 2.5 a-c. (This is the spectral scattering over an angle of 5 - 180°, calculated by subtracting the combined absorption spectra (Figs. 2.5.c or the sum of spectra given in Fig. 2.6 and 2.7.a) from the seston attenuation spectra (Fig. 2.5.a)).*

Fig. 2.8 shows the spectral scattering for the same seston samples as used before to measure absorption spectra. The spectral scattering was calculated from the beam attenuation measurements minus the true total absorption (Eqs. 2.1 - 2.13); it is the spectral scattering over an angle of 5 - 180°. The scattering values are high compared to those found for ocean waters. In general an increase in scattering was associated with an

increase in slope of the spectral scattering towards shorter wavelengths. An effect especially noticeable for the filamentous algae dominated lakes in accordance by the findings of Davies-Colley *et al.* (1986) and Morel & Bricaud (1986). An increase in scattering is closely correlated to an increase in particulate matter as expressed in seston dry weight concentration and in absorption by particulate matter. The shape of the scattering spectrum is mainly a function of the scattering properties of the particles. In general a steepening of the slope toward shorter wavelengths may be caused by a decreasing optical cross section of the average particle size in the samples. In inland water samples the particulate matter will always be a mixture of particle types and sizes. Scattering by algae is quite complex: an alga is semitransparent and contains a variety of different materials within its cell structure. Cyanobacteria contain gas vacuoles that cause high scattering at large angles (Dubelaar *et al.*, 1987). Ganf *et al.* (1989) calculated a spectral slope of scattering for isolated gas-vesicles from *Microcystis* of $\lambda^{-2.56}$. Although scattering by algae is generally regarded to be inversely related to wavelength, scattering spectra of freshwater algae by Klepper *et al.* (1984) show low scattering at the two chlorophyll *a* absorption maxima and higher scattering in between with a peak at 565 nm. Dubelaar *et al.* (1987) show spectra of *Microcystis aeruginosa* from which scattering due to gas vacuoles may be deduced as being inversely related to wavelength.

2.2.4.1 *The specific scattering coefficient*

Several specific scattering coefficients may be calculated depending on the parameter serving as the independent variable. The seston specific scattering coefficient may be determined through calculating the amount of seston scattering at 550 nm ($b(s)_{550}$) nm per unit seston dry weight. A wavelength of 550 nm is often chosen as it represents the centre of the PAR wavelength range thus giving a first approximation for use in PAR-based studies and models. In the water bodies of this study between 550 and 600 nm the phytoplankton absorption is lowest within the PAR range (see Figs. 2.7.a & b); 550 nm is therefore a convenient wavelength for possible estimation of $b(s)^*_{550}$ from a remotely sensed spectral measurement of upwelling radiance, for the absorption by phytoplankton may be assumed low. $b(s)^*_{550}$ consists of a phytoplankton-specific scattering, $b(ph)^*_{550}$, and of a tripton-specific scattering coefficient, $b(t)^*_{550}$.

For ocean waters Morel (1987) defined the chlorophyll-specific scattering coefficient b* as that part of the scattering coefficient of an algal suspension (or of a water body) which is due to the presence of algal cells, $b(ph)$, once it has been divided by the chlorophyll *a* concentration.

In inland waters the composition of the seston is more variable than in ocean waters. The scattering of phytoplankton per mg dry weight contribution is higher than the scattering contribution of the tripton when both are expressed per mg seston dry weight. Thus the seston b^*_{550} will only be a useful parameter, for analytical modelling of the underwater light field, if the partial contributions of the tripton and the phytoplankton to the seston are known. The seston b^*_{550} for the waters with high tripton to phytoplankton

ratios will give a first order approximation of the tripton b^*_{550}, whereas the seston b^*_{550} for the waters with a low tripton to phytoplankton ratio will give the first order approximation of the phytoplankton b^*_{550}. The waters with low and high tripton to phytoplankton can be identified by the $a(s)_{438}$: $a(s)_{676}$ ratio: as the ratio increases (from a value of 2 onwards) the tripton to phytoplankton ratio increases (see Table 2.5). The values change with water type. The waters with high tripton to phytoplankton ratios, for example the canal/river and the mesotrophic lake samples, have lower seston b^*_{550} values than the deep and shallow eutrophic lakes. For the shallow eutrophic lakes the average seston b^*_{550} lies high at 0.79 m^2 mg^{-1} indicating that the dry weight connected b^*_{550} of algae is more than that of tripton, as was expected.

Table 2.6 shows that the deep lakes and shallow mesotrophic lakes have average b^*_{550} per unit chlorophyll *a* values of ~0.12 m^2 mg^{-1}, whilst the filamentous prokaryote dominated waters have b^*_{550} per unit chlorophyll *a* of ~0.18 m^2 mg^{-1}. This may be explained by the differing optical properties of the different algal species. The filamentous prokaryotes probably scatter light more intensely than the other algal species. The values for the mesotrophic lakes compare well with those found by Davies-Colley(1986) for freshwater algal cultures where chlorophyll *a*-specific b^*_{550} ranges from 0.044 to 0.139 m^2 mg^{-1}. The high b^*_{550} per unit chlorophyll *a* of the river and canal samples are, of course, caused by the low chlorophyll *a* to seston ratios for these waters.

2.3 The effects of the combined spectral absorption and scattering properties of inland waters on reflected irradiance from the water column

The subsurface irradiance reflectance *R(0-)* is a function of solar zenith angle, the volume scattering function and the absorption and scattering properties of a water (see § 3 and 4). The spectral absorption will cause a reduction in *R(0-)*, the spectral scattering will cause an increase in *R(0-)*. Details of this relationship are presented in further chapters. In this section an outline is presented for selecting the most appropriate parts of the spectrum for extracting information from a reflectance spectrum as measured by an *in situ* spectrometer or by a remote sensor.

The combined absorption curves are shown in Fig. 2.9, calculated by summing the absorption curves for humus, tripton, phytoplankton and water.

At short wavelengths humus, tripton and the first chlorophyll *a* absorption peak cause high total absorption. This is the reason for the low reflectance observed in this spectral area (Fig. 3.4 a & b ;see § 3 and further). Beyond 500 nm absorption decreases and reflectance increases correspondingly allowing a better discrimination of spectral features in reflectance spectra. The lowest total absorption values occur at 550 to 600 nm, at 650 nm and at 700 - 710 nm, conversely coinciding with maxima in reflectance.

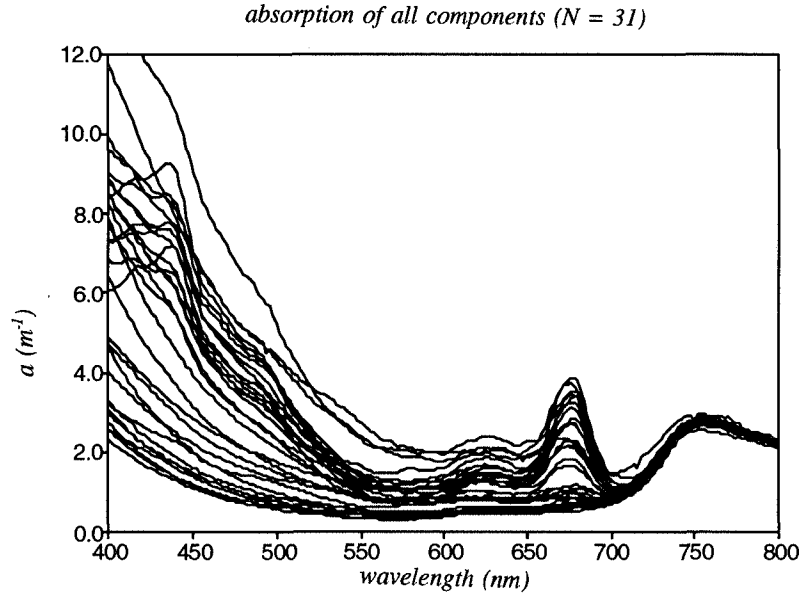

Figure 2.9 *The combined absorption spectra for pure water (Fig. 2.2), aquatic humus (Fig. 2.3), phytoplankton (Fig. 2.7.a) and tripton (Fig. 2.6).*

The combined effects of humus, tripton and algal pigment absorption at short wavelengths (< 500 nm) together with the opposing effects of an increased scattering towards shorter wavelengths make this spectral region inappropriate for extracting information from the resultant reflectance (Dekker *et al.*, 1990, 1991, 1992 b-d).

At 550 nm the algae rich spectra have a minimum absorption; at 624-628 nm an absorption peak due to CP-cyanin is visible; at 648 nm another local minimum in absorption is visible; at 676 nm the red chlorophyll *a* peak is clear; the lowest combined absorption over the entire spectrum is found at 700 - 710 nm. It is also evident from the total absorption spectra that beyond 720 nm water absorption is the dominant factor. These results support earlier research results that information extraction from the reflectance spectra of inland waters should take place in the spectral green to nearby infrared areas (Dekker *et al.*, 1990, 1991, 1992 b-d; Gitelson & Kondratyev, 1991). This is significantly different from ocean colour remote sensing practice where the blue to green spectral area is considered the most appropriate for water quality feature information extraction.

2.4. Conclusions and recommendations

A method developed by Davies-Colley (1986) for the spectrophotometric determination of spectral absorption and scattering was investigated and applied to samples of natural waters. Measurements of the spectral attenuation of samples were carried out using a spectrophotometer with and without an integrating sphere accessory. Analysis of both sets of measurements indicated that volume scattering functions of natural waters may vary significantly. Dividing apparent scattering by total scattering gave a range of 5 to 25 %, suggesting that an assumption of a fixed volume scattering function for modelling the underwater light field or for radiative transfer applications in inland waters may not be correct. However, the scattering at small angles (< 5°) is still an unknown parameter in the determination of total scattering coefficients.

It is possible to spectrally distinguish four components contributing to the spectral absorption: pure water, aquatic humus, phytoplankton and tripton. The aquatic humus analysis indicated large variations in exponential slope within samples from a relatively small geographical region. The possible causes for this variation may be changes in fulvic to humic acid concentrations possibly due to the influence of pH. Absorption by aquatic humus may influence the height and location of the total absorption and reflectance up to 720 nm and beyond in inland waters.

A model for dividing the seston absorption spectrum into component phytoplankton and tripton spectra was applied to the data obtained in this study. However, additional research is necessary in order to determine spectral absorption indices specifically for distinguishing freshwater phytoplankton from tripton. In oligotrophic and mesotrophic waters as well as in a river and a canal, tripton absorption was high compared to phytoplankton absorption. In the shallow eutrophic lakes tripton absorption was less than phytoplankton absorption. Deep mesotrophic to eutrophic lakes were intermediary in this respect.

From the phytoplankton absorption spectra it was possible to determine specific absorption coefficients for chlorophyll *a* at 676 nm and for CP-cyanin at 624 nm. The large variations in the chlorophyll *a* specific absorption coefficients was partly explained by the differing species composition occurring in the various water types encountered. The ratio of the $a(ph)_{438}$: $a(ph)_{676}$ lay in the order of 1 to 2 and may be used to estimate the contribution of tripton to the seston absorption signal: a value significantly higher than 2 will indicate a high tripton to phytoplankton ratio. This ratio may also be used as a control on the correctness of the tripton absorption calculation.

The spectral scattering estimates enabled an approximation of seston dry weight and chlorophyll *a*-specific scattering coefficients for these waters. Specific scattering coefficients at 550 nm were chosen to compare the values with published values. An indication of the relative contribution of the two specific scattering parameters was obtained by determining the chlorophyll *a*-specific b^*_{550} on eutrophic lake samples where the

phytoplankton contributed mostly to scattering and by determining the seston dry weight-specific b^*_{550} on the canal and oligotrophic lake samples where the tripton dominated scattering. Algae scatter light intensely, with the filamentous prokaryote dominated lakes having the highest chlorophyll *a*-specific b^*_{550} values.

From the combined absorption and scattering coefficients it may be deduced that for remote sensing purposes the spectral areas where only one dominant spectral feature (besides pure water) is present will be the most useful for determining inland water quality parameters. Such features include the 624 nm CP-cyanin and the 676 nm chlorophyll *a* absorption features or the absorption minimum at 700-710 nm. Below 500 nm the effects of absorption by aquatic humus, phytoplankton and tripton are compounded and combined with the high level of scattering, present a four-parameter equation of influence on the reflectance signal measured by remote sensing.

A general conclusion pertaining to the determination of inherent optical properties for application in radiative transfer equations can be drawn: the variability in specific absorption and scattering coefficients within and between different water types indicates that the development of remote sensing algorithms for inland water quality analysis must reckon with adjustable parameterisation of absorption and scattering variables for each water type studied.

3 DERIVATION OF SUBSURFACE IRRADIANCE REFLECTANCE FROM REMOTELY SENSED UPWELLING RADIANCE USING *IN SITU* SPECTRORADIOMETRIC MEASUREMENTS

3.1 Introduction

Spectroradiometric measurements play an important role in the development of remote sensing applications. If atmospheric influence, scale effects and instrument differences are ignored, a passive optical remote sensing instrument measures exactly the same upwelling radiance signal as an *in situ* spectroradiometer pointing downwards above the water surface. A remote sensing instrument may thus be thought of as a spectroradiometer with two-dimensional viewing capabilities.

In situ spectroradiometric measurements of reflectance are also important for the development of remote sensing algorithms, because they function as a bridge between laboratory optical measurements and remote sensing measurements.

The desired information from the remotely sensed signal of an area (pixel) of surface water is the subsurface irradiance reflectance *R(0-)*. Undesirable contributions to the remotely measured signal are surface reflectance and backscatter from the atmosphere. Undesirable losses to the *R(0-)* are downward reflection beneath the water surface and absorption and scattering during transmission through the atmosphere. Correction methods for these extraneous effects exist, but residual systematic effects remain and contribute to decreased signal-to-noise ratios.

In any water body part of the light which penetrates the water will, by scattering within the water, pass up through the surface again. Of this emergent flux, 90% originates within the depth (equal to $1 / K_d$) in which downward irradiance falls to 37% of the subsurface value (Kirk, 1983). The detection and quantification of any vertical inhomogeneities in the water column is complex, if possible at all; it was not investigated in this research.

The aim of this study is to develop multitemporal algorithms (i.e. independent of sky conditions, sun zenith angle and state of the water surface) for extraction of water quality information from a remotely sensed upwelling radiance signal L_{rs}. Because L_{rs} varies linearly with the total downwelling irradiance E_{ad}, an algorithm based on L_{rs} is not valid for conditions varying from those that occurred during the measurements used for development of the algorithm. This problem is overcome by determining the ratio of the subsurface upwelling (E_{wu}) to subsurface downwelling irradiance (E_{wd}), giving the subsurface irradiance reflectance, *R(0-)*. *R(0-)* is thus independent of variations in irradiance. However, *R(0-)* is influenced to some extent by angles of irradiance and by measurements at more than 40° from nadir. On the basis of *R(0-)* it is possible to derive multitemporally valid algorithms for applications in remote sensing and from *R(0-)* information can be extracted on those components in the water that interact with the natural light field. This interaction takes place through changes in the inherent optical

properties of absorption and scattering and is dependent on the volume scattering function (see § 2).

In this chapter the theory and practice of determining subsurface irradiance reflectance *R(0-)* from the remote sensed signal L_{rs} is presented. Also described is how to obtain information from the different methods of radiance measurement, including the possible error sources.

The application potential of results presented here for remote sensing of other inland waters is illustrated by a survey of reflectance spectra published in the literature. Similar subsurface irradiance spectra as encountered in the Vecht lakes area are reported by Miyazaki *et al.* (1987) for the Lake Kasumigaura in Japan, by Vos *et al.* (1986) for Frisian lakes in The Netherlands and by Dekker *et al.* (1991) for measurements carried out in 1988 in the southern part of the Vecht lakes area. Similar subsurface reflectance spectra for eutrophic water bodies are those of Davies-Colley *et al.* (1988) for New Zealand lakes and Seyhan *et al.* (1974) for ditch water in The Netherlands. Normalised spectra with similar shape to those encountered in this study are given by Gitelson *et al.* (1986) for Lake Balaton in Hungary and by Gitelson & Nikanorov (1988) for the Don and Seversky Donetz Rivers in the former Soviet Union. However, most of these studies did not clarify the spectral absorption and scattering features of these spectra.

The theory presented in § 3.2 is used as a basis for discussing the *in situ* spectroradiometric measurements. In § 4 the relationship of *R(0-)* to the inherent optical properties is discussed. Multitemporal algorithms are developed in § 5 based on the results of § 2, 3 and 4. Application of these algorithms to remote sensing measurements are discussed in § 6.

This chapter presents the pertinent theory augmented by results from measurements both from this research and from the literature. Appendix A contains the supporting theory and the technical and practical aspects of field-based spectroradiometric measurements of radiance and irradiance.

3.2 Theory

The waters for which a theoretical model is discussed are presumed to be optically infinitely deep, i.e. the influence of bottom reflectance has been ignored.

The radiance as measured by a remote sensor in the direction of view (θ,φ), with θ the zenith or look angle and φ the azimuth angle, is defined by

$$L_{rs}(\theta,\varphi)_\lambda = T_a(\theta,\varphi)_\lambda L_a(\theta,\varphi))_\lambda + L_p(\theta,\varphi)_\lambda \qquad [3.1a]$$

where T_a is the atmospheric transmittance along the direction (θ,φ), L_p the path radiance scattered by air molecules and dust particles in the direction of view (θ,φ) and L_a the

upwelling radiance just above the water surface in the direction of view (θ,φ). In the following, the spectral dependency of the (ir)radiances and reflectances will no longer be expressed and since all our observations are in nadir view $(\theta,\varphi) = (0,0)$, Eq. 3.1.a becomes:

$$L_{rs} \equiv L_{rs}(0,0) = T_{az}\, L_{az} + L_{pz} \qquad [3.1b]$$

The suffix z implies a nadir view direction from the target. In the case of observations made at low altitude where the influence of the atmosphere may be ignored, L_{rs} would be equal to L_{az}.

A reflectance parameter that is frequently used in remote sensing studies is apparent reflectance (R_{az}), which is equal to the bi-directional reflectance factor of a target (BRF: Milton, 1987). R_{az} is defined as the radiant flux reflected in a solid angle divided by the radiant flux reflected by a perfectly reflecting Lambertian panel at the same finite solid angle under identical irradiance conditions (Austin, 1974). For radiant flux reflected in nadir view the apparent reflectance can be defined by

$$R_{az} = L_{az} / L_o \qquad [3.2]$$

where L_o is the radiance reflected from a perfectly diffuse reflecting Lambertian panel:

$$L_o \equiv E_{ad} / \pi \qquad [3.3]$$

with E_{ad} the downwelling irradiance in air. L_o (or E_{ad}) is estimated by measuring the radiance reflected from a diffuse reflecting reference panel or by using a cosine-corrected hemispherical diffuser which measures irradiance.

The downwelling irradiance at the water surface E_{ad} consists of a direct sun light or solar beam component E_{sun}, and a diffuse sky light component E_{dif}:

$$E_{ad} = E_{sun} + E_{dif} \qquad [3.4]$$

The fraction of diffuse to total downwelling irradiance F can then be defined as:

$$F = E_{dif} / E_{ad} \qquad [3.5]$$

F increases as the wavelength decreases and as the sky becomes more hazy (Robinson & Biehl, 1979; Kimes & Kirchner, 1982; Baker & Smith, 1990; also see Appendix A). An increase in F with decreasing sun elevation is also described by Baker & Smith (1990).

To derive information about the water constituents we must consider L_{az} as a sum:

$$L_{az} = L_u + L_{ar} \qquad [3.6]$$

where L_u is the radiance transmitted upward from beneath the water surface, referred to as the water leaving radiance, and L_{ar} the upwelling radiance that has not penetrated the water surface, also known as Fresnel or surface reflected radiance (L_{ar} is described in § 3.3.4). L_u contains the information on optical water quality parameters and is defined by:

$$L_u = L_{az} - L_{ar} \qquad [3.7]$$

Taking into account transmittance of light across the water/air interface ($1-r^0$) and the effect of the radiant flux being confined to a wider solid angle as it passes the water/air interface ($1 / n^2$), knowing L_u leads to the subsurface upwelling radiance L_{wu}:

$$L_{wu} = (n^2 / (1-r^0))L_u = (1 / 0.544)L_u = 1.84\ L_u \qquad [3.8a]$$

for ocean waters (Austin, 1980; Carder & Cleveland 1985) and

$$L_{wu} = (n^2 / (1-r^0))L_u = (1 / 0.551)L_u = 1.82\ L_u \qquad [3.8b]$$

for fresh waters; where n is the index of refraction (n = 1.341 for ocean waters and 1.333 for freshwaters) and r^0 is the Fresnel coefficient for 0° angle of incidence (r^0 = 0.021).

Since most underwater light climate models are based on irradiances or ratios of irradiance (i.e. irradiance reflectances), it is necessary to derive the upwelling irradiance E_{wu} from L_{wu}. The assumption is often made that the upwelling radiance, below and above the water surface, is completely diffuse and unpolarized; that is, the water body is a Lambertian reflector and thus E_{wu} is equal to $\pi\ L_{wu}$. In fact, the radiance distribution is not Lambertian (Kirk, 1983). Measurements in Lake Pend Oreille at a solar altitude of 57° showed that E_{wu} was equal to 5.08 L_{wu} near the surface in this water body (Tyler, 1960) where Q is the angular distribution factor of spectral radiance:

$$E_{wu} = Q\ L_{wu} \qquad [3.9]$$

Bukata *et al.* (1988) carried out Monte Carlo simulations to estimate values of Q. Inherent optical properties of Great Lakes waters were assumed in their calculations. For backscattering probabilities (b_b:b) of 0.013 to 0.044 they found a Q value of 3.79 at a solar zenith angle of 36.5°. With increasing solar zenith angles Q increased to 4 (b_b:b = 0.044) or 4.18 (b_b:b = 0.013) at θ = 45° and to 4.21 (b_b:b = 0.044) or 4.80 (b_b:b = 0.013) at θ = 60°. Monte Carlo modelling calculations by Kirk (1983) gave values of E_{wu} / L_{wu}, just below the surface, of about 4.9 for waters with b / a values in the range 1.0 to 5.0, at a solar altitude of 45°. For intermediate solar altitudes Kirk concluded that E_{wu} / $L_{wu} \approx 5$, and that the ratio was not likely to vary greatly at other solar altitudes. There is thus some contradiction in the results from Kirk (1983) and Bukata *et al.* (1988), as to whether or not there is a solar elevation angle dependency of E_{wu} on L_{wu}. Further information is required in order to compare these results; neither author

presents complete information on all input parameters, initial boundary conditions or Monte Carlo simulation computer code.

According to theoretical prediction (Gordon & Morel, 1983), Q is also dependent to some extent on wavelength λ. Wavelength dependency should therefore be taken into consideration. For example, if radiance ratios or $L_{wu}(\lambda_1) / L_{wu}(\lambda_2)$ are used for the two wavelengths λ_1 and λ_2, the spectral change in Q should be taken into account. For the purposes of this study the spectral dependence has not been considered due to the lack of experimental data. However, the influence of this quantity on the algorithms discussed below was considered to be small.

From a knowledge of E_{wu} it is possible to derive the inherent irradiance reflectance $R(0)$ as defined by Jerlov (1968):

$$R(0) = E_{wu} / E_{ad} \qquad [3.10]$$

Studies of the underwater light climate are concerned with the behaviour of light under the water surface. In these studies the subsurface irradiance reflectance $R(0-)$:

$$R(0-) = E_{wu} / E_{wd} \qquad [3.11]$$

plays an important role. To derive $R(0-)$ from $R(0)$, E_{ad} must be replaced by E_{wd} in Eq. 3.10:

$$R(0-) = (E_{ad} / E_{wd})\, R(0) \qquad [3.12]$$

The main part of E_{wd} is the fraction of E_{ad} that has penetrated the water:

$$(1-\rho)E_{ad} = (1-\rho_{sun})E_{sun} + (1-\rho_{dif})E_{dif} \qquad [3.13]$$

where ρ is the global surface irradiance reflectance at the air/water interface (the term ρ is reserved for those reflectances that relate to the interface solely; i.e. there is no contribution by reflectance from substances in the water column), as defined by Baker & Smith (1990). ρ_{sun} is the reflectance of the direct solar beam and ρ_{dif} is the reflectance of the skylight against the air/water interface.

With Eq. 3.5

$$F = E_{dif} / E_{ad} \quad \text{and} \quad (1-F) = E_{sun} / E_{ad}$$

Eq. 3.13 can be written as

$$(1-\rho)E_{ad} = (1-\rho_{sun})(1-F)E_{ad} + (1-\rho_{dif})F\, E_{ad} \qquad [3.14]$$

Since ρ_{sun} is the reflectance of a direct beam for a perfectly smooth water surface it is equal to the Fresnel coefficient (Jerlov, 1968). According to Austin (1974) this reflectance, is little affected by roughening of the surface up to wind speeds of 10 m s^{-1}, for angles of incidence smaller than 70°. Assuming a uniform radiance distribution due to the sky, the reflectance of skylight ρ_{dif} for a smooth water surface was found to be 6.6% (Preisendorfer, 1976; Baker & Smith, 1990). For reflectance in the case of a cardiodal distribution of sky radiation, assumed for completely overcast skies, Preisendorfer (1957: in Jerlov, 1968) has given 5.2%.

The other contribution to E_{wd} is $\rho_w E_{wu}$, where ρ_w is the downward reflectance of the diffuse upwelling irradiance against the water/air interface. ρ_w varies from 0.485 to 0.463 as wind speed increases from 0 to 16 m s^{-1} (Austin, 1974). With average windspeeds between 3 to 4 m s^{-1} for this study ρ_w was assumed equal to 0.48. This is the same value for ρ_w found by Jerlov (1968) (however, he assumed the upwelling radiance distribution to be isotropic. This in contradiction with the fact that the factor Q, described above, is not equal to π, thus the assumption of isotropy by Jerlov is not correct).

Combining the two contributions to E_{wd}, E_{wd} can be determined for both clear and hazy skies through:

$$E_{wd} = (1-\rho)E_{ad} + \rho_w E_{wu} \qquad [3.15a]$$

$$E_{wd} = (1-\rho_{sun})(1-F)E_{ad} + (1-\rho_{dif})FE_{ad} + \rho_w E_{wu} \qquad [3.15b]$$

Eqs. 3.11 and 3.15.b lead to

$$R(0-) = E_{wu} / E_{wd}$$

$$= E_{wu} / \{(1-\rho_{sun})(1-F)E_{ad} + (1-\rho_{dif})FE_{ad} + \rho_w E_{wu}\} \qquad [3.16]$$

$$= R(0) / \{(1-\rho_{sun})(1-F) + (1-\rho_{dif})F + \rho_w R(0)\} \qquad [3.17]$$

Equation 3.17 can be used to deduce the subsurface irradiance reflectance $R(0-)$ from $R(0)$ if the ratio of diffuse irradiance to total irradiance, F, is known and with ρ_{dif} estimated as 0.066. In the case of a completely overcast sky, $F = 1$, ρ_{dif} is estimated to be 0.052 and Eq. 3.17 reduces to:

$$R(0-) = R(0) / \{1-\rho_{dif} + \rho_w R(0)\} \qquad [3.18]$$

3.3 Spectroradiometric measurements of radiance and irradiance

3.3.1 *Introduction*

During the remote sensing flights with the CAESAR instrument on 3 September 1990 and the CASI instrument on 14 September 1990, simultaneous spectroradiometric measurements of *in situ* upwelling and downwelling radiance were carried out. However, because of the number of water bodies included in the study in the 1990 programme all imaged waters were measured over the period 28 August - 14 September. For example, measurements also had to be made on days before and after the remote sensing flights. In conjunction with the spectroradiometric measurements, water samples were taken and other *in situ* limnological measurements were carried out. The link between remotely sensed upwelling radiance and underwater inherent optical properties is thus made through the spectroradiometric measurements. It is not necessary, therefore, that sampling and laboratory analyses are made simultaneously with the remote sensing data acquisition, as long as the water quality parameters within a water body do not vary markedly between the two sets of measurements.

Field-based spectroradiometric measurements are necessary in remote sensing studies for three reasons. Firstly, spectroradiometric measurements are required for determining $R(0-)$ from the L_{rs} measurement. Secondly, spectroradiometric measurements are essential for determining the atmospheric effect between the airborne sensor and the ground. Although atmospheric interference may be removed through a "removal of atmospheric influence" model, actual field-based spectroradiometric measurements were preferred for this study, because the amount of data to be corrected would have required an atmospheric correction model for high spectral resolution directly implementable in the available data analysis environment. Such a model was not available. Thirdly, spectroradiometric measurements may be used to predict the potential performance of existing or planned remote sensing instruments. Such measurements may be used to determine optimal bandwidths and spectral and radiometric resolution. In this manner spectroradiometric measurements can be a cost-effective way of determining the relevance of application of a remote sensor for a specific task, as illustrated by Dekker *et al.* (1990, 1991, 1992 b-d) and Dekker and Peters (1993).

3.3.2 *The measuring equipment*

In order to correctly interpret the data presented, a technical description of the spectroradiometers used in this study, and their limitations, is presented in Appendix B.

The Spectron SE590 portable spectroradiometer was used in the 1990 remote sensing campaign. This is a portable spectroradiometer which measures a target spectrum with a slit band width (half-power) of 8 nm every 2.8 nm over the wavelength range of 400 - 1100 nm.

In this study the wavelength range 400-850 nm was used. Two sensorheads may be fitted to the instrument: for this study one sensorhead was fitted with a 15° field of view (FOV) aperture and the other with a cosine corrected hemispherical diffuser. To facilitate subsurface upwelling radiance measurements, the 15° FOV aperture was fitted with a 50 cm long and 4 cm diameter perspex tube, coated on the outside with black tape. The sensor heads were attached to a two metre boom, thus enabling upwelling radiance measurements to be made away from the boat to prevent erroneous radiance effects on the measured signal.

Because measurements of the fraction of diffuse to downwelling irradiance were not performed in 1990, spectroradiometric measurements of downwelling irradiance from the 1992 remote sensing campaign were analysed and are included in this study.

A PSII portable spectroradiometer was used in 1992. This measures the target spectrum with a minimal slit bandwidth (half-power) of 1 nm every 1.4 nm over the wavelength range of 360 - 1100 nm. In the 1992 study only the wavelength range 400-850 nm was used. The optical fibre sensor may be fitted with a range of apertures from 1° to 18° FOV. For measuring upwelling radiance from low reflecting targets such as natural waters, the 18° FOV is used due to the relatively low radiometric sensitivity of the instrument. A two meter long boom similar to that available for the Spectron was used.

In the 1990 campaign a polytetrafluorethylene (PTFE), also known as halon, panel was used. Halon is not a perfect Lambertian reflector. However the panel is sturdy, hydrophobic and easy to clean, and therefore very suitable for field-based research. In the 1992 campaign a LabSphere 50% diffuse reflecting Spectralon panel was used for measurements of the downwelling irradiance.

The calibration, radiative transfer theory and estimates of the inherent error made in assuming a panel to be a perfect Lambert diffuser is given in Appendix A.

3.3.3 *Spectroradiometric measurements of downwelling irradiance*

3.3.3.1 *Introduction*

Two methods for measuring downwelling irradiance were carried out. The first method used a (imperfect Lambertian) reference panel for diffusely reflecting irradiance, measured by the 15 FOV aperture; the second method used a cosine corrected hemispherical diffuser attached to the spectroradiometer. Downwelling irradiance, E_{ad}, has a diffuse and a direct component. The measurement of these components is not only pertinent to the derivation of *R(0-)* from the remotely sensed signal but also to assessment of the inherent error made through assuming the reference panel to be an ideal Lambertian reflector.

During the 1990 measurements no estimates of the diffuse component of downwelling irradiance were made; they were made in the 1992 campaign. Estimates of diffuse radiation for the 1990 data were derived from the 1992 data.

3.3.3.2 *Definitions*

The directional reflectance of a target depends on both the irradiating flux and the direction along which the reflected flux is detected. Ignoring skylight, energy from the sun and the energy reflected to a sensor can be thought of as being confined to two slender elongated cones, each subtending a small angle at the target surface, termed solid angles and measured in steradians (*sr*). If these solid angles are sufficiently small, the reflectance of the target can be defined as the 'bi-directional reflectance distribution function' or BRDF (Milton, 1987). To specify the reflectance field at the target completely, reflectance must be measured at all possible source/sensor positions resulting in the BRDF. However, this is frequently not feasible in the field environment and an alternative to the BRDF must be found (Milton, 1987). The assumption of an absence of skylight is also erroneous; *in situ* the target surface is irradiated with a combination of near-specular (direct solar) and hemispherical (atmospherically and cloud scattered) radiant flux.

Two alternatives to the BRDF exist (Milton, 1987). The first is measurement of the bi-directional reflectance factor BRF by using a reference panel; the second is to monitor the irradiation directly using an upward looking spectral sensor with a cosine corrected hemispherical diffuser receptor. Both of these alternative measurements were applied during the 1990 measurement campaign.

The BRF is defined as the radiant flux reflected into a solid angle divided by the radiant flux reflected by a perfectly reflecting Lambertian panel into the same finite solid angle under identical irradiance conditions. Because a Lambertian panel is specified to be perfectly diffuse and completely reflecting, then E_{ad} is equal to $\pi\ L_o$ (Eq.3.3) by definition. The "bi-directional reflectance factor" of the water R_{az} is defined as:

$$R_{az} = L_{az}(\theta_r,\varphi_r) \,/\, L_o \qquad [3.19]$$

where the subscript r denotes the reflected radiance. In practice, true Lambertian panels do not exist and a correction R_p, defined as the ratio of the radiance reflected by the panel to the radiance reflected by an ideal Lambertian reference panel, has to be made:

$$R_{az} = \{L_a(\theta_r,\varphi_r) \,/\, L_p(\theta_r,\varphi_r)\}\ R_p \qquad [3.20]$$

where R_p (the bi-directional reflectance factor of the reference panel) is

$$R_p = L_p(\theta_r,\varphi_r) \,/\, L_o \qquad [3.21]$$

The reference panel should be calibrated under the same irradiance conditions as existed during the measurements with the panel in the field (Jackson *et al.* 1987). However, this is complex and was not performed in this study. Instead with the assumption of the absence of sky light, we get the bi-directional reflectance factor (BRF) as defined by Milton (1987):

$$R_{az}(\theta_i,\varphi_i;\theta_r,\varphi_r) = \{L_a(\theta_r,\varphi_r) / L_p(\theta_r,\varphi_r)\}\ R_p(\theta_i,\varphi_i;\theta_r,\varphi_r) \qquad [3.22]$$

with (θ_i,φ_i) the angle of incidence of the solar beam. The assumed irradiance conditions can be simulated in the laboratory to determine $R_p(\theta_i,\varphi_i,\theta_r,\varphi_r)$.

$R_{az}(\theta_i,\varphi_i;\theta_r,\varphi_r)$ is sometimes called the "bi-conical reflectance factor" (Kimes & Kirchner, 1982) because the energy from the source and the energy reflected to the sensor can be thought of as being confined to two slender elongated cones.

For practical purposes $R_{az}(\theta_i,\varphi_i;\theta_r,\varphi_r)$ can, for an azimuthal uniform surface and a view direction of $0°$, be defined as $R_a(\theta,0°)$.

In the case of irradiance measurement using a cosine corrected hemispherical diffuser, which is assumed to measure downwelling irradiance perfectly, Eq. 3.2 becomes:

$$R_{az} = \pi\ L_{az}(\theta_r,\varphi_r) / E_{ad} \qquad [3.23]$$

In practice a cosine corrected hemispherical diffuser (CCHD) will not measure total downwelling irradiance perfectly and a correction factor E_{CCHD} must be applied. Therefore equation 3.24 becomes:

$$R_{az} = \pi\ \{L_{az}(\theta_r,\varphi_r) / E_{ad}\}\ \{1 / E_{CCHD}\} \qquad [3.24]$$

3.3.3.3 *Results*

The diffusely reflected downwelling irradiance from the PTFE reference panel was measured using the 15° FOV apertured Spectron sensor head. This is equivalent to L_o corrected for the panel deviation from a perfectly diffuse Lambertian panel. Fig. 3.1.a shows the 37 L_o spectra measured during the 1990 campaign on 5 different days and under varying overhead conditions (overcast to clear sky). Fig. 3.1.b presents the same data as Fig. 3.1.a. but the data is normalised at 550 nm (middle of the *PAR* range). With normalisation the spectral differences between varying solar elevation and sky conditions are enhanced. No systematic spectral variation with overhead irradiance conditions was found. However, several spectral features were prominent in the spectra and are caused by the shape of the extraterrestrial solar irradiance spectrum and atmospheric absorption by ozone, water vapour and oxygen.

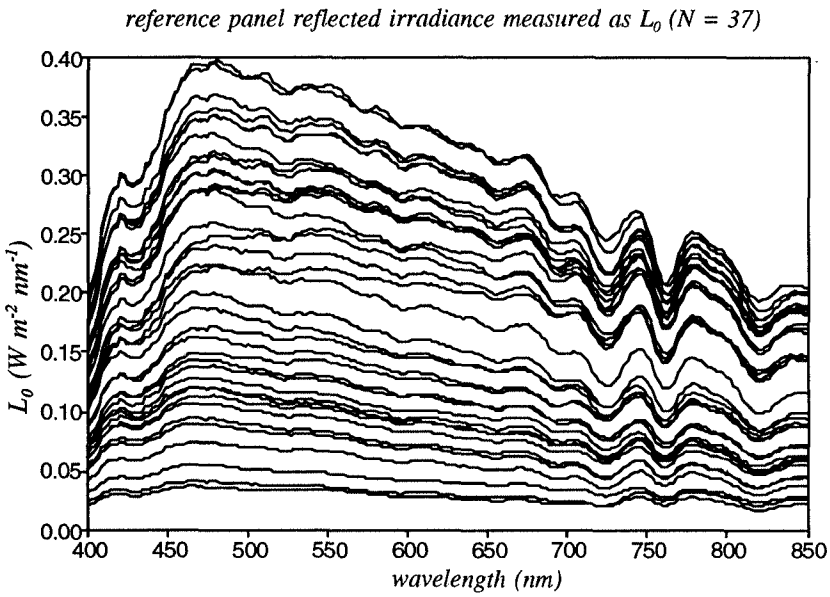

Figure 3.1.a *L_o: the irradiance reflected from the PTFE reference panel during 37 measurements in 1990 under widely varying circumstances (overcast to clear blue sky) on five days. The lowest spectra were measured under completely overcast conditions; the highest values under clear sky conditions at maximum local zenith angle of 42°.*

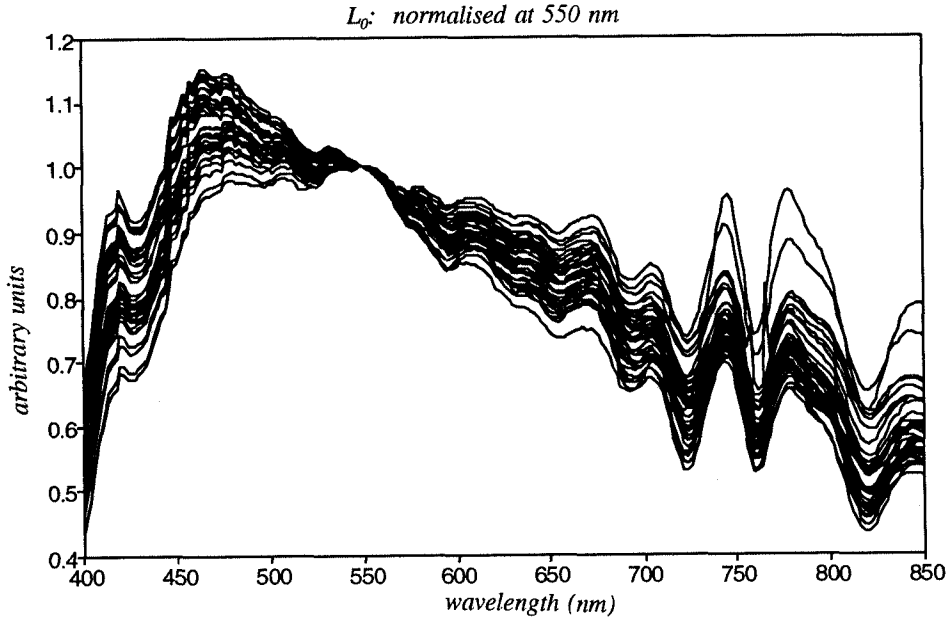

Figure 3.1.b *The same data as in Fig. 3.1.a, normalised at 550 nm (middle of the PAR range). The spectral differences between varying solar elevation and sky conditions are enhanced.*

These features include:

- Irradiance is low at 400 nm: being approximately 50 % of the irradiance at 480 nm which is the peak value for the clear sky measurements. The 400 to 480 nm range has marked peaks and troughs.
  From 480 to 600 nm a relatively featureless gradual decrease in irradiance is found, more profound for clear than for hazy skies.
  Marked spectral features occur form 600 to 850 nm which are attributable to absorption by water vapour and oxygen. The oxygen absorption peak at approximately 760 nm is a constant feature useful for verifying first order calibration of spectral measuring devices.

Within the wavelength ranges defined above, shoulders and troughs occur in the irradiation. Some of these features occur near the wavelength ranges where light harvesting pigments occur; for example, at 632 and 694 nm near to absorption by CP-cyanin at 624 nm and chlorophyll *a* at 676 nm respectively, and at wavelengths where reflectance in inland waters is often high, due to a minimum in absorption (at 706 nm). Absolute variations in intensity and spectral variations caused by changing overhead conditions suggest that an analysis of the upwelling radiance, which is a function of downwelling irradiance, will be strongly influenced by spectral and radiometric variations in irradiance conditions. For this reason the results of remote sensing research making use of upwelling radiance (e.g. Dekker *et al.* 1990, 1992b-d and Dekker & Peters, 1993) will have little multi-temporal validity, as previously suggested by Dekker *et al.* (1992a). Multitemporally valid algorithms may only be defined on the basis of reflectance data, preferably recalculated to subsurface irradiance reflectance. The resultant *R(0-)* data is maximally independent of irradiance, atmospheric path radiance and surface reflectance effects.

The spectra displayed in Fig. 3.1.a & b consist of a direct (solar beam) and a diffuse (skylight) component as described in Eqs. 3.4 and 3.5. In 1990 these components were not measured separately. During the 1992 campaign measurements were made to determine the diffuse component of the downwelling irradiance.

An estimation of the fraction of diffuse downwelling irradiance (F) is necessary when the surface reflected Fresnel radiance L_{ar} needs to be estimated, in order to determine L_u from L_{az} or L_{rs} measurements (Eq. 3.7.). If L_{wu} measurements are available, knowledge of the fraction of diffuse to total downwelling irradiance is less important.

During the 1992 campaign F was estimated by measuring the diffuse downwelling radiance L_{dif} using the PS11 spectroradiometer. Often the diffuse skylight component is measured by blocking out the direct solar disk irradiance with a shield (Epema, 1992); for water-based measurements this method is not feasible due to boat motions.

For *in situ* spectroradiometric measurements using a boat as measuring platform, the sun zenith and azimuth angle may be used as a fixed reference point. By measuring L_{dif} at fixed angles to the sun, boat motions are compensated. L_{dif} was estimated by pointing

the 18° FOV aperture at the sky at a 90° angle to the direct solar beam in the sun-zenith plane (= 180° azimuth). By holding the aperture at 90° to the sun elevation angle no internal reflection of direct solar radiance within the aperture could occur. F is approximated, under the assumption of a completely isotropic radiance distribution of sky light, by L_{dif} divided by the reflected radiance from a diffuse reflecting reference panel (in this case the 50% reflecting LabSphere panel).

Usually, however, sky light under clear sky conditions is not completely diffuse and its angular distribution is primarily affected by solar zenith and azimuth angle and by atmospheric scattering. For the sun-zenith plane the observed radiance at 90° to the direct solar beam (at a solar zenith angle of 45°) is not the minimum radiance; the direction where the minimum is measured is more towards zenith (Kondratyev, 1969).

De Haan (1987) calculated the diffuse radiance distribution in a moderately turbid atmosphere (at λ = 550 nm) for a solar elevation of 45° for four different aerosol types: small water-soluble, large dustlike, soot and of oceanic origin. Table 3.1 tabulates the effects of the aerosols. Depending on the atmospheric conditions and aerosol composition prevailing at the time of the irradiance measurement, L_{dif} measured at a 90° angle to the sun-zenith plane will have to be multiplied by the appropriate aerosol factors (up to 1.96 according to the values in Table 3.1) to arrive at a correct estimation of L_{dif} at zenith.

Table 3.1 *The ratio of L_{dif} at 90° to the sun in the sun-zenith plane and L_{dif} at zenith for a moderately turbid atmosphere, for a solar elevation of 45° (based on data from de Haan, 1987).*

aerosol type	ratio of L_{dif} at 90° to sun and L_{dif} at zenith for a solar elevation of 45°
small water-soluble	1.96
large dustlike	1.56
soot	1.40
oceanic origin	1.96

According to Baret & Andrieu (pers.comm.) more than 50% of the diffuse radiation is located very close to the sun position. With a hazy sky, the sky radiance is more concentrated around the solar disk and does not increase towards the horizons as it does for a clear sky. The zenith values for diffuse downwelling irradiance are thus more relevant than the 90° for the direct solar beam measurements, because the reflectance measurement over the panel and over the water all take place at nadir angles where diffuse irradiance input would be greater.

Table 3.2 *The diffuse fraction of irradiance, F, measured using the PSII spectrometer in 1992 by pointing the 18° FOV aperture at the sky at a 90° angle to the direct solar beam in the sun-zenith plane and at 180° from the sun azimuth (see also Fig. 3.2 and Table A.2)*

	N	*F* λ=400 nm	*F* λ=850 nm
measurement conditions			
clear sky	5	0.30	0.07
clear to hazy sky	2	0.46	0.10
hazy sky	4	0.63	0.23
all measurements	11	0.45	0.13

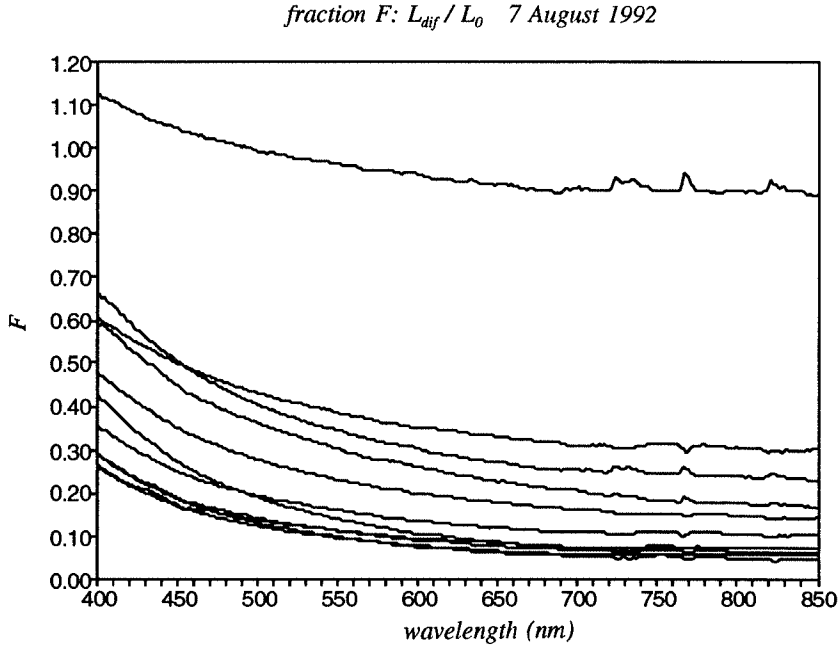

Figure 3.2 *Spectra of the E_{dif} : E_{ad} ratio or F ratio on 7 August 1992. The lowest values are representative of the clearest skies encountered at this geographical location; as the values of F increase, the haziness increases until the sky is completely overcast and F should be equal to 1. (See Tables 3.2 and A.2).*

Therefore, if L_{wu} measurements cannot be made and clear sky conditions exist, an approximation of the L_{dif} at zenith can be made by multiplying the L_{dif} measured at 90° angle to the sun in the sun-zenith plane (at a sun zenith angle of 45°) by the appropriate factor calculated from Table 3.1. It is recommended that zenith L_{dif} is measured as well, although an error will be caused in the case of direct sunlight reflecting inside the aperture opening. Therefore the inside coating of the aperture will have to be black and non-specularly reflecting.

The spectroradiometric measurements made on 7 August 1992 were initially made under conditions approximating the clearest skies encountered at this geographical location. After a few hours the sky conditions became more hazy until the sky was completely overcast. Table 3.2 presents F values for 400 nm and 850 nm for clear, clear-to-hazy and hazy skies as well as the average over these three categories. The average values are close to those of F for the clear-to-hazy skies and are approximately 50% higher than values for the clearest skies. The spectra of F are displayed in Figure 3.2 and show an increase in F (defined as L_{dif} / L_o, at 90° angle to the sun-zenith plane; i.e. a close-to-minimum value) as the sky conditions deteriorated from clear blue to completely overcast. Also evident in Figure 3.2 is an exponential increase of F with decreasing wavelength. As the sky conditions deteriorated the fraction of diffuse irradiance increased strongly, by a factor of 2 at short wavelength to a factor of 3 at longer wavelengths. Between 450 and 500 nm crossovers in the spectra occur, indicating changes in spectral shape of the diffuse downwelling radiance to total radiance ratio. The single measurement made under completely overcast conditions showed values greater than 1 for wavelengths below 500 nm and less than 1 for higher wavelengths. For a highly reflecting surface a ratio of 1 for L_{dif} / L_o might be expected under completely overcast conditions; this deviation may be caused by the non-Lambertian properties of the reference panel used or by the sky radiance distribution being non-isotropic.

Increases in F with decreasing wavelength and with increasing haze levels are in accordance with the findings of Robinson & Biehl (1979), Kimes & Kirchner (1982) and Baker & Smith (1990). On the basis of these results it is recommended that F be estimated from measurements made at the time of remote sensing since F is apparently variable at short time scales. A dependence of the fraction of diffuse irradiance on solar elevation angle as was reported by Baker & Smith (1990), could not be shown from the measurements of this study, possibly due to the changes in atmospheric condition being stronger than those due to solar elevation angle. Because the values of F in Figure 3.2 are close-to-minimum values, these should be multiplied by a factor according to the atmospheric conditions and aerosol types and concentrations (Table 3.1) when used in calculations such as Eqs. 3.14 to 3.17. In this way the best approximation of the zenith downwelling radiance (which is by definition diffuse in case of the sun not being in zenith) to total downwelling radiance is calculated. The average values of F for clear to hazy skies measured in August 1992 were used in calculations involving the remote sensing measurements of 1990 outlined in Chapter 6. The remote sensing data in 1990 were obtained under clear to slightly hazy sky conditions. No information on aerosol type and concentrations, or on total atmospheric turbidity, was available.

By using the average values for F for clear to hazy skies a best estimate based on the available information was made. Moreover, as will be discussed in § 3.3.5.1, F may be relatively inaccurate provided subsurface upwelling radiance measurements (L_{wu}) are available. In the absence of L_{wu} measurements, however, F needs to be known accurately.

3.3.4 *Spectroradiometric measurements of upwelling radiance*

Upwelling radiance above the water surface, L_{az}, is the sum of radiance transmitted upward from beneath the water surface and upwelling radiance that has not penetrated the water surface (i.e. the Fresnel, or surface reflected radiance). The radiance that contains information about water constituents is the upwelling radiance (Eq. 3.7): $L_u = L_{az} - L_{ar}$. Taking into account transmittance through the water/air interface and the effect of the flux being confined to a wider solid angle as it passes the interface, then knowing L_u leads to knowing the subsurface upwelling radiance (Eq.3.8.a): $L_{wu} = 1.84\ L_u$ for ocean water and $L_{wu} = 1.82\ L_u$ for fresh water. The surface reflected radiance may be defined as:

$$L_{ar} = r^{\rho}\ L_{dif} + r^{\theta}\ L_{sun} \qquad [3.25]$$

However, L_{ar} will be calculated from measurements by:

$$L_{ar} = r^{\rho}\ F\ L_o + r^{\theta}(1\text{-}F)L_o \qquad [3.26]$$

where $r^{\rho}\ L_{dif}$ and $r^{\rho}\ F\ L_o$ denote the reflected skylight component and $r^{\theta}\ L_{sun}$ and $r^{\theta}(1\text{-}F)L_o$ denote the specularly reflected direct sunlight component. r^{θ} is dependent on the solar angle of incidence, θ, and the state of the water surface. The reflectance of skylight can be estimated by the Fresnel coefficient for normal incidence r^{ρ} (2.1%) since it only slightly increases with increasing angle of incidence. For observation angles greater than 30° to 40° from the solar specular point, measurements obtained when wind speeds are less than 10 m s^{-1} are not significantly affected by the surface reflected sky light (Austin, 1974). The wind speed is not supposed to influence this reflectance for nadir view. In practice, however, with a 15° FOV aperture, given the relatively long integration times required for upwelling radiance measurements and given that measurements are typically made from unstable platforms, such as boats, a significant contribution attributed to the specularly reflected direct solar radiance is measured.

Although equation 3.8.b is essential for deriving L_{wu} from the remotely sensed upwelling radiance L_{rs}, a more reliable method is the measurement of *in situ* L_{wu} directly, achieved by lowering the aperture of the spectroradiometer into the water. Measurements of L_{wu} made with the Spectron instrument in 1990 were obtained using a perspex extension (§ 3.3.2). The fraction of the radiance transmitted through the tube, $(1\text{-}\alpha)$, was estimated using the reference panel measurements. $(1\text{-}\alpha)$ shows a spectral dependence: 90 % of the radiance is transmitted for wavelengths between 500-700 nm, but less is transmitted for wavelengths < 500 nm and > 700 nm. A local minimum in

transmittance is evident at λ = 730-734 nm. The wavelength independent standard deviation was 6 %. The wavelength averaged transmittance was 87%, which indicates that 13 % of the radiance is lost in the tube.

Figure 3.3 shows 24 L_{wu} measurements collected during the 1990 remote sensing fieldwork. The spectral features caused by the spectral absorption and scattering characteristics for each waterbody are evident and are discussed below with the *R(0-)* spectra calculated using these L_{wu} measurements. As described previously (§ 3.3.3.3) L_{wu} measurements have no multitemporal validity in developing algorithms for remote sensing applications. However, L_{wu} measurements may serve as a calibration for L_{rs} measurements as discussed in § 6.

Making underwater measurements introduces errors associated with the requirement that the sensor (i.e. the perspex tube) must be lowered below the wave amplitude. Consequently, subsurface upwelling radiance measurements are generally made at a depth which is between half the wave height to that which is greater than the highest wave occurring during the measurements. If depth profiles of subsurface upwelling radiance are available a spectral vertical attenuation coefficient may be calculated, which allows correction of the shallow subsurface measurements. This correction procedure was not performed on the 1990 data.

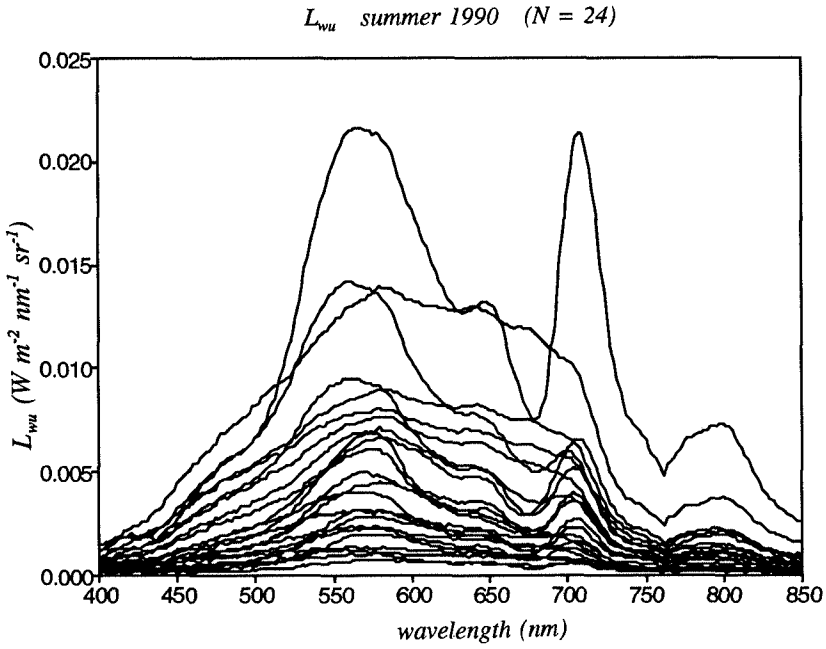

Figure 3.3 *24 L_{wu} measurements collected during the 1990 remote sensing fieldwork.*

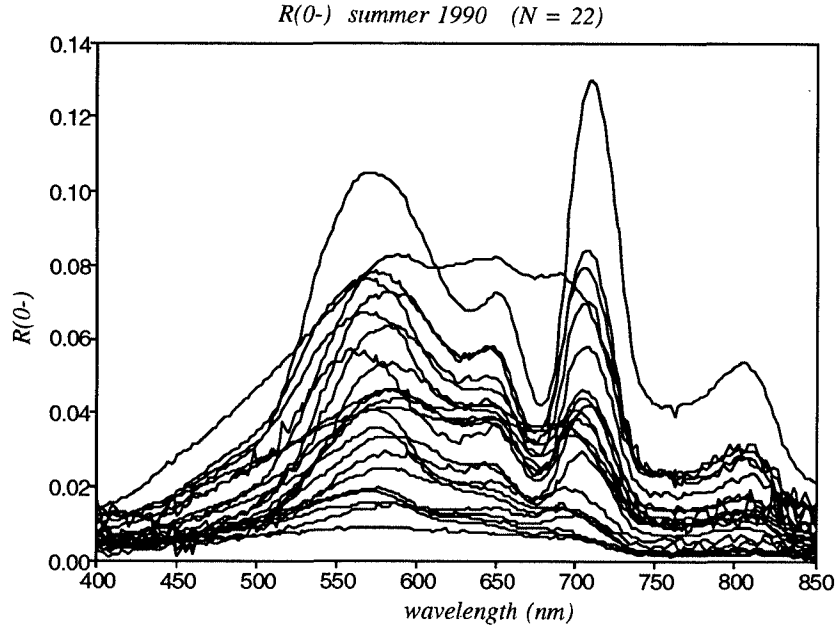

Figure 3.4.a *22 R(0-) spectra for 1990 (same measurements as Fig. 3.3).*

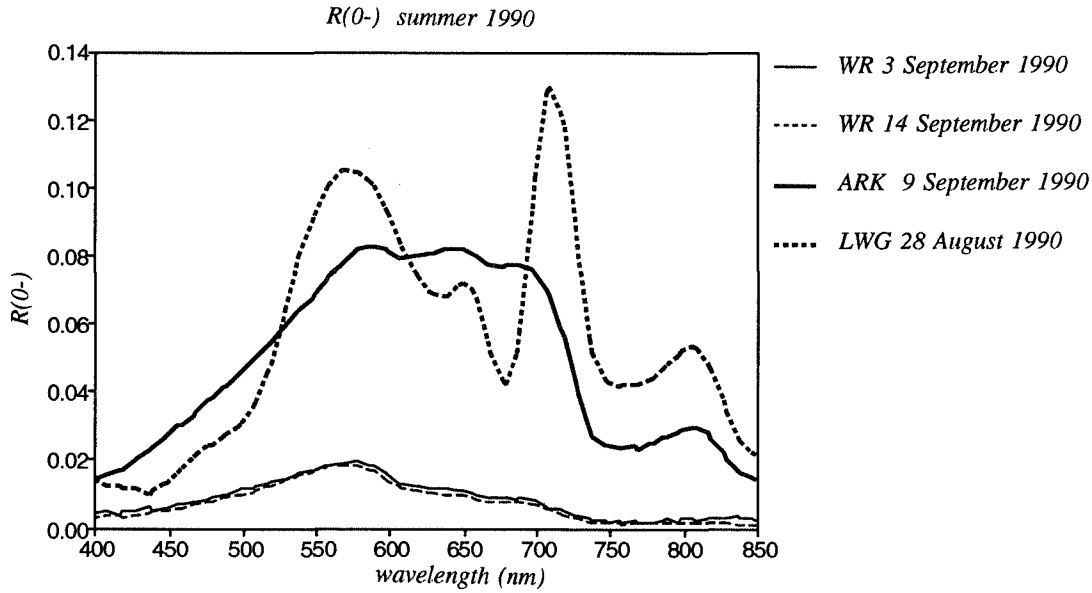

Figure 3.4.b *R(0-) spectra which represent the three major water types to be found in this area: the Water Reservoir (WR), as an example of a clear lake, with low phytoplankton and suspended matter concentrations; the Amsterdam-Rijn Kanaal (ARK), with low phytoplankton, but high suspended matter concentrations; Lake Wijde Gat (LWG), with high phytoplankton and suspended matter concentrations. The aquatic humus levels are high in all waters, with the highest levels found in the shallow eutrophic lakes.*

3.3.5 *Irradiance reflectance calculations*

3.3.5.1 *Introduction*

The most accurate *in situ* measurements for calculating the subsurface irradiance are L_o and L_{wu}. From these measurements E_{ad} and E_{wu} were calculated using Eqs. 3.3 and 3.9. The ratio of E_{wu} and E_{ad} is the inherent subsurface irradiance reflectance *R(0)* as defined by Jerlov (1968). The subsurface irradiance reflectance *R(0-)*, that is generally used in underwater light climate models, was estimated from *R(0)* using Eq. 3.17 for clear and hazy skies and from Eq. 3.18 for overcast conditions.

F ratio values were not available for the 1990 spectroradiometric measurements, which were performed on five different days under varying sunny to hazy weather conditions. For these data the average *F* value for the 1992 measurements of *R(0)* was taken, using the sunny to hazy measurements. This will produce an error in calculation of transmittance across the interface of maximally 1% according to Baker & Smith (1990). Baker & Smith found that for an *F*-ratio change of 50 %, global transmittance across the interface is changed by less than one percent for solar angles less than 70°. It is thus assumed that an estimate of *F* for the 1990 measurements derived from the 1992 measurements provides a relatively accurate estimate of *R(0-)*.

3.3.5.2 *Results*

Fig. 3.4.a shows results of the *R(0-)* calculations for the 1990 data. Roughly the same spectral shapes occur as for the L_{wu} spectra. The difference is that the *R(0-)* data have multitemporal validity because the effects of variations in diffuse radiance (and its reflectance) and in absolute irradiance variations (solar elevation, sky condition etc.) are accounted for.

The results for the *R(0-)* data are discussed according to the results in § 2.5 for the combined absorption and scattering properties in these waters. Figure 3.4.b shows three selected spectra which represent three major water optical types found in this area. The examples chosen were spectra from the Water Reservoir (WR), as an example of a clear lake with low phytoplankton and suspended matter concentrations, the Amsterdam-Rijn Kanaal (ARK) with low phytoplankton but high suspended matter concentrations, and Lake Wijde Gat (LWG) with both high phytoplankton and suspended matter concentrations. The aquatic humus concentrations were high in all waters, with the highest levels found in the shallow eutrophic lakes.

At wavelengths between 400 and 500 nm humus, tripton and the blue chlorophyll *a* absorption peak cause high light absorption. This is the reason for the low reflectance observed in this spectral area. Beyond 500 nm the spectral information becomes less

ambiguous with the reflectance increasing, allowing a better discrimination of spectral features. The lowest total absorption values occur at 550 to 600 nm, at 650 nm and at 705 nm, causing maxima in reflectance in the LWG spectrum and shoulders in the spectra from the ARK and the WR. The figure also clearly shows that nearby infrared reflectance is still high for LWG and the ARK.

Table 3.3 *An inventarisation and recommendation of possible and desired in situ spectroradiometric measurements for application in remote sensing - valid for field-based spectroradiometers with a capability of only one measurement at a time.*

measurement	***required***	***reason***
Irradiance		
E_{ad}	N	L_o measurements more convenient (same sensor head)
E_{au}	N	Too noisy due to influence of surface reflectance effects
E_{wd}	N	May be calculated from L_{ad} and L_o measurements
E_{wu} with L_{wu}	Y/N	Y = to determine Q more accurately in combination N = once Q is known
Radiance		
L_{ad}		
- 90° to θ, 180° to ϕ zenith	Y	Guaranteed absence of direct sunlight in aperture; gives an almost minimal value of L_{dif}
	Y	Most relevant L_{dif} measurement
L_{az}	Y	For calibration of L_{rs}, only useful if simultaneous with L_{rs} measurements
L_o	Y	Essential as measure of downwelling irradiance, preferably using a diffuse reflecting panel approaching a Lambertian surface at a reflectance of 5 - 10% in the order of magnitude of the water reflectance. This minimizes calibration errors due to varying integration times and non-linearity of radiometric response.
L_{wd}	N	Only required to determine transmission across the air/-water interface measurements; may also be calculated from L_o or L_{dif} zenith measurements.
L_{wu}	Y	The desired radiance signal in remote sensing.

The combined effects of humus, tripton and algal pigment absorption at wavelengths smaller than 500 nm, and the increased scattering towards shorter wavelengths make this spectral region inappropriate for extracting information from the resultant low reflectance (Dekker *et al.* 1990, 1991, 1992 b-d). It is between 500 and 720 nm that the contribution to absorption of algal pigments can be most easily discriminated. At 550 nm the spectra of algal rich waters have a minimum absorption causing a reflectance peak; at 628 nm a slight absorption peak due to CP-cyanin is visible as a relative reflectance low; at 648 nm another local minimum in absorption is visible, causing a local reflectance peak; at 676 nm the red chlorophyll *a* absorption peak is evident as the most prominent low in *R(0-)*. The highest *R(0-)* beyond the peak at 550 nm lies at 700 - 710 nm. This peak is caused by the lowest absorption over the entire spectrum found at 700 - 710 nm. It is also evident from the total absorption spectra that beyond 720 nm absorption of light by water is dominant, contributing to low reflectance. These results support earlier research results that information extraction from inland waters should take place in the spectral green to nearby infrared areas (Gitelson & Kondratyev, 1991a & b; Dekker *et al.* 1990, 1991, 1992b-d). This is in contrast to passive optical remote sensing of oceans where the blue to green spectral area is considered the most appropriate for water quality feature information extraction.

3.3.6 *Conclusions and recommendations*

The results of the theoretical survey and data analysis indicate that there exists a minimum set of *in situ* spectroradiometric measurements which provide sufficient data to enable:

a) accurate modelling, calibration of remotely sensed data;
b) testing and development of algorithms for the determination of water quality parameters from reflectance measurements obtained at altitude.

Table 3.3 presents and discusses the possible measurements available if one or two sensor heads are connected to a spectroradiometer; the usual configuration on most available portable spectroradiometric equipment. Simultaneous measurement of both E_{ad} and L_{wu} with one sensor head would be ideal. From an operational point of view an optimal spectroradiometric program should measure the minimum required parameters as accurately as possible. From Table 3.3 it is clear that irradiance measurements are not essential to remote sensing, except for verification and model parameterisation. However, radiance measurements are vital, for the remote sensing instrument measures the radiance at nadir.

The results indicate that *R(0-)* is the single most important parameter necessary for the multitemporal validity of algorithms for determining water quality parameters using passive optical remote sensing techniques. In general, all *in situ* spectroradiometric and remotely sensed data should be calculated to *R(0-)*.

The value of Q, the angular distribution factor for conversion of subsurface upwelling radiance to subsurface upwelling irradiance, requires further study. Especially for water bodies high in concentrations of phytoplankton and tripton as encountered in the study area. Published values of Q may not be appropriate for waters such as these. The spectral dependency of Q should also be investigated. The anisotropy of the underwater upwelling irradiance field also influences the calculated diffuse reflectance ρ_w value, assumed to be 0.48. This ρ_w factor needs to be measured or calculated for turbid inland waters as well.

Both spectroradiometers used in this research showed large spectral calibration shifts between the calibrations supplied by the instrument manufacturers and the measurements made at the time of remote sensing measurement campaigns. This suggests that frequent and accurate radiometric and spectral calibration of spectroradiometers to be used in the field is essential. Factory-based calibrations are frequently no longer applicable at the time of actual field measurements. In addition, spectroradiometric measurements made over low reflectance targets such as water, require instruments of high radiometric sensitivity in order to minimise the integration time taken for a single measurement.

All subsurface measurements are influenced by the layer of water between sensor and surface, which is necessary to prevent wave action from exposing the sensor to the air. Under measurement conditions where waves are present, the sensor will have to be located at a depth minimally deeper than the maximum wave amplitude.

The fraction F of diffuse to total radiance is dependent on wavelength, atmospheric condition (aerosol content and type) and on the solar zenith and azimuth angle. If only one spectroradiometer is available and it is equipped with a radiance measuring aperture, it is advisable to measure total downwelling irradiance from a reference panel approximating a perfect Lambertian diffuser (see Appendix A). The diffuse component of downwelling radiance should also be determined by a measurement at 90° to the sun-zenith plane (at 180° azimuth) and a measurement at zenith (assuming measurements at intermediate solar zenith angles of ± 30° to 60°, typical of mid-latitudes).

4 SUBSURFACE IRRADIANCE REFLECTANCE AS A FUNCTION OF ABSORPTION AND BACKSCATTERING

4.1 Introduction

The subsurface irradiance reflectance *R(0-)* is the essential parameter for applications of the analytical model for remote sensing. It is essential because *R(0-)* can be determined from the inherent optical properties of a, b and $\beta(\theta)$ or from spectroradiometric measurements or from remote sensing measurements as explained in the model discussed in § 3. *R(0-)* is only slightly dependent on solar elevation, atmospheric or water surface conditions. Algorithms developed on the basis of *R(0-)*, irrespective of the mode of calculation or measurement, have multitemporal validity.

4.2 The model for relating subsurface irradiance reflectance as a function of absorption and backscattering

The relationship between the subsurface irradiance reflectance, *R(0-)*, and the inherent properties, a and b_b, of lake and river waters was investigated. *In situ* spectroradiometric measurements of reflectance and laboratory-based spectrophotometric measurements of spectral absorption and scattering were used to test published models relating reflectance to the inherent optical properties.

According to Gordon *et al.* (1975), *R(0-)* varies with $b_b/(b_b+a)$ in a manner which can be described by the polynomial equation:

$$R(0-) = r_0 + r_1(b_b/(b_b+a)) + r_2(b_b/(b_b+a))^2 \qquad \text{for } \omega_0 < 0.95 \qquad [4.1]$$

with coefficients r_n depending on illumination conditions and where ω_0 is the scattering albedo (b/c). Morel & Prieur (1977) and Kirk (1991) have found through Monte Carlo simulations that it is sufficient to approximate equation 4.1 by replacing $b_b / (b_b+a)$ with b_b / a and ignoring the nonlinear term. This leads to:

$$R(0-) = r_1 \, b_b / a \qquad [4.2]$$

where Morel & Prieur (1977) defined

$$r_1 = 0.33$$

whereas Kirk (1991) defined

$$r_1 = 0.33 \text{ for } b_b < 0.25 \text{ m}^{-1}$$
$$r_1 = C(\mu_0) \text{ for } 0.4 < b_b < 2.6 \text{ m}^{-1}$$

Table 4.1 *Scattering properties of different water types taken from the literature for waters with high scattering albedo values, $\omega_0 = b/c > 0.8$ (see text for explanation of symbols).*

	b	b_b/b	b_b/b'	b/c
Petzold (1972; λ=530 nm)				
San Diego Harbor				
- sample 1	1.583	0.019	0.23	0.824
- sample 2	1.824	0.020	0.23	0.833
- sample 3	1.205	0.018	0.23	0.906
Visibility Laboratory freshwater:				
filtered	0.009	0.119	0.51	0.093
+ scattering material	0.544	0.018	0.25	0.798
+ absorbing material	0.573	0.017	0.25	0.430
Whitlock *et al.* (1981; λ=550 nm)				
A1 Appomatox River	14	0.04	0.27	0.85
A2 Appomatox River	16	0.07	0.30	0.85
A3 Back River	8.8	0.025	0.26	0.92
Krijgsman (*in prep*)				
(polystyrene particles : 1.6 μm diameter)				
λ=400 nm		0.064	0.339	
λ=550 nm		0.019	0.221	
λ=800 nm		0.011	0.197	
Privoznik (1978)				
Unicellular algal suspension of *C. pyrenoidosa*)				
			0.2	0.9

where $C(\mu_0)$ is dependent on solar altitude and water type. $C(\mu_0)$ is a coefficient in the expression for reflectance as a function of b_b/a and μ_0, as defined by Kirk (1991). μ_0 is the cosine of the zenith angle of refracted solar photons just beneath the water surface. No restrictions for ω_0 were presented in either study, but $R(0-)$ was calculated for relatively clear oceanic waters and might therefore not be valid for the turbid waters studied here. Most of the waters described in the literature have high scattering albedo values, $\omega_0 = b/c > 0.8$ (Table 4.1). Figure 4.1.a & b present $\omega_0(\lambda)$ values for this study being the average values of ω_0 for each water type. The ω_0 decreases from samples for the shallow eutrophic lakes (highest value of $\omega_0 = 0.94$ at 560 nm), the river and canal, the deep lakes to the shallow mesotrophic lakes (lowest value of $\omega_0 = 0.23$ at 750 nm).

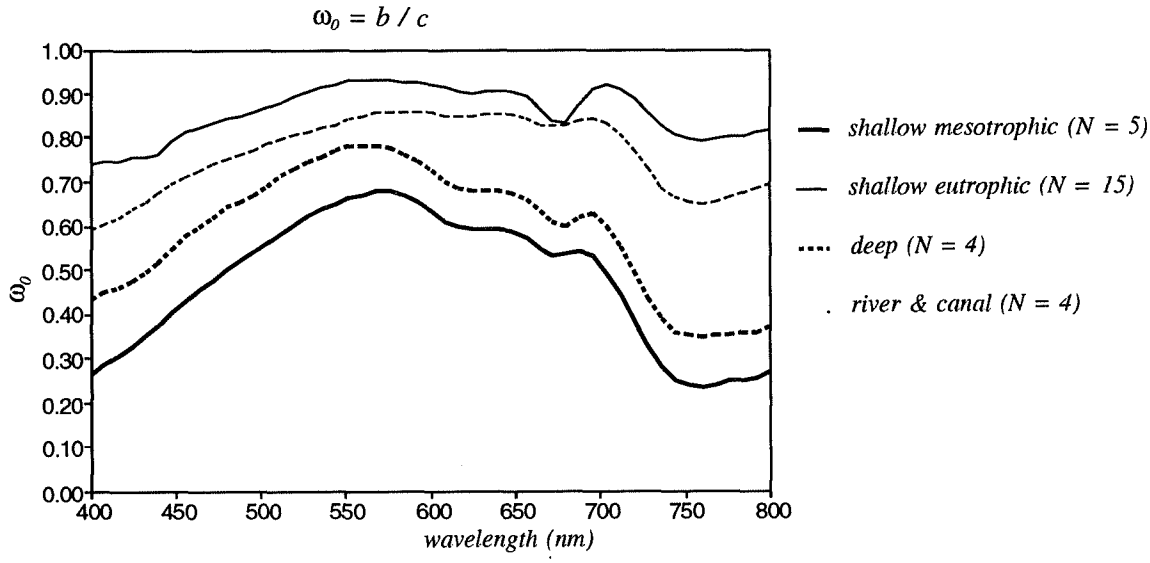

Figure 4.1.a *Plots of spectral scattering albedo ω_0 (= b/c) averaged for each of the four water types investigated in this study.*

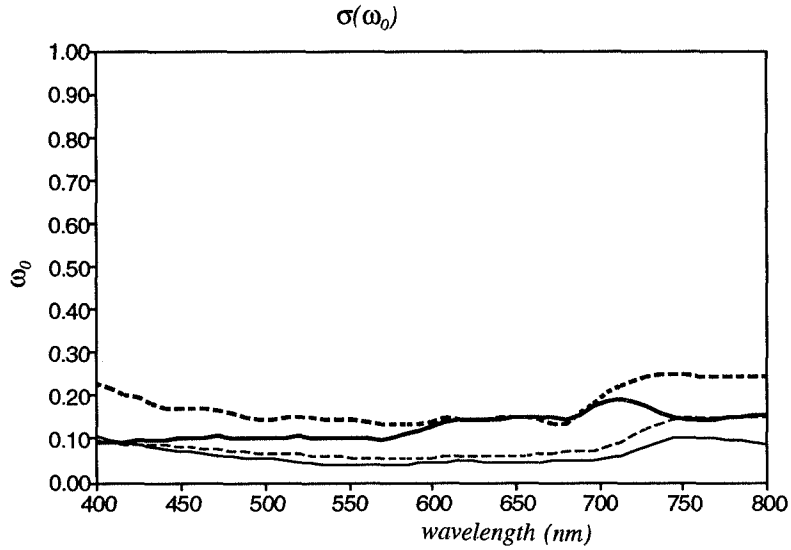

Figure 4.1.b *Plots of the standard deviation of spectral scattering albedo ω_0 (= b/c) averaged for each of the four water types investigated in this study presented in Fig. 4.1.a.*

There is also a clear spectral dependency of ω_0 on wavelength, becoming more pronounced with decreasing ω_0 values. Kirk (1991) investigated the reflectance averaged over the PAR range, $R(0-)_{PAR}$. This research concentrates on the spectral reflectance, $R(0-)_\lambda$, possibly introducing variation from the PAR based model.

Whitlock *et al.* (1981) found that reflectance for turbid river waters did not vary in a linear manner with b_b / a but was correctly described by Eq. 4.1. The authors obtained experimental values of reflectance, absorption and backscattering for waters with scattering albedos ranging from 0.7 to 0.93 and concluded that data from different water samples did not fit a single curve. This result appears to support Kirks (1991) findings for $C(\mu_0)$ outlined above. It is clear, then, that equation 4.1 requires further analysis in order to derive a relationship between measured reflectance and the absorption and backscattering values for the waters in this study. Absorption was evaluated by the method described in Chapter 2; further investigation is needed to estimate backscattering b_b and the coefficients r_n.

4.3 Estimation of the backscattering coefficient b_b

The backscattering coefficient, b_b (representing the total scattering over angles from 90° to 180°: $b_{90\text{-}180}$), was estimated from the apparent absorption and beam attenuation measurements as follows. Chapter 2 detailed how the total scattering coefficient b (= $b_{5\text{-}180}$) and scattering over angles from 40° to 180° (b' = $b_{40\text{-}180}$), were deduced from spectrophotometric measurements (see § 2.1.2.2). b_b can be expressed as a fraction of either b or b', the value depending on water type (Kirk, 1991; Whitlock *et al.*, 1981; this study: Table 4.1) and wavelength (Krijgsman, *in prep*). However, calculations on volume scattering functions by Petzold (1972) and Whitlock *et al.* (1981) have shown that the ratio of b_b to b' is more constant over the different water types than the ratio of b_b to b.

Table 4.1 indicates that values for b_b /b' generally range from 0.2 to 0.3 from different studies covering a range of different water types. For purposes of this study, the median value b_b / b' = 0.25 was selected. The table also shows that b_b / b' values tend to be less variable than those for b_b / b. This selection may introduce an error of 20 %. The ratio was also assumed to be wavelength independent (Whitlock *et al.*, 1981); this assumption was further made for the determination of actual absorption from the apparent absorption and scattering measurements (see § 2.1.2.2.1). Additional measurements of volume scattering functions for a variety of fresh water types are required to test the validity of these assumptions.

Thus, in this study, the following equation was used to calculate b_b from the estimated b' values:

$$b_b = 0.25\ b' \qquad [4.3]$$

4.4 The variation of $R(0-)$ with $b_b / (b_b+a)$

The relationship between $R(0-)$ and $b_b / (b_b+a)$ was investigated. Figures 4.2.a-h show the spectral nature of the relationship between measured $R(0-)$ and $b_b / (b_b+a)$ for each of the four water types, with an example of the lowest and the highest correlations for each water type of $R(0-)$ with $b_b / (b_b+a)$. The figures indicate that a linear dependence of $R(0-)$ on $b_b / (b_b+a)$ can be expected, thus reducing equation 4.1 to

$$R(0-) = r_0 + r_1 \, b_b / (b_b+a) \qquad [4.4]$$

A bivariate linear regression analysis was performed for those cases where both $R(0-)$, b_b and a values were available (Table 4.2.); in 15 out of 20 cases r_0 was smaller than the standard error of the Y estimate, $S_{y\cdot}$. The term was thus removed from Eq. 4.4:

$$R(0-) = r_1 \, b_b / (b_b+a) \qquad [4.5]$$

Three of the five cases which did not meet this criterion were River Vecht and Amsterdam-Rijn Kanaal samples. These turbid, but low algal samples deviated markedly from the lake samples. The lowest correlations between measured $R(0-)$ and $b_b / (b_b+a)$ for each water type in Table 4.2 can be compared to Figs. 4.2.a, c, e and g. From the comparison it may be deduced that a low correlation is caused by a spectral dependency of r_1, most markedly for the eutrophic lakes.

Table 4.3 presents values for r_1, ω_0, b and b_b / a integrated over 400 - 700 nm, as an indication of water type. Values of r_1 ranged from 0.12 to 0.56 with an average of 0.29. The relative error ranged from 1 % to 5 % for the 20 samples. The variation in r_1 between the water bodies was large. This suggests that the conclusions of Whitlock *et al.* (1981) and Kirk (1991), that the coefficient(s) change with changing water type are confirmed. A change of coefficients with solar zenith angle cannot be deduced from the results in Table 4.3. This may be caused by a masking effect of the change of the coefficients with water type. Whitlock *et al.* (1981) did not present the values for the coefficients of the polynomial (Eq. 4.1); Kirk (1991) presented the sun angle dependence for $C(\mu_0)$ on μ_0 for seven different waters. The highest scattering coefficient presented by Kirk (b = 1.54 m^{-1}) for San Diego Harbour) lay in the range of the lowest values for waters considered here. The values of $b_{5\text{-}180}$ for this study range from 0.6 to 25 m^{-1}.

The only relationship that can be deduced from the values of r_1 and its relative error as a function of illumination condition (sun angle and sky condition) and water type (b/c, b_b / a and b) is a general increase in error with increasing b and ω_0 . Since the relative error does not increase with increasing b_b / a, this cannot be fully explained by the error that results from approximating equation 4.1 by equation 4.4.

The values of r_1 obtained in this study and those from the literature indicate that the prediction of a generalised r_1 for all water bodies is currently not possible. Available data on volume scattering functions for different water types are scarce, especially for

inland waters. *In situ* optical measurements enabling the estimation of *R(0-)* and *a* and *b* remain necessary until appropriate volume scattering functions for freshwaters are available.

Table 4.2 *Bivariate linear regression analysis results for measured R(0-) and* $b_b/(b_b+a)$ *(r_1 is equal to the x-coefficient in the regression equation; $S_{x'}$ = standard error of the x-coefficient; $S_{y'}$ = standard error of the y estimate; r^2= coefficient of determination)*

Sample	*Constant*	r_1	$S_{x'}$	$S_{y'}$	r^2
shallow eutrophic					
LHA	-0.0134	0.481	0.0120	0.0079	0.89
LWG	-0.0279	0.497	0.0134	0.0053	0.87
LWL	-0.0002	0.135	0.0017	0.0008	0.97
LEL1	-0.0032	0.266	0.0101	0.0065	0.78
LEL2	-0.0017	0.151	0.0060	0.0042	0.76
LEL3	-0.0037	0.206	0.0079	0.0068	0.77
LVU	-0.0029	0.286	0.0145	0.0115	0.66
LLO	-0.0104	0.376	0.0147	0.0116	0.77
LBR	-0.0057	0.253	0.0108	0.0088	0.73
shallow mesotrophic					
LNS	+0.0003	0.186	0.0037	0.0012	0.93
LSA	-0.0007	0.200	0.0021	0.0011	0.98
deep meso-eutrophic					
LSP1	-0.0000	0.564	0.0085	0.0020	0.96
LSP2	-0.0019	0.498	0.0066	0.0021	0.97
LWB1	-0.0029	0.121	0.0039	0.0046	0.83
LWB2	0.0048	0.153	0.0044	0.0053	0.86
WR	-0.0003	0.274	0.0036	0.0010	0.97
river & canal					
HIK	-0.0022	0.241	0.0051	0.0030	0.92
ARK	-0.0101	0.235	0.0042	0.0059	0.94
RVE1	-0.0041	0.201	0.0018	0.0015	0.98
RVE2	-0.0057	0.526	0.0033	0.0012	0.99

Table 4.3

Values for r_l and its relative errors, in combination with sun angle and sky condition at the time of measurement and with ω_b(PAR), b(PAR) and b_b(PAR)/a(PAR) as an indication of water type. (%E = percentage error in estimation of r_l; θ = solar zenith angle; sky = sky condition: s=clear sky(sun), s/h = sunny-to-hazy, h = hazy, o = completely overcast, c = intermittent clouds); see main text for explanation of other symbols.

Sample	r_l	% E	θ	sky	b/c(PAR)	b_b /a(PAR)	b(PAR)
shallow eutrophic							
LHA	0.48	2	67	h	0.85	0.13	14.55
LWG	0.50	3	43	s/h	0.89	0.22	22.76
LWL	0.14	1	57	s	0.66	0.08	3.13
LEL1	0.27	4	43	c	0.86	0.13	14.45
LEL2	0.15	4	46	c	0.87	0.15	14.71
LEL3	0.21	4	67	o/c	0.89	0.18	15.60
LVU	0.29	5	55	o	0.90	0.16	22.09
LLO	0.38	4	50	o	0.89	0.16	22.05
LBR	0.25	4	49	s	0.91	0.17	25.03
shallow mesotrophic							
LNS	0.19	2	51	s	0.59	0.06	1.17
LSA	0.20	1	61	h	0.71	0.09	3.35
deep meso-eutrophic							
LSP1	0.56	2	45	s/h	0.61	0.03	0.78
LSP2	0.50	1	47	s/h	0.55	0.05	0.67
LWB1	0.12	3	46	s/h	0.88	0.54	13.84
LWB2	0.15	3	44	s/h	0.78	0.24	2.52
WR	0.27	1	50	s	0.46	0.04	0.60
river & canal							
HIK	0.24	2	42	h	0.80	0.09	15.38
ARK	0.24	2	59	s	0.86	0.45	7.78
RVE1	0.20	1	52	s/c	0.81	0.21	6.38
RVE2	0.53	1	57	s/c	0.68	0.08	2.46
average	0.29	2					

Figure 4.2 *(general caption) Spectral nature of the relationship between measured R(0-) and $b_b/(b_b+a)$ for each of the four water types, with an example of the lowest and the highest correlations of R(0-) with $b_b/(b_b+a)$. (See Table 4.2 and 4.3 for additional information on the regression equations, solar zenith angles etc.)*

Figure 4.2.a
Lake Vuntus

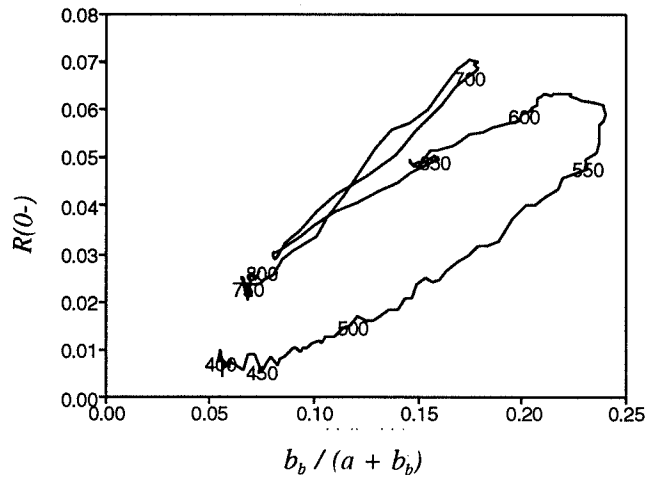

Figure 4.2.b
Lake Western Loenderveen

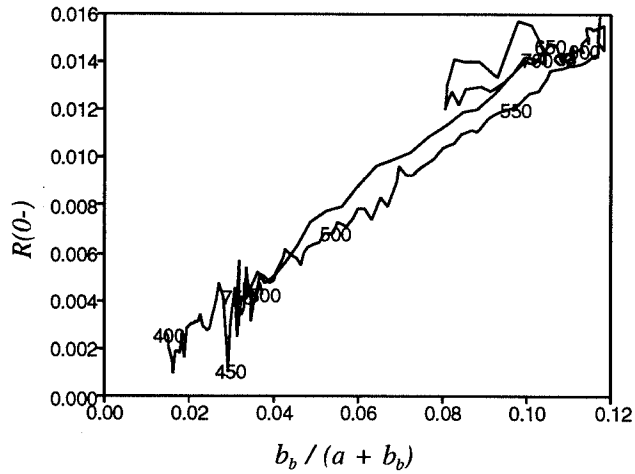

Figure 4.2.c
Lake Naardermeer Spookgat

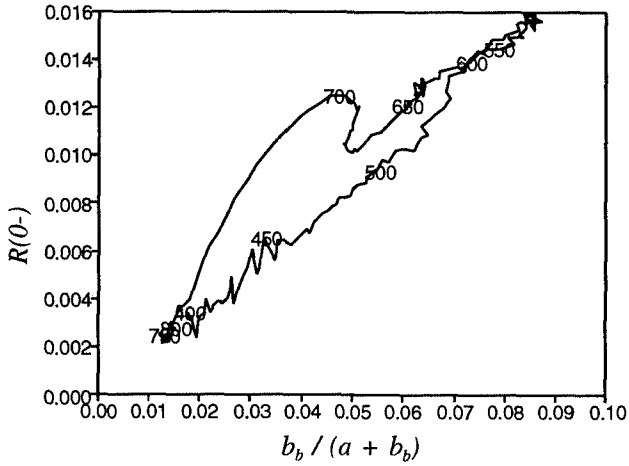

Figure 4.2.d
Lake Hollands Ankeveen

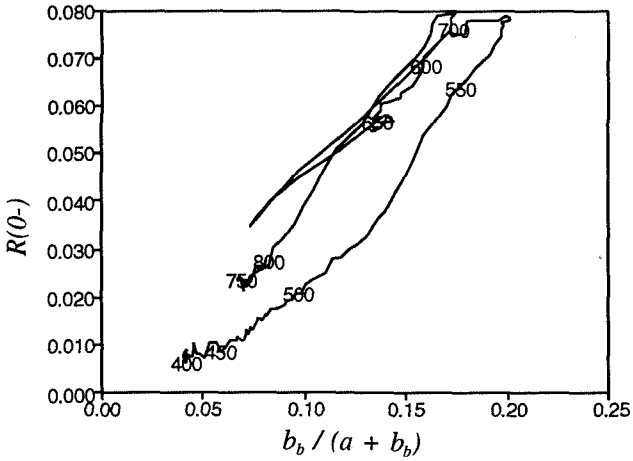

Figure 4.2.e
Lake Wijde Blik

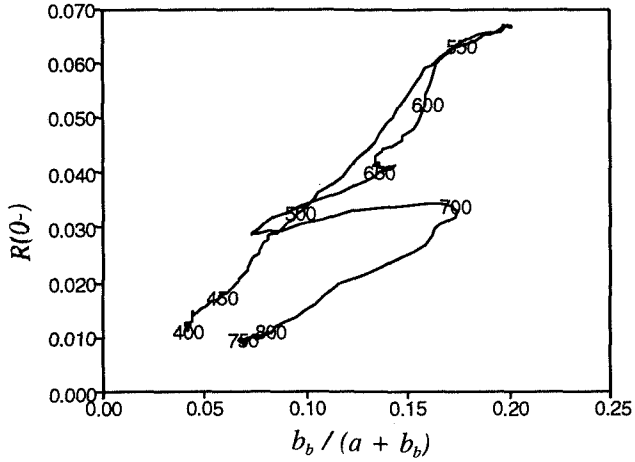

Figure 4.2.f
Water Reservoir

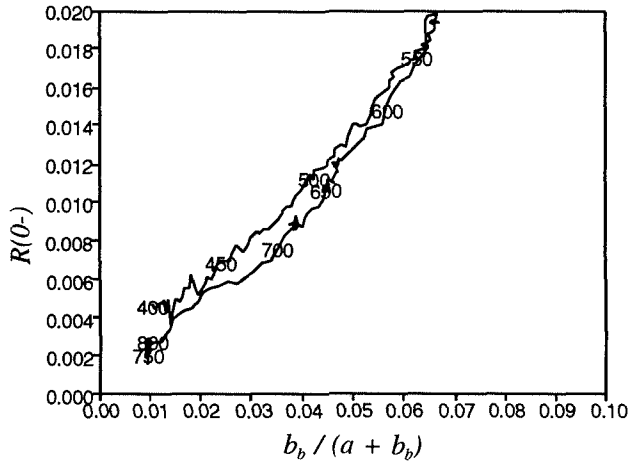

Figure 4.2.g
Amsterdam-Rijn Kanaal

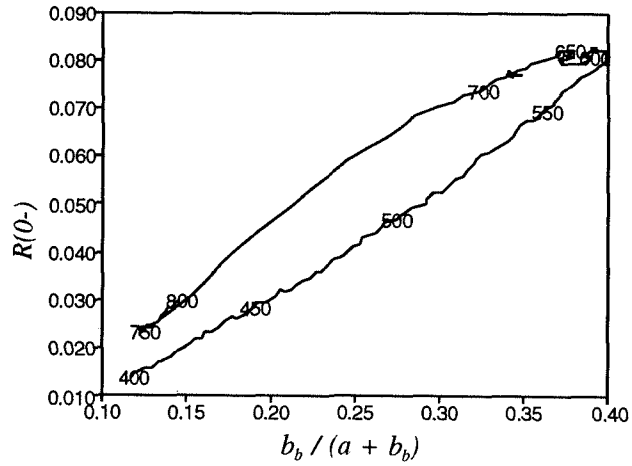

Figure 4.2.h
River Vecht

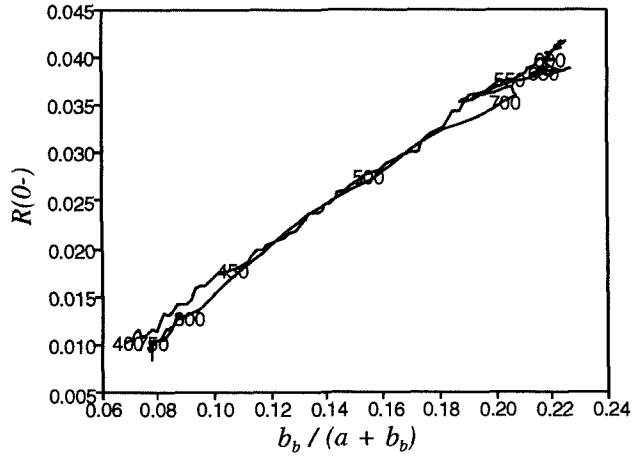

For the purpose of information extraction from reflectance spectra it is therefore recommended that algorithms which are independent of r_1 values be used. This requirement would suggest the use of algorithms that combine information from more than one spectral band in such a manner that r_1 values are normalised. Alternatively, algorithms which require information about the spectral behaviour of backscattering and absorption can be used.

4.5 Summary and conclusions

With respect to the accuracy of measurements in this study, it was sufficient to describe $R(0-)$ as a linear function of $b_b/(b_b+a)$:

$$R(0-) = r_1 \, b_b/(b_b+a)$$

Values of b_b were best estimated as a fraction of scattering over 40° to 180°; the value for the fraction used in this study was 0.25:

$$b_b = 0.25 \, b'$$

The coefficient r_1 varied with changing optical water type and illumination conditions; values for r_1 derived from the data ranged from 0.12 to 0.56, with an average of 0.29. At the moment it is not possible to predict a value for r_1 which is applicable to a wide range of water bodies. A spectral dependence of r_1 was most markedly evident in the samples from the shallow eutrophic lakes. Therefore, information extraction from reflectance spectra requires the use of algorithms which are preferably independent of r_1 values. Spectral band ratioing, derivative analysis or alternatively, acquisition of spectral absorption, scattering and backscattering properties are the most promising methods for information extraction from *in situ* spectroradiometric or from remote sensing measurements.

For the further development of an analytical method for inland water measurements of volume scattering functions for the various fractions of freshwater related suspended matter (detritus, inorganic matter and phytoplankton) are required.

5 ALGORITHM DEVELOPMENT BASED ON THE *R(0-)* DATA

5.1 Introduction

The subsurface irradiance reflectance *R(0-)* is an essential parameter in the development of multitemporal remote sensing algorithms. *R(0-)* acts as the link between:

1 laboratory-based determination of inherent optical properties (§ 2 and 4);
2 *in situ* measured parameters of the (ir)radiance field (§ 3 and 4);
3 the remotely sensed upwelling radiance signal (§ 3 and 6).

The method for estimating water quality parameters from remote sensing data consists of determining the relationships between the inherent optical properties (spectral absorption and scattering and the volume scattering function) and the water quality parameters.

Once the relationships between the inherent optical properties and *R(0-)* and between *R(0-)* and the remote sensing signal are known, there should ideally be no need for simultaneous field sampling for determination of water quality parameters from remote sensing measurements. However, simultaneous measurements of the *in situ* diffuse and direct downwelling (ir)radiance components will remain necessary to determine *R(0-)* from L_{rs}, as described in § 3; unless L_{wu} measurements are available, in which case an estimation of the diffuse component is less important.

The aim of this study was to develop remote sensing algorithms for estimation of concentrations of chlorophyll *a*, cyanophycocyanin and seston dry weight, and values of vertical attenuation of downwelling irradiance and Secchi depth transparency, following the analytical method described in § 1. By basing the algorithms on values of *R(0-)* a high level of multitemporal validity could be obtained. If the analytical approach was not possible, a semi-empirical algorithm was developed with as much multitemporal validity as possible.

For each parameter algorithms were developed for 2 nm intervals, and for spectral band intervals equivalent to an Inland Water Mode bandset. Attention was paid to the location of the spectral intervals required for the algorithms. Attention was also paid to locating spectral areas for inclusion in algorithms that would enable measurement of a sufficiently high reflectance signal in at least one of the spectral bands to assure sufficient signal-to-noise levels. Sensitivity estimates were performed to determine the effect of variations in optical water quality parameters other than those for which the algorithm was intended. It was also investigated whether one algorithm was valid for all types of waters or whether it was necessary to adjust parameters in the algorithms for them to perform correctly (see § 2.4).

In chapter 6 the algorithms developed in this chapter are applied to remote sensing data from two flights on different days under differing atmospheric and irradiance condi-

tions, using different remote sensing instruments, thus illustrating the validity of the approach outlined below.

The algorithms for estimation of water quality parameters are treated in order of decreasing possibilities for application of the analytical algorithm as caused by lack of information concerning the exact nature of the effect of water quality parameters on the inherent optical properties. The parameters most influenced by this lack of knowledge are K_d and *SD* because they are determined by the inherent optical properties of absorption, scattering and the volume scattering function.

5.2 Algorithm development

5.2.1 *Criteria for algorithm development based on the inherent optical properties*

For the estimation of water quality parameters based on calculations or measurements of *R(0-)* a distinction must be made between water quality parameters that influence the inherent optical properties and those that are determined by the inherent optical properties. The water quality features which are, in principle, directly determinable from *R(0-)* through their effects on the inherent optical properties of absorption, scattering and the volume scattering function are:

aquatic humus
light harvesting pigments
seston, which is separable into:
- phytoplankton and
  tripton, which is separable into:
  - detritus and other organic material
    inorganic material

Water quality parameters which are determined by the inherent optical properties, which in turn are a function of the above named parameters, include:

Secchi depth transparency
vertical attenuation of downwelling irradiance

Transparency and vertical attenuation can only be determined analytically from *R(0-)* measurements if the inherent optical properties of the water constituents are determined first.

In § 2 it was explained that absorption of light by aquatic humus and light harvesting pigments and absorption and scattering by phytoplankton and tripton at short wavelengths (400 to 500 nm) were essentially inseparable from a combined attenuation or reflectance signal. In addition, high absorption at low wavelengths causes *R(0-)* to be low, resulting in low remotely sensed L_{rs} values and thus low signal-to-noise levels in a

spectral area where atmospheric influence is high and sensor sensitivity is low. Thus none of the water quality parameters can be estimated with any accuracy at short wavelengths in eutrophic inland waters.

Table 5.1 shows the information available for the inherent optical properties of the inland water quality parameters in this study. For each parameter the absorption properties are reasonably well known. The scattering properties of the seston are well known; the backscattering, however, has been estimated from an assumed fixed relation between the scattering within an angle of 40 - 180° and the backscattering at angles of 90 - 180° (see § 4.3). Because some samples had abundant phytoplankton and some had abundant tripton, approximations of the scattering of phytoplankton and tripton were obtained. Important data lacking were $\beta(\theta)$ functions of the water quality constituents.

Table 5.1 *The desired and available inherent optical properties of inland waters constituents Y = known, Y* is approximated but not separately determined, N = not known, N* = not known for the parameters of this research but given for other (often ocean water related) water types.*

	a	b	b_b	$\beta(\theta)$
Aquatic humus	Y	Y(=0)		Y(=0)
CP-cyanin	Y	N*	N*	N
Chlorophyll *a*	Y	Y*	N*	N*
Phytoplankton	Y	Y*	Y*	N*
Tripton	Y*	Y*	Y*	N
- Detritus	Y*	Y*	N*	N
- Inorganics	N*	N*	N*	N

The lack of information on the inherent optical properties of the water constituents implies that the apparent optical parameters (*SD* and K_d) and the concentration of seston expressed as seston dry weight (*DW*) may not be determined analytically from the *R(0-)* signal. If these parameters are required for water quality management purposes, they will have to be estimated in the semi-empirical manner; i.e. through correlation with *R(0-)* at a wavelength preferably highly correlated with *SD*, K_d and *DW* and at wavelength intervals with a sufficiently high signal-to-noise level to obtain a reliable remote sensing signal.

Based on the available information on the inherent optical properties, chlorophyll *a* and, to a certain extent, CP-cyanin, are the only parameters that may be determined by the

analytical method for remote sensing (as defined in § 1). Chlorophyll *a* and CP-cyanin are defined in concentration units based on their specific absorption coefficients.

Unlike chlorophyll *a*, for CP-cyanin the analytical solution cannot be fully determined because it is a superimposed pigment absorption feature for which the specific absorption may be determined, but for which a specific scattering may be difficult to derive. The CP-cyanin-specific scattering cannot be determined for any of the samples in which this pigment occurs (mainly in the highly eutrophic lakes). For the shallow eutrophic lakes CP-cyanin is dependent on the species ratio of *Oscillatoria spp.* to *Prochlorothrix hollandica* without any clear relationship with the total chlorophyll *a* absorption or chlorophyll *a*-correlated (back)scattering (see § 5.2.3.2: *step 2* for definitions). Using measured values of inherent optical properties an approximation for an analytical solution can, however, be made for CP-cyanin for eutrophic lakes with high scattering coefficient values.

5.2.2 *Criteria for algorithm development based on requirements for remote sensing data acquisition*

Algorithm development based on *R(0-)* data for implementation in remote sensing using an analytical or semi-empirical method has to take into account additional criteria to determine the optimal number and placement of spectral bands from which to calculate water quality parameters. Three spectral band configurations were considered; a single spectral band, a spectral band ratio of two bands and combinations of three or more bands. In general, indices for water quality parameter estimation based on combinations of two or more bands are preferred because they utilize the spectral information in a reflectance signal from water analytically. Of these techniques the ratioing of spectral bands is the best known and most useful (Hilton, 1984).

5.2.2.1 *Water quality parameter estimation from a single spectral band*

One advantage of being able to use a single spectral band for water quality parameter estimation lies in the ease with which data manipulation will produce a map of the water quality parameter(s). Also the increase in noise through combining spectral bands, caused by uncorrelated noise present in the separate spectral bands, is avoided (Lillesand & Kiefer, 1987; Dekker *et al.*, 1991, 1992c; Dekker & Peters, 1993).

In general, a single spectral band will be located at an absorption feature or at a reflectance feature, with the aim of extracting information causing the spectral feature. In the first case the signal-to-noise ratio (S/N) will be lower and in the second case the S/N will be higher.

In order to maximise the fraction of upwelling radiance from an inland water contained in L_{rs}, the remotely sensed signal should be measured with the least amount of atmos-

pheric interference. Wavelengths where atmospheric components absorb significantly should perhaps also be avoided. Alternatively, corrections for atmospheric absorption may be made based on the concentration of these constituents at the time of remote sensing data acquisition. For airborne remote sensing *in situ* spectroradiometric measurements were considered to be sufficient (depending on altitude and atmospheric conditions). (However, results from the analysis of remote sensing data from 1990 question the correctness of this assumption: see § 6). The main atmospheric components which absorb in the visible region are (Gregg & Carder, 1990): 1) water vapour - between 586 and 600 nm with a maximum at 590 nm; between 647 and 658 nm with a maximum at 651 nm and from 691 to beyond 700 nm with a maximum at 698 nm; 2) ozone - a gradual increase in absorption from low values below 523 nm to a high at 603 nm after which a gradual decrease occurs down to 666 nm; 3) oxygen - between 686 and 694 nm with a maximum at 687 nm.

Information from a single spectral band is subject to variation in the coefficient r_1, necessary for relating *R(0-)* to the inherent optical properties (Eq. 4.5). r_1 is dependent on the volume scattering characteristics of the water and to a lesser extent on the solar zenith angle and state of the water surface.

5.2.2.2 *Water quality parameter estimation from spectral band ratios*

An important feature of spectral band ratios is that the results are not subject to variation in r_1 in Eqs. 4.5 and 5.1 because the $r_{1,\lambda}$ for each band will be divided by the $r_{1,\lambda}$ of the other band, provided r_1 is not dependent on wavelength for the interval between the two spectral bands (the results from chapter 4 showed that r_1 is probably spectrally dependent for the shallow eutrophic waters). Atmospheric influences may also be annulled in a similar fashion. However, atmospheric influence is dependent on wavelength. In the case of atmospheric scattering this influence will be low in spectral bands positioned close together. Philpot (1990) advises a maximum spectral distance of 50 nm when applying derivative algorithms to avoid atmospheric effects in remote sensing. In the case of an absorption feature such as water vapour or ozone in one of the bands of a spectral band ratio, this effect must be compensated.

To extract information on a spectral absorption feature, a spectral band ratio should have one spectral band with a high reflectance, to ensure a high S/N value, as well as a spectral band located at the maximum of the absorption feature to be estimated. The absorption feature should be as unique as possible, i.e. preferably not in a spectral area where another absorption feature may be variable and highly absorbing.

The wavelengths involved in a spectral ratio should be spectrally as close as possible in order to:

- annul T_{az} and L_p contributions
  prevent non-desired spectral absorption features introducing errors
  prevent the spectral scattering features introducing errors

prevent sensor-specific sensitivities (e.g. low radiometric sensitivity at short wavelengths) introducing errors
prevent errors in the estimation of the fraction of diffuse irradiance (F) introducing errors in the calculation of $R(0-)$ from L_{rs}.

5.2.2.3 *Water quality parameter estimation from other spectral band combinations*

All the criteria for spectral band ratios also apply to other spectral band combinations. The criteria concerning high S/N are especially important because uncorrelated noise vectors acting in each band included in the algorithm will increase the noise (Lillesand & Kiefer, 1987, Dekker *et al.*, 1991, 1992c, Dekker & Peters, 1993). For this reason the number of spectral bands used in an algorithm should be kept to a minimum. The application of algorithms with more than three spectral bands may not be successful in remote sensing due to decreasing S/N levels.

The above criteria also suggest that the blue end of the spectrum will be less useful for algorithm development because of high atmospheric interference, low sensor sensitivities and a high and variable fraction of diffuse downwelling irradiance.

5.2.3 *General models for water quality parameter estimation*

5.2.3.1 *A general model for water quality parameter estimation for a single band*

The model for water quality parameter estimation using a single spectral band is as follows. First Eq. 4.5 has to be written as:

$$R(0-)_{\lambda 1} = r_1 \, [(b_b(i) \,/\, (b_b(i)+a(i))]_{\lambda 1} \qquad [5.1]$$

where i denotes optical active parameters and $b_b(i)$ and $a(i)$ are the sum of b_b and a for $i = 1$ to n. Not all parameters have both a and b_b characteristics: e.g. aquatic humus only absorbs light.

If the desired information is the concentration of one of the parameters in the equation the parameter must be defined as $C_i \, b_{bi}^*$ or $C_i \, a_i^*$, where C_i is the concentration of parameter i, b_{bi}^* the parameter-specific backscattering coefficient and a_i^* the parameter-specific absorption coefficient.

In the case of a pigment extraction feature in the waters studied here Eq. 5.1. becomes

$$R(0-)_{\lambda 1} = r_1 \, [(b_b(t)+b_b(ph)) \,/\, (b_b(t)+b_b(ph)+a(w)+a(ah)+a(t)+a(ph))]_{\lambda 1} \qquad [5.2]$$

where $a(ph)_{\lambda I}$ is equal to $C\ a_{\lambda I}^*$ with C equal to the concentration of the pigment and $a_{\lambda I}^*$ the pigment-specific absorption coefficient at wavelength λ_I. Equation 5.2 can be written as

$$R(0-)_{\lambda I} = r_I\ [(b_b(t)+b_b(ph))\ /\ (b_b(t)+b_b(ph)+a(w)+a(ah)+a(t)+(C\ a_{\lambda I}^*))]_{\lambda I} \qquad [5.3]$$

and solved for C.

5.2.3.2 *A general model for water quality parameter estimation from a spectral band ratio*

As has been demonstrated in § 4.4, r_I is highly variable in each of the waters sampled. The use of a single band will therefore be less suitable for multitemporal comparisons. However, the dependence on r_I may be circumvented by use of a spectral band ratio. For example, if a wavelength can be found where the $a_{\lambda I}^*$ is zero the equation for the estimation of pigment concentration becomes:

$$\begin{aligned} &R(0-)_{\lambda I}\ /\ R(0-)_{\lambda 2} = \\ &\quad (r_I\ [(b_b(t)+b_b(ph))\ /\ (b_b(t)+b_b(ph)+a(w)+a(ah)+a(t))]_{\lambda 1})\ / \\ &\quad (r_I\ [(b_b(t)+b_b(ph))\ /\ (b_b(t)+b_b(ph)+a(w)+a(ah)+a(t)+(C\ a^*))]_{\lambda 2} \end{aligned} \qquad [5.4]$$

which can be solved for C:

$$C = (R(0-)_{\lambda 2}\ b_{b\lambda I}\ [b_b+a(r)]_{\lambda 2})\ /\ (R(0-)_{\lambda I}\ b_{b\lambda 2}\ a^*_{\lambda I}-[b_b+a(r)]_{\lambda 1})\ /\ (a^*_{\lambda I}) \qquad [5.5]$$

where $a(r)$ is the sum of the non-pigment absorption coefficients: $a(w) + a(ah) + a(t)$ and b_b is the sum of $b_b(t)+b_b(ph)$. The calculation of C from equation 5.4 is given in Appendix C for an example where C is the chlorophyll a concentration.

5.3 The analytical model applied to determination of chlorophyll *a*

5.3.1 *The algorithm for chlorophyll a estimation from R(0-)*

Seven steps were necessary to develop an algorithm for chlorophyll a estimation from $R(0-)$, including an analysis of the sensitivity of the algorithm to varying concentrations of non-algal material.

Step 1 Determination of spectral location(s) of absorption maxima and minima of chlorophyll a and the associated chlorophyll a-specific absorption coefficients.

The average spectral chlorophyll a-specific absorption was calculated for 25 samples, by dividing the $a(ph)$ for each sample with the measured chlorophyll a concentration (Fig. 5.1). The graph shows two spectral areas of high chlorophyll a-specific absorption;

at 438 nm and at 676 nm. Not all spectral features in Fig. 5.1 are chlorophyll *a* related; at approximately 624 nm for example the presence of CP-cyanin in samples containing cyanobacteria covaries with chlorophyll *a*.

Chlorophyll *a*-specific absorption at 438 nm is almost twice as high as the absorption at 676 nm, yet it was not chosen as a pigment absorption maximum for algorithm development due to the occluding effects of the high values of *a(ah)*, *a(t)*, *b(t)* and *b(ph)*. Furthermore, the standard deviation for the chlorophyll *a*-specific absorption at 676 nm (a^*_{676}) was lower than for a^*_{438}.

Figure 5.2 shows the correlation diagram between *a(ph)* and measured chlorophyll *a* concentrations at each wavelength. The coefficient of determination (r^2) lies between 0.70 and 0.88 over the 400 to 704 nm wavelength range. Above 704 nm r^2 approaches zero. Between 500 and 585 nm and between 650 and 690 nm the correlations are highest. Between 585 and 650 nm the r^2 is lower ($r^2 = 0.70$). A probable cause for this lower correlation is CP-cyanin with an *in vivo* absorption peak at 624 nm.

There are two spectral regions which could be chosen as minima of chlorophyll *a* absorption for inclusion in a spectral ratio. Figure 5.1 shows that these areas are located around 550 to 560 nm and beyond 700 nm. The chlorophyll *a*-specific absorption values at 550-560 nm amount to approximately 30% of the values at 676 nm. This spectral region is also located over 100 nm away from the chlorophyll *a*-specific absorption at 676 nm, thus perhaps not meeting the criterion for ratio spectral bands to be spectrally close. Furthermore, this region also coincides with absorption by phycoerythrin, a pigment present in some cyanobacteria, with an absorption maximum around 565 nm. Compared to wavelengths beyond 700 nm, there is still marked aquatic humus and tripton absorption at 560 nm (Fig. 2.2). Thus, the minimum chlorophyll *a*-specific spectral band seems to be more appropriately located at 700 nm or beyond. The rapidly increasing absorption by water at these wavelengths, however, prevents the use of wavelengths beyond approximately 720 nm, where the absorption by water has doubled compared to that at 700 nm (Figs. 2.3 and 5.3).

The choice of a reference wavelength for the algorithm based on the analytical model for chlorophyll *a* concentration estimation is based on the following additional criteria. The local *R(0-)* maximum in lakes with chlorophyll concentrations higher than 10 $\mu g\ l^{-1}$ lies at 706 nm (Fig. 3.4.a & b), thus giving the highest signal-to-noise ratio in the remotely sensed signal. 706 nm is also the spectral location where the average chlorophyll *a*-specific a^* becomes less than 10 % of a^*_{676} and where the standard deviation in the estimate becomes equal to the average value of a^*_{706} (Fig. 5.1).

Therefore, the best combination of spectral bands for estimation of chlorophyll *a* absorption is considered to be a band centred at 676 nm and a band centred at 706 nm.

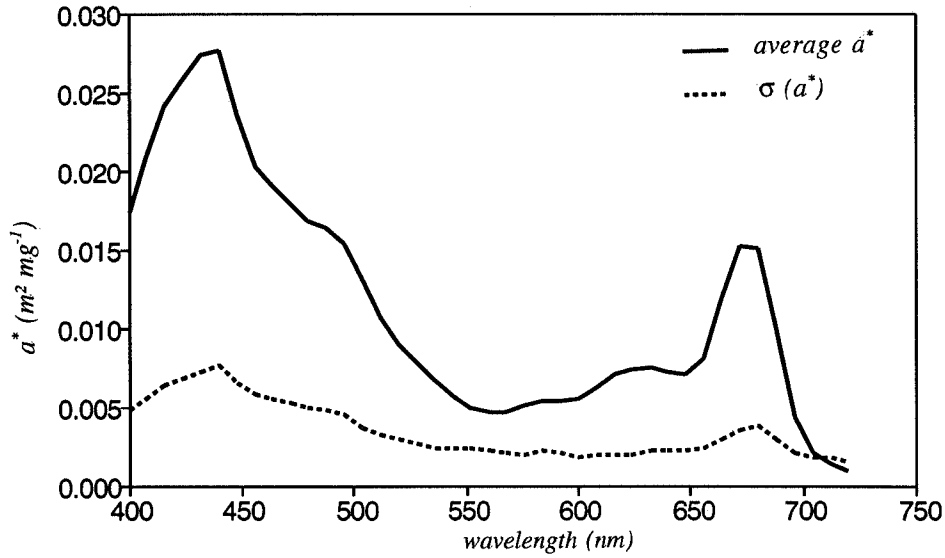

Figure 5.1 *Spectral chlorophyll a-specific absorption (m^2 mg^{-1}) calculated by dividing the spectral absorption by phytoplankton by the measured chlorophyll a concentrations (N = 25; River Vecht and Amsterdam-Rijn Kanaal samples were omitted because of high tripton relative to phytoplankton concentrations).*

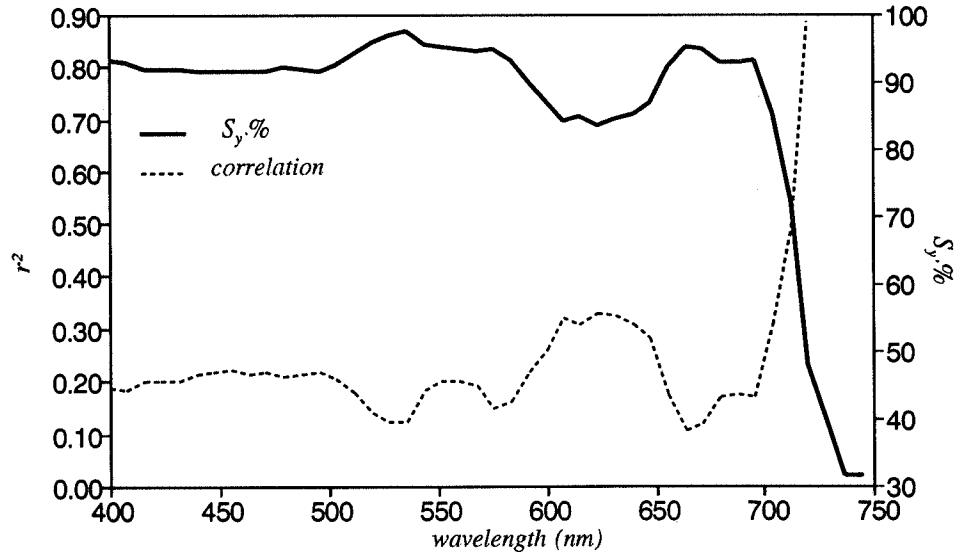

Figure 5.2 *Correlation spectrum of a(ph) and measured chlorophyll a concentration for the same samples used in Fig. 5.1, including the omitted values. The correlation was performed at 2 nm intervals from 400 to 750 nm.*

Step 2 Non-chlorophyllous absorption features at the spectral location of the chosen chlorophyll a-specific absorption maxima and minima.

Water, aquatic humus and tripton also contribute to absorption at 676 nm and beyond. Figure 5.3.a shows the absorption by water and the range in spectral absorption by phytoplankton measured during this study; Fig.5.3.b. shows the range in spectral absorption by aquatic humus and tripton for 600 to 720 nm.

Water absorption becomes the dominant absorption feature beyond 700 nm (Fig. 5.3.a). The crossing of the absorption spectra of water and phytoplankton between 685 and 699 nm for *a(ph)* are an indication that the location of the reflectance peak around 700 nm is partly determined by the width of the *a(ph)* feature centred at 676 nm, as was also established by Gitelson (1992). In this study the *a(ph)* at 676 nm varied from 0.04 to 6.6 times the water absorption at the same wavelength.

The absorption values for aquatic humus and tripton are of the same magnitude although the slopes vary (Fig. 5.3.b). Water absorption becomes dominant at approximately 640 nm for the highest values of aquatic humus and tripton absorption encountered during this study. However, it is probable that the combined absorption features of water, aquatic humus, tripton and phytoplankton determine the location of the reflectance peak at 700 nm in turbid eutrophic waters.

As a demonstration of the possible influence of non-chlorophyllous absorption features to absorption at 676 nm, Table 5.2 presents the contribution to absorption of *a(w)*, *a(ah)* and *a(t)* expressed as the equivalent chlorophyll *a* absorption. The calculations are based on a a^*_{676} of 0.0164 $m^2\ mg^{-1}$, which is the average value of a^*_{676} for the deep and shallow eutrophic lakes from Table 2.6. The average values for absorption of *a(w)*, *a(ah)* and *a(t)* are together equivalent to the absorption of 38 $\mu g\ l^{-1}$ chlorophyll *a*.

Table 5.2 *The contribution to absorption of a(w), a(ah) and a(t) expressed as the equivalent chlorophyll a absorption, based on a chlorophyll a-specific absorption at 676 nm of 0.0164 $m^2\ mg^{-1}$.*

	Chlorophyll *a* equivalent absorption ($\mu g\ l^{-1}$)		
	average	minimum	maximum
$a(w)_{676}$	27.1		
$a(ah)_{676}$	8.2	2.5	15.3
$a(t)_{676}$	2.9	0.3	10.8

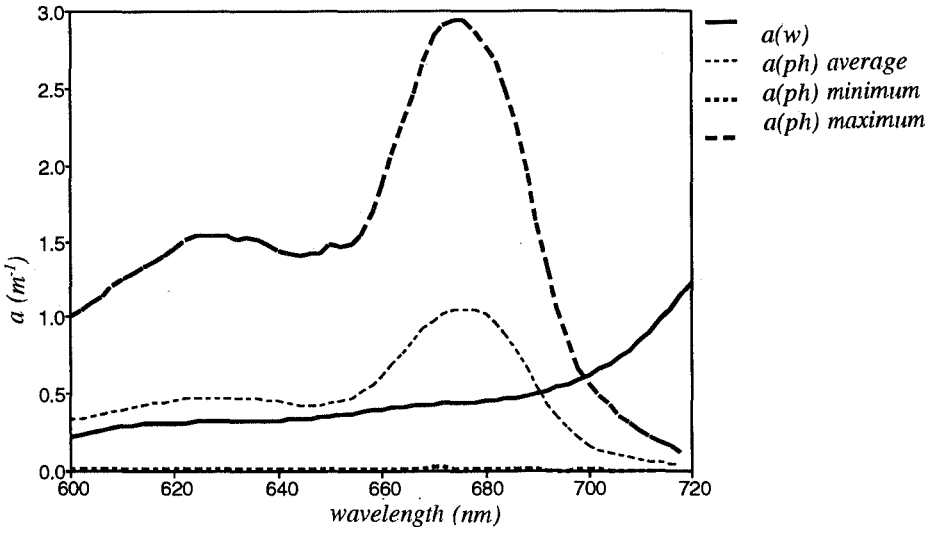

Figure 5.3.a *Absorption by water a(w) and the average, minimum and maximum absorption by phytoplankton a(ph) (N = 27).*

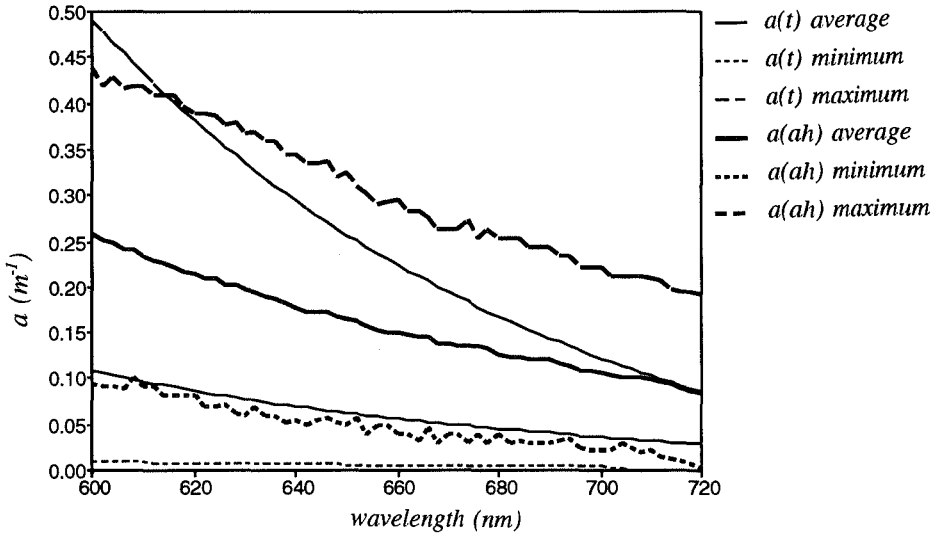

Figure 5.3.b *Average, minimum and maximum absorption by aquatic humus a(ah) and tripton a(t) (N = 27).*

Step 3 Determination of spectral (back)scattering and chlorophyll a-correlated (back)-scattering coefficients.

In order to calculate $R(0-)_{676}$ and $R(0-)_{706}$ as a function of chlorophyll *a*, information is required on the increase in backscattering associated with an increase in algal concentrations expressed by the chlorophyll *a* concentration (Eq. 5.3): the chlorophyll *a*-specific backscattering at 676 and at 706 nm (b_{b676}^* and b_{b706}^*). Backscattering increases more rapidly than absorption with increased algal concentration as shown in Fig. 3.4, where at *676* nm an increase of $R(0-)_{676}$ with increasing trophic status is clear. Increased *R(0-)* with increased chlorophyll *a* levels may also be caused by increases in detritus levels associated with increasing algal concentrations.

No information was available on the scattering and backscattering properties of the dominant algae in these lakes. Therefore, spectral chlorophyll *a*-specific backscattering could not be determined. It was possible, however, to calculate a chlorophyll *a*-correlated backscattering, defined as the increase in backscattering of both algae and tripton associated with an increase in chlorophyll concentration. According to Gons *et al.* (1991) much of the fine-sized detritus (< 15 µm) in the shallow eutrophic Lake Loosdrecht arises from degradation of cyanobacteria and still contains chlorophyll *a*, supporting the correlation between chlorophyll *a* and the sum of algae and tripton scattering. Under conditions of resuspension of bottom sediment in the shallow lakes this relationship may be markedly altered. For deep lakes, River Vecht and Amsterdam-Rijn Kanaal water types this relationship will need separate investigation.

To calculate the chlorophyll *a*-correlated backscattering coefficient (b_b^{**}) at 676 and 706 nm from the chlorophyll *a*-correlated scattering coefficient (b^{**}) at the same wavelengths, the b_b:*b* ratio must be derived. In § 4 it was determined that the $\beta(\theta)$ for these waters varies significantly. Therefore, b_b:*b* was calculated for each sample, b_b (scattering over 90° to 180°) being estimated from *b'* (scattering over 40° to 180°), using equation 4.3 and *b* calculated as described in § 2.

Table 5.3 presents b_b:*b* and r_1 coefficient values for the measurements calculated as average values for the four main water types (Table 4.1 presents published values for b_b:*b*). An increase in values of b_b:*b* from shallow eutrophic lakes through shallow mesotrophic lakes and deep lakes to the river and canal waters is evident. Except for the b_b:*b* ratio for the shallow eutrophic lakes the b_b:*b* values deviate from the value calculated by Kirk (1980, 1983, 1991) using the $\beta(\theta)$ for San Diego Harbour water obtained by Petzold (1972; b_b:*b* = 0.019). The lowest value of 0.017 for the eutrophic lakes is probably caused by the optical characteristics of the mainly organic particles. Lower values for b_b:*b* in eutrophic waters were predicted by Kirk (1983). The results from Table 5.3 demonstrate the need for more $\beta(\theta)$ measurements to be made in inland waters. However, the relatively low variance for the eight shallow eutrophic lake samples in Table 5.3 is an indication of the validity of using this b_b:*b* ratio for these water bodies.

Table 5.3 *Backscattering to scattering ratio b_b:b for the measurements of this study.*

	b_b:b	σ(b_b:b)	r_1	σ(r_1)	N
water type					
shallow eutrophic	0.017	0.003	0.254	0.106	8
shallow mesotrophic	0.033	0.004	0.143	0.040	3
deep	0.042	0.013	0.320	0.193	5
river & canal	0.047	0.012	0.290	0.135	3
all	0.030	0.004	0.258	0.141	20

The average values of b^{**} and b_b^{**} at 676 and 706 nm are presented in Table 5.4. The average value of b^{**} at both wavelengths was 0.133 m^2 mg^{-1}. Average b_b:b ratios of 0.017 and 0.030 and average b_{b676}^{**} of 0.0023 and 0.0040 m^2 mg^{-1} were calculated for shallow eutrophic lakes and for the combined lake samples respectively, from 20 measurements.

Table 5.4 *Chlorophyll a-correlated scattering $b_{b\lambda}^{*}$ and backscattering $b_{b\lambda}^{**}$ values at λ= 676 and λ= 706 nm. The samples of the River Vecht and the Amsterdam-Rijn Kanaal are excluded as they are composed mainly of tripton. Two samples of Lake Wijde Blik which contained M. aeruginosa in colonies in situ are excluded because the chlorophyll a concentrations were subject to large variations, probably caused by the chance process of sampling different amounts of colonies of M. aeruginosa.*

Water types		r^2	$S_{y.}$	N
chlorophyll a-correlated scattering $b_{b\lambda}^{*}$ (m^2 mg^{-1})				
shallow eutrophic	b_{676}^{**}= 0.132 *C*	0.72	2.43	11
all lakes	b_{676}^{**}= 0.133 *C*	0.94	1.76	22
shallow eutrophic	b_{706}^{**}= 0.134 *C*	0.76	2.29	11
all lakes	b_{706}^{**}= 0.133 *C*	0.94	1.66	22
chlorophyll a-correlated backscattering $b_{b\lambda}^{**}$ (m^2 mg^{-1})				
shallow eutrophic	$b_b676,706^{**}$= 0.133 x 0.017 = 0.0023			
all lakes	$b_b676,706^{**}$= 0.133 x 0.030 = 0.0040			
river & canal	$b_b676,706^{**}$= 0.133 x 0.047 = 0.0062			

Step 4 Calculation of $R(0-)_{676}$ and $R(0-)_{706}$ and the ratio $R(0-)_{706}$ / $R(0-)_{676}$ as a function of chlorophyll a concentration.

Once the appropriate spectral band locations, associated chlorophyll *a*-specific absorption coefficients and chlorophyll *a*-correlated specific backscattering coefficients are known, it is possible to calculate the effect of an increase in chlorophyll *a* on $R(0-)_{676,706}$ and on the ratio of $R(0-)_{706}$ / $R(0-)_{676}$ using the equations:

$$R(0-)_{676} = r_1 \, [C \, b_{b676}^{**} / (C \, b_{b676}^{**} + a(r) + (a^*_{676} \, C))]_{676} \qquad [5.6]$$

$$R(0-)_{706} = r_1 \, [C \, b_{b706}^{**} / (C \, b_{b706}^{**} + a(r))]_{706} \qquad [5.7]$$

Calculations were performed over chlorophyll concentrations from 0 to 200 µg l^{-1} assuming average values of inherent optical properties for shallow eutrophic and deep lakes with a^*_{676} = 0.0164 m^2 mg^{-1}, b = 0.133 C, b_b:b = 0.017 and b_{b676}^{**} = 0.0040 m^2 mg^{-1}, and assuming an average $a(ah)$ and $a(t)$ as given in Fig. 5.3.b. The increase in $R(0-)_{676}$ with increasing concentrations of chlorophyll *a* is at first rapid, but decreases to an almost asymptotic level at higher concentrations of chlorophyll *a* (Fig. 5.4). Figure 5.5 shows the change in $R(0-)_{676}$, $R(0-)_{706}$ and $R(0-)_{706}$ / $R(0-)_{676}$ caused by an increase of one µg l^{-1} chlorophyll *a* over the range of 0 - 200 µg l^{-1} chlorophyll *a* (i.e. the derivative of Fig. 5.4). The change in $R(0-)_{676}$ decreases rapidly with increasing chlorophyll *a* levels, whereas the change in $R(0-)_{706}$ remains fairly stable.

This suggests that for $R(0-)_{676}$ the increase in backscattering is almost compensated by the increase in absorption of chlorophyll *a*. $R(0-)_{706}$ continually increases with increasing concentrations of chlorophyll *a*, the rate of increase decreasing slightly at higher concentrations. Consequently $R(0-)_{706}$ / $R(0-)_{676}$ increases in a similar manner to $R(0-)_{706}$ at higher concentrations of chlorophyll *a*.

The effect of different b_b:b ratios on the ratio $R(0-)_{706}$ / $R(0-)_{676}$ was simulated. Using the same values as for Figure 5.4, $R(0-)_{706}$ / $R(0-)_{676}$ was calculated for b_b:b values of 0.017, 0.030 and 0.047 (Fig. 5.6). Deviations in the ratio are evident at concentrations of approximately 40 µg l^{-1} chlorophyll *a* and greater. This result indicates that $R(0-)_{706}$ / $R(0-)_{676}$ depends significantly on the b_b:b ratio. For example, a $R(0-)_{706}$ / $R(0-)_{676}$ ratio of 2 leads to an estimated chlorophyll *a* concentration of 75 µg l^{-1} chlorophyll *a* for b_b:b = 0.0170 and to 110 µg l^{-1} for b_b:b = 0.047: a difference of 35 µg l^{-1} chlorophyll *a*.

The model was used to investigate the effect of changes in backscattering unrelated to changing phytoplankton concentrations caused, for example, by resuspension of bottom material. The results are presented in Fig. 5.7 where a b_b of 0.1 m^{-1} was added to the backscattering variables in Eqs. 5.3 and 5.5 (thus $b_b = b_b(t) + b_b(ph) + 0.1$). In general, an increase in b_b lowers the ratio $R(0-)_{706}$ / $R(0-)_{676}$. Thus, for turbid tripton-rich waters where b_b:b is usually high, the ratio $R(0-)_{706}$ / $R(0-)_{676}$, will be lowered due to the mitigating effect of chlorophyll *a*-independent backscattering.

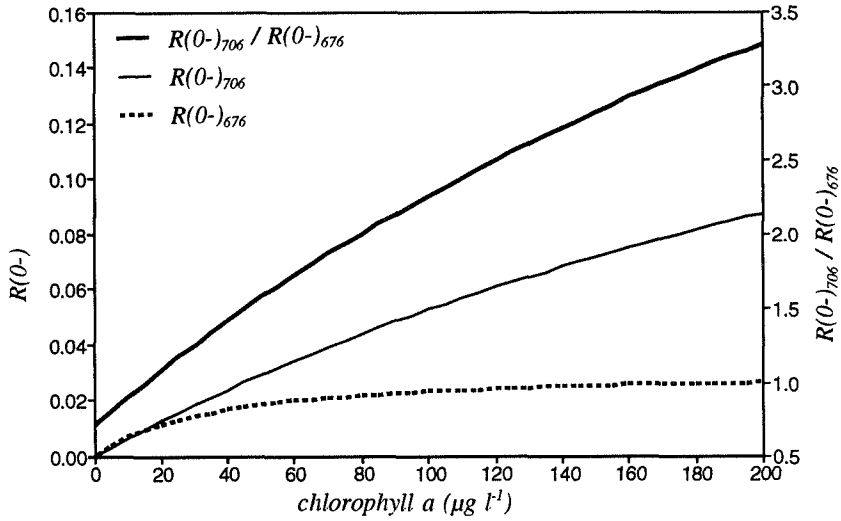

Figure 5.4 *Effect of chlorophyll a on the ratio of $R(0-)_{706}$ / $R(0-)_{676}$ for average values of deep and shallow eutrophic lakes with the chlorophyll a specific absorption a^*_{676} = 0.0164 m^2 mg^{-1}, b = 0.133 * Chlorophyll a, b_b:b = 0.017 and chlorophyll a-correlated $b_{b676}{}^{**}$=0.004 m^2 mg^{-1}, assuming an average a(ah) and a(t) as given in Fig. 5.3.b.*

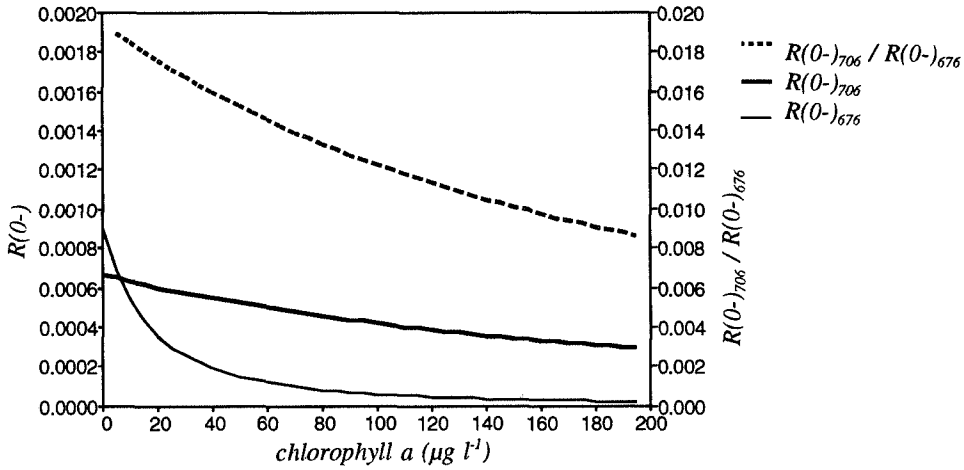

Figure 5.5 *Change in $R(0-)_{676}$, $R(0-)_{706}$ and in the ratio of $R(0-)_{706}$ / $R(0-)_{676}$ caused by adding 1 µg l^{-1} chlorophyll a at continuously increasing chlorophyll a levels.*

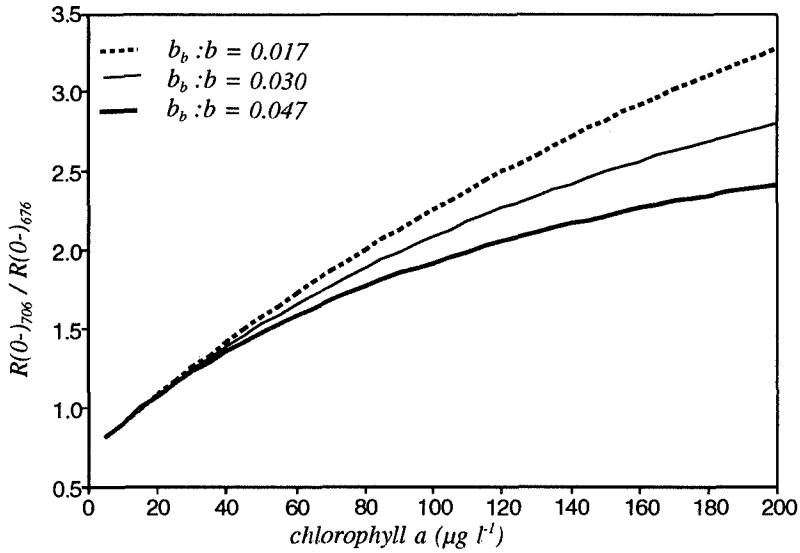

Figure 5.6 *Effect of different b_b:b ratios on the ratio of $R(0-)_{706}$ / $R(0-)_{676}$. Using the same values as for Figure 5.4 the b_b:b values of 0.017, 0.030 and 0.047 were calculated.*

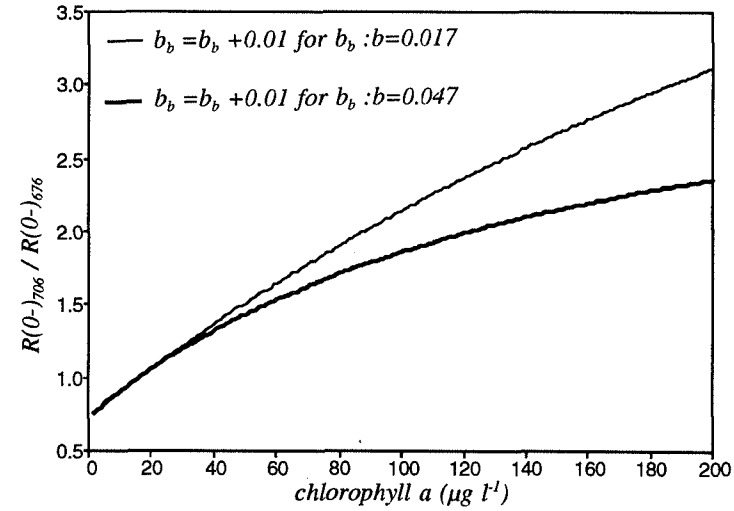

Figure 5.7 *Effect of adding a background backscattering of 0.1 m^{-1} on the ratio of $R(0-)_{706}$ / $R(0-)_{676}$.*

These results are dependent on the accuracy of the determinations of the parameters in the equations and their implied stability with increasing chlorophyll *a* concentration. Nevertheless the simulations confer understanding of the underlying mechanisms involved in the determination of chlorophyll *a* from subsurface irradiance reflectance ratios.

Step 5 Sensitivity of $R(0-)_{676}$ and $R(0-)_{706}$ and the ratio $R(0-)_{706}$ / $R(0-)_{676}$ to variations in a(ah) and a(t).

In order to estimate the sensitivity of $R(0-)_{676}$, $R(0-)_{706}$ and $R(0-)_{706}$ / $R(0-)_{676}$ to variations in aquatic humus and tripton absorption, Eqs. 5.6 and 5.7 were used using the same chlorophyll *a*-related inherent optical property parameters applied for Fig. 5.4. In the first instance the minimum and maximum *a(ah)* and average *a(t)* values were used followed by the minimum and maximum *a(t)* and the average *a(ah)*. The results are shown in Figs. 5.8.a & b.

Variations in *a(t)* and *a(ah)* levels had the most marked effect on $R(0-)_{706}$. $R(0-)_{676}$ is less influenced because absorption by phytoplankton decreases the relative effects of *a(ah)* and *a(t)*. Absorption by phytoplankton does not influence $R(0-)_{706}$, causing reflectance at this waveband to be more sensitive to variations in *a(ah)* and *a(t)*. From Fig. 5.8.a. it may be deduced that the maximum error in chlorophyll *a* estimation caused by variations in *a(ah)* levels is approximately 35 µg l^{-1} at chlorophyll *a* concentrations of 150 - 200 µg l^{-1}.

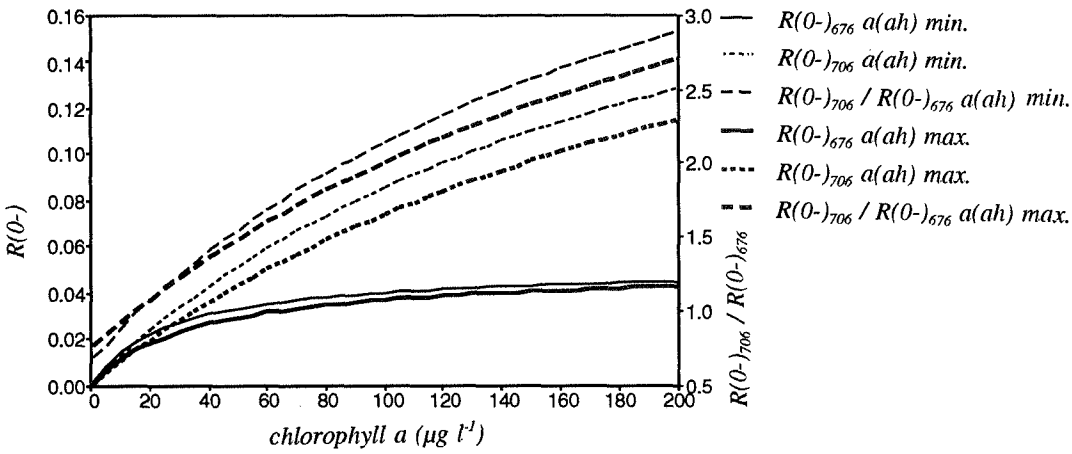

Figure 5.8.a *Effect on $R(0-)_{676}$, $R(0-)_{706}$ and $R(0-)_{706}$ / $R(0-)_{676}$ caused by minimum and maximum values of measured a(ah) at continuously increasing chlorophyll a levels.*

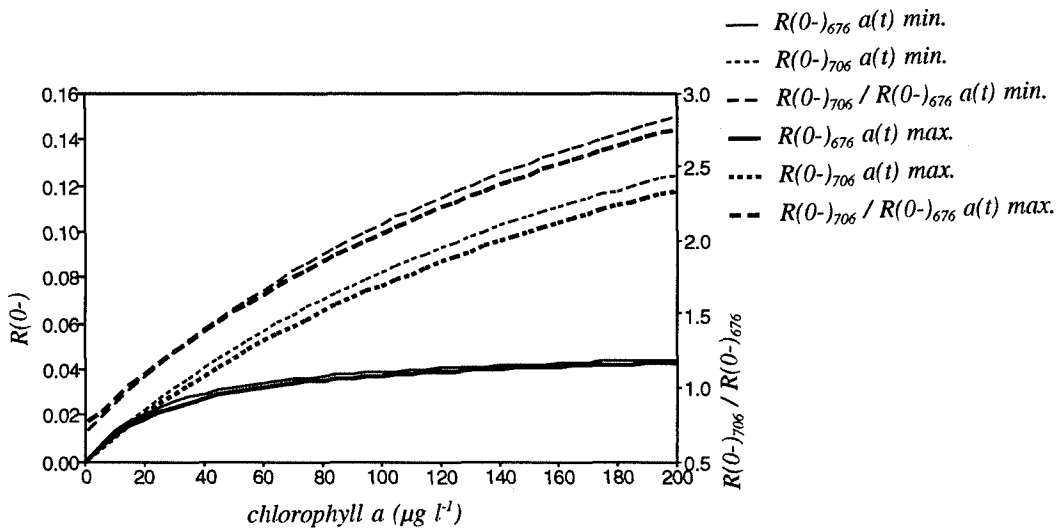

Figure 5.8.b *Effect on $R(0-)_{676}$, $R(0-)_{706}$ and on $R(0-)_{706}$ / $R(0-)_{676}$ caused by minimum and maximum values of estimated a(t) at continuously increasing chlorophyll a levels.*

Similarly, the maximum error for varying tripton levels is 10 µg l^{-1} chlorophyll *a* (Fig. 5.8.b). However, for the waters studied here the maximum error caused by variations in *a(ah)* and *a(t)* will generally be smaller because tripton and aquatic humus appear to vary independently within a waterbody. Furthermore, non-algal correlated scattering will decrease the errors caused by variations in *a(ah)* and *a(t)* as demonstrated before, but will lead to greater errors generally.

It is demonstrated, however, that variations in *a(ah)* and *a(t)* are not negligible at these red to nearby infra-red wavelengths.

Step 6 Determination of optimal spectral band width and location

A narrow spectral band interval of 2 nm, as was used for the previous calculations, can generally only be attained by (imaging) spectrometers. The absolute amount of photons reaching the detector in such a narrow spectral interval is relatively low. Sufficient S/N levels can be obtained through one or more of the following system configurations: an increase in radiometric sensitivity, a decrease in the spatial resolution (thus imaging a larger reflecting surface) or a decrease in spectral resolution.

Increases in radiometric sensitivity may be costly and have the accompanying problem of increased susceptibility to overexposure (mainly caused by land surfaces adjacent to inland water bodies). Decreasing the spatial resolution may not be practical, particularly when remotely sensing inland waters, where the water bodies and the studied features are small. Therefore, provided the accuracy is not severely influenced, the increase in S/N could be reached by using broader spectral bands. Increases in spectral band widths have the additional advantages of being simpler to achieve instrumentally and less susceptible to calibration errors.

The relationship between the chlorophyll *a*-specific absorption at spectral band widths wider than 2 nm and centred at 676 nm was investigated. Spectral a^* was calculated as a function of increasing spectral band width intervals of 2 nm (676±2 nm, 676±4 nm, etc.). The results, presented in Fig. 5.9, indicate that the decrease in a^* with wider spectral band widths is low for band widths up to 10 to 15 nm, beyond which the rate of decrease becomes greater. An optimal spectral band width and location for the chlorophyll *a* absorption peak at 676 nm would therefore be approximately between 670±2 and 682±2 nm.

The width of the spectral band centred at 706 nm will be principally determined by increasing water absorption at infrared wavelengths and decreasing *a(ph)* beyond 676 nm. For the waters studied here the peak in *R(0-)* in this spectral region was found to be located at 698 nm (σ = 8 nm, N = 24) for all samples, at 706 nm (σ = 2 nm, N = 9)

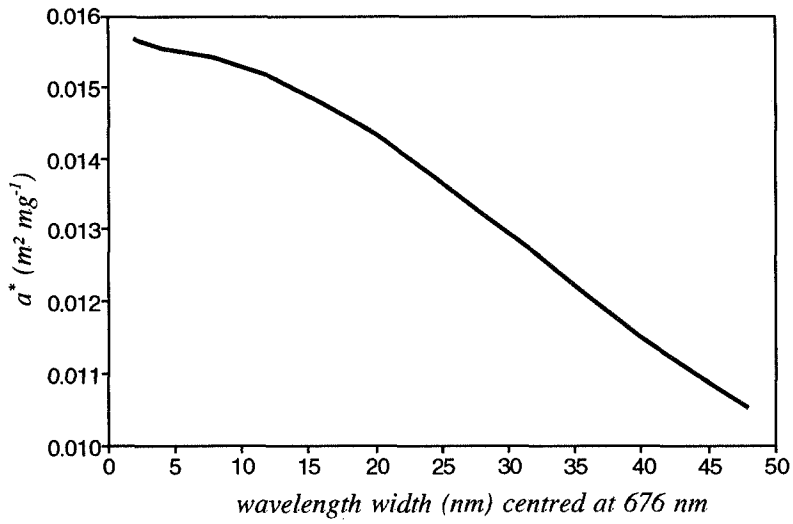

Figure 5.9 *Decrease in chlorophyll a-specific absorption as a function of spectral band width, based on the same samples as used for the calculations given in Fig. 5.1.*

for the shallow eutrophic lakes and at 692 nm (σ = 4 nm, N = 15) for the other lakes and waters. The peak is less pronounced for the shallow mesotrophic and the deep lakes. A choice of 706 minus 8 nm = 698 nm as the lower limit seems appropriate for the lower wavelength boundary; it will incorporate most of the high reflectance peaks without coming too near to chlorophyll *a* absorption shoulders due to high *a(ph)* levels (Fig. 2.7; Fig. 5.1); increases in *a(ah)* and *a(t)* are also avoided. The maximum wavelength for a *R(0-)* peak was 710 nm for Lake Wijde Gat. The main criterion for choosing the actual cutoff position of a long wavelength limit for this spectral band is the water absorption increasing strongly beyond 710 nm. Thus, for reasons of symmetry around the average peak reflectance for eutrophic lakes at 706 nm, the spectral band is chosen at 16 nm wide between 698 and 714 nm.

Step 7 Calculate $R(0-)_{706}$ / $R(0-)_{676}$ with these spectral bands, based on modelled and measured R(0-).

Step 7.a Calculation of $R(0-)_{706}$ / $R(0-)_{676}$ based on the inherent optical properties.

For application of the analytical model $R(0-)_{706}$ / $R(0-)_{676}$ is investigated. Following the general model outlined in Eqs. 5.1 to 5.5, the ratio for the subsurface irradiance reflectance can be calculated from the inherent optical properties by:

$$R(0-)_{706} / R(0-)_{676} = r_1 [b_b / (b_b+a(w)+a(ah)+a(t)+a(ph))]_{706} / r_1 [b_b / (b_b+a(w)+a(ah)+a(t)+a(ph))]_{676} \quad [5.8]$$

Because the aim is to estimate the concentration of chlorophyll *a*, $a(ph)_{676}$ is expressed as:

$$a(ph)_{676} = a^*_{676} C \quad [5.9]$$

where *C* is the chlorophyll *a* concentration. Assuming absorption by chlorophyll *a* is zero at 706 nm equation 5.9 becomes :

$$R(0-)_{706} / R(0-)_{676} = [b_b / (b_b+a(w)+a(ah)+a(t))]_{706} / [b_b / (b_b+a(w)+a(ah)+a(t)+(a^*_{676} C))]_{676} \quad [5.10]$$

Taking the absorption by *a(w)+a(ah)+a(t)* at both wavelengths to be independent of the chlorophyll *a* absorption, *a(w)+a(ah)+a(t)* is represented by *a(r)*. Solving equation 5.10 for *C* (as given in Appendix C):

$$C = [R(0-)_{706} b_{b676} (b_b+a(r))_{706})] / [(R(0-)_{676} b_{b706} a^*_{676}-(b_b+a(r))_{676})) / (a^*_{676})] \quad [5.11]$$

The value a^*_{676} was taken to be 0.0164 m^2 mg^{-1} for the average of the deep and shallow eutrophic lakes from Table 2.6. This value was assumed to be the most accurate because the tripton absorption was relatively low in these waters thus providing a more reliable estimate of a^*_{676}.

Table 5.5 *Results from the bivariate linear regression equations for estimating chlorophyll a concentration from equation 5.11, based upon the inherent optical properties:* a^*_{676} *= 0.0164 m² mg⁻¹ for the average of deep and shallow eutrophic lakes and* a^*_{676} *= 0.0180 m² mg⁻¹ for the average of the shallow eutrophic lakes, taken from Table 2.6;* C_{est} *= estimated chlorophyll a concentration in μg l⁻¹;* C_{meas} *is the measured chlorophyll a concentration in μg l⁻¹;* $S_{y\cdot}$ *is the standard error of estimate of Chlorophyll a in μg l⁻¹; N = 19; (Fig. 5.10 shows the data).*

	r^2	$S_{y\cdot}$
for a^*_{676} = 0.0164 m² mg^{-1}		
C_{est} = -3.2 + 1.04 C_{meas}	0.95	12.4
with a forced zero intercept: C_{est} = 1.01 C_{meas}	0.95	12.2
for a^*_{676} = 0.0180 m² mg^{-1}		
C_{est} = -2.9 + 0.95 C_{meas}	0.95	11.3
with a forced zero intercept: C_{est} = 0.92 C_{meas}	0.95	11.2

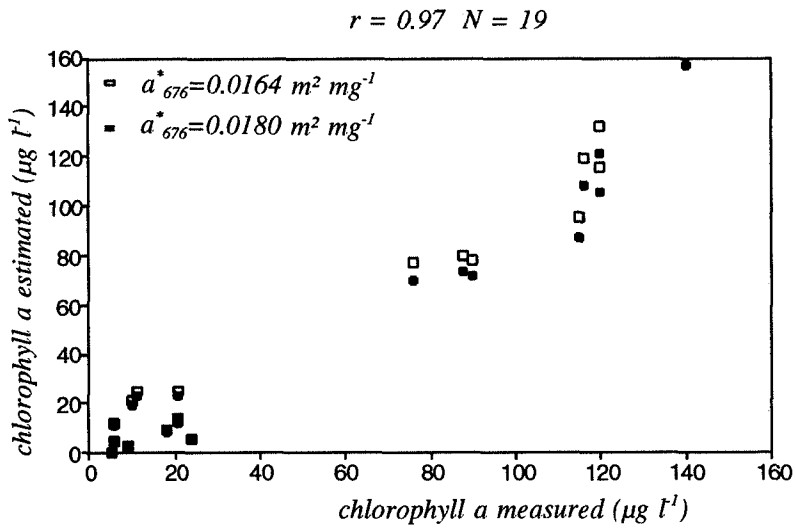

Figure 5.10 *Estimated and measured concentrations of chlorophyll a using the regression equations given in Table 5.5. Values used for* a^*_{676} *were 0.0164 and 0.0180 m² mg⁻¹.*

Table 5.5 and Fig. 5.10 show a high correlation ($r^2 = 0.95$) between the calculated and measured values for *C*. Also evident is the low value that the Y-intercept had on the regression equation and correlation results. If the measured chlorophyll *a* values are considered to be independent and correct, chlorophyll *a* concentrations may be estimated through calculations of $R(0-)_{706} / R(0-)_{676}$ (at 2 nm resolution) using equation 5.4 with an accuracy of 12.2 µg l^{-1} (average a^*_{676} is 0.0164 m^2 mg^{-1} and a forced Y-axis intercept of zero). The X-coefficient of 1.01 is closest to unity for this equation.

It should be noted, however, that the assumption that the measured chlorophyll *a* is independent is incorrect because the chlorophyll analysis produces its own errors (§ 1). Part of the error in the estimation of *C* may arise from errors in the measurement of chlorophyll *a*.

Step 7.b *Chlorophyll a concentration from values of $R(0-)_{706} / R(0-)_{676}$ derived from the spectroradiometric measurements.*

Using *R(0-)* derived from the *in situ* spectroradiometric measurements (§ 3), regression equations for $R(0-)_{706} / R(0-)_{676}$ as a function of measured chlorophyll *a* concentration were calculated. The inversion of this equation was also studied since remote sensing data will be used to estimate chlorophyll *a* concentrations. Table 5.6 and Fig. 5.11 give the results of the linear regression equations between chlorophyll *a* and the measured $R(0-)_{706} / R(0-)_{676}$. Because remote sensing data were acquired with spectral bands of the CAESAR Inland Water Mode spectral bandset, the spectral bands 7 (671-684 nm) and 8 (698-714 nm) were also simulated and regressed against chlorophyll (Table 5.6).

Chlorophyll *a* can be estimated from the *in situ* measurements of $R(0-)_{706} / R(0-)_{676}$ with an accuracy of 9.64 µg l^{-1}, with $r^2 = 0.96$. The results are slightly improved by using wider spectral band widths close to those proposed in Step 6 and equivalent to the CAESAR Inland Water Mode spectral bands.

The regression results for measured $R(0-)_{706} / R(0-)_{676}$ with chlorophyll *a* concentrations are slightly higher than for the modelled $R(0-)_{706} / R(0-)_{676}$ values. This may be caused by:

1) errors in the spectrophotometric measurements and analysis as discussed in § 2;
2) incorrect assumptions concerning spectral invariability of the r_1 coefficient in Eq. 5.1;
3) errors caused by assuming a^*_{706} to be zero and the error in assuming a chlorophyll *a*-correlated specific backscattering coefficient.

Table 5.6 *Results from the bivariate linear regression equations for estimating in situ spectro-radiometric derived $R(0-)_{706}$ / $R(0-)_{676}$ from chlorophyll a concentrations, and the inverse equation at 2 nm spectral band width and at the optimal spectral band width for remote sensing, slightly modified to fit the full width half peak (FWHP) dimensions of the CAESAR Inland Water Mode spectral bands. Fig. 5.11 shows the data); N=19.*

		r^2	$S_{y'}$
$R(0-)_{706}$ / $R(0-)_{676}$	= 0.75 + 0.0145 C_{meas}	0.96	0.142
C_{meas}	= -48.2 + 66.5 $R(0-)_{706}$ / $R(0-)_{676}$	0.96	9.64
For CAESAR spectral bands $R(0-)_{671-684}$ and $R(0-)_{698-714}$			
$R(0-)_{698-714}$ / $R(0-)_{671-684}$	= 0.78 + 0.0123 C_{meas}	0.97	0.118
C_{meas}	= -59.0 + 78.9 $R(0-)_{698-714}$ / $R(0-)_{671-684}$	0.97	9.47

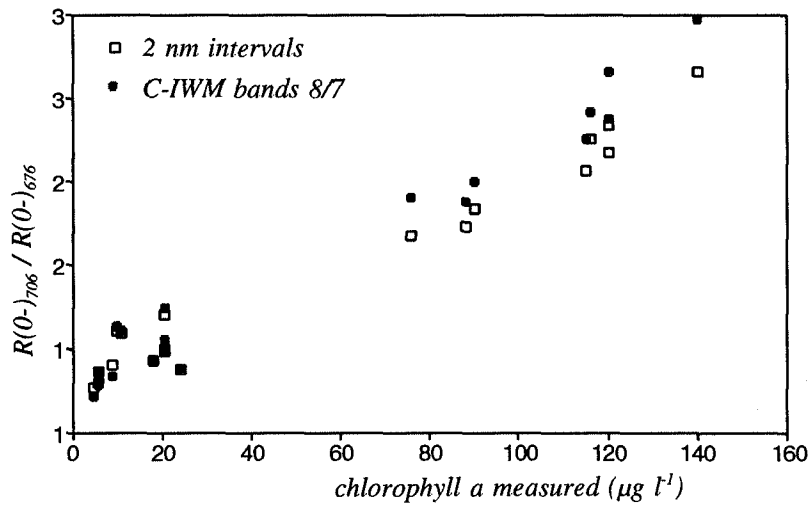

Figure 5.11 *Relationship between in situ measured $R(0-)_{706}$ / $R(0-)_{676}$ and measured chlorophyll a concentrations. Table 5.6. presents results of the regression equations describing this relationship.*

5.3.2 *Calculation of required signal-to-noise ratio for the estimation of 1 µg l^{-1} chlorophyll a*

For remote sensing applications it is desirable to know what sensitivity a remote sensor must have to obtain the required accuracy for the estimation of a water quality parameter, in this case chlorophyll *a*. The equations were used to calculate the required S/N performance of a remote sensing instrument, because *R(0-)* is related to L_{rs} as described in § 3. A useful parameter for the expression of the S/N ratio for remote sensing purposes is the noise equivalent reflectance difference (δR), which is defined here as the reflectance difference necessary to discriminate 1 µg l^{-1} chlorophyll *a* (see § 6). The subsurface irradiance reflectance difference ($\delta R(0-)$), necessary to discriminate 1 µg l^{-1} chlorophyll *a*, was first determined.

For the average values of the lakes with:
a^*_{676} = 0.0164 m^2 mg^{-1}
b = 0.133 C
$b_b:b$ = 0.017
b_b676^{**} = 0.0023 m^2 mg^{-1}
assuming an average *a(ah)* and *a(t)* as given in Fig. 5.3.b, the $\delta R(0-)$ was calculated for $R(0-)_{706}$, $R(0-)_{676}$ and the ratio $R(0-)_{706}$ / $R(0-)_{676}$. The results are given in Fig. 5.7. It is necessary to define the range in *R(0-)* to be measured by a (remote) sensor to determine the required signal-to-noise expressed as the $\delta R(0-)$. For example, if a sensor must measure 0 - 100 % or 0 - 20% reflectance this will change the required $\delta R(0-)$ by a factor of 5. If a range in $R(0-)_{676,706}$ of 0 - 20 %, considered to be the maximum value for *R(0-)* encountered in the waters studied here (see Fig. 3.4.a & b), needs to be estimated this would require:

Simulation for $b_b:b$ = 0.0170 based on Eqs. 5.6 and 5.7

S/N ratio of a spectral band at 676 nm to be
20 / 0.09% = 220:1 at low concentrations of chlorophyll *a*
20 / 0.002% = 10000:1 at high concentrations of chlorophyll *a*.
(these values may be directly derived from Fig. 5.7)

S/N ratio of a spectral band at 706 nm to be
20 / 0.07% = 390:1 at low concentrations of chlorophyll *a*
20 / 0.03% = 670:1 at high concentrations of chlorophyll *a*.

Because the ratio is more dependent on an increase in *R(0-)* at 706 nm than at 676 nm, a S/N of slightly more than 700:1 will be required to estimate 1 µg l^{-1} chlorophyll *a* from low to high concentrations under the assumption that the inherent optical properties as a function of chlorophyll *a* concentration are invariable and correct.

The same simulation was performed with b_b:b = 0.030 :

Simulation for b_b:b = 0.030 based on Eqs. 5.6 and 5.7

S/N ratio of a spectral band at 676 nm to be
20 / 0.16% = 125:1 at low concentrations of chlorophyll *a*
20 / 0.005% = 4000:1 at high concentrations of chlorophyll *a*.

S/N ratio of a spectral band at *706* nm to be
20 / 0.12% = 167:1 at low concentrations of chlorophyll *a*
20 / 0.04% = 500:1 at high concentrations of chlorophyll *a*.

Because the ratio is more dependent on an increase in *R(0-)* at 706 nm than at 676 nm, a S/N of slightly more than 500:1 will be required to estimate 1 µg l^{-1} chlorophyll *a* from low to high concentrations under the assumption that the inherent optical properties as a function of chlorophyll *a* concentration are invariable and correct.

5.3.3 *Conclusions and recommendations*

It was possible to determine algorithms for estimation of chlorophyll *a* concentrations based on the analytical method. The algorithm uses *R(0-)* as the independent variable. Because *R(0-)* is relatively stable under varying solar angles, atmospheric conditions and states of the water surface, these algorithms have a multitemporal validity. The analytical model allows calculation of the sensitivity of the algorithm to varying values of the non-chlorophyllous optically active water constituents. It also allows calculation of required signal-to-noise levels for measuring a unit quantity of chlorophyll *a*.

A method was developed involving seven steps for applying the analytical model to the determination of chlorophyll *a*. It involved the determination of:

- spectral location(s) of absorption maxima and minima of chlorophyll *a*
  chlorophyll *a*-specific absorption coefficients and chlorophyll *a*-correlated (back)scattering coefficients
  spectral absorption and (back)scattering of all non-chlorophyllous components.

Using this information the effects could be calculated of varying dimensions of any of the input parameters on the ratio $R(0\text{-})_{706}$ / $R(0\text{-})_{676}$, based on both modelled and measured values of $R(0\text{-})_{706}$ and $R(0\text{-})_{676}$.

It was calculated that the average values for absorption of *a(w)*, *a(ah)* and *a(t)* are together equivalent to the absorption of 38 µg l^{-1} chlorophyll *a*. With increasing concentrations of chlorophyll *a* $R(0\text{-})_{676}$ remained fairly constant whereas $R(0\text{-})_{706}$ values increased with increasing chlorophyll *a*-correlated backscattering values.

b_b:b ratios were calculated. The values varied between the water types from 0.017 for the shallow eutrophic lakes to 0.047 for the river and canal samples. These values for b_b:b demonstrate that the volume scattering functions for these inland waters are also highly variable. The effect of this range of b_b:b on the calculation of chlorophyll *a* by the algorithm was estimated to be 35% at approximately 100 µg l^{-1} chlorophyll *a* concentration levels. Similar calculations for the effect of maximum and minimum *a(ah)* and *a(t)* showed errors in estimation of chlorophyll *a* of 20% and 5% respectively.

The value for chlorophyll *a*-specific absorption: a^*_{676} was taken to be 0.0164 m^2 mg^{-1} for the average of the deep and shallow eutrophic lakes. A high correlation (r^2 = 0.95) occurred between the calculated and measured values for chlorophyll *a* concentration using the algorithm. Chlorophyll *a* concentrations may be estimated through calculations of $R(0\text{-})_{706}$ / $R(0\text{-})_{676}$ (at 2 nm resolution) based on modelled *R(0-)* with an accuracy of 12.2 µg l^{-1} and based on the *in situ* measured *R(0-)* values with an accuracy of 9.64 µg l^{-1}. For the eutrophic lakes these accuracies are of the same order of magnitude as the accuracies for the laboratory-based chlorophyll *a* measurements of the samples, which was approximately 10% (see § 1).

For application in remote sensing, appropriate spectral band widths were determined to be 670±2 to 682±2 nm and 698 to 714 nm. Algorithm calculations showed little influence on estimation of chlorophyll *a* concentrations using these wider spectral bands. Signal-to-noise ratios for *R(0-)* required for the estimation of 1 µg l^{-1} chlorophyll *a* were calculated to be 700:1 for b_b:b = 0.017 and 500:1 for b_b:b = 0.030 (under the assumption that only 0-20 % reflectance will cover the entire required radiometric sensitivity range of a sensor).

Improvements to the results obtained using an analytical model such as presented in this study may be achieved by:

- increased knowledge of the chlorophyll *a*-specific inherent optical properties of the algal species abundant in these lakes; the empirically derived chlorophyll *a*-correlated backscattering coefficient should be replaced by a chlorophyll *a*-specific backscattering coefficient, preferably for each main algal species occurring in these waters. More reliable estimates at low concentrations of chlorophyll *a* may then be made;
  increasing the accuracy of the chlorophyll *a* measurements for samples in the laboratory. For the northern Vecht lakes and the Amsterdam-Rijn Kanaal and the River Vecht the chlorophyll *a* determinations were single measurements, thus preventing an assessment of accuracy. Triple measurements of chlorophyll *a* per sample are recommended.

The regression equations for the 2 nm fieldspectroradiometric data should be directly applicable to the remote sensing data acquired with the CASI instrument in spectral mode. The regression equations for the CAESAR Inland Water Mode bands 7 and 8 should be directly applicable to the remote sensing data acquired with CAESAR on 3 September 1990 and to the data acquired with the CASI imaging spectrometer operating

in spatial mode with a similar Inland Water Mode spectral band setting on 14 September 1990.

First, however, the *R(0-)* will have to be determined from the L_{rs} data following the method presented in § 3. Results of applying the algorithms (§ 5 : Table 5.6) to the remote sensing data are presented in § 6.

5.4 The analytical model applied to the estimation of CP-cyanin

5.4.1 The algorithm for CP-cyanin estimation from *R(0-)*

CP-cyanin-specific spectral absorption coefficients (a^*_{624}) were calculated for 8 samples and are displayed in Table 2.7. The average a^*_{624} of 0.0032 m^2 mg^{-1} was approximately 5 times lower than the chlorophyll *a*-specific absorption (a^*_{676}). The method for the calculation of a^*_{624} was different from that used for calculating a^*_{676} because CP-cyanin absorption is superimposed on the red absorption shoulder of chlorophyll *a*, and on accessory pigment absorption such as allophycocyanin *B* (with an *in vitro* absorption peak at 618 nm: Kirk, 1983), chlorophyll *c* (*in vitro* absorption peak at 628 nm: Korthals & Steenbergen, 1985) and chlorophyll *b* (*in vitro* absorption peak at 643 nm: Burger-Wiersma *et al.*, 1986; or at 645 nm: Korthals & Steenbergen, 1985).

The change in a^*_{624} with increasing spectral band width was calculated using the average spectral a^*_{624} for the 8 samples (Fig. 5.12). As for chlorophyll *a*, CP-cyanin-specific absorption decreased more rapidly at band widths larger than 10 to 15 nm, indicating an initial limit to a spectral band width for potential use in a remote sensing algorithm.

CP-cyanin contents of other samples for which *a(ph)* spectra were available were calculated by dividing the result of subtraction of the baseline value over 600 to 648 nm from the *a(ph)* value (see § 2), by the value of a^*_{624} = 0.0032 m^2 mg^{-1} (Figure 5.13 and Table 5.7). Of the 27 samples 16 contained 5 µg l^{-1} or more CP-cyanin. Thus, this data set of 16 samples was available for further analysis. This increased number of samples allowed an expansion of the available *R(0-)* spectra for developing a CP-cyanin algorithm.

Other factors which absorb in the 600 to 648 nm spectral region are not only chlorophyll *a* and accessory pigments as detailed above, but also water, aquatic humus and tripton (Fig. 5.3.a & b). Figure 5.12 shows that the maximum CP-absorption at *624* nm is approximately 0.4 m^{-1} which is similar to the maximum absorption of *a(ah)*, *a(t)* and *a(w)*; all in the range of 0.35 to 0.39 m^{-1}. This indicates that absorption by these extraneous parameters will have a strong influence on a ratio for the estimation of CP-cyanin absorption using a spectral band centred at 648 nm and at 624 nm as proposed by Dekker *et al.* (1992a). The slopes of these non-CP-cyanin absorption features will therefore introduce errors in remote sensing algorithms for estimating CP-cyanin concentrations based on spectral band ratios.

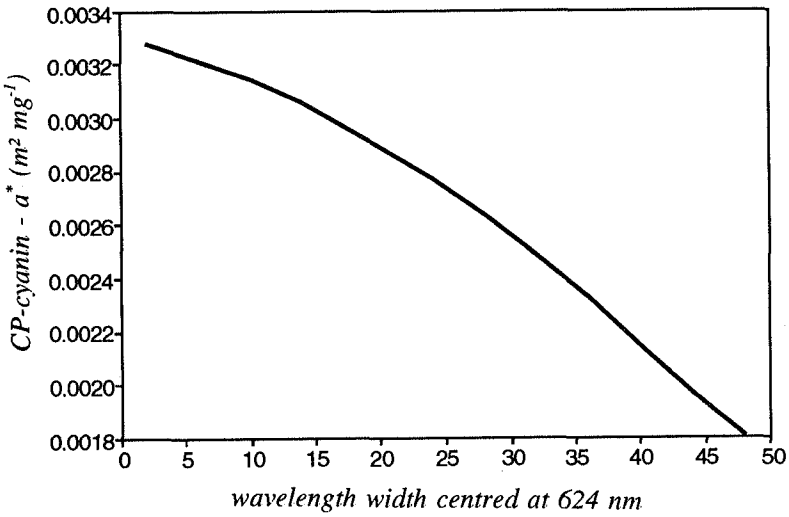

Figure 5.12 *Decrease in CP-cyanin-specific absorption as a function of band width, based on the same samples given in Table 5.7.*

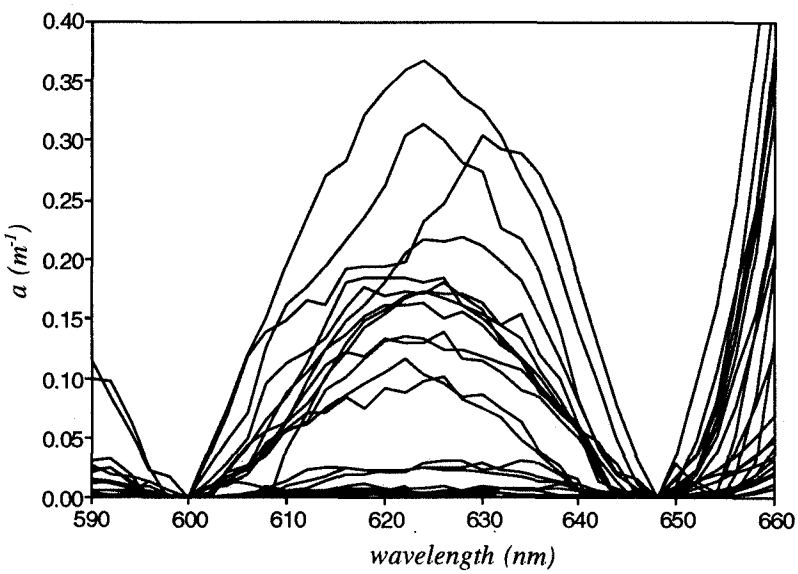

Figure 5.13 *Absorption by CP-cyanin calculated from the a(ph) spectra of 27 samples after a baseline subtraction from 600 to 648 nm.*

Table 5.7 *Measured values of CP-cyanin for the 8 samples of Table 2.7 (marked with an *) and the 8 samples for which a CP-cyanin pigment concentration was calculated based on a CP-cyanin-specific absorption of 0.0032 m^2 mg^{-1}.*

	Measured CP-cyanin µg l^{-1}	Date of sampling CP-cyanin measurement	Calculated CP-cyanin µg l^{-1}	Date of sampling for *a(ph)* measurement
LNB	130	12 Sep	96	12 Sep
LHA	110	"	51	12 Sep
LSA	7		7	12 Sep
LWG	92		67	28 Aug
LWB1	110		113	28 Aug
LWL1	8		29	03 Sep
LVU	38		66	10 Sep
LLO	49		53	10 Sep
LBR	46	"	53	10 Sep

Calculated CP-cyanin (µg l^{-1}) by applying the average CP-specific a^*_{624} of 0.0032 m^2 mg^{-1} to the *a(ph)* measurements

	Calculated CP-cyanin µg l^{-1}	Date of sampling for *a(ph)* measurement
LEL1	42	03 Sep
LEL2	40	03 Sep
LEL3	34	10 Sep
LWB3	8	10 Sep
LWL2	53	03 Sep
HIK	57	28 Aug
LWB2	7	28 Aug

For the development of a multitemporally valid remote sensing algorithm for CP-cyanin the influence of CP-cyanin concentration on *R(0-)* over the wavelength region of interest should be investigated. However, this would require a value for the increase in backscattering associated with an increase in cyanobacterial concentrations as expressed through the CP-cyanin concentration; the CP-cyanin-specific backscattering at 624 nm. As mentioned earlier, no information was available on the scattering and backscattering properties of the dominant algae in the lakes studied and thus the CP-cyanin-specific backscattering could not be determined.

It was also not possible to calculate a CP-cyanin-correlated backscattering through correlation with chlorophyll *a*-correlated backscattering, because a change in cyanobacterial CP-cyanin concentration may not necessarily imply a similar change in chlorophyll *a* concentration, due to changes in species composition. For example, a lake with a high *Prochlorothrix hollandica* to *Oscillatoria spp.* content may have a similar CP-cyanin pigment concentration to a lake without *P. hollandica* but with a low level of *Oscillatoria* (*P. hollandica does not contain any CP-cyanin*). Thus *in situ* CP-cyanin concentration changes may not necessarily be related to variations in scattering.

An alternative method to a spectral band ratio is proposed for the determination of CP-cyanin concentrations from *R(0-)* data. This method also enables calculation of the effect of variations in CP-cyanin on *R(0-)*. The basis of the method is the determination of the decrease in subsurface irradiance reflectance at *624* nm ($R(0-)_{624}$), caused by increasing CP-cyanin concentrations. In order to obtain an absolute value for this decrease, two spectral bands, located as close as possible to but not influenced by CP-cyanin absorption were defined. Based on initial work by Dekker *et al.* (1992a) and on the calculation of CP-cyanin-specific absorption (§ 2) and CP-cyanin spectral absorption (Fig. 5.12), the wavelengths chosen were located at 600 and at 648 nm.

A method for the determination of reflectance decrease due to an increase in the concentration of CP-cyanin ($C_{CP\text{-}cyanin}$) is proposed as the difference between the average value of $R(0-)_{600}$ and $R(0-)_{648}$ and the $R(0-)_{624}$ value:

$$C_{CP\text{-}cyanin} = f(0.5\ (R(0-)_{600}+R(0-)_{648})-R(0-)_{624}) \qquad [5.12]$$

The result of this algorithm will be less influenced by the spectral absorption and scattering slopes caused by parameters unrelated to CP-cyanin than a two-band spectral ratio of $R(0-)_{648}$ / $R(0-)_{624}$. A two-band spectral ratio at these wavelengths could, in theory, produce ambiguous results because a ratio may have similar values at low and high *R(0-)* values. This is less likely for the chlorophyll *a* algorithm based on spectral band ratios, because of the higher constant value of water absorption and the higher chlorophyll *a*-specific absorption as well as lower aquatic humus and tripton absorption levels at 676 and 706 nm.

One drawback of the proposed algorithm for CP-cyanin is the influence of the coefficient r_1 (necessary for calculating *R(0-)* from the inherent optical properties, see Eq. 4.5 and 5.1), which in this case will not be divided to unity through ratioing. Another disadvantage over a two-band spectral ratio is that another band is added to the algorithm, contributing to the total uncorrelated noise in the algorithm.

With the appropriate spectral locations and the CP-cyanin-specific absorption coefficients it is possible to calculate the effect of an increase of CP-cyanin on *R(0-)* at the three bands using the equations:

$$R(0\text{-})_{624} = r_l\ [b_b / (b_b + a(r) + (a^*_{624}\ C))]_{624} \quad [5.13a]$$
$$R(0\text{-})_{600} = r_l\ [b_b / (b_b + a(r))]_{600} \quad [5.13b]$$
$$R(0\text{-})_{648} = r_l\ [b_b / (b_b + a(r))]_{648} \quad [5.13c]$$

where $a(r)$ is the average absorption by aquatic humus, tripton, water and phytoplankton (minus the CP-cyanin absorption) and b was taken as the average scattering coefficient, all calculated from the average values for 10 shallow eutrophic lake samples. This simulation was thus based on the assumption that the only change taking place is an increase by CP-cyanin, analogous to an increasing *Oscillatoria spp.* to *P. hollandica* ratio as may occur in some of the shallow lakes in the study area.

The effect of an increase in CP-cyanin concentration on the algorithm

$$0.5\ (R(0\text{-})_{600} + R(0\text{-})_{648}) - R(0\text{-})_{624}$$

was subsequently determined (Fig. 5.14). As expected, the values of the algorithm increased proportionally with the increase in concentration of CP-cyanin. The change in the algorithm could be described by a linear function:

$$C_{CP\text{-}cyanin} = -24.6 + 13686\ (0.5\ (R(0\text{-})_{600}+R(0\text{-})_{648})-R(0\text{-})_{624}) \quad [5.14]$$

with a $r^2 = 0.996$ and $S_{y\cdot} = 2.34\ \mu g\ l^{-1}$.

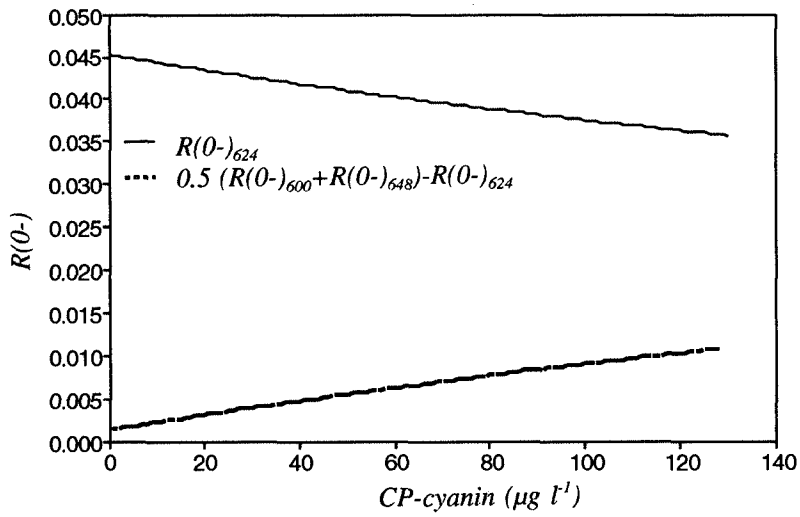

Figure 5.14 *R(0-) at 624 nm and values for the proposed algorithm equation: 0.5 $(R(0\text{-})_{600}$ + $R(0\text{-})_{648})$ - $R(0\text{-})_{624}$ as a function of increasing CP-cyanin levels, assuming an average scattering and absorption for water, aquatic humus, tripton and phytoplankton (from which the CP-cyanin has been subtracted) calculated for 10 of the shallow eutrophic lake samples.*

Table 5.8 *Bivariate linear regression equations for the determination of $C_{CP\text{-}cyanin}$ from $(0.5\ (R(0\text{-})_{600} + R(0\text{-})_{648}) - R(0\text{-})_{624})$ as a function of increasing CP-cyanin levels with varying non CP-cyanin related inherent optical properties. Except for the inherent optical property that was varied, the average values of the inherent optical properties for the 10 shallow eutrophic lakes were used.*

	$a(ah)$ (m^{-1})			
	minimum	maximum		
600 nm	0.25	0.41		
624 nm	0.19	0.34		
648 nm	0.15	0.25		
			r^2	$S_{y'}$
$a(ah)$ minimum: $C_{CP\text{-}cyanin} = -22.9 + 12790\ (0.5\ (R(0\text{-})_{600}+R(0\text{-})_{648})-R(0\text{-})_{624})$			0.996	2.42
$a(ah)$ maximum: $C_{CP\text{-}cyanin} = -27.9 + 5071\ (0.5\ (R(0\text{-})_{600}+R(0\text{-})_{648})-R(0\text{-})_{624})$			0.997	2.23

	$a(ph)$ (m^{-1})			
	minimum	maximum		
600 nm	0.29	0.93		
624 nm	0.34	1.07		
648 nm	0.39	1.22		
			r^2	$S_{y'}$
$a(ph)$ minimum: $C_{CP\text{-}cyanin} = -23.7 + 9336\ (0.5\ (R(0\text{-})_{600}+R(0\text{-})_{648})-R(0\text{-})_{624})$			0.994	2.83
$a(ph)$ maximum: $C_{CP\text{-}cyanin} = -28.3 + 21202\ (0.5\ (R(0\text{-})_{600}+R(0\text{-})_{648})-R(0\text{-})_{624})$			0.998	1.88

	b_b (m^{-1})			
	minimum	maximum		
600 nm	0.22	0.54		
624 nm	0.20	0.51		
648 nm	0.19	0.48		
			r^2	$S_{y'}$
b_b minimum: $C_{CP\text{-}cyanin} = -34.7 + 17491\ (0.5\ (R(0\text{-})_{600}+R(0\text{-})_{648})-R(0\text{-})_{624})$			0.996	2.45
b_b maximum: $C_{CP\text{-}cyanin} = -13.9 + 9621\ (0.5\ (R(0\text{-})_{600}+R(0\text{-})_{648})-R(0\text{-})_{624})$			0.997	2.07

The sensitivity of this algorithm to varying levels of $a(ah)$, $a(t)$ and $a(ph)$ and to scattering was determined by calculating the same regression equation but with inherent optical properties varying between the lowest and the highest values occurring in the shallow eutrophic lake samples. The results are presented in Table 5.8 and Figure 5.15.

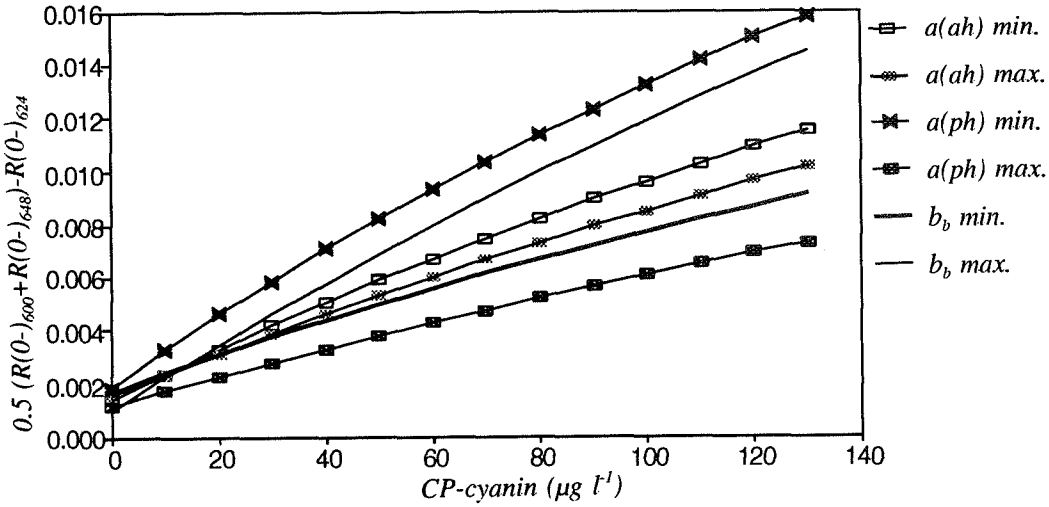

Figure 5.15 *Results from the algorithm* $C_{CP\text{-}cyanin} = 0.5\ (R(0\text{-})_{600} + R(0\text{-})_{648}) - R(0\text{-})_{624}$ *as a function of the range of inherent optical properties measured for 10 shallow eutrophic lakes; the inherent optical properties are averaged values except for the subject inherent optical property for which the minimum and maximum values were taken (see Table 5.8 for regression equations and results and the range of inherent optical properties).*

The regression equations for varying *a(t)* were not calculated because *a(t)* was similar to *a(ah)* at approximately one-third of the aquatic humus concentration. Changes in the algorithm due to *a(ah)* were low compared to the changes caused by variations in *a(ph)* and by b_b. Variations in *a(ph)* had the most marked effect on the values obtained from the algorithm. The slope of the relationship decreased with increasing phytoplankton contents; this also occurred for increasing *a(t)*, *a(ah)* and decreasing b_b. These changes can be explained by the fact that as the sum of the absorption and scattering components in the denominator of the equation increases, the relative effect of an addition of CP-cyanin absorption diminishes. A consequence is that a sensor will require increased sensitivity to distinguish similar levels of CP-cyanin in water bodies with high absorption and scattering values caused by non-CP-cyanin optical water quality parameters.

The implication of a strong dependence of the X-coefficient on phytoplankton absorption is that if a high accuracy is desired for CP-cyanin concentration retrieval prior to applying a CP-cyanin algorithm as proposed here, the phytoplankton concentration needs to be determined. This is also true for the influence of varying backscattering levels.

Determination of spectral band width

Following the same method, regression equations were calculated to determine the effect of wider spectral bands on the algorithm. Band width was varied from a 2 nm wide band at 600, 624 and 648 nm (Eq. 5.14) by adding 2 nm to both sides of the bands: 598-602, 622-626 and 646-650 nm, and so on. CP-cyanin-specific absorption was taken from the values used for calculating Fig. 5.13 for each of the band widths chosen. The CAESAR and CASI Inland Water Mode bands were also simulated in this manner. The results are given in Table 5.9.

Table 5.9 *Bivariate linear regression equations for the determination of $C_{CP\text{-}cyanin}$ from $(0.5 * (R(0\text{-})_{\lambda 1} + R(0\text{-})_{\lambda 2}) - R(0\text{-})_{\lambda 3})$ as a function of increasing CP-cyanin levels with increasing spectral band width and with simulated bands of the CAESAR and CASI Inland Water Mode spectral bands. The average values of the inherent optical properties for the 10 shallow eutrophic lakes were used.*

Band-width (nm)	$\lambda 1$ (nm)	$\lambda 2$ (nm)	$\lambda 3$ (nm)	a^*_{624} (m^2 mg^{-1})
4	598..602	622..626	646..650	0.00321
8	596..604	620..628	644..652	0.00315
12	594..606	618..630	642..654	0.00308
16	592..608	616..632	640..656	0.00294
	B3	B4	B5	
CAESAR Inland Water Mode				
	592..610	620..641	645..654	0.00271
CASI Inland Water Mode				
	592..610	624..640	645..652	0.00264

		r^2	$S_{y'}$ (μg l^{-1})
2	$C_{CP\text{-}cyanin} = -24.6 + 13686\ (0.5\ (R(0\text{-})_{\lambda 1}+R(0\text{-})_{\lambda 3})\text{-}R(0\text{-})_{\lambda 2})$	0.996	2.34
4	$C_{CP\text{-}cyanin} = -22.6 + 13654\ (0.5\ (R(0\text{-})_{\lambda 1}+R(0\text{-})_{\lambda 3})\text{-}R(0\text{-})_{\lambda 2})$	0.996	2.34
8	$C_{CP\text{-}cyanin} = -21.8 + 13839\ (0.5\ (R(0\text{-})_{\lambda 1}+R(0\text{-})_{\lambda 3})\text{-}R(0\text{-})_{\lambda 2})$	0.996	2.30
12	$C_{CP\text{-}cyanin} = -20.3 + 14103\ (0.5\ (R(0\text{-})_{\lambda 1}+R(0\text{-})_{\lambda 3})\text{-}R(0\text{-})_{\lambda 2})$	0.996	2.26
16	$C_{CP\text{-}cyanin} = -17.1 + 14648\ (0.5\ (R(0\text{-})_{\lambda 1}+R(0\text{-})_{\lambda 3})\text{-}R(0\text{-})_{\lambda 2})$	0.997	2.16
CAESAR Inland Water Mode:			
	$C_{CP\text{-}cyanin} = -28.1 + 15904\ (0.5\ (R(0\text{-})_{\lambda 1}+R(0\text{-})_{\lambda 3})\text{-}R(0\text{-})_{\lambda 2})$	0.997	2.00
CASI Inland Water Mode:			
	$C_{CP\text{-}cyanin} = -28.1 + 15904\ (0.5\ (R(0\text{-})_{\lambda 1}+R(0\text{-})_{\lambda 3})\text{-}R(0\text{-})_{\lambda 2})$	0.997	1.96

For spectral bands up to and including 12 nm intervals the results remain fairly constant. At wider spectral band intervals the slope changes rapidly and the constant decreases. The regression equation results for the CAESAR and CASI simulated bands show a high constant and a steep slope compared to spectral bands centered at the chosen wavelengths. At the time of development of the CAESAR Inland Water Mode band set, information was not available on the *in situ* absorption peak of CP-cyanin and therefore the spectral bands in this region were not changed from the original CAESAR Sea Mode spectral band set (Dekker *et al.*, 1992b). For comparison purposes the CASI was flown in 1990 with spectral bands simulating the CAESAR Inland Water Mode. On the basis of the currently available data, bands of up to approximately 12 nm wide centred at 600, 624 and 648 nm are recommended for detecting and quantifying CP-cyanin concentrations.

5.4.2 *Calculation of required signal-to-noise ratio for the estimation of 1 µg l^{-1} CP-cyanin*

The noise equivalent subsurface irradiance reflectance difference ($\delta R(0-)$) required for detecting 1 µg l^{-1} CP-cyanin was determined by taking the reciprocal value of the X-coefficient in the regression equations given in Tables 5.8 and 5.9. At 2 nm resolution a $\delta R(0-)$ of 1:13686 = 0.0073 % is required. For the CAESAR and CASI Inland Water Mode band settings a $\delta R(0-)$ of 1:16000 = 0.0063 % is required for detecting 1 µg l^{-1} CP-cyanin. If a reflectance range of 20 % needs to be recorded accurately (as was chosen for the chlorophyll *a* algorithm) the required S/N of the remote sensing instrument, expressed in $R(0-)$ terms varies from: 20 / 0.0073 = 1:2740 to 20 / 0.0063= 1:3175. These are high values of required sensitivity. In the following chapter the surface radiance reflectance difference will be calculated from the $\delta R(0-)$ values.

5.4.3 *Conclusions and recommendations*

The results for the CP-cyanin algorithms based on $R(0-)$ are dependent on the accuracy of the determinations of the varying parameters and their implied stability with increasing CP-cyanin contents. They are simulations, and as such lead to understanding the mechanisms for determining CP-cyanin concentrations from subsurface irradiance reflectance measurements. The algorithms for CP-cyanin concentration estimation are only valid for turbid phytoplankton rich waters, because the averaged optical properties from 10 of the shallow eutrophic lakes were used as input parameters. Nevertheless, the results do indicate that a three-band algorithm for CP-cyanin concentrations is worthy of further investigation.

The average CP-cyanin-specific absorption a^*_{624} of 0.0032 m^2 mg^{-1} was approximately 5 times lower than the chlorophyll *a*-specific absorption at 676 nm. CP-cyanin absorption is superimposed on the red absorption shoulder of chlorophyll *a* and accessory pigments.

The maximum CP-cyanin absorption at *624* nm is approximately 0.4 m^{-1}, which is similar to the maximum absorption of *a(ah)*, *a(t)* and *a(w)*. Therefore, a two-band ratio technique was not applied. Instead the following algorithm was determined:

$$C_{CP\text{-}cyanin} = -24.6 + 13686\ (0.5\ (R(0\text{-})_{600} + R(0\text{-})_{648}) - R(0\text{-})_{624})$$

with $r^2 = 0.996$ and $S_{y\cdot} = 2.34$ µg l^{-1}, based on averaged inherent optical properties data from 10 shallow eutrophic lakes.

A sensor will require increased sensitivity to distinguish similar levels of CP-cyanin in water bodies with high absorption and scattering values, caused by the effect of non-CP-cyanin parameters on the inherent optical properties. If a high accuracy is desired for CP-cyanin estimation, the phytoplankton concentration needs to be determined prior to applying the CP-cyanin algorithm. This is also true for the influence of independently varying backscattering levels.

Spectral bands of up to approximately 12 nm wide centered at 600, 624 and 648 nm are recommended for detecting and quantifying CP-cyanin concentrations from remotely sensed data. A signal-to-noise ratio defined as $\delta R(0\text{-})$ of 1:3000 is required for estimating 1 µg l^{-1} CP-cyanin in shallow eutrophic lakes (under the assumption that only 0 - 20% reflectance will cover the entire required radiometric sensitivity range of a sensor).

More CP-cyanin samples are required to improve the results of the CP-cyanin algorithm. Information is also required on the CP-cyanin and chlorophyll *a*-specific backscattering properties in order to develop an algorithm applicable to other water types.

The regression equations for the field-based spectroradiometric data (at 2nm intervals) should be directly applicable to the remote sensing data acquired with the CASI instrument in spectral mode. The regression equations for the CAESAR Inland Water Mode bands 3, 4 and 5 (see Table 6.1) should be directly applicable to the remote sensing data acquired with CAESAR on 3 September 1990 and to the data acquired with the CASI imaging spectrometer operating in spatial mode with similar spectral bands on 14 September 1990.

First, however, *R(0-)* will have to be determined from the L_{rs} data following the method presented in § 3. Results of applying the algorithms (§ 5: Table 5.6) to the remote sensing data are presented in § 6.

5.5 Algorithm for estimating seston dry weight *DW* from subsurface irradiance reflectance *R(0-)* measurements.

5.5.1 *Introduction*

The seston concentration was expressed as seston dry weight or *DW* (see also § 2). For development of an algorithm for application in remote sensing information on the optical characteristics of the seston is important. Seston consists of phytoplankton and tripton; the tripton is in turn comprised of organic and inorganic matter. The organic matter is comprised of detritus from phytoplankton and zooplankton and of resuspended bottom material such as peat fragments and organic decay material of larger aquatic flora and fauna. The inorganic matter is mineral matter, mostly occurring as (re)suspended bedload for the river and canal and as resuspended material for the lakes.

Each of these material fractions has its own characteristic particle size distribution, colour, transparency and refractive index and hence will have their own characteristic optical properties. For the development of an analytical model the inherent optical properties for each of these seston components should be known. Table 5.1 gives the desired and available inherent optical properties of the main inland water constituents. The lack of information on the inherent optical properties for most of the constituents limits the possibilities for developing a remote sensing algorithm based on the analytical model.

An alternative approach is to apply the semi-empirical method; i.e. a statistical analysis of the spectrophotometrically and spectroradiometrically derived *R(0-)* data and the seston dry weight measurements. The results could then be interpreted using the available knowledge of the inherent optical properties. Because the algorithm is developed using the *R(0-)* data, any algorithms so derived could still be used for multitemporal comparisons due to the wide variation in water types studied. The minimum requirements for development of an analytical algorithm for retrieval of seston dry weight concentration are discussed at the end of this section.

The semi-empirical model

For the 21 samples for which *R(0-)* values were determined from the *in situ* spectroradiometric measurements the values of *DW* varied from 1 to 45 mg l^{-1}. Correlations were performed between *DW* and *R(0-)* for each wavelength interval of 2 nm from 400 to 850 nm. The resulting correlation spectrum for the coefficient of determination (r^2) is presented along with the average *R(0-)* spectrum for the 21 measurements in Fig. 5.16. The r^2 for 400 to 500 nm is very low, confirming the findings in previous sections that at wavelengths below 500 nm absorption by aquatic humus, tripton and blue light harvesting pigments, coupled with high values for scattering, interacts in a complicated and analytically unsolvable manner. Beyond 500 nm r^2 increases until it reaches a plateau at 600 to 650 nm at a value of $r^2 = 0.56$. Towards the 676 nm chlorophyll *a* absorption

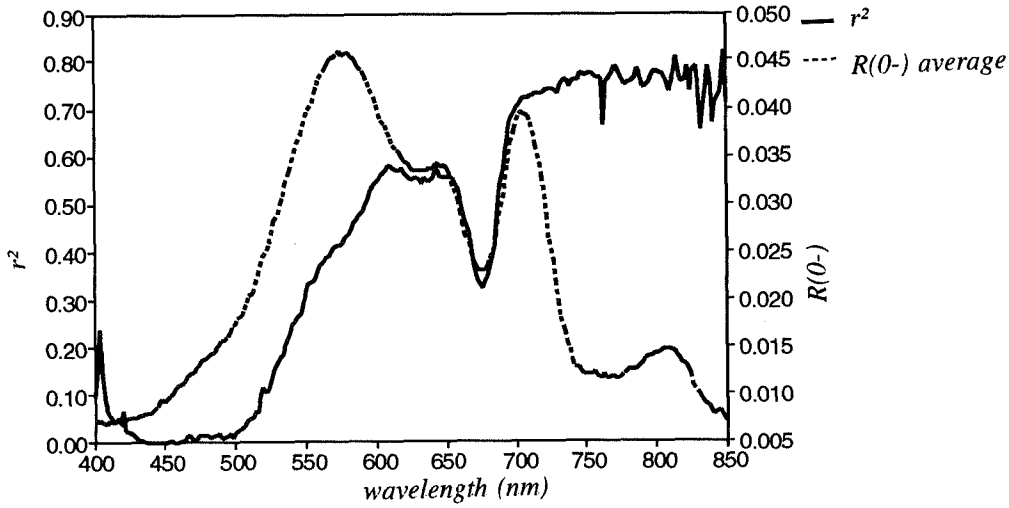

Figure 5.16 *Bivariate linear correlation (r^2) between R(0-) values determined from the in situ spectroradiometric measurements and the values of DW for each wavelength interval of 2 nm from 400 to 850 nm (N = 21). Also given is the average R(0-) spectrum for the 21 measurements.*

maximum the correlation decreases. Since the combined effects of absorption by aquatic humus, tripton and chlorophyll *a* approach zero beyond 720 nm, scattering variations induced by variations in seston concentrations cause an increase in r^2 values from 0.70 in the near-infrared at 700 nm to a maximum of 0.78 at 748 nm.

Regression equations were calculated between *R(0-)* and *DW* at 748 nm because the highest correlation occurred at 748 nm (r^2 = 0.78). However, the average value for *R(0-)* at 748 nm was just 20 % of that at 706 nm. Therefore, the regression equation was also calculated for 706 nm where correlations were still high (r^2 = 0.72). The regression equation was also calculated for the spectral band 698-714 nm, corresponding to an Inland Water Mode spectral band for both CAESAR and CASI.

The regression equations at 706 and 748 nm are given in Table 5.10 for the relationship between *R(0-)* and *DW* concentration. Figure 5.17.a & b show the scatter plots and the linear regression lines for these relationships. Upon first inspection the results of the regression analyses imply that 748 nm would be the best location for a spectral band for *DW* estimation. However, Fig. 5.16 shows that the highest signal for average *R(0-)* was obtained at 706 nm and is approximately 5 times higher than *R(0-)* at 748 nm. The X-coefficients in the regression equations reflect this change in magnitude of *R(0-)*.

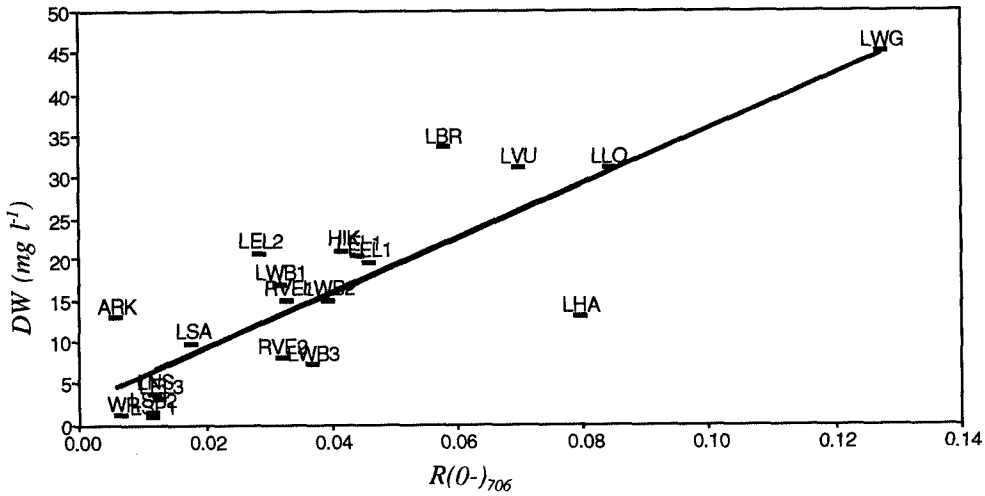

Figure 5.17.a *Scatter plot and regression line for $R(0\text{-})_{706}$ values determined from the in situ spectroradiometric measurements and measured values of DW (see Table 5.10 for results of the regression equations).*

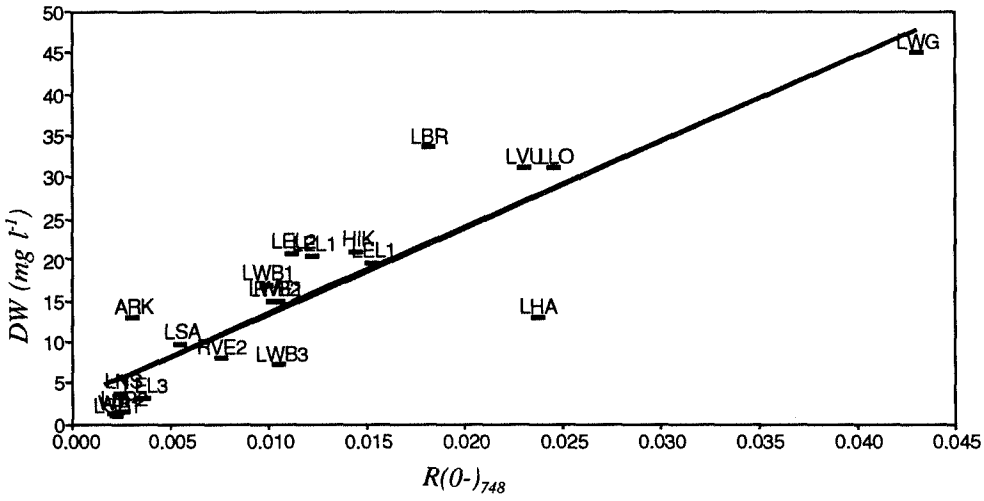

Figure 5.17.b *Scatter plot and regression line for $R(0\text{-})_{748}$ values determined from the in situ spectroradiometric measurements and measured values of DW (see Table 5.10 for results of the regression equations).*

From the equation it may be deduced that by selecting 706 nm rather than 748 nm as the wavelength for determining *DW* the S/N will increase by a factor of 3.5. This reduction in S/N will probably more than compensate for the lower r^2 value of 0.72 instead of 0.78. An additional advantage is that the Inland Water Mode band 8, already recommended for estimation of chlorophyll *a*, may also be used for *DW* concentration estimation using remote sensing measurements.

The correlation for the simulated Inland Water Mode band 8 (centred at 706 nm) with *DW* was also high. This strength of the relationship was markedly improved when two outlying points, ARK and LHA, were removed from the regression.

Table 5.10 *Regression equations at 706 nm and at 748 nm for the relationship between R(0-)λ and DW concentration; as well as for the Inland Water Mode spectral band from 698-714 nm: and for the Inland Water Mode spectral band excluding the two outliers of the ARK and LHA (see Figs. 5.17.a & b).*

		r^2	S_y.	N
DW	= 1.99 + 1170 $R(0-)_{748}$	0.78	4.46	21
DW	= 2.69 + 331 $R(0-)_{706}$	0.72	6.46	21
DW	= 2.59 + 346 $R(0-)_{698\text{-}714}$	0.72	6.46	21
DW(ex. ARK & LHA)	= 0.71 + 406 $R(0-)_{698\text{-}714}$	0.85	4.93	19

The ARK sample was taken a day after the *in situ* optical measurements and therefore may not be reliable. There is no apparent reason for the LHA sample to deviate markedly from the correlation between *R(0-)* and *DW* for the other samples. This deviation could be the result of errors in the *DW* measurement or be caused by differences in the coefficient r_1, or by differences in particle size and hence tripton-specific or algal pigment-specific scattering differences.

5.5.2 *Calculation of required signal-to-noise ratio for estimating of 1 mg l^{-1} DW*

The noise equivalent subsurface irradiance reflectance difference $\delta R(0-)$ required for discriminating 1 mg l^{-1} difference in *DW* was determined by taking the reciprocal value of the X-coefficients in the regression equations given in Table 5.10. Thus at 2 nm resolution a $\delta R(0-)$ of 1:1170 = 0.0855 % would be required for a spectral band at 748 nm and a $\delta R(0-)$ of 1:331 = 0.3021 % would be required for a spectral band at 706 nm. If a reflectance range of 20 % covers the full range of sensitivity required from a sensor the required S/N of the remote sensing instrument, expressed in terms of *R(0-)*, needs to be 20 / 0.0855 = 234:1 at 748 nm and 20 / 0.3021 = 66:1 at 706 nm. The surface radiance reflectance difference will be calculated from the $\delta R(0-)$ values in Chapter 6.

5.5.3 *Requirements for developing an analytical model for DW estimation using remote sensing*

A simple analytical model for estimating *DW* from *R(0-)* measurements requires information on the DW-specific (back)scattering and absorption properties and volume scattering functions of the two main fractions of which the seston is composed: the phytoplankton and the tripton.

For phytoplankton a fixed relationship must be determined between the chlorophyll *a* concentration and the biomass of the algae and subsequently between *DW* and biomass. Determination of the presence or absence of CP-cyanin and the value of the chlorophyll *a* will give a first order indication of the water type (oligotrophic, mesotrophic or eutrophic). Based on this information a *DW* concentration attributable to algal concentration may be estimated. The remaining seston dry weight concentration will be composed of tripton. Gons *et al.* (1992) calculated a relationship between chlorophyll *a* and *DW* for a laboratory-scale-enclosure batch culture of *Prochlorothrix hollandica* under light limited conditions of 0.048 g of chlorophyll *a* to 1 g of seston dry weight. This type of information for *in situ* conditions for the main algae in these waters needs to be determined.

The next step will be determination of the chlorophyll *a*-specific (back)scattering. With the scattering and absorption due to the phytoplankton known, calculations can be carried out to remove the influence of phytoplankton on the *R(0-)*; for example, at 676 and at 706 nm. The remaining *R(0-)* signal will be attributable to scattering by tripton alone and to the absorption by aquatic humus, tripton and water. At approximately 706 nm a minimum in the combined absorption will occur, thus potentially providing the best spectral location for estimating tripton-induced scattering. Provided a reliable tripton specific (back)scattering can be estimated the tripton concentration may be determined. If the tripton-specific absorption coefficient is known, the absorption contribution due to tripton can be estimated and the influence of absorption and scattering by tripton can be removed from the *R(0-)* signal. This would leave a *R(0-)* signal influenced only by aquatic humus absorption and by water absorption. In principle this should produce *R(0-)* values of zero across the spectrum, for without backscattering there can be no reflectance; thus automatically providing a test of the accuracy of the modelling.

The main obstacles to applying such a model are the likely large variations in:
1) phytoplankton pigment values for different algal species;
2) tripton-specific absorption and (back)scattering for different tripton materials.
It may be feasible, however, to determine these values for separate types of water bodies; for example, in this research a differentiation of these optical properties into general values for deep lakes, shallow mesotrophic lakes, eutrophic lakes and river and canal water types seems possible.

5.5.4 *Conclusions and recommendations*

The lack of information on the inherent optical properties of most of the seston constituents limits the possibilities for developing an algorithm for *DW* based on the analytical model for application in remote sensing. Therefore the semi-empirical method was applied. It is likely that in future, as more data becomes available, this semi-empirical method can be fine-tuned to different types of water (e.g. in this study deep lakes, shallow eutrophic lakes, shallow mesotrophic to oligotrophic lakes and river and canal water).

Because seston does not have any discriminatory spectral features at a specific wavelength the ratio method could not be applied. From a correlation spectrum it was deduced that at either 706 nm ($r^2 = 0.72$) or at 748 nm ($r^2 = 0.78$) a sufficient correlation existed for applying a single spectral band algorithm. The spectral band centred at 706 nm was chosen since it had 3.5 times higher signal-to-noise ratio for *R(0-)*. If a reflectance range of 20 % covers the full range of sensitivity required from a sensor then the required S/N of the remote sensing instrument, expressed in terms of *R(0-)*, needs to be 66:1 at 706 nm.

The required information on inherent optical properties and the method for developing an analytical model for estimating seston dry weight concentrations from *R(0-)* were analysed. A possible method would be the consequent analytical determination of each inherent optical property: first determination and subtraction of the non-seston properties of water and aquatic humus. Next, determination and subtraction of the phytoplankton optical properties. Finally, the tripton optical properties would have to be determined. The derived concentrations of tripton and phytoplankton could then be recalculated to *DW* concentration.

5.6 A semi-empirical model based on *R(0-)* for estimating the vertical attenuation coefficient K_d and Secchi disk transparency *SD*

5.6.1 *Introduction*

Measurement of the vertical attenuation, K_d, of photosynthetically active radiation (wavelength range of 400-700 nm) has become standard procedure for deriving lake optical conditions. Vertical attenuation measurements are useful for determining the amount of radiance available to phytoplankton and submerged macrophytes, for determining the transparency of water for swimming water standards, for primary production studies and as an indication of turbidity. The range of K_d values for this study was between 0.63 m^{-1} for the Water Reservoir to 4.58 m^{-1} for the highly eutrophic Lake Wijde Gat.

The Secchi disk is a device used visually to measure the clarity of natural waters. Secchi disk transparency (*SD*), is often considered to be a crude measure of water quality. It is, however, an easy, fast and low cost measurement. For these reasons it has been widely employed and has become one of the primary parameters for water quality description. The *SD* is a measure for the transparency of waters and is inversely proportional to the average amount of organic and inorganic materials along the path of sight in the water (Preisendorfer, 1986). The range of *SD* in the waters studied here was from as low as 25 cm in the LWG to 490 cm in the Water Reservoir.

5.6.2 *The relationship between the inherent optical properties and K_d and SD*

The vertical attenuation of subsurface downwelling irradiance K_d is defined as

$$K_d = \mathrm{d} \ln E_{wd} / \mathrm{d}z \qquad [5.15]$$

where E_{wd} is the subsurface downwelling irradiance and z the depth. Kirk (1991) investigated the relationship between K_d and the inherent optical properties and presented the general equation:

$$K_d = 1 / \mu_0[a^2 + G(\mu_0)\, a\, b]^{1/2} \qquad [5.16]$$

where μ_0 is the cosine of the angle of refracted incident photons and $G(\mu_0)$ a coefficient that is a function of μ_0 and a shape factor of the volume scattering function $\beta(\theta)$. This shape factor of $\beta(\theta)$ is a function of the average cosine of scattering, μ_s, derived from the $\beta(\theta)$ in question. The exact relationships between $G(\mu_0)$ and μ_s are determined through modelling of the data.

From equation 5.16 it follows that, ideally, a knowledge of $\beta(\theta)$ and μ_s is required to develop a remote sensing algorithm for the retrieval of K_d from *R(0-)* measurements using the analytical method. Applying an analytical approach was therefore beyond the scope of the more limited information on inherent optical properties determined in this study (see also Table 5.1).

SD is a function of the beam attenuation coefficient, c, and the vertical attenuation coefficient K_d (Preisendorfer, 1986); c is defined as the sum of a and b (§ 2.1.1). Thus for application of an analytical algorithm for estimation of *SD* from remote sensing derived *R(0-)* measurements, the estimation of a, b and K_d for each wavelength interval over the visible spectrum would be required. Analytical modelling of *SD* therefore requires an analytical model for K_d as well as sufficient information on the inherent optical properties a and b.

Given the limited available data on inherent optical properties, the semi-empirical method was investigated for the estimation of K_d and *SD* values from *R(0-)* measurements, with the aim of estimating these properties from the remote sensing data.

5.6.3 *Algorithms using the semi-empirical method for estimation of K_d and SD from R(0-).*

5.6.3.1 *Introduction*

For an initial identification of wavelengths for K_d and *SD* estimation bivariate linear correlations between K_d and *SD* with *R(0-)* were determined at 2 nm intervals. Figure 18.a shows results for the spectral correlation between the measured K_d values and *R(0-)* and Figure 18.b. shows results for the spectral correlation between the measured *SD* and *R(0-)* at 2 nm intervals.

Similar to the calculations for chlorophyll *a*, CP-cyanin and *DW*, there was a low correlation for K_d and *SD* with *R(0-)* up to 500 nm, confirming the findings that high absorption by several components in this spectral region contributes to low *R(0-)* in all waters.

For K_d the correlation increases gradually from $r^2 = 0$ at 520 nm to $r^2 = 0.40$ between 600 and 650 nm. After a local minimum, centred at the chlorophyll *a* induced *R(0-)* minimum at 676 nm, r^2 increases to 0.60 at 700 nm and rises to 0.70 between 750 nm and 850 nm. The highest correlations thus occurred at wavelengths where the absorption of phytoplankton, tripton and aquatic humus are all low and differences in *R(0-)* are predominantly determined by varying levels of scattering.

The correlations between *R(0-)* and K_d over 400 to 850 nm were all below $r^2 = 0.70$. The use of a single band algorithm for the estimation of K_d from remotely sensed reflectance would therefore be of limited accuracy. The use of spectral ratio algorithms were therefore investigated to determine if improved estimates of K_d could be made.

For *SD* the correlation with *R(0-)* increased beyond 500 nm to $r^2 = 0.36$ at 640 nm (Fig. 5.18.b). After a local minimum at the chlorophyll *a* induced *R(0-)* minimum at 676 nm, a maximum value occurred of $r^2 = 0.41$ at 688 nm. Beyond this wavelength the r^2 values remained relatively stable at approximately $r^2 = 0.35$. The correlation calculations beyond 700 nm are by definition not directly linked to the *SD* measurement since Secchi disk transparency is defined for the human eye sensitive wavelength range of 400 - 700 nm.

The correlations between *R(0-)* and *SD* were all relatively low ($r^2 < 0.41$). This suggests that for retrieval of *SD* from remotely sensed reflectance, an algorithm based on a single spectral band is not appropriate. Algorithms involving two spectral bands were therefore investigated.

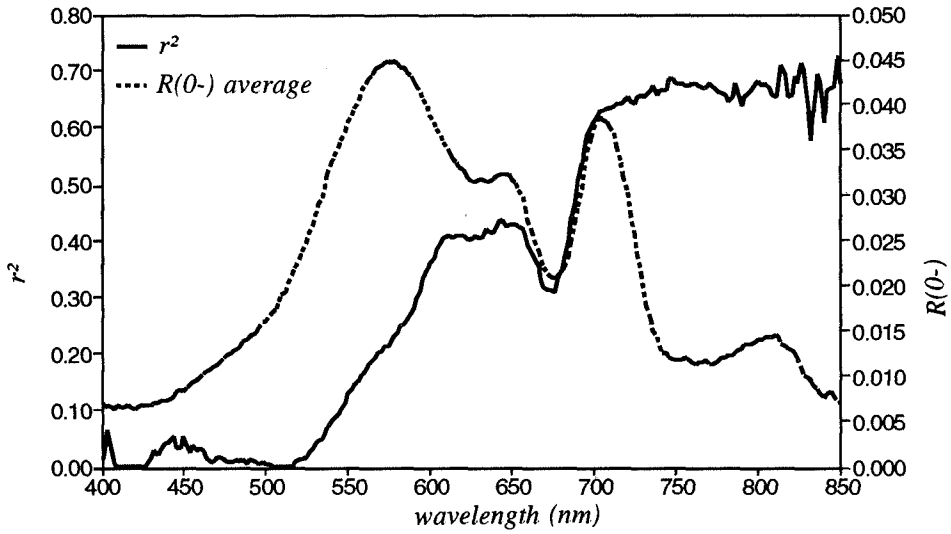

Figure 5.18.a *Bivariate linear correlation (r^2) between R(0-) values (determined from the in situ spectroradiometric data) and the values of K_d for each wavelength interval of 2 nm from 400 to 850 nm (N = 20).*

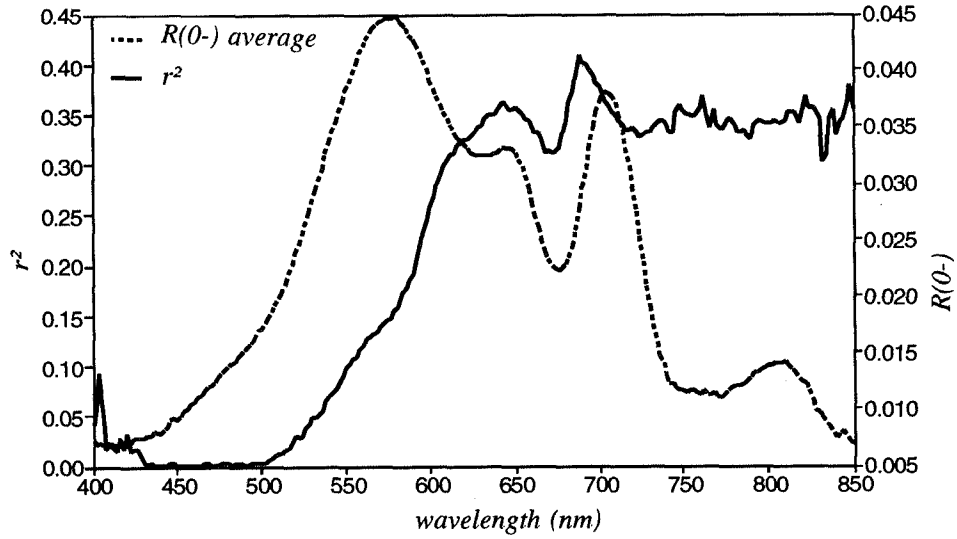

Figure 5.18.b *Bivariate linear correlation (r^2) between R(0-) values (determined from the in situ spectroradiometric data) and the values of SD for each wavelength interval of 2 nm from 400 to 850 nm (N = 22).*

5.6.3.2 Results of the correlation analysis for K_d and *SD* correlated with $R(0\text{-})_{706}$ / $R(0\text{-})_{676}$ at 2 nm intervals over 400 to 850 nm

Part of the reason for the relatively low correlations between *R(0-)* and K_d and *SD* may be variations between the measurements in the r_1 coefficient relating *R(0-)* to absorption and scattering as defined in chapter 4. A spectral band ratio has the advantage that, apart from spectral variations in r_1, any r_1 induced differences are divided to unity (see § 5.2.2.2).

The results of the bivariate linear correlation analysis between K_d and *R(0-)* as a function of wavelength indicated that K_d was more correlated to scattering in those regions of the spectrum where the influence of absorption was reduced (Fig. 18.a). In spectral regions where absorption was relatively high, such as the chlorophyll *a* absorption at 676 nm, correlations were lower. Results from earlier semi-empirical studies where correlations for E_{us} and K_d (Dekker *et al.*, 1990) and E_{us} and L_{rs} and K_d were investigated (Dekker *et al.*, 1990, 1991 & 1992d), showed that a ratio of spectral bands centred at 676 nm and 706 nm had a high correlation (r^2 of 0.83 to 0.94). The reason for these high correlations probably lies in the correlation of chlorophyll *a* with algal biomass determining significant parts of the scattering and absorption. The correlation of K_d and chlorophyll *a* for 29 samples from the 1990 data set was $r^2 = 0.86$.

A scatter plot of the relationship between K_d and the ratio of $R(0\text{-})_{706}$ and $R(0\text{-})_{676}$ is shown in Fig. 19.a and indicates that a linear relation describes the data reasonably well. The Amsterdam-Rijn Kanaal sample deviated, probably because the ARK water had a relatively low chlorophyll *a* content and high tripton content, thus preventing the ratio from following a chlorophyll *a* correlated relationship. The LW3 sample also deviated markedly from the general linear relationship. A possible cause for this deviation may be that the aquatic humus concentration was very high for this sample whereas a low chlorophyll *a* level was determined. Thus K_d may have been less related to algal biomass for LW3. These results suggest that the $R(0\text{-})_{706}$ / $R(0\text{-})_{676}$ ratio may only be applied to water types similar to those from which the regression equation was calculated.

The ARK and River Vecht samples may probably be best estimated using a single band at 700 nm or a longer wavelength where the K_d and *R(0-)* will be largely related to scattering which is a dominant optical feature in these waters. However, further investigation is required to develop a valid regression equation for these water types.

Bivariate linear regressions of K_d with $R(0\text{-})_{706}$ / $R(0\text{-})_{676}$ for all the samples (N = 20), for the samples excluding the ARK and LW3 (N = 18), the shallow lakes (N = 11) and the deep lake samples (N = 7), are presented in Table 5.11. A considerable improvement in r^2 to values between 0.90 and 0.97, compared with the $r^2 < 0.70$ for the single band approach, indicates that such a spectral band ratio based algorithm is appropriate. The lower r^2 values for the shallow lakes compared to r^2 for the deep lakes may be an-

other indication of a strong correlation of *Kd* with chlorophyll *a*; the tripton and aquatic humus levels in the shallow lakes probably influence this relationship.

Table 5.11 *Bivariate linear regression results for $R(0\text{-})_{706}$ / $R(0\text{-})_{676}$ as the independent variable and K_d as the dependent variable (see Fig. 5.19.a).*

bivariate linear regression equation	r^2	$S_{y.}$	N	samples
K_d = -0.3457 + 1.6224 $R(0\text{-})_{706}$ / $R(0\text{-})_{676}$	0.90	0.42	20	: all samples
K_d = -0.5331 + 1.7046 $R(0\text{-})_{706}$ / $R(0\text{-})_{676}$	0.93	0.35	18	: all (ex. ARK & LW3)
K_d = +0.2134 + 1.3786 $R(0\text{-})_{706}$ / $R(0\text{-})_{676}$	0.91	0.31	11	: shallow lakes
K_d = -0.2467 + 1.1966 $R(0\text{-})_{706}$ / $R(0\text{-})_{676}$	0.97	0.06	7	: deep lakes

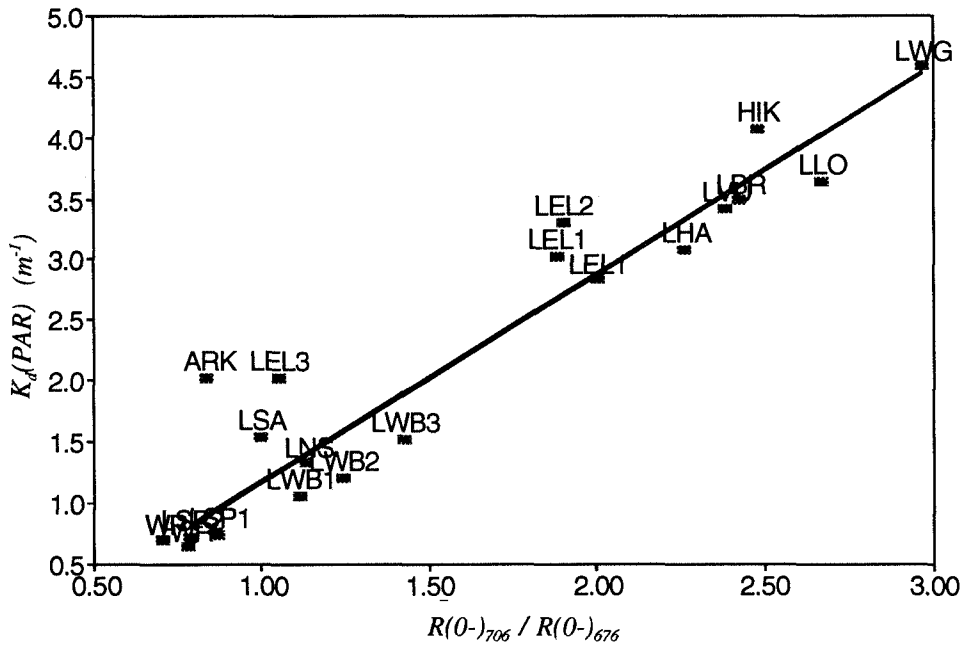

Figure 5.19.a *Scatter plot of in situ measured values of K_d and the ratio of in situ measured $R(0\text{-})_{676}$ and $R(0\text{-})_{706}$.*

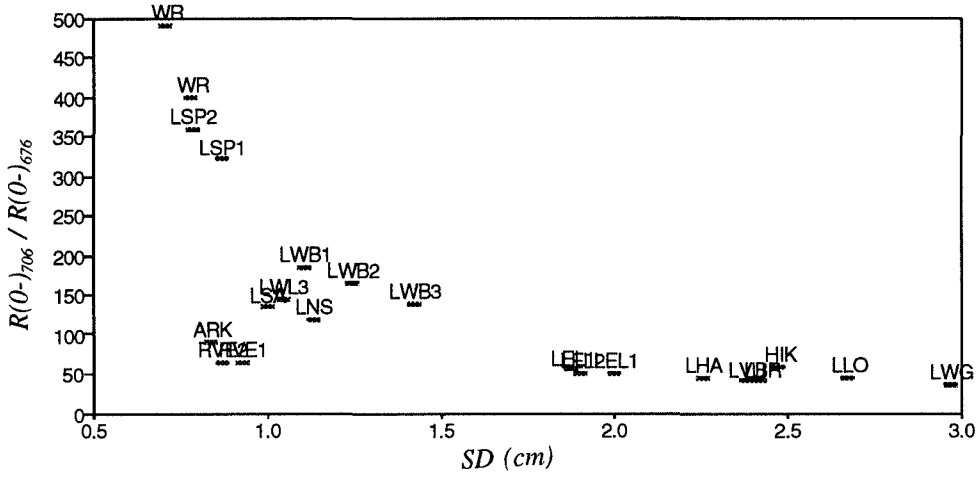

Figure 5.19.b *Scatter plot of in situ measured values of SD and the ratio of in situ measured* $R(0\text{-})_{676}$ *and* $R(0\text{-})_{706}$.

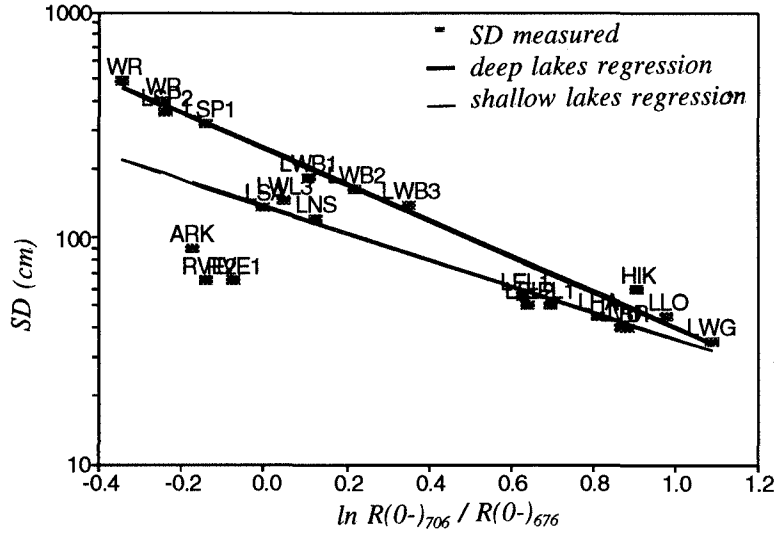

Figure 5.19.c *Scatter plot with logarithmic X and Y axes of in situ measured values of SD and the ratio of in situ measured* $R(0\text{-})_{676}$ *and* $R(0\text{-})_{706}$.

Because no analytical model could be derived to relate K_d to $R(0-)$ through the inherent optical properties, calculations could not be made of the required sensitivity in $R(0-)_{706}$ or $R(0-)_{676}$ for the detection of a 0.1 m^{-1} change in K_d. However, from the linear regression equations, the reciprocal value of the X-coefficient gives an indication of the change in $R(0-)_{706}$ / $R(0-)_{676}$ required for detecting such a change in K_d. Using the measured values for the lowest K_d value, which corresponds to the lowest $R(0-)_{706}$ and $R(0-)_{676}$ measurement, the noise equivalent subsurface irradiance reflectance difference $\delta R(0-)$ required for detecting 0.1 m^{-1} K_d was calculated to be approximately 320:1.

Results from the bivariate linear correlation analysis between *SD* and $R(0-)$ as a function of wavelength indicated that the spectral area at 688 nm gave the highest correlation (Figure 18.b). As for K_d, results from previous semi-empirical studies (Dekker *et al.* 1990, 1991 and 1992d), where correlations were analysed between E_{us} or L_{rs} data and *SD*, showed that the spectral band ratio $R(0-)_{676}$ / $R(0-)_{706}$ gave high correlations, particularly with log-transformed data (r^2 of 0.91 to 0.98).

Scatter plots for the relationship between *SD* and $R(0-)_{676}$ / $R(0-)_{706}$ are shown in Fig. 19.b for the untransformed data and in Fig. 19.c for the log-transformed data. Comparison of the two figures indicates that an exponential or power relation would best describe the data. The four water types appear as grouped sets of data points in the figures. The shallow eutrophic lakes *SD* were between 25 and 60 cm, the canal and river between 60 and 90 cm, the shallow mesotrophic lakes between 120 and 150 cm and the deep lakes between 140 and 490 cm. For all the samples and for each of the water types bivariate linear regression analysis was performed on the log-transformed data. The results are presented in Table 5.12. The results for the shallow eutrophic and mesotrophic lakes were so similar (< 1% difference) that the values were combined.

An improvement in r^2 for all samples to a value of 0.67, compared to $r^2 < 0.41$ for the single band approach, indicates that such a spectral band ratio based algorithm is more appropriate. The results in Table 5.12 indicate that separation of the points into water types increased the correlation for *SD* with $R(0-)_{706}$ / $R(0-)_{676}$ to $r^2 = 0.96$ for the shallow lakes and to $r^2 = 0.98$ for the deep lakes. The regression equation for the ARK and River Vecht is highly tentative, because it was based on three samples only. The regression equations are only valid for the range of Secchi depth transparencies for which they were calculated, with limited possibilities for extrapolation. Due to the negative correlation of *SD* with increasing values for $R(0-)_{706}$ / $R(0-)_{676}$, the constant in the regression equation sets a limit on the possible values for $R(0-)_{706}$ / $R(0-)_{676}$ beyond which negative transparencies will be calculated. In the case of the power equations the results become particularly sensitive to variations at low values for $R(0-)_{706}$ / $R(0-)_{676}$. This is illustrated in the following discussion on the required sensitivity for determining a 10 cm transparency change (10 cm is approximately the accuracy obtained for Secchi depth transparency estimates between 25 and 500 cm).

Table 5.12 *Bivariate linear regression results for the untransformed and for the log-transformed data with $R(0-)_{706}$ / $R(0-)_{676}$ as the independent variable and SD as the dependent variable (see Fig. 5.19.b & c.*

untransformed data			r^2	$S_{y\cdot}$	N		samples
SD =	323 -119	$R(0-)_{706}$ / $R(0-)_{676}$	0.43	102	22	:	all samples
SD =	180 - 56	$R(0-)_{706}$ / $R(0-)_{676}$	0.83	18	11	:	shallow lakes
SD =	752 -462	$R(0-)_{706}$ / $R(0-)_{676}$	0.90	47	7	:	deep lakes
SD =	284 -240	$R(0-)_{706}$ / $R(0-)_{676}$	0.61	13	3	:	canal & river

log-transformed data	r^2	$S_{y\cdot}$%	N		samples
$\ln SD = 5.05 - 1.795 \ln (R(0-)_{706} / R(0-)_{676})$	0.67	63	22	:	all samples
$SD = e^{(5.05 - 1.795 \ln R(0-)706 / R(0-)676)}$		"	"		"
$\ln SD = 4.92 - 1.342 \ln (R(0-)_{706} / R(0-)_{676})$	0.96	11	11	:	shallow lakes
$SD = e^{(4.92 - 1.342 \ln (R(0-)706 / R(0-)676)}$		"	"		"
$\ln SD = 5.51 - 1.815 \ln (R(0-)_{706} / R(0-)_{676})$	0.98	7	7	:	deep lakes
$SD = e^{(5.51 - 1.815 \ln (R(0-)706 / R(0-)676)}$		"	"		"
$\ln SD = 3.92 - 2.793 \ln (R(0-)_{706} / R(0-)_{676})$	0.61	27	3	:	canal & river
$SD = e^{(3.92 - 2.793 \ln (R(0-)706 / R(0-)676)}$		"	"		"

Table 5.13 *Bivariate linear regression results for $R(0-)_{698-714}$ / $R(0-)_{671-684}$ as the independent variable and K_d as the dependent variable:*

bivariate linear regression equation	r^2	$S_{y\cdot}$	N		samples
K_d = -0.6256 + 1.9187 $R(0-)_{698-714}$ / $R(0-)_{671-684}$	0.89	0.43	20	:	all samples
K_d = -0.7950 + 1.9984 $R(0-)_{698-714}$ / $R(0-)_{671-684}$	0.92	0.38	18	:	all (ex. ARC&LW3)
K_d = 0.0492 + 1.5950 $R(0-)_{698-714}$ / $R(0-)_{671-684}$	0.89	0.34	11	:	shallow lakes
K_d = -0.4045 + 1.3600 $R(0-)_{698-714}$ / $R(0-)_{671-684}$	0.99	0.04	7	:	deep lakes

As for K_d, the lack of an analytical model relating *SD* to *R(0-)* meant that changes in $R(0-)_{706}$ or $R(0-)_{676}$ required for the detection of a 10 cm change in *SD* could not be calculated directly. The reciprocal values of the X-coefficient from the linear regression equation were therefore used as an indication of the change in $R(0-)_{706}$ / $R(0-)_{676}$ required for detecting such a change in *SD*. The $\delta R(0-)$ required for detecting 10 cm *SD* was

calculated for the highest *SD* measured (WL1) and was found to be 1020:1. That the power equation is particularly sensitive at low values of the $R(0-)_{706}$ / $R(0-)_{676}$ ratio can be illustrated by calculating the required S/N for detecting a 10 cm *SD* change for WL1 using the power regression equations. Through iterative calculation and assuming a stable $R(0-)_{676}$ it was determined that a change in $R(0-)_{706}$ of 0.0084% changed the estimated *SD* by 10 cm. This is equivalent to a S/N of 20 / 0.0084:1 = approximately 2600:1. Based on the two highest measurements of *SD* (i.e. sample WL1 with a *SD* of 450 cm and WL2 with a *SD* of 380 cm) a required S/N of 1:1000 was calculated for determining a 10 cm change across this range of *SD*, close to the value of 1020:1 calculated from the linear regression equations. Thus, at the upper limits of the data for which the power regression equation was calculated, the sensitivity to small variations in the independent variable $R(0-)_{676}$ / $R(0-)_{706}$ is high.

For the Inland Water Mode spectral bands 7 (CAESAR: 670-684 nm; CASI: 674-686 nm) and band 8 (CAESAR:696-714 nm; CASI: 699-711) the same regression calculations were performed to determine the relationship between K_d and *SD* and the ratio of band 8 to band 7 (Table 5.13 and 5.14: Since the CASI values were similar to those for CAESAR values,CASI values are not presented separately).

Table 5.14 *Bivariate linear regression results for the untransformed and for the log-trans formed data with* $R(0-)_{698\text{-}714}$ / $R(0-)_{671\text{-}684}$ *as the independent variable and SD as the dependent variable.*

untransformed data	r^2	$S_{y'}$	N	samples
SD = 344 - 141 $R(0-)_{698\text{-}714}$ / $R(0-)_{671\text{-}684}$	0.44	102	22	: all samples
SD = 191 - 68 $R(0-)_{698\text{-}714}$ / $R(0-)_{671\text{-}684}$	0.84	18	11	: shallow lakes
SD = 796 - 509 $R(0-)_{698\text{-}714}$ / $R(0-)_{671\text{-}684}$	0.85	55	7	: deep lakes

log-transformed data	r^2	$S_{y'}$%	N	samples
$\ln SD = 5.05 - 1.615 \ln (R(0-)_{698\text{-}714} / R(0-)_{671\text{-}684})$	0.67	62	22	: all samples
$SD = e^{(5.05 - 1.615 \ln R(0-)698\text{-}714 / R(0-)671\text{-}684)}$	"		"	"
$\ln SD = 4.89 - 1.464 \ln (R(0-)_{698\text{-}714} / R(0-)_{671\text{-}684})$	0.96	12	11	: shallow lakes
$SD = e^{(4.89 - 1.464 \ln (R(0-)698\text{-}714 / R(0-)671\text{-}684)}$	"		"	"
$\ln SD = 5.51 - 2.038 \ln (R(0-)_{698\text{-}714} / R(0-)_{671\text{-}684})$	0.96	11	7	: deep lakes
$SD = e^{(5.51 - 2.038 \ln (R(0-)698\text{-}714 / R(0-)671\text{-}684)}$	"		"	"

The differences between the results of the regression analyses for the 2 nm resolution spectra compared with the Inland Water Mode spectral bands are small. The main differences between the narrow and broad spectral band regressions were in the slope of the relationships. With the broader spectral bands the X-coefficients increased in value, thus indicating a decreasing slope. This result suggests that a higher S/N ratio will be required for a broad band than for a narrow band remote sensing system. The effect of varying band widths on the correlation between K_d and *SD* with *R(0-)* was not determined because this was considered to be useful only if based on an analytical model.

5.6.4 Conclusions and recommendations

Given the limited available data on inherent optical properties, the semi-empirical method was investigated for the estimation of K_d and *SD* values from *R(0-)* measurements with the aim of estimating these properties from the remote sensing data.

The use of spectral ratio algorithms improved estimates of K_d and *SD* over single band algorithms. r^2 values for K_d and $R(0-)_{676}$ / $R(0-)_{706}$ of 0.91 for the shallow lakes to 0.97 for the deep lakes were calculated. r^2 values for ln *SD* and ln $R(0-)_{676}$ / $R(0-)_{706}$ of 0.96 for the shallow lakes to 0.98 for the deep lakes were also derived.

If a reflectance range of 20 % covers the full range of sensitivity required from a sensor the required S/N of the remote sensing instrument, expressed in terms of *R(0-)*, needs to be 320:1 for estimating K_d value differences of 0.1 m^{-1} at 676 and 706 nm. The same calculation of S/N for estimating *SD* differences of 10 cm was found to be 1000:1 at 676 and 760 nm. For the spectral bands of the Inland Water Mode the results were similar; however, higher S/N ratios were required for measuring 0.1 m^{-1} K_d or 10 cm *SD*.

It is likely that in future, as more data becomes available, the semi-empirical method can be fine-tuned to different types of water (e.g. in this study deep lakes, shallow lakes and river and canal water).

The analytical determination of $K_{d\lambda}$ from $R(0-)_\lambda$ data will probably be the most useful (where λ is a wavelength between 550 and 720 nm). The greatest light penetration in the shallow eutrophic lakes takes place between 550 and 720 nm (Malthus & Dekker, 1990) with a local minimum centered at 676 nm. Because absorption by aquatic humus and tripton is relatively low and the slope of scattering decreases after 500 to 550 nm, reasonable accuracy may be obtained in determining $K_{d\lambda}$ once information on the backscattering and $\beta(\theta)$ is available for these waters. For *SD* determination all the inherent optical properties for all substances influencing the underwater light field over the entire visible wavelength region need to be known. An analytical model for *SD* retrieval from *R(0-)* measurements would therefore require availability of spectral information on *a(ah)*, *a(t)*, *a(ph)*, *b(t)*, *b(ph)*, $b_b(t)$, $b_b(ph)$ and on $\beta(\theta)$ for all the scattering substances.

5.7 General conclusions, recommendations and discussion.

Only general conclusions, recommendations and discussion will be presented here (for parameter-specific conclusions and recommendations see the appropriate sections).

Although the analytical approach is the preferred method for algorithm development, it was not always possible to follow this approach, due to insufficient information on parameter-specific inherent optical properties. Even in the case of the chlorophyll algorithm an empirical approximation of the backscattering of phytoplankton had to be made. Major improvements are possible if more knowledge concerning the scattering and backscattering (and, thus, volume scattering functions) of the phytoplankton and the tripton are available. Research aimed at obtaining such information is strongly recommended.

In successive order, a decrease in analytical and an increase in semi-empirical elements were required for the algorithms for estimation of chlorophyll *a*, CP-cyanin, seston dry weight, vertical attenuation coefficient and Secchi disk transparency. Chlorophyll *a*, CP-cyanin and seston are parameters that influence the optical characteristic of water, whereas K_d and *SD* are a function of the optical properties of the waters. This explains the increasing level of semi-empirical approach from chlorophyll to *SD*: for each parameter in the successive order given above, information on the preceding parameter is required for an analytical algorithm approach. Thus, the parameter for which an analytical algorithm will require analytical models of all the other properties, is Secchi disk transparency.

Because all algorithms presented are based on *R(0-)* data, even the semi-empirical algorithms will show consistency when applied multitemporally as illustrated in chapter 6. Of course the optical characteristics of the waters should not vary beyond the range existing during the 1990 remote sensing campaign.

The algorithms developed in this study are intended to be used in further research where validation, augmentation of the results and possibly development of further precision, may take place. The strength of this approach also lies in the possibility of combining information and results from underwater light climate research as well as *in situ* and remote sensing measurements.

6 WATER QUALITY PARAMETER ESTIMATION FROM REMOTE SENSING DATA USING ALGORITHMS BASED ON *R(0-)*.

6.1 Introduction

A remote sensor measures upwelling radiance in the direction of view (θ,φ): $L_{rs}(\theta,\varphi)$. $L_{rs}(\theta,\varphi)$ is a function of solar zenith and azimuth angles, atmospheric condition, the state of the water surface and subsurface reflectance. Because a remote sensor measures $L_{rs}(\theta,\varphi)$ over a swath of several hundreds to several thousands of pixels most radiance detectors in an array will register $L_{rs}(\theta,\varphi)$ up to a maximum angle determined by the field of view of the instrument. In the case of remote sensing from an aircraft, movement of the aircraft in three dimensions: roll, pitch and yaw, will also introduce additional angles to the $L_{rs}(\theta,\varphi)$. L_{rs} at nadir $(=L_{rs}(0,0))$ is presumed in the remainder of this chapter unless otherwise defined.

The development of remote sensing algorithms that may be used over different time periods requires the calculation of *R(0-)* from L_{rs}. Chapters 2 to 5 of this study discussed the development of multitemporally valid algorithms for the detection of water quality parameters using data from high spectral and radiometric resolution remote sensing systems. In this chapter these algorithms are applied to remotely sensed data acquired during the field measurement campaign. The results presented here are intended as a demonstration of the validity of the algorithms. A method is presented for converting remotely sensed upwelling radiance values to *R(0-)* values based upon the spectral radiance measurement and modelling results of Chapter 3.

From the results of the application of the algorithms to remotely sensed data, criteria were obtained for determining whether imaging spectrometry or multispectral remote sensing should be preferred for water quality parameter detection.

6.1.1 *The airborne remote sensing instruments*

A flight with the multispectral airborne instrument CAESAR (Charge Coupled Device Airborne Experimental Scanner for Applications in Remote Sensing) over the study area took place on 3 September 1990 between 14:23 and 15:37 solar time with one flight track flown at an altitude of 3 km and the other tracks flown at 6 km. The flight tracks are shown in Figure 6.1.a.

The CAESAR instrument was equipped with the Inland Water Mode spectral band filter set, measuring in nine wavelength bands positioned between 500 to 800 nm each with a spectral resolution of 10 to 30 nm. The characteristics for each spectral band are given in Table 6.1. The Inland Water Mode spectral band set was developed in earlier studies using the semi-empirical method applied to subsurface spectroradiometric and remotely sensed upwelling radiance (Dekker *et al.* 1990, 1991, 1992c & d).

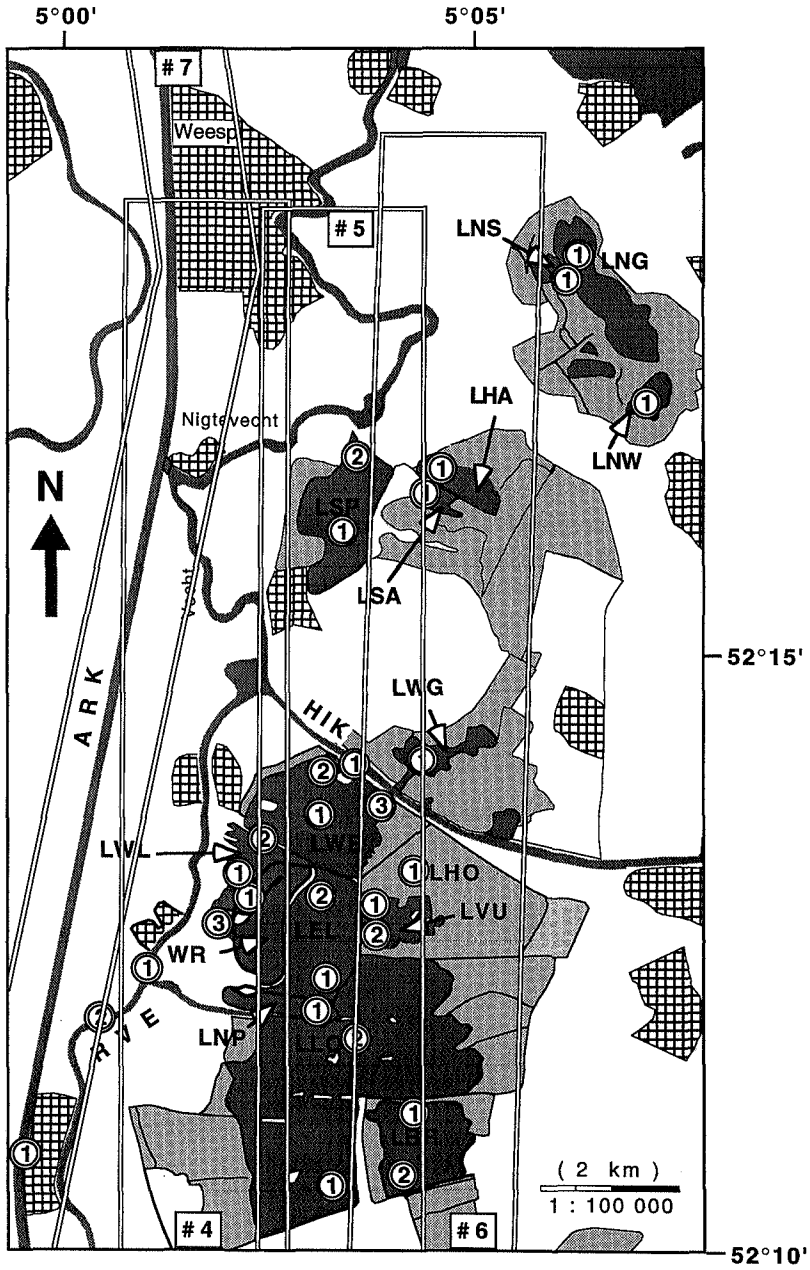

Figure 6.1.a *Flight tracks of the CAESAR remote sensing flight on 3 September 1990; tracks 4, 5 and 6 were flown at 6 km A.G.L, track 7 was flown at 3 km A.G.L.*

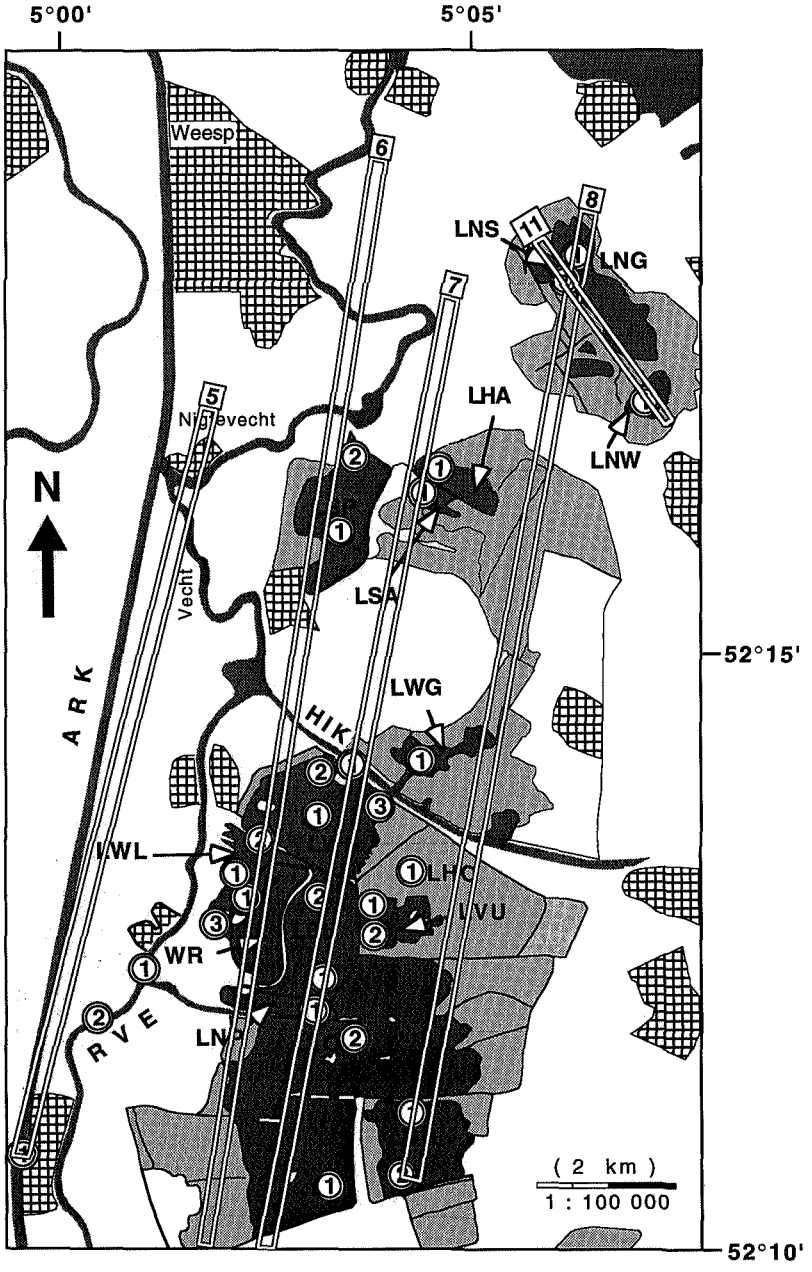

Figure 6.1.b *Flight tracks of the CASI remote sensing flight on 14 September 1990. The tracks were flown at an altitude of 450 m A.G.L. The tracks drawn in the figure are the spatial mode tracks; the spectral mode tracks cover an area within 40% of the width of the spatial mode tracks.*

Table 6.1. *Spectral band specifications for the CAESAR and CASI Inland Water Mode. The array code identifies the channel in the CAESAR coding system. The central figures (1-3) indicate the camera in the module and A/C/B stands for Ahead/-Central/Backwards which indicate the arrays in the camera.*

INLAND WATER MODE				
	CAESAR		CASI	
Array code	Centre λ (nm)	width	Centre λ (nm)	width
D1C	521	23	520	22
D2C	567	20	565	24
D1A	601	18	601	20
D2A	630	21	633	17
D3A	649	9	648	8
D1B	664	9	664	8
D2B	677	13	680	11
D3B	705	16	705	11
D3C	778	34	791	23

The CAESAR instrument is the property of the National Remote Sensing Programme of The Netherlands; it is operated by the National Aerospace Laboratories of The Netherlands and it is calibrated by the TPD-TNO-TU (TNO Institute of Applied Physics-Netherlands Organization for Applied Scientific Research at the Delft University of Technology).

The Compact Airborne Spectrographic Imager (CASI) was flown over the study area on 14 September 1990 between 10:45 and 12:54 solar time at an altitude of 0.45 km (Fig. 6.1.b). Dependent on measurement mode this instrument is an imaging spectrometer with the dual capability of measuring as a line spectrometer (with 39 parallel lines or pixels) in the spectral mode or as a programmable multispectral imager (with 512 pixels across track) in the spatial mode. A true imaging spectrometer mode, which has the highest spatial and spectral resolution, is also available, but one image recording requires 1.5 seconds and is therefore only suitable for application from fixed platforms in field and laboratory experiments. The CASI instrument used (nr 201) was operated by the owner: AeroSpace Image Productions, Heidelberg, FRG. It was manufactured by Itres Research, Calgary, Canada.

In spectral mode a contiguous spectrum from 430 to 900 nm at 1.8 nm intervals across a rake of 39 interspaced lines parallel to the flight direction is recorded. In spatial mode the CASI can be programmed to function as a multispectral system with the capability of pre-flight or in-flight programming of up to 15 spectral bands between 430 to 900

nm. In this study the instrument was flown in multispectral, or spatial mode, using a spectral band set closely approximating the Inland Water Mode spectral filter set of the CAESAR instrument. Table 6.1 presents the CASI spectral band configuration used.

The main differences between the two remote sensing instruments are that the CASI simultaneously registers all the spatial and spectral information in one scan line. In addition, with CASI, the ability to select the operating mode and required spectral band settings within each mode in-flight confers great flexibility. The CASI can also be mounted in most vertical aerial photography mounts in aircraft. Major modifications in order to fit the instrument are therefore not required.

In this chapter the CASI instrument, and the remote sensing data acquired with the CASI will be presented and discussed first. The spectral mode results will be presented initially, because the spectra enable a comparison of the *in situ* spectroradiometric data with the remotely sensed upwelling radiance or L_{rs} spectra. The results of the CASI spatial mode recordings will be subsequently discussed.

The CAESAR data, with a more limited sampling of the reflectance spectrum, can best be discussed in relation to a system which measures the entire spectrum. The CAESAR instrument and data will therefore be discussed after the CASI measurements. Moreover, due to calibration problems, only two spectral bands on this instrument were finally proven to have functioned correctly.

6.2 The CASI imaging spectrometer

6.2.1 *The CASI instrument description*

The CASI is a pushbroom imaging spectrometer. The basic concept is that a line perpendicular to the aircraft is imaged along one dimension of a two-dimensional charge coupled device (CCD) array (the "pushbroom" concept), while the spectrum is dispersed along the other dimension. The along-track ground resolution is a function of aircraft speed and integration time, while the across-track ground resolution is a function only of aircraft altitude. The CASI has three operating modes: 1) spatial mode; 2) spectral mode and 3) full frame mode.

As previously stated, in spatial mode up to 15 spectral bands (of any width, but never overlapping) may be defined and implemented immediately at the highest spatial resolution of 512 pixels across track. In spectral mode spectra at 1.8 nm intervals with a resolution of 3.0 nm are acquired over 39 lines in a "rake" across the scene. The 288 * 1.8 = 520 nm spectral coverage may be positioned anywhere between 410 and 980 nm, though calibration is only guaranteed between 430 and 780 nm. A simultaneous "Scene Recovery Channel" is acquired in full spatial mode in a selected wavelength interval. This may be useful in locating the position of the less easily visualised "raked" spectral lines.

In full-frame mode the entire CCD sensor area is digitized, acquiring 288 spectral samples for each of 512 spatial pixels. This mode is used for the acquisition of calibration data and in applications where hyperspectral data sets are desired. One full frame acquisition requires 1.5 seconds and is therefore only useful when employed from a fixed platform.

6.2.2 *The flight specifications*

Data were acquired in the first two CASI modes at an altitude of 450 m A.G.L. over a variety of clear to turbid, mesotrophic to highly eutrophic, waters in the central western part of The Netherlands (Fig.6.1.b) on 14 September 1990. The CASI was mounted in a WILD RC40 aerial camera mount in a twin-engined aircraft with an air speed of 120 knots. In spectral mode the integration time was set at 202 ms (milliseconds) providing an along-track resolution of 13.6 m and an across-track resolution of 0.6 m. In spatial mode the integration time was 57 ms providing an along-track resolution of 3.9 m. The swath width in the spatial mode was 512 * 0.6 = 307 m, whereas the swath width for the spectral mode was {(39 * 0.6)+(39 * 0.6 * 4)}= 117 m. It should be pointed out that on this mission CASI was operated at very low altitudes. This configuration was near the limits of the recommended specifications.

6.2.3 *Calibration and performance*

The CASI data suffered from various types of noise. The noise occurred as a fixed high frequency noise pattern across the spectra acquired in the spectral mode and across the image line in the spatial mode, and as a low frequency noise across the rake or swath of the spectral mode and across the image line of the spatial mode. The high frequency noise was probably the result of leakage in the CCD chamber causing frost deposition on the cooled (-30°C) CCD arrays (pers. comm. ASIP and ITRES), but could also be caused by incorrect or no application of calibration files by the supplier. The exact calibration routine carried out on the data during preprocessing could not be reconstructed. The low frequency effect resembled an optical lens effect with lower radiance values at the outsides of the CCD array. This effect was probably due to incorrect or no application of calibration files specifically meant to correct for optical lens-related errors.

Both the high and low frequency noise in the data showed a fixed pattern for each flight track and could thus be corrected by using a post-flight uniformity correction routine developed during the study for this purpose. This correction depended on the selection of homogeneous areas, preferably across a substantial number of image lines (minimum of 30), from which the average response per group of CCDs responsible for imaging a part of the spectrum or a part of the image was determined. The deviation of each CCD group from the average of all the CCD groups necessary for a complete spectrum or a complete image line gives a measure for the high frequency noise.

Because the central CCDs of the array were least influenced by the optical lens effect causing the low frequency noise, the average of the central pixels (50% of the pixels between pixel or CCD number 128 and 384) was calculated. The raw data were subsequently corrected to this fixed average value using both the high and low frequency determined deviations.

This method of data correction, which requires the assumption of a homogeneous area in the water body, is contrary to one of the aims of remote sensing: determining the spatial variation of detected optical water quality features. If the homogeneous area is in fact heterogeneous, the error which is meant to be corrected for is replaced by another error. Such post-flight uniformity correction procedures, making use of scene data, is the least desirable method for calibrating remote sensing data. The correct application of pre-flight and in-flight calibration routines are essential for developing reliable remote sensing methodologies.

For the calculation of radiance values from the digital number values a peak spectral radiance unit (PSRU) is required. The PSRU applied was determined postflight and as such determines the range of raw digital numbers recorded to be fitted into a maximum range of zero to 4092 digital numbers (12 bits representation) of corrected data. This corrected data is subsequently transformed to 16 bit data. For the CASI data acquired in this study a PSRU of 0.24 W m^2 nm^{-1} sr^{-1} was applied to the spectral mode data. One digital number (DN) is equal to 0.24/65536 = 3.67 10^{-6} W m^2 nm^{-1} sr^{-1}.

The PSRU for the spatial mode data was not supplied with the data and could not be recovered. In order to derive a PSRU for the spatial mode data 48 sample points (each point corresponding to a 3 by 3 pixel matrix average value) were sampled across all tracks and water bodies in both the spatial and spectral modes. From the spectral mode data average digital numbers were calculated integrated over the corresponding wavelengths of the spectral bands selected for the inland water mode settings. The digital number values of the spatial mode were approximately 5 times (with a maximum variation of 10%) as high for each band. Thus for each band of the spatial mode a PSRU was derived from the PSRU of 0.24 W m^2 nm^{-1} sr^{-1} for the spectral mode, divided by an empirically derived factor to convert from spectral to spatial mode.

There appeared to be no quality control employed by the operators of CASI in the process of recording and calibration. No specific reason was apparent for the differing PSRU values. A consequence of the PSRU being approximately 5 times higher for the spatial mode than for the spectral mode is that the signal-to-noise levels are higher for the spatial mode.

The samples extracted from the spectral mode data for further analysis still showed considerable noise between adjacent lines. For the spectral mode 3 by 3 pixel averages were sampled to suppress this noise remaining after the post-flight uniformity correction discussed above. This was equivalent to a 40.8 m area in the along track direction (each along track pixel = 13.6 m) and an average of three samples each of 0.6 m width with

interspaces of 4 pixels or 2.4 m between each pixel (due to the "rake" sampling characteristics in spectral mode) in the across track direction.

The spectra required smoothing to remove high frequency noise not removed by the post flight uniformity correction. A 5 channel interval moving box filter was applied, reducing the resolution from 3 nm at 1.8 nm intervals to 10.2 nm (5 * 1.8 nm + 0.6 nm at each side due to the difference between the interval (1.8 nm) and the resolution (3 nm)) at 1.8 nm intervals. Since the resolution of the field-based spectroradiometer (Spectron) was approximately 8 nm, the effective spectral resolutions of the spectroradiometric and the imaging spectrometer data were in the same range.

Finally, a cubic spline interpolation was applied to convert the smoothed spectral data to 2 nm intervals for comparison with the other spectrophotometric and spectroradiometric spectral data.

6.2.4 *Calculation of R(0-) from L_{rs} measurements*

6.2.4.1 *Method*

In order to apply the algorithms developed in the previous chapters for *R(0-)* measurements the CASI L_{rs} spectra needed to be recalculated to the equivalent *R(0-)* spectra. This required removal of the atmospheric path radiance, the water surface reflection and the air/water interface effects as well as a conversion of radiance to irradiance data. The equations necessary for this data conversion were derived from § 3.

6.2.4.2 *Calculation of R(0-) from the CASI L_{rs} measurements*

The CASI spectral L_{rs} measurements were corrected for atmospheric path radiance, the water surface reflection and the air/water interface effects and converted to irradiance, by using *in situ* L_o and L_{wu} measurements from the Spectron SE-590 spectroradiometer equipped with a 15° FOV aperture as described in Chapter 3. The most appropriate spectroradiometric measurement took place at the sampling point on the Water Reservoir (WR1: Fig. 6.1.a). The CASI flew over this sampling point at 11:42 solar time; the *in situ* spectroradiometric measurement was performed 42 minutes later at 12:24 solar time. The corresponding sun zenith angles were 48.5° and 48.7° respectively and the atmospheric conditions were fairly stable during this 42 minute interval (Fig. 6.2.a). Fig. 6.3 shows the CASI L_{rs} spectrum and the *in situ* spectroradiometric measurements of subsurface and above surface upwelling radiance (L_{az} and L_{wu}) made at the Water Reservoir on 14 September 1990. The procedure to calculate the corresponding spectral *R(0-)* signal from the L_{rs} signal is given below.

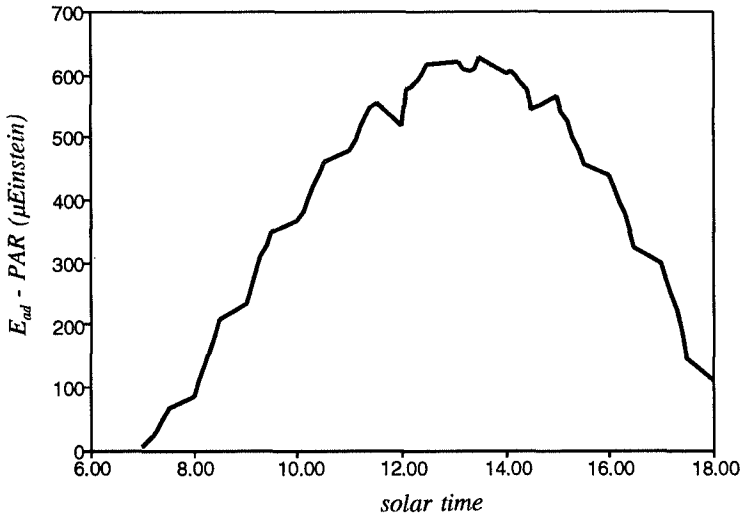

Figure 6.2.a *Registration of PAR downwelling irradiance at 10 minute intervals calculated from 20 measurements each registered at 30 seconds interval time at Lake Maarsseveen 5 km to the south of Lake Loosdrecht on the day of the CASI remote sensing flight.*

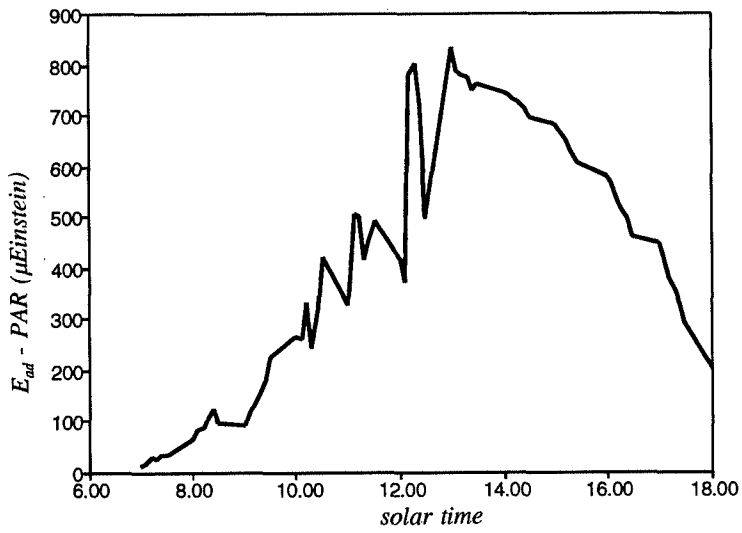

Figure 6.2.b *Registration of PAR downwelling irradiance at 10 minute intervals calculated from 20 measurements each registered at 30 seconds interval time at Lake Maarsseveen 5 km to the south of Lake Loosdrecht on the day of the CAESAR remote sensing flight.*

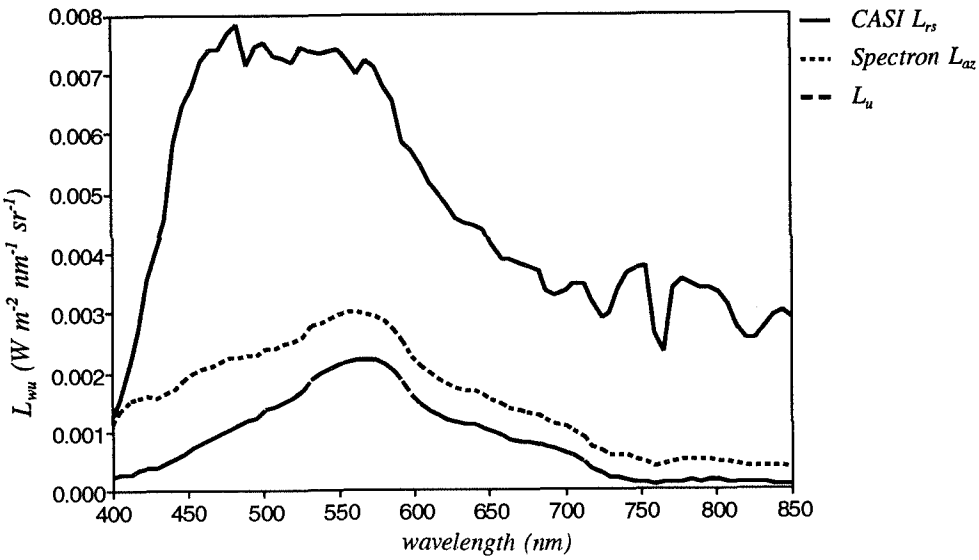

Figure 6.3 *CASI L_{rs} spectrum and the in situ spectroradiometric measurement of upwelling radiance above the surface L_{az} at the Water Reservoir on 14th September 1990.*

R(0-) is defined as E_{wu} / E_{wd}. E_{wu} was calculated from L_{rs} and E_{wd} was derived from the reference panel measurement of downwelling radiance L_o. First the L_{rs} signal required conversion to L_{az}. According to equation 3.1.b this entails determination and removal of T_{az} as well as L_p from the L_{rs} signal. If this removal of T_{az} and L_p takes place using *in situ* spectroradiometric measurements the most direct approach is to take the *in situ* L_{az} measurement and to subtract this from the L_{rs} signal. According to equation [3.1.b] this is not a correct procedure because T_a is a multiplicative factor whilst L_p is an additive factor. However, in the absence of atmospheric modelling to enable the calculation of T_a the two atmospheric factors are jointly approximated by L_{rs} - L_{az}. If, as is the case in this study, L_{wu} measurements are available, it is also possible to calculate the atmospheric and the surface reflectance effects by calculating L_u from L_{wu} using equation 3.6.b. In this manner an above-surface spectroradiometric measurement subject to the possible errors discussed in § 3 is not required. Thus the combined atmospheric and water surface effects can be calculated by L_{rs} - L_u which is equal to L_p' + L_{ar}, where L_p' is the atmospheric path radiance with an atmospheric transmittance effect included. The low altitude (450 m A.G.L.) at which the L_{rs} measurements were made caused L_p to be almost equal to L_p'. E_{wu} was thus calculated by:

$$\{(L_{rs}-(L_p'+L_{ar})\} * 1.8159 * 5 \qquad [6.1]$$

where 1.8159 is the factor required for converting L_u to L_{wu} and where 5 is the factor Q needed for calculating E_{wu} from L_{wu} (§ 3). E_{ad} was calculated from the reference panel measurement of reflected downwelling radiance L_o according to equation [3.2.a] and E_{wd} was calculated from E_{ad} using equation [3.14].

Table 6.2. *S/N requirements defined as δR(0-) based on values calculated in Chapter 5 and S/N ratios for remote sensing data defined as δR_{rs}. The conversion factor for determining δR_{rs} from δR(0-) was calculated to be 2.89. See text for derivation and further details.(Chl-a = chlorophyll a; CPC = cyanophycocyanin; DW = seston dry weight; K_d = vertical attenuation coefficient for subsurface downwelling irradiance; SD = Secchi disk transparency)*

	calculated		actual detection limit : δR_{rs}		
	$\delta R(0-)$	δR_{rs}	528:1 950:1 485:1 (for CPC)		
for measuring unit quantity			CASI	CAESAR	
Chl-*a*:	700:1	2020:1	4	2	µg l^{-1}
CPC	3000:1	9670:1	20	--	µg l^{-1}
DW	66:1	190:1	0.36	0.2	mg l^{-1}
K_d	320:1	920:1	0.17	0.10	m^{-1}
SD	1000:1	2890:1	55	30	cm

With this information it was possible to calculate the required conversion factor for determining the δR_{rs} from the $\delta R(0-)$ as determined in § 5. Table 6.2 presents the calculated values for the S/N ratio expressed as $\delta R(0-)$ for the water quality parameter detection. The conversion from $\delta R(0-)$ to δR_{rs} is required in order to determine the accuracy demanded of a remote sensor for determining a unit measure of a water quality parameter. The derivation is as follows:

R_{rs} is defined as L_{rs}/L_o from equation 3.2, substituting subscript *rs* for *az*.
$R(0-)$ is converted to R_{rs} by dividing $R(0-)$ by a factor 2.89. This factor is calculated as follows:

- a conversion factor of E_{wu} to L_u is 1.816 * 5 = 9.08;
  the conversion factor of E_{wd} to E_{ad} is 0.97;
  the conversion of E_{ad} to L_o is a factor π;
  thus $R(0-)$ to R_{rs} is $9.08/\pi = 2.89$.

Because all measurements (including L_p and L_{ar}) of L_{rs} over water targets are less than 20% in terms of R_{rs}, this correction factor is valid for converting *R(0-)* to R_{rs} as required for the calculation of $\delta R_{rs}$from $\delta R(0-)$.

The results in Table 6.2 for the detection limit of the CASI in spatial mode are minimum values because CASI performed below capacity due to the calibration and system errors during and after the flight. The detection limit of 55 cm for *SD* was calculated for the deep lakes; for the shallow lakes this value will be in the range of 10-20 cm.

The CASI spectral and spatial mode tracks were flown consecutively and a cosine correction for the increase in solar zenith angle with time was made for the L_{rs} data. This correction made it possible to apply the same L_{rs} to *R(0-)* correction for all the CASI data. For the CASI spatial mode data the same conversion factors were applied using integrated values over the equivalent wavelength bands of which the inland water mode bands were composed. In this manner *R(0-)* data were acquired from the remote sensing measurements. With these *R(0-)* values derived from L_{rs} measurements, concentrations of chlorophyll *a*, CP-cyanin, seston dry weight and values for Secchi depth transparency and vertical attenuation were calculated using the appropriate algorithms presented in § 5 and summarised in Table 7.1.

6.2.5 *The estimation of water quality parameters from CASI remote sensing data using multitemporal algorithms.*

The algorithms for estimating water quality parameters from *R(0-)* given in § 5 and summarised in Table 7.1 were applied to the *R(0-)* data derived from both the CASI spectral and spatial mode data. The algorithms developed from the spectral data at intervals of 2 nm were applied to the spectral mode data. The algorithms developed for the Inland Water Mode spectral band settings were applied to the spatial mode data.

Spectral samples were extracted from locations in the water bodies where maximum and minimum L_{rs} radiance values occurred, based on images of the 706 nm spectral band for the spectral mode (equal to a swath of 39 lines) and on images of spectral band 8 (698-714 nm) of the spatial mode. It was assumed that minima and maxima in this band would correspond with approximate minima and maxima of the water quality parameters detected.

The results of the algorithms for *R(0-)* data, applied to converted *R(0-)* data derived from L_{rs} data, are presented in Tables 6.2 a-e for chlorophyll *a*, CP-cyanin, seston dry weight, vertical attenuation and Secchi depth transparency. Also given are the values of water quality parameters obtained during *in situ* sampling on days immediately before, during and immediately after the remote sensing flight. This allows a comparison to be made between the water quality parameter values determined by remote sensing and the *in situ* measured values. Furthermore, the sampling data give an estimate of the range of the water quality parameters in question during the remote sensing campaign. The

water quality parameter measurements, based on *in situ* determinations and water samples, will each have their own sources of error as explained in Chapter 1. In the following discussion on the remote sensing results it was assumed that measurement errors in the field and in the laboratory did not cause systematic errors in the data.

Chlorophyll a

In general the results for chlorophyll *a* detection (Table 6.3.a) using both CASI spectral and spatial mode data compare well. For the shallow eutrophic lakes there is a tendency for higher values of calculated chlorophyll *a* levels to be estimated from the spatial mode data than from the spectral mode data. One reason for this may be errors caused by the indirect method of establishing the PSRU for the spatial mode data. Another reason may be that selection of minima and maxima on the spatial mode data took place on a higher quality (spatial resolution) image and across a larger swath width (512 instead of 39 pixels), thus enabling more points to be sampled.

The higher radiometric sensitivity shown in the spatial mode data, as indicated by the empirically derived PSRU being 5 times lower for this mode than for the spectral mode, may also explain the differences observed.

The correctness of the method applied is supported by the good correspondence between the measured values of chlorophyll *a* and those estimated from the remotely sensed data at the Water Reservoir (WR) and at Lake Eastern Loenderveen (LEL) on 14 September, as well as for all the other waters sampled on previous days. From minimum *R(0-)* values in Lake Spiegel (LSP) negative estimates for chlorophyll *a* were calculated indicating that the algorithm does not always function well at low levels of chlorophyll *a*.

CP-cyanin

In Table 6.3.b the values of CP-cyanin estimated from the CASI data are presented together with both the measured CP-cyanin concentrations from samples taken on 12 September and with estimated values based on applying the CP-cyanin-specific absorption coefficient of 0.0032 m^2 mg^{-1} to the phytoplankton absorption spectra derived from samples taken between 28 August and 10 September 1990 (see § 5).

The back cover of this publication presents a CASI spatial mode image covering part of Lake Wijde Blik, Lake Western Loenderveen and the Water Reservoir (see Fig. 1.1 and 6.1.b for location). The CP-cyanin algorithm was applied to the CASI data converted from $\underline{Lrs}$ to *R(0-)*. These three lakes represent three entirely different water types: a deep eutrophic lake (LWB) with abundant *Microcystis aeruginosa* floating at or near the water surface, a shallow eutrophic lake (LWL) with a mixture of the filamentous prokaryotic algae *Prochlorothrix hollandica* and *Oscillatoria spp.*, and a deep oligotrophic lake (WR) without measurable concentrations of cyanobacteria.

Samples	in situ samples 28-8	in situ samples 3-9	CAESAR 6 km A.G.L. Min 3-9	CAESAR 6 km A.G.L. Max 3-9	in situ samples 4-9	in situ samples 5-9	in situ samples 10-9	in situ samples 12-9	in situ samples 14-9	CASI 0.45 km A.G.L. Spectral Min 14-9	CASI 0.45 km A.G.L. Spectral Max 14-9	CASI 0.45 km A.G.L. Spatial Min	CASI 0.45 km A.G.L. Spatial Max
shallow eutrophic													
LNW						162		130		85	116		
LHA	112		127	127	140			115		113	128	120	124
LWG*	140		135	138	212			191		125	135		
LVU			96	146		130	120	87					
LWL		21-70	56	64				41		53	60	60	66
LEL		88-90	83	98		84	76		69-77	70	77	72	89
LNP			131	131		134				135	135	129	160
LLO			101	183		170	120	106-147		111	171	129	173
LBR			91	104		128	116	85- 86					
shallow mesotrophic													
LNG		4						42				17	56
LNS		10						14					
LSA	15		54	56	27			21		36	60	26	40
LHO			59	73				12					
deep													
LSP	6		30	54		17		10		0	17	0	16
LWB	11		23	70	52-219		25	40		37	111	36	169
WR		5	0	27					5	4	27	0	10
river canal													
RVE			34	83	11- 18			9- 37		29	65	16	72
ARK			34	49		8- 10		9- 11		10	14	8	16
HIK	174		69	86				93		15	95	19	31

Table 6.3.a(opposite page) *Chlorophyll a (in µg l^{-1}): algorithm from Table 5.6. Although the CASI spatial mode band setting was slightly different from the CAESAR Inland Water Mode the same algorithm equation was used:*

CASI spectral mode : $C_{meas} = -48.2 + 66.5\ R(0\text{-})_{706} / R(0\text{-})_{676}$

CAESAR & CASI IWM : $C_{meas} = -59.0 + 78.9\ R(0\text{-})_{698\text{-}716} / R(0\text{-})_{671\text{-}684}$

Table 6.3 - General caption:

Water quality parameter estimation based on

1) in situ samples on days before during and after the remote sensing flights

2) calculated from remotely sensed upwelling radiance (L_{rs}) converted to R(0-) applying the appropriate multitemporal algorithm from Chapter 5.

The minimum and maximum values for the water bodies are based on selection of highest and lowest upwelling radiance (L_{rs}) measurements for spectral bands centered at 706 nm. The HIK samples are estimated according to the shallow lakes algorithms, where applicable. Although it is a canal its water quality is determined by the in and outflow of the surrounding lakes (such as LWB and LWG) and there is no heavy shipping causing turbulence and thus a high suspended load. The LWG measurements from the CASI spectral mode are located in a smaller connected lake just to the north east of LWG and are designated with LWG.*

The range of CP-cyanin derived from the image lies between 0 for the WR to more than 148 µg l^{-1} for LWB. LWL seems to have a fairly homogeneous distribution of CP-cyanin whereas LWB shows patterns in the distribution of CP-cyanin probably related to near-surface or floating layers of *M. aeruginosa.* Due to the differing nature of the algae and the water bodies the accuracy of the CP-cyanin concentration estimation is unsure. Not enough data was available to calculate CP-cyanin-specific absorption for *M. aeruginosa.* Furthermore, the effect of layers of concentrated algae on the algorithm results needs to be investigated. However, from Table 6.2 it was already evident that the accuracy for CP-cyanin detection based on the δR_{rs} of the CASI was 20 µg l^{-1} CP-cyanin. If the CASI had functioned according to its specifications a threefold increase in sensitivity would seem possible, resulting in a detection accuracy based on δR_{rs} of 7 µg l^{-1} CP-cyanin.

For Lake Naardermeer Wijde Blik (LNW), Lake Hollandsch Ankeveen (LHA) and Lake Stichts Ankeveen (LSA) the calculated values from the CASI spectral mode data were lower than those for the *in situ* samples. Estimates from the spatial mode data were higher for LHA (LNW data were not recorded in spatial mode).

The values estimated for CP-cyanin from the CASI spectral mode for lakes Wijde Gat (LWG), Loosdrecht (LLO) and Wijde Blik (LWB) were all within expected ranges. The large range in values observed in LWB was caused by a gradient in surface or near-to-surface floating *Microcystis aeruginosa* colonies, increasing in concentrations towards the shores. For these lakes the CP-cyanin concentrations estimated from the spatial mode data were generally higher than estimates from the spectral mode. This difference could be caused by either a systematic error in the calibration or by the higher radiometric resolution of the spatial mode.

For the shallow mesotrophic lakes, the deep lakes (with the exception of LWB) and for the Hilversumsch Kanaal (HIK) negative values of CP-cyanin were calculated. This is a clear indication that the algorithm is only applicable to turbid waters with high algal concentrations, similar to the lake waters from which the algorithm was developed.

Seston dry weight (DW)

Estimated seston dry weight concentrations are presented along with measured values in Table 6.3.c. The Lake Eastern Loenderveen (LEL) sample of 14 September corresponded well with the CASI derived concentrations. The concentration in the WR was overestimated from the CASI data compared to a sample taken on the same date. This could be caused by the errors associated with calibration of the CASI or by the *in situ* sampling and laboratory-based measurement of *DW*, as well as by the influence on *R(0-)* of the r_1 coefficient in equation 4.5. An incorrect atmospheric correction may also have a relatively strong influence at low water reflectance values.

Samples	<--calculated from a(ph)--> 28-8	3-9	5-9	10-9	measured from sample 12-9	CASI 0.45 km A.G.L. Spectral Min	Spectral Max	Spatial Min	Spatial Max
						14-9			
shallow eutrophic									
LNW					130	0	42		
LHA				51	110	59	63	81	94
LWG*	67			96	92	116	124		
LVU					38				
LWL		29			8	5	26	40	77
LEL		40-41	34			29	54	39	111
LNP						92	92	105	110
LLO			53		49	66	92	65	119
LBR					46			123	154
shallow mesotrophic									
LNG								0	0
LSA				7	7	0	0	0	0
deep									
LSP						0	14	0	34
LWB	7-113		8		110	24	166	52	203
WR						0	0	0	5
canal									
HIK	57					0	20	0	20

Table 6.3.b *CP-cyanin (in μg l^{-1}): the CASI spectral mode algorithm is given in Eq. 5.14 The Inland Water Mode algorithm equations are derived from Table 5.9. (C_{CPC} = concentration of CP-cyanin (μg l^{-1})*

CASI spectral mode : $C_{CPC} = -24.6 + 13686\ (0.5\ (R(0-)_{600}+R(0-)_{648})-R(0-)_{624})$

CAESAR IWM : $C_{CPC} = -28.1 + 15904\ (0.5\ (R(0-)_{B3}+R(0-)_{B5})-R(0-)_{B4})$

CASI IWM : $C_{CPC} = -28.1 + 15904\ (0.5\ (R(0-)_{B3}+R(0-)_{B5})-R(0-)_{B4})$

Samples	in situ samples 28-8	3-9	CAESAR 6 km A.G.L. Min 3-9	Max	in situ samples 4-9	5-9	10-9	12-9	14-9	CASI 0.45 km A.G.L. Spectral Min 14-9	Max	Spatial Min	Max
shallow eutrophic													
LNW						37		30		26	29		
LHA			25	25	19			13		29	34	33	34
LWG*	45		38	39	36			31		43	44		
LVU			22	22		30	31	31					
LWL		3-13	12	16				12		17	17	18	19
LEL		20-21	16	17		22	21		19	19	23	14	25
LNP			21	21		24				27	27	31	35
LLO			20	23		37	31	30-33		26	30	31	42
LBR			26	27		37	34	32-34				43	47
shallow mesotrophic													
LNG		3						1				5	7
LNS		4						3					
LSA			14	14	4			10		9	10	6	9
LHO			13	14				4					
deep													
LSP	9-16		8	13				1- 4		4	7	2	5
LWB	15-17		12	25	3			2- 6		9	38	16	57
WR		1	3	7					1	5	8	3	4
river canal													
RVE			13	37	8-15	6- 8		1-19		10	38	16	36
ARK			14	32		13-14	28	7-13		30	35	31	41
HIK	21		13	21				7		17	21	16	16

Table 6.3.c *Seston dry weight (in mg l^{-1}): The algorithm for DW estimation (excluding the ARC and the LHA samples) from Table 5.10 was applied. The algorithm for the CAESAR Inland Water Mode band 8 was also applied to the CASI Inland Water Mode band 8.*

CASI spectral mode : $DW = 2.69 + 331\ R(0-)_{706}$

CAESAR & CASI IWM : $DW = 0.71 + 406\ R(0-)_{698-716}$

	in situ samples		CAESAR 6 km A.G.L.		in situ samples				CASI 0.45 km A.G.L.			
									Spectral		Spatial	
			Min	Max					Min	Max	Min	Max
Samples	28-8	3-9	3-9		5-9	10-9	12-9	14-9	14-9			
shallow eutrophic												
LNW									2.97	3.63		
LHA			3.84	3.84			3.08		3.57	3.86	3.66	3.75
LWG*	4.58		3.99	4.00					3.80	4.01		
LVU			3.19	3.76	3.49	3.42	3.16					
LWL		2.02-2.75	2.38	2.56			2.51		2.31	2.45	2.45	2.48
LEL		3.02-3.31	2.93	3.24		2.83		2.38-2.40	2.66	2.81	2.70	3.03
LNP			3.90	3.90					4.01	4.01	3.85	4.47
LLO			3.31	3.74	4.30	3.64	3.38-3.80		3.95	4.76	3.95	4.86
LBR			3.27	3.36		3.49	3.59-3.89				4.23	4.28
shallow mesotrophic												
LNG		0.82									1.58	2.38
LNS		1.32										
LSA			2.36	2.40			1.54		1.96	2.46	1.77	2.05
LHO			2.46	2.73								
deep												
LSP	0.72-0.74		1.15	1.56					0.39	0.92	0.29	0.89
LWB	1.06-1.20		1.03	1.84		1.52			1.29	2.62	1.19	3.53
WR		0.69	0.60	1.08				0.64	0.69	1.10	0.40	0.79
river canal												
RVE			1.95	2.94							1.19	2.34
ARK			1.96	2.26		2.02					1.04	1.20
HIK	4.07		2.65	3.01					1.53	3.19	1.63	1.87

Table 6.3.d *Vertical attenuation coefficient (in m^{-1}) for subsurface downwelling irradiance (K_d: units m^{-1}): the values for RVE and ARC were based on the algorithm based on all samples. The 2 nm algorithms are from Table 5.11. The IWM algorithms come from Table 5.13*

CASI spectral mode	$: K_d = -0.5331 + 1.7046\ R(0-)_{706}/R(0-)_{676}$	*(all waters)*
	$: K_d = +0.2134 + 1.3786\ R(0-)_{706}/R(0-)_{676}$	*(shallow lakes)*
	$: K_d = -0.2467 + 1.1966\ R(0-)_{706}/R(0-)_{676}$	*(deep lakes)*
CAESAR & CASI IWM	$: K_d = -0.7950 + 1.9984\ R(0-)_{B8}/R(0-)_{B7}$	*(all waters)*
	$: K_d = 0.0492 + 1.5950\ R(0-)_{B8}/R(0-)_{B7}$	*(shallow lakes)*
	$: K_d = -0.4045 + 1.3600\ R(0-)_{B8}/R(0-)_{B7}$	*(deep lakes)*

Samples	in situ samples 28-8	3-9	CAESAR 6 km A.G.L. Min 3-9	Max	in situ samples 4-9	5-9	10-9	12-9	14-9	CASI 0.45 km A.G.L. Spectral Min 14-9	Max	Spatial Min	Max
shallow eutrophic													
LNW						30		25		41	54		
LHA	35		38	38	50			45		37	42	39	40
LWG*	35		35	35	40			35		35	38		
LVU			39	49		40	40	35					
LWL		65-145	68	76				50		72	78	68	73
LEL		50- 55	48	56			50		45-50	59	63	53	63
LNP			37	37						35	35	30	37
LLO			39	47		35	45			28	36	26	36
LBR			46	48		40	40	30				32	32
shallow mesotrophic													
LNG		>100				>120		80				76	141
LNS													
LSA	120		76	77	120			135		71	100	96	119
LHO			62	87				>150					
deep													
LSP	320-365		116	189		440		290-450		260	775	273	974
LWB	165-185		89	221	70			150-175		51	157	28	178
WR		490	206	463					400	199	387	321	729
river canal													
RVE			60	117		60-120		70- 80		11	46	63	172
ARK			92	117		70- 90	90	60- 65		60	74	171	207
HIK	60		54	65				60		49	146	110	134

Table 6.3.e *Secchi disk transparency (in cm): for the CASI spectral mode the algorithm from Table 5.12 was applied, for the CAESAR and CASI Inland Water Mode the algorithms from Table 5.14 were applied: The ARC and RVE estimations were based on the "all" water algorithms.*

CASI spectral mode : $ln\ SD = 5.05 - 1.795\ ln\ (R(0-)_{706}/R(0-)_{676})$ *(all waters)*

: $ln\ SD = 4.92 - 1.342\ ln\ (R(0-)_{706}/R(0-)_{676})$ *(shallow)*

: $ln\ SD = 5.51 - 1.815\ ln\ (R(0-)_{706}/R(0-)_{676})$ *(deep lakes)*

CAESAR & CASI IWM : $ln\ SD = 5.05 - 1.615\ ln\ (R(0-)_{B8}/R(0-)_{B7})$ *(all waters)*

: $ln\ SD = 4.89 - 1.464\ ln\ (R(0-)_{B8}/R(0-)_{B8})$ *(shallow)*

: $ln\ SD = 5.51 - 2.038\ ln\ (R(0-)_{B8}/R(0-)_{B7})$ *(deep lakes)*

Values for *DW* determined on 12 September were lower, in general, than those estimated from the CASI data on 14 September. The weather was similar on both days with low wind speeds, thus resuspension of bottom material may be ruled out as a possible cause for the difference. The CASI spatial mode derived values were generally higher than those calculated from the spectral mode measurements except for two deep lakes: LSP and the WR. The reason for this may be an incorrect estimation of the atmospheric influence, a non-linear response in the CASI two-dimensional CCD-array or a calibration error caused either by errors in the preprocessing of data or by the post flight uniformity correction method applied subsequently.

Vertical attenuation coefficient (K_d)

In general there was good agreement between the spectral and spatial mode remotely sensed estimates and the *in situ* measured values of K_d (Table 6.3.d). This is due to the application of separate algorithms for the shallow lakes and for the deep lakes. The high correlations for the regression equations given in Tables 5.11 & 5.13 for K_d were an indication of the possibility of attaining high accuracies for estimating K_d from remotely sensed data using the appropriate equations for the water bodies involved.

Secchi depth transparency (SD)

In general there was also good agreement between the *in situ* measurements and the remotely sensed values for SD (Table 6.3.d). However, the maximum *SD* values of 7 m and more calculated for the WR and Lake Spiegel (LSP) were higher than expected from the *in situ* measurements, and for LSP higher than measured during a monthly sampling program over 1990 (maximum *SD* measured in 1990 was 450 cm on 12 September 1990). The remotely sensed values could be correct, because remote sensing offers the opportunity to select sites with the lowest L_{rs}, thus enabling the detection of extreme values, which would be difficult to locate from a boat. However, as mentioned in Chapter 5, the algorithm becomes highly sensitive and thus possibly inaccurate at low *R(0-)* values for the spectral bands centred at 676 and 706 nm. Applying the linear regression equation for the deep lakes from Tables 5.12 & 5.14, maximum values for the WR were 5.06 m in spectral mode and 5.36 m in spatial mode, and for LSP 3.91 m and 4.97 m respectively. This is an indication that at low *R(0-)* values the exponential algorithm needs adaptation or that a linear algorithm is preferable.

6.3 The CAESAR multispectral scanner

The CAESAR instrument malfunctioned during the overflight on 3 September 1990 and errors in the pre- or postflight calibration were probably made. Thus only two spectral bands were available for further analysis. These two bands were, however, the spectral bands located at 671-684 nm and at 698-716 nm, thus enabling estimation of chlorophyll *a*, seston dry weight, Secchi depth transparency and vertical attenuation coef-

ficients. The quality of the data from the spectral bands required for the CP-cyanin algorithm was insufficient, preventing the estimation of CP-cyanin concentration.

6.3.1 *The CAESAR instrument description*

CAESAR was designed to make land and sea observations in up to nine different spectral bands. These nine spectral bands are grouped in three sets, each belonging to one camera of a (3-camera) down-looking module (see Table 6.1). One camera points 11.5° backwards, one is vertical and one looks ahead with a 11.5° tilt. CAESAR's advantages are the capability of measuring directional reflectances, a stereoscopic potential, high spatial resolution, the ability of applying user-specified filter sets and the absolute and relative geometric, radiometric and spectral calibration of the data. Another feature of CAESAR is the possibility of tilting the down-looking module over an angle varying from 0 to 20° in order to avoid sunglint. This feature is relevant for the water modes of CAESAR operation. A technical description and application possibilities of the CAESAR scanner are given in Donze *et al.* (1989).

The Inland Water Mode of nine spectral bands was developed for the CAESAR scanner as an illustration of how to use high resolution spectrometric data for modelling and data reduction in future imaging spectrometry remote sensing missions. Based on spectral signature analysis, spectral band simulated values of upwelling (ir)radiance and water quality parameters were used as input data for statistical analysis. The selected spectral bands in the wavelength range 500 to 800 nm were sufficient to obtain high correlations between spectral band combination values with water quality parameters (Dekker *et al.*, 1990).

For the preprocessing of CAESAR data, the National Aerospace Laboratories (NLR: The Netherlands) developed a special software package (OPTIPARES) to compensate for in-flight aircraft motion and attitude as well as for specific sensor distortions. During the flight aircraft motion parameters are measured by an Inertial Reference System (IRS). In the case of CAESAR, specific sensor corrections deal with the optical aspects of the scanner and the radiometric calibration, required for all individual elements and for all CCD-arrays. The geometric correction makes no use of topographic maps or geodetic reference points (Looyen & Dekker, 1991).

6.3.2 *The flight specifications*

Four tracks were flown across the study area with CAESAR on 3 September 1990 between 14:23 and 15:37 solar time at an altitude of 3 km and 6 km A.G.L. The flight tracks are shown in Figure 6.1.a. Corresponding swath widths were 1.3 km and 2.6 km. The data preprocessing and geometric correction were carried out to produce 4 m pixels.

CAESAR was tilted at 15° in the flight direction which was approximately from south to north to prevent sunglint affecting the remotely sensed signal. Because of this tilt the back looking array had an angle of 6.5° forward (-11.5°+ 3°pitch + 15° tilt), the central looking arrays had an angle of 18° forward (0°+ 3°+ 15°) and the ahead looking arrays had an angle of 29.5° forward (+11.5°+ 3°+ 15°).

The CAESAR data were geometrically corrected using the aircraft IRS data as described above.

6.3.3 *Calibration and performance*

The CAESAR system has been calibrated relatively and absolutely. In order to fulfil the objective that the detector should be able to detect a ground reflectance variation *Ned*ρ < 0.5% and *Ned*ρ < 0.05% over land and over sea respectively, the performance of CAESAR in terms of radiometric resolution was investigated (see Looyen & Dekker, 1991 for details; *Ned*ρ is defined as the noise-equivalent reflectance at a solar zenith angle of 60° at a flight altitude of 6 km A.G.L. and a full range of radiometric sensitivity over 0 - 25 % reflectance) and was found to be in order, except for one channel at 410 nm for the Sea Mode. For the Inland Water Mode the *Ned*ρ was not determined.

During the 1990 mission CAESAR data showed aberrant increases in measured radiances towards both outer ends of the central CCD arrays. A subsequent calibration was carried out at the TPD-TNO-TU and showed internal scattering of light out of the direct field of view in the central look CCD optical pathways. Baffles were mounted to suppress this scattering. A laboratory-based test under diffuse illumination conditions showed no measurable internal scattering (Smorenburg *et al*, 1991). The 1990 data was also affected, however, and therefore only data from the ahead and backward-looking modules were available for further analysis.

The data from each of the spectral bands in the ahead looking module (Bands 3-4-5, Table 6.1) seemed to be in order when analysed separately. Upon application of the CP-cyanin algorithm, involving determination of the average radiance of bands 3 and 5 and subsequent subtraction of band 4 values, the result was a scene-independent across track low frequency noise vector. Virtually all differences between land and water pixels were obscured by this effect. One factor partly responsible for this poor performance could be the strong tilt of 29.5° forward for the ahead looking module, causing a longer atmospheric path length, and a different reflectance angle.

It is possible that an operator error such as swapped spectral band data files caused this effect. Also, the calibration procedure applied to the CAESAR remote sensing data has acquired a "black box" nature for the scientist receiving data from the National Aerospace Laboratories, due to the non-modular and complex nature of the data preprocessing. Only at high cost and with considerable time effort could the procedure be check-

ed. It is strongly recommended that the calibration table application procedure be made transparent to users of the CAESAR data.

Spectral band 6 of the Inland Water Mode was inoperative due to incompatibility between the filters used for spectral band selection as specified by Dekker *et al.* (1990) and grey filters mounted on the lens of the D1 camera module by the TPD-TNO-TU. A superposition of the filters caused a reduction in sensitivity to 3% of the full radiance scale.

Thus, for the 1990 CAESAR remote sensing flight only data from spectral bands 7 (671-684 nm) and 8 (698-716 nm) were available. Fortunately, these bands were the spectral bands required for the estimation of all the water quality parameters treated in this study, except for CP-cyanin concentration.

6.3.4 *Calculation of R(0-) from the CAESAR L_{rs} measurements*

In general the same method that was used for the CASI data for calculating *R(0-)* from L_{rs} was applied to the CAESAR data. Therefore, only differences in the method are discussed here.

The CAESAR spectral L_{rs} measurements were corrected for atmospheric path radiance, water surface reflection and the air/water interface effects as well as a conversion of radiance to irradiance, by using *in situ* L_o and L_{wu} measurements from the Spectron SE-590 spectroradiometer. In the case of the CAESAR flight between 14:23 and 15:37 solar time, the nearest spectroradiometric measurement of L_o took place at a sampling point on Lake Naardermeer-Spookgat (LNS) at 14:00 solar time, corresponding to a solar zenith angle of 50.4°. This location was approximately 100 m to the east from the northern part of track 6 (Fig. 6.1.a). Figure 6.2 shows the relatively stable nature of the irradiance after 13:00 at Lake Maarsseveen in the south of the study area. Because the nearest spectroradiometric measurements did not correspond with the points on the CAESAR imagery, an alternative method was found for an estimation of L_{wu} at a location where CAESAR L_{rs} data were available.

On 3 September 1990 *in situ* spectroradiometric measurements were also made at lakes Western Loenderveen (LWL), Eastern Loenderveen (LEL) and the Water Reservoir (WR). The WR spectroradiometric measurements were performed at 10:01 solar time with a solar zenith angle of 50.4°. By calculating the difference between L_o measurements at the WR and at the LNS the L_{wu} measurement at the WR could be computed as if it had been taken at 14:00. Assuming a decrease in irradiance corresponding to the solar zenith angle increase with time in the afternoon during the CAESAR flight, it was possible to calculate a corresponding L_o for each flight track of CAESAR and a corresponding L_{wu} for those tracks recording above the WR. Apart from the similar solar zenith angles between the WR and the LNS measurements the homogeneous water quality at the WR was also an important criterion for selection.

According to equation 3.1.b, T_a is a multiplicative factor whilst L_p is an additive factor. However, in the absence of atmospheric modelling enabling calculation of T_z the two atmospheric factors may be jointly approximated by L_{rs} - L_a. Because L_{wu} measurements were available, albeit estimated, it was possible to calculate the atmospheric and the surface reflectance effects by calculating L_u from L_{wu} using equation 3.6.b. Thus the combined atmospheric and water surface effects were calculated from L_{rs} - L_u, which is equal to L_p' + L_{ar}, where L_p' is the atmospheric path radiance with an atmospheric transmittance effect included. The higher altitude (3000 / 6000 m A.G.L.) at which the L_{rs} measurements were taken using CAESAR compared to the CASI probably caused L_p' to be markedly different from L_p. The exact nature of this effect was not calculated due to the lack of information on T_a. Thus E_{wu} was calculated using equation 6.1 and *R(0-)* was subsequently calculated in the same manner as for the CASI data.

6.3.5 *The estimation of water quality parameters from CAESAR remote sensing data using multitemporal algorithms*

Spectral samples were extracted from locations in the water bodies where maximum and minimum L_{rs} radiance values occurred based on images of spectral band 8 (698-716 nm) of the spatial mode. It was again assumed that minima and maxima in this band would correspond with approximate minima and maxima of the water quality parameters detected.

Chlorophyll a

The chlorophyll *a* concentration estimates from the CAESAR data (Table 6.3.a) were in good agreement with measured chlorophyll *a* concentrations.

The front cover of this publication presents a CAESAR Inland Water Mode image covering Lake Wijde Gat (LWG) in the north to parts of Lake Loosdrecht (LLO) in the south (see Fig. 1.1 and 6.1.a for location; the legend is located on the back cover). The sinusoidal sides of the image are caused by the geometric correction for aircraft movements as explained in § 6.3.1. The image may be superposed on a topographic map with high accuracy. The chlorophyll *a* algorithm was applied to the CAESAR data converted from L_{rs} to *R(0-)*. These lakes cover the entire range in chlorophyll *a* encountered in the Vecht lakes area. LWG (top right hand corner of image) has high concentrations of chlorophyll *a* from ca. 90 to 150 µg l^{-1}. Water with a lower concentration of chlorophyll *a* (ca. 50 µg l^{-1}) can be seen flowing into LWG from the Hilversumsch Kanaal (HIK). Lake Wijde Blik (LWB) shows a gradient in chlorophyll *a* concentration from low values (ca. 20 µg l^{-1}) in the west to concentrations of 80 µg l^{-1} in the east. Lakes Eastern Loenderveen (LEL) and Lake Vuntus (LVU) show a north-south gradient in chlorophyll *a* concentration. This contrasting gradient orientation has no obvious reason, but may be related to the depths of the lakes (LEL and LVU are shallow (ca. 2 m); LWB is deep (ca 30 m)). LLO, LVU and Lake Nieuwe Polder are fairly homogeneous at high concentrations of chlorophyll *a* (ca 80 - 120 µg l^{-1}).

This image is an illustration of the value of remote sensing for detecting gradients within water bodies. Point samples taken in LWG, LWB, LEL and LVU would not be representative for the water body whereas a point sample in LWL, WR, LLO and LNP would be reasonably representative.

From Table 6.3.a the LWL, LEL and WR samples are all within the range estimated from CAESAR data. For the shallow mesotrophic lakes LSA and Lake 't Hol (LHO), the deep LSP and for the ARK and RVE, the chlorophyll *a* concentration estimates were higher than measured. This may be attributed to an inaccurate correction for the atmospheric transmittance and path radiance due to the indirect determination method. It is also possible that the algorithm requires modification at low concentrations of chlorophyll *a*. The results in chapter 5 indicated a non-linear nature at low concentrations for the simulations carried out involving fixed chlorophyll *a* to backscattering ratios. Only a few low chlorophyll measurements were available for this study. With more information on the scattering by algae and by tripton an improved algorithm may be developed for estimating chlorophyll *a* more accurately in phytoplankton-poor lakes, rivers and canals.

Seston dry weight (DW)

The *DW* estimates calculated from the remotely sensed data are presented along with measured values in Table 6.3.c. Estimates for LEL, LWL and WR from the same day corresponded reasonably well to the *in situ* sampled dry weight concentrations. At low measured concentrations, such as for LSA, LHO, LSP, the WR and the River Vecht and ARK samples the CAESAR derived seston dry weight concentrations were higher. This result may be caused by an incorrect estimation of the atmospheric influence, a non-linear response in the CAESAR CCD-arrays or a calibration error caused either by errors in the pre- or postflight processing of the data; sampling error or laboratory measurement error may also contribute. Because estimated *DW* was based on the single Band 8 (696-714 nm) reflectance value, variations in the coefficient r_1 relating *R(0-)* to the inherent optical properties (equation 4.3) could contribute to this error.

Vertical attenuation coefficient (K_d)

As for the CASI data there was general agreement between the remotely sensed estimates and the *in situ* measured values of K_d (Table 6.3.d). The *in situ* measured K_d values on the day of the CAESAR flight were all within the range measured calculated from the CAESAR data.

Secchi depth transparency (SD)

The Secchi depth transparencies (*SD*) calculated from the remotely sensed data are presented along with measured transparencies in Table 6.3.d. As for the CASI estimates there was good agreement between the *in situ* measurements and the CAESAR derived

remotely sensed values for *SD*. There were no apparent systematic variations between waters with higher or lower transparency.

6.4 Conclusions

L_{rs} data from two flights using different types of remote sensing instruments carried out 11 days apart, at different solar zenith angles and atmospheric conditions and at different flight altitudes, were converted to *R(0-)* values. It was demonstrated that analytical and semi-empirical algorithms for water quality feature extraction, developed on the basis of *in situ R(0-)* measurements, could be successfully applied to both sets of remotely sensed data to yield useful results.

Making use of two spectral bands, centred at 676 nm and at 706 nm, estimations could be made of concentrations of chlorophyll *a* and seston dry weight and of vertical attenuation coefficients and Secchi depth transparency. Cyanophycocyanin concentrations, requiring the measurement in spectral bands centered at 600, 624 and 648 nm, were measured by the CASI in both spectral and spatial mode. However, the required sensitivity of the remote sensor needs to be of high order to measure this parameter. CAESAR data was insufficiently calibrated to perform these measurements.

The calculation of *R(0-)* values from remotely sensed upwelling radiance is possible when estimates of the downwelling irradiance and subsurface upwelling radiance are available. In the absence of subsurface upwelling radiance measurements, however, the fraction of diffuse to total downwelling irradiance is required. Because *R(0-)* is largely independent of irradiance, atmospheric condition and water surface state, it was possible to make use of *in situ* spectroradiometric measurements made several hours before the remote sensors flew over the target area. However, simultaneous *in situ* spectroradiometric measurements of L_{wu} and L_o at the time of the overflight are always preferable for the required calibrations and calculations necessary to derive *R(0-)* from L_{rs}.

The lack of quality control for calibration of both the CAESAR and the CASI instruments and their data sets limited the accuracy of the water quality estimates. In the case of CAESAR seven out of nine spectral bands were partly or wholly inoperative due to design, calibration and operator errors. In the case of the CASI instrument it was not clear whether calibration tables were applied or not. An instrument error also increased noise in the data.

Given data from multispectral remote sensing systems, with a spectral band set such as the Inland Water Mode, it is possible to determine chlorophyll *a* and CP-cyanin with analytical algorithms and *DW*, K_d and *SD* with semi-empirical algorithms. The remote sensing of these water quality parameters requires five spectral bands centered at 600, 624, 648, 676 and at 706 nm. The inclusion of further spectral bands may allow discrimination of other water quality parameters. For example, it is probable that inclusion of spectral bands located at 545, 565 and 585 nm will allow discrimination of CP-erythrin.

7 GENERAL CONCLUSIONS, DISCUSSION AND RECOMMENDATIONS

7.1 General conclusions on remote sensing of inland waters

This research marks a significant change in research methodology pertaining to development and implementation of remote sensing of inland waters. During remote sensing missions it is no longer necessary to gather large quantities of *in situ* samples for statistical analyses in support of the empirical or semi-empirical methods. Research can now focus on increasing understanding of the relationship between water quality parameters and the inherent optical properties, and on the relationship between the inherent optical properties and subsurface irradiance reflectance, *R(0-)*.

The multitemporal (and multisensor) applicability of the derived algorithms has been demonstrated by the successful application to remote sensing data from two different instruments, flown on two days under different atmospheric conditions and solar zenith angles.

The algorithms developed in this study are intended to be used in further research, where validation, augmentation of the results and possible development of further precision may take place. The strength of this approach also lies in the ability for combining information and results from underwater light climate research as well as *in situ* and remote sensing reflectance measurements.

7.2 Conclusions concerning multitemporal algorithms for remote sensing of inland waters

The remote sensing algorithms developed in this study are presented in Table 7.1. Although the analytical approach is the preferred method for algorithm development, it was not always possible to follow this approach due to lack of information on essential parameter-specific inherent optical properties. Even in the case of the chlorophyll *a* algorithm an empirical approximation for the backscattering of phytoplankton had to be made. Improvements in the analysis would be possible if more information concerning the scattering and backscattering (and, therefore, volume scattering functions) of the phytoplankton and the tripton was available. Research aimed at obtaining such information is strongly recommended.

A decrease in analytical and an increase in semi-empirical elements in the algorithms were required, in successive order, for chlorophyll *a*, CP-cyanin, seston dry weight, vertical attenuation coefficient and Secchi disk transparency. Chlorophyll *a*, CP-cyanin and seston are parameters that influence the optical characteristics of water, whereas K_d and *SD* are a function of the optical properties of the water. This explains the increasing incorporation of semi-empirical techniques from chlorophyll to *SD*: for each parameter in the above sequence, information on the preceding parameter is required in order to develop remote sensing algorithms based on the analytical approach.

Table 7.1 *Summary of remote sensing algorithms based on R(0-) data (see Chapter 5 for more information).*

At 2 nm intervals:						
Chlorophyll *a*	=	-48.2		66.5	$R(0-)_{706}$ / $R(0-)_{676}$	all
CP-cyanin		-24.6		13686	$(0.5(R(0-)_{600}+R(0-)_{648})-R(0-)_{624})$	shallow eutrophic
DW		2.69	+	331	$R(0-)_{706}$	
K_d	=	-0.5331	+	1.7046	$R(0-)_{706}$ / $R(0-)_{676}$	all
K_d	=	+0.2134	+	1.3786	$R(0-)_{706}$ / $R(0-)_{676}$	shallow lakes
K_d	=	-0.2467	+	1.1966	$R(0-)_{706}$ / $R(0-)_{676}$	deep lakes
ln *SD*	=	5.05		1.795	ln ($R(0-)_{706}$ / $R(0-)_{676}$)	all samples
ln *SD*	=	4.92		1.342	ln ($R(0-)_{706}$ / $R(0-)_{676}$)	shallow lakes
ln *SD*	=	5.51		1.815	ln ($R(0-)_{706}$ / $R(0-)_{676}$)	deep lakes
For CAESAR and the CASI Inland Water Mode bands the algorithms were approximately the same: the spectral band subscripts for the CAESAR Inland Water Mode are given.						
Chlorophyll *a*	=	-59.0		78.9	$R(0-)_{698-716}$ / $R(0-)_{671-684}$	all waters
CP-cyanin	=	-28.1	-	15904	$(0.5(R(0-)_{592-609}+R(0-)_{645-654})-R(0-)_{620-641})$	shallow eutrophic
DW	=	0.71		406	$R(0-)_{698-716}$	all waters
K_d	=	-0.7950	+	1.9984	$R(0-)_{698-716}$ / $R(0-)_{671-684}$	all waters
K_d	=	0.0492	+	1.5950	$R(0-)_{698-716}$ / $R(0-)_{671-684}$	shallow lakes
K_d	=	-0.4045	+	1.3600	$R(0-)_{698-716}$ / $R(0-)_{671-684}$	deep lakes
ln *SD*	=	5.05		1.615	ln ($R(0-)_{698-716}$ / $R(0-)_{671-684}$)	all waters
ln *SD*	=	4.89		1.464	ln ($R(0-)_{698-716}$ / $R(0-)_{671-684}$)	shallow lakes
ln *SD*	=	5.51	-	2.038	ln ($R(0-)_{698-716}$ / $R(0-)_{671-684}$)	deep lakes

The parameters for which an analytical algorithm will require analytical models for all other properties are thus K_d and subsequently *SD*.

The large range in optical water quality parameters in the study area has led to new insights concerning the range of inherent optical properties encountered in inland waters. A general conclusion pertaining to the determination of inherent optical properties for application in radiative transfer equations is that the variability in specific absorption and scattering coefficients within and between the four different water types indicates that the development of remote sensing algorithms for inland water quality analysis must reckon with adjustable parameterisation of absorption and scattering variables for each water type studied.

The subsurface irradiance reflectance *R(0-)* is the essential parameter for applications of the analytical model for remote sensing. It is essential because *R(0-)* can be determined from the inherent optical properties of *a*, *b* and $\beta(\theta)$, from *in situ* spectroradiometric measurements and from remote sensing measurements.

Once the relationships between the inherent optical properties and *R(0-)* and between *R(0-)* and the remote sensing signal are known, there should ideally be no need for simultaneous field sampling in order to determine water quality parameters from the remote sensing measurements. However, simultaneous measurements of the *in situ* diffuse and direct downwelling (ir)radiance components will remain necessary to enable determination of *R(0-)* from the remotely sensed upwelling radiance L_{rs}, as described in § 3.

Because all algorithms presented are based on *R(0-)* data, even the semi-empirical algorithms will show consistency when applied on a multitemporal basis as illustrated in chapter 6. However, for the semi-empirical algorithms validity can only be assumed for optical characteristics of the waters within the range of those that existed during the *in situ* sampling and measurements in the 1990 remote sensing campaign.

For chlorophyll *a* and CP-cyanin concentration estimation the analytical model provided the means to perform a sensitivity analysis on the influence of the variation in inherent optical properties of other parameters such as aquatic humus and tripton. Naturally occurring variations in aquatic humus and tripton levels in these waters led to 35 $\mu g\ l^{-1}$ and 10 $\mu g\ l^{-1}$ chlorophyll *a* equivalent error respectively. This indicates that estimates of the other inherent optical properties are required for successful application of these algorithms.

Size, shape and variability of the aquatic humus spectra were investigated. The approximately exponential slope was highly variable and was possibly related to changing fulvic- to humic acid ratios and to pH. Although exponentially decreasing with wavelength, aquatic humus absorbs significantly ($> 0.1\ m^{-1}$) up to and beyond 720 nm, eventually becoming relatively insignificant due to the high water absorption.

From the combined absorption and scattering coefficients of all parameters it was deduced that for remote sensing purposes the spectral areas where only one dominant spectral feature (besides pure water) is present, will be the most useful for determining inland water quality parameters. Such features include the 624 nm CP-cyanin and the 676 nm chlorophyll *a* absorption features and the overall absorption minimum at 700 - 710 nm. Below 500 nm the effects of absorption by aquatic humus, phytoplankton and tripton and the high level of scattering are compounded, presenting a four-parameter equation of influence on the reflectance signal measured by remote sensing.

The coefficient r_1 relating *R(0-)* to the inherent optical properties by (see Eqs. 4.4 and 5.1):

$$R(0-) = r_1 \; b_b / (a + b_b)$$

was studied for ocean and coastal waters with low scattering and absorption values by Gordon *et al.* (1975), Morel & Prieur (1977) and Kirk (1991), and was found to be dependent on solar zenith angle and the volume scattering function of the water. For the waters studied here, in which the scattering and absorption values were much higher, r_1 varied from 0.12 to 0.56 with no apparent relationship with solar zenith angle. It was concluded that the volume scattering functions for the waters studied varied greatly from those determined for ocean and coastal waters. Information extraction from reflectance spectra requires the use of algorithms which are preferably independent of r_1 values. Spectral band ratioing, derivative analysis or alternatively, acquisition of spectral absorption, scattering and backscattering properties are the most promising methods for information extraction from *in situ* spectroradiometric or from remote sensing measurements because these are independent of r_1.

The successful application in earlier semi-empirical studies of ratios of spectral bands centred at 676 ± 5 nm and at 706 nm ± 5 nm by Dekker *et al.* (1990, 1991 and 1992 b-d), Dekker & Donze (1992), Gitelson (1990, 1991) and Kondratyev & Podzniakov (1990) can now be explained by the analytical model:

1) Through ratioing of spectral bands the r_1 coefficient in Eqs. 4.4 and 5.1 is annulled (apart from a possible spectral dependence of r_1);

2) the increase in reflectance of the spectral band at 676 nm with increasing chlorophyll concentration remains relatively low, especially at concentrations above 40 µg l^{-1}, due to the associated increase in backscattering. The reflectance at 706 nm increases with increasing backscattering because no chlorophyll *a* absorption occurs here. Through this mechanism the spectral band ratio $R(0-)_{706} / R(0-)_{676}$ measures the absorption feature at 676 nm.

7.3 Recommendations to improve remote sensing algorithms

7.3.1 *Introduction*

Recommendations concerning areas of research where improvements to the analytical models may be achieved are given. Recommendations are also made for further research required in order to determine analytical algorithms for *DW*, K_d and *SD*.

DW, K_d and *SD* algorithms following the analytical method will probably require measurement of spectral absorption, scattering and backscattering of all the optical water quality parameters.

7.3.2 *The inherent optical properties*

Recommendations regarding further research on inherent optical properties are:

To determine the effect of varying pH and fulvic- to humic acid ratios on the slope *S* for aquatic humus.

To measure volume scattering functions ($\beta(\theta)$) of inland waters: specifically of the tripton and of the dominant phytoplankton in these waters such as the filamentous prokaryotic species. These measurements should include the scattering at small angles (< 5°); still an unknown parameter in the determination of total scattering coefficients for the inland waters studied.

To calculate specific scattering and specific backscattering coefficients for tripton and the phytoplankton species (i.e via the $\beta(\theta)$).

To perform more measurements of CP-cyanin concentration, with the aim of increasing information on the CP-cyanin-specific absorption of different algal species such as *Oscillatoria spp.* or *Microcystis spp.* as well as other cyanobacteria often occurring in eutrophic inland waters.

A published model for ocean waters to estimate of tripton from the combined seston (= tripton + phytoplankton) was tested and modified to encompass all the absorption data encountered. Thus, the physically non-separable (or very difficult to separate) tripton component of the seston was estimated, based on spectral indices of phytoplankton absorption. These indices were empirically modified and require testing and validation; e.g. based on laboratory cultures of freshwater phytoplankton.

7.3.3 *The field-based spectroradiometric measurements*

Results of the theoretical study and data analyses indicate that a minimal set of *in situ* spectroradiometric measurements exists, thus providing sufficient data to enable

a) accurate modelling and calibration of remotely sensed L_{rs} (converted to $R(0-)$) data and
b) testing and development of algorithms for the determination of optical water quality parameters from reflectance measurements obtained at altitude.

Table 3.3 presents and discusses the possible measurements available if one or two sensor heads are connected to a spectroradiometer, the usual configuration for most available field portable spectroradiometric equipment. Simultaneous measurement of both E_{ad} and L_{wu} with one sensor head would be ideal. From an operational point of view an optimal spectroradiometric program should measure the minimally required parameters as accurately as possible. Irradiance measurements are not essential to remote sensing, except for verification and model parameterisation. However, at least one up and downwelling radiance measurement is vital, since the remote sensing instrument also measures the radiance.

It is recommended that for future irradiance measurements to irradiance is determined using reflectance panels. Only when calibration is assured, are simultaneous measurements of upwelling radiance and downwelling irradiance advised.

Simultaneous measurements of the *in situ* diffuse and direct downwelling (ir)radiance components will remain necessary in order to determine $R(0-)$ from L_{rs}.

The fraction F of diffuse to total radiance is dependent on wavelength, atmospheric condition (aerosol content and type) and on the solar zenith and azimuth angle. The diffuse component of the downwelling radiance should also be determined by a measurement at 90° to the sun-zenith plane (at 180° azimuth) and a measurement at zenith (assuming measurements at intermediate solar zenith angles of ± 30° to 60°, typical of mid-latitudes).

The value of Q, the angular distribution factor for conversion of subsurface upwelling radiance to subsurface upwelling irradiance, requires further study. This is especially the case for water bodies high in concentrations of phytoplankton and tripton as encountered in this study area. Published values of Q may not be appropriate for waters such as these. The spectral dependency of Q should also be investigated.

The anisotropy of the underwater upwelling irradiance field probably also influences the calculated diffuse reflectance ρ_w value, assumed to be 0.48. This ρ_w factor needs to be measured or calculated for highly scattering and absorbing inland waters.

7.3.4 *Calibration of spectroradiometric instruments including remote sensing instruments*

Too much time and effort was spent on analysing and improving the data quality from field-based and airborne spectroradiometric equipment. In future, calibration information on all spectroradiometric equipment (laboratory, field-based and remote sensors) must be made available to researchers. In the case of unavailability of pre-flight calibration information in-flight and post-flight calibration routines become necessary.

7.4 Discussion

7.4.1 *Multispectral remote sensing or imaging spectrometry?*

It has been demonstrated that two spectral bands centred at 676 and 706 nm are sufficient for estimation of chlorophyll *a*, *DW*, K_d and *SD*. The addition of three spectral bands centred at 600, 624 and 648 nm enables the determination of CP-cyanin and another two bands centred at 545 and 565 nm may enable the measurement of cyanophycoerythrin. Thus a seven spectral band multispectral remote sensing system could remotely sense all optically retrievable parameters discussed in this study.

It may be concluded that optical water quality parameter detection techniques require the use of multispectral scanners, but not necessarily the use of imaging spectrometers. Algorithm development and testing, however, does require the use of imaging spectrometers. By virtue of measuring an entire spectrum, data from an imaging spectrometer can also be referred to at any time after the flight for the application or further development of algorithms.

For example, remote sensing of aquatic humus might become possible if the tripton and algal-specific (back)scattering and absorption coefficients were available; this would certainly require coverage of the spectrum between e.g. 400 and 550 nm. The data set acquired with the CASI in 1990 could be used for verification purposes, whereas the CAESAR data could not be used (presuming all spectral channels had functioned).

Spectral band changes such as replacement of the spectral band from 621 to 640 nm by a spectral band from e.g. 618 to 630 nm, necessary for improved estimation of CP-cyanin may also be achieved in real time with an instrument such as the CASI, whereas this would require months of preparation, testing and calibrating for a multispectral filter-based system such as the CAESAR.

If analytical models for seston dry weight, K_d and SD are to be developed, it is uncertain whether a selection of spectral bands would be sufficient. It is tentatively proposed that these analytical algorithms will probably require full spectral information over the visible and near infrared range.

7.4.2 *Error analysis*

Where possible in this study, sources of errors in measurements or assumptions were identified. These errors were, however, generally not quantified. Error propagation takes place at all stages of algorithm development which, for the chlorophyll *a* algorithm, was complex. The coefficients of determination, standard errors of estimate and the standard deviations were presented whenever possible. These statistically derived parameters were the net result of the error propagation and as such give a degree of accuracy for the algorithms.

Special attention must also be given to the errors involved in the measurement of the "independent variables" of chlorophyll *a*, CP-cyanin, *DW*, K_d and *SD*.

In future it is advised for related studies to perform an error analysis of each step in the process of developing and applying the analytical algorithm. Amongst others this will entail determination of the error associated with:

the *in situ* sampling (scale and site selection);

the *in situ* measurements of the radiance field (angle dependencies, non-Lambertian reference panel properties, short term variations);

the transport, laboratory storage and processing of the samples;

the laboratory analyses of concentrations of pigments and seston dry weight: it is advised to perform triple measurements in order to determine a first order approximation of these errors;

the atmospheric path radiance and transmission measurements (or assumptions necessary to derive these parameters);

the air/water interface effects;

the calibration of all spectrometric measurement instruments: in particular the field-based spectroradiometers and the remote sensing instruments.

The propagation of errors through parameters involved in calculations, leading to remote sensing algorithms must be calculated. The information obtained will enable identification of the research areas where the highest gain in improved results may be expected.

7.4.3 *Remote sensing of stream flows of different water types*

The algorithms for CP-cyanin, *DW*, K_d and *SD* are all dependent on the water types measured (Table 7.1). A problem arises when waters of one type flow into waters of another type: e.g. when water from a shallow eutrophic lake flows into a deep lake. A remote sensing image must be processed according to the most appropriate algorithm. Such a situation will probably require the use of an "all water types" algorithm, often associated with a decrease in estimation accuracy for the target parameter.

A remote sensing algorithm based on the analytical method would not show the above mentioned problems. This, therefore, is an additional argument for analytical algorithm development.

APPENDIX A MEASUREMENT OF DOWNWELLING IRRADIANCE

A.1 Introduction

Any error in the measurement of downwelling irradiance will produce a similar error in the irradiance or radiance reflectance calculations in remote sensing (atmospheric influences excepted). Unspoken assumptions are often made concerning the validity of these measurements. It is necessary to define accurately what is measured, what errors are made during the measurements and what assumptions are made concerning these measurements. Principles of field spectroradiometry in general have been reviewed by Milton (1987). Measurement of reflected downwelling irradiance from reference panels and the associated error sources are discussed in Biggar *et al.* (1988), Che *et al.* (1985), Duggin & Cunia (1983), Jackson *et al.* (1987 & 1988) and Kimes & Kirchner (1982).

In the 1990 remote sensing campaign two measurements of downwelling irradiance were made: the first measured the reflected irradiance from a diffuse reflecting reference panel using a 15° FOV aperture mounted on a Spectron sensor head; the second measured the downwelling irradiance directly using a cosine corrected hemispherical diffuser (CCHD) mounted on another Spectron sensor head (see App. B). The aim of duplicating measurements of E_{ad} was to determine which method is most suitable for remote sensing related fieldwork.

In 1990 a polytetrafluorethylene panel (PTFE, also known as halon) was used as a reference panel. PTFE is not a perfect Lambertian reflector. However the panel is sturdy, hydrophobic and easy to clean, making it suitable for field research conditions being easily transportable and usable under non-optimal conditions, in the field.

In the 1992 campaign reference panel measurements of E_{ad} were made. The sensor-panel configuration was different to that used in 1990. As a reference panel a Spectralon 50% diffuse reflecting panel was used. A field spectroradiometer (Personal Spectrometer PS II) equipped with a 18° FOV aperture was used for the radiance measurements (see App. B).

In general, field measurements should be kept simple and made as fast as possible. A reduction in the type of measurements made, preferably limited to a single sensor, would minimise the time needed for the scans. This would allow more sites to be measured during the often limited time available. For the operational use of remote sensing it is essential that the required field measurements can be made by suitably trained field staff. In the 1992 campaign elimination of the CCHD E_{ad} measurements contributed to meeting these criteria.

A.2 Reference panel calibration

A.2.1 *The PTFE panel (1990 measurements)*

At the NERC Equipment Pool for Fieldspectrometry a primary standard reference panel of $BaSO_4$ is calibrated in terms of reflectance relative to a perfect diffuser, traceable to National Physics Laboratory (UK) standards. The PTFE panel was calibrated relative to this primary standard. The illumination source was a 1000 Watt quartz-halogen lamp. The PTFE panel was calibrated with the sensor at nadir and with illumination at 45° to the panel over the wavelength range 400 to 850 nm. Values for *R(45°,0°)* were used to estimate the total downwelling irradiance from the reflected radiance of the panel. Using this calibration, a correction for non-Lambertian properties of the panel was made on the condition that only direct sunlight with an angle of incidence of 45° was considered. The calibration generated was less valid for diffuse sky light and different sun angles typical of those encountered in field situations. The 1990 *in situ* spectro-radiometric measurements were made at sun zenith angles of 67° to 42°, under varying sky conditions.

A correlation analysis of the radiance reflected from a diffuse reflecting reference panel L_o to E_{ad} ratio with varying solar zenith angles gave no significant correlation indicating that the panel calibration made by the NERC EPFS was appropriate for the circumstances encountered during this fieldwork.

The panel was also calibrated by F. Baret of the INRA (Avignon) in 1990. This calibration gives an indication of the non Lambertian properties of the PTFE. Measurements were made using a three band CIMEL radiometer, resembling wavelength bands of the SPOT-HRV sensor XS1, XS2 and XS3 centered at 545, 650 and 845 nm respectively. Measurements of directional reflectance factors were made for incidence-angles ranging from 10° to 90°.

Table A.1 *Bi-directional reflectance factors of the PTFE panel used for this study in 1990 for the XS2-band (650 nm) by Baret & Andrieu (pers.comm.). The solar zenith angles for the measurements of this study were between 41° and 67° (θ is the incidence angle of radiance, R(0,θ) the directional reflectance factor, and Δ(R0, θ) is the percentage error of R(0,θ)).*

θ	*R(0,θ)*	*ΔR(0,θ)*
40°	0.88	0.00
45°	0.88	0.00
50°	0.88	0.00
60°	0.85	0.03
70°	0.80	0.08

The calibration results showed that the directional reflectance factors, $R(0,\theta)$, were approximately constant for angles of 0° to 50°, but decreased markedly for angles greater than 60°. As an example the bi-directional reflectance factors for the XS2-band (650 nm) are given in Table A.1. At Grignon absolute directional reflectance was measured and seen to be approximately 1.0 for 0° to 50°.

Ideally, the calibration of a reference panel should be performed under the same illumination conditions as during the measurements in the field (Jackson *et al.*, 1987) if atmospheric conditions are stable. If atmospheric conditions are unstable laboratory determinations are required (Biggar *et al.*, 1988; Epema, 1992). For this study *in situ* calibration was not possible due to changing atmospheric conditions. Therefore, the laboratory-based calibration was used.

Additional errors could be caused by the blue colour of the outside casing of the Spectron sensor heads: this could possibly have influenced some or all of the measurements. Another error source, not investigated here, could be caused by self-shading of the instrument as it is positioned directly above the reference panel.

A.2.2 *The Spectralon panel (1992 measurements)*

A 50 % diffuse reflecting Spectralon (Labsphere, USA) reference panel was used in 1992 for downwelling irradiance reflectance measurements. The panel hemispherical spectral reflectance factor was measured under 8° zenith angle illumination and the reflectance characteristics are traceable to National Institute of Standards and Technology (USA; NIST) master standards. The material is highly Lambertian; a BRDF of a 99% reflecting Spectralon panel is published by the LabSphere company and deviates less than 5% from a Lambertian target down to 80° zenith angle. Spectralon is a waterproof, washable and durable material suitable for use in water-based field measurements.

A.3 Errors in irradiance determination caused by using a reference panel

Derivation of true irradiance from measurements of a reference panel requires a summation over all sources of incident radiations with their corresponding directional reflectance factors $R(0,\theta)$ from the panel. By neglecting diffuse sky light and the changing angle of incidence of direct sun light, an inherent error, due to non-Lambertian properties of the reference panel, is made. Kimes & Kirchner (1982) used published values to estimate irradiance measurement errors due to the assumption of a Lambertian reference panel. From Dave (1978) they obtained ratios of diffuse over total irradiance at λ= 678 nm. The results given in Table A.2. show a threefold increase of E_{dif} / E_{tot} for clear to hazy skies. As the solar zenith angle increases the percentage E_{dif} increases more rapidly for clear skies than for overcast skies. The ratios by Kimes & Kirchner are greater than those given by Slater (1980).

Table A.2 *Ratios of diffuse over total irradiance for Dave's (1978) atmospheric models #3 and #4, λ =678 nm (from Kimes & Kirchner, 1982: Table 1). See Fig. 3.2 for spectra of F (= E_{dif} / E_{tot}).*

θ	E_{dif}/E_{tot}	
	clear	hazy
45°	0.14	0.44
60°	0.18	0.56
70°	0.25	0.69

Table A.3 *An estimation of the percentage error of measuring direct irradiance using a reflectance panel at λ=650 nm due to changing sun angle. Calculations were made with data from Table A.1 and using Eq. A.1: $\Delta E_{dir}(\theta) / E_{dir}(\theta) = \Delta R / R(0,\theta)$*

	$\Delta E_{dir}(\theta)/E_{dir}(\theta)$ *(at 650 nm)*	
θ	(PTFE:Table A.1)	(data from Kimes & Kirchner) (1982: Fig.3)
	%	%
40°	0.0	4.0
45°	0.0	5.5
50°	0.0	7.5
60°	3.5	13.0
70°	6.0	25.0

The errors in irradiance estimates using a reference panel derived by Kimes & Kirchner (1982) are probably greater than the errors for measurements made during this research for two reasons:

A) Kimes & Kirchner (1982) estimate the error that is made by assuming that $R(0,\theta) = 1$ for all angles of incidence θ, neglecting non-Lambertian properties of the panel. The calibration of the reference panel at an incidence angle of 45° *($R(0,45°)$)* in this research prevents this error to a large degree. An estimation of the percentage error due to changing sun angle for the PTFE panel for direct irradiance measurement at λ=650 nm, due to the sun angle not being 45°, using Table A.1 and the equation :

$$\Delta E_{dir}(\theta) / E_{dir}(\theta) = \Delta R / R(0,\theta) \qquad [A.1]$$

is presented in Table A.3. These results indicate much lower errors associated with the PTFE panel. Because measurements were made at solar zenith angles of 42° to 67°, it was estimated that the errors in irradiance for this study caused by the reference panel were between 0 and 5 %.

The error for diffuse irradiance is also smaller when using a panel calibrated for direct sunlight since the sky radiance is concentrated around the solar disk. More than 50 % of the diffuse radiation is located close to the sun position (Baret & Andrieu, pers. comm). For a hazy sky, the sky radiance is more concentrated around the solar disk and does not increase at the horizons as it does for a clear sky.

B) The spectral bi-conical reflectance factors of the PTFE-panel show a more Lambertian character than the barium sulfate panel examined by Kimes & Kirchner (data from Fig. 2, Kimes & Kirchner, 1982). The values for the $BaSO_4$ panel were: *R(0, 40°)* = approximately 0.95 and *R(0, 70°)* = approximately 0.7. Therefore, together with the reasons given above, the percentage error for diffuse irradiance $\Delta E_{dif} / E_{dif}$, as presented by Kimes & Kirchner (1982) for λ = 678 nm (Table A.4), is greater than the error in our measurements. The data of Kimes & Kirchner (1982) is used as an indication of the upper limit in the error of $\Delta E_{dif} / E_{dif}$ measured, using reference panels.

Table A.4 *Percentage error for diffuse irradiance, as presented by Kimes & Kirchner (1982) for λ = 678 nm, using a relatively non-Lambertian $BaSO_4$ reflectance panel.*

θ	$\Delta E_{dif}(\theta)/E_{dif}(\theta)$	
	clear	hazy
	%	%
40°	10.0	8.5
45°	11.0	9.0
50°	12.5	11.5
60°	16.0	12.5
70°	18.5	14.5

The total error in total irradiance is assumed to be smaller than that derived with the use of Tables A.2-4 and equation A.2 (See Table A.5):

$$(\Delta E_{tot} / E_{tot})^2 = \{(\Delta E_{dif} / E_{dif})(E_{dif} / E_{tot})\}^2 + \{(\Delta E_{dir} / E_{dir})(E_{dir} / E_{tot})\}^2 \qquad [A.2]$$

because the PTFE panel is more Lambertian than that used by Kimes & Kirchner (1982) and because the calibration of the PTFE panel was carried out at incidence angles θ of 45°, close to the actual solar zenith angles during the field-based measurements.

Table A.5 *Maximum error in total irradiance calculated with the use of Tables A.2-4 and equation A.2.*

	calibrated PTFE panel for θ = 45°		Data from Kimes & Kirchner (1982) Fig.3. : uncalibrated panel	
	$(\Delta E_{tot}/E_{tot})$ *as a %*			
θ	clear	hazy	clear	hazy
45°	1.5	4	6.0	7.0
60°	4.0	7	13.5	13.0
70°	6.5	10	23.0	17.5

Robinson and Biehl (1979) calculated that the reflectance factor measured over 500 to 600 nm on a hazy day (visibility = 8 km) will differ from the true reflectance factor by a systematic 3% due to the presence of sky light. This is smaller than the expected maximum error of 4% for a 45° solar zenith angle (Table A.5); if it is assumed that 50 % of the diffuse radiation is located near to the sun position (Baret & Andrieu, pers. comm.) then the estimation of maximum error for the PTFE panel measurements is 2 - 4%. This error is, however, probably dependent on the wavelength of irradiance due to the spectral dependency of the scattering properties of the reference panel and the radiance distribution. For shorter wavelengths (blue light) the proportion of diffuse radiance increases, causing the error to increase.

A.4 Conclusions and recommendations concerning the Lambertian panel

The results of Robinson and Biehl (1979), Kimes and Kirchner (1982) and Che *et al.* (1985) suggest that the error associated with assuming a panel is perfectly Lambertian is larger for hazy than for clear atmospheres, that it decreases with increasing wavelength, and is dependent on the solar zenith angle. For reference reflectance panels the estimated error ranged, for a solar zenith angle of 60°, from 0 to 3% for clear skies and up to 7% for hazy skies and for a solar zenith angle of 45° from approximately 1% for clear skies and 4% for hazy skies. The proportion of diffuse light increases with decreasing wavelength causing the error to increase as well. According to Jackson *et al.* (1987), improved estimates of the error may be obtained from studies using atmospheric models to assess the non-isotropic nature of the diffuse component.

Recommendations for the use of a reference panel:

In addition to the recommendations by Milton (1987) concerning the use of reference panels (i.e.: use a fixed geometry between sensor, panel and target if possible; the sensor should have a minimum distance from the target of 1 m; measure at known positions to the sun; the reference panel should fill the FOV of the sensor; prevent sensor selfshading; use of a continuous recording solarimeter; remove coloured objects at least 3 m away from measurement scene) additional recommendations, based on this research are:

* Panel and target reflectance must be measured as close in time as possible.
* Calibration of the panel should be made with the instruments that will be used in the field with the same field of view and spectral band width.
* Calibrations should be made determining $R_p(0°,\theta)$, with θ the solar zenith angle during the *in situ* irradiance measurements.
* Measurements should be performed under clearest possible sky conditions.

A.5 Measuring the downwelling irradiance E_{ad} using a CCHD

An alternative approach to using a reference panel is to measure the irradiance directly by using an upward looking spectral sensor with a cosine corrected hemispherical diffuser (i.e. a sensor which shows no dependence on the zenith or azimuthal angle of the incident flux). The cosine corrected hemispherical diffuser (CCHD) is an aperture which can be fitted to the Spectron SE-590 optical head. The term cosine-corrected implies that the irradiance due to a beam is proportional to the cosine of the incident angle of that beam to the horizontal plane (naturally, the CCHD is considered to be horizontal). A radiometer, whose response to beams of light coming from different directions follows the same relationship, is said to be "cosine-corrected".

If the "cosine-corrected hemispherical diffuser" treats radiance coming from all directions equally, it is expected that measurements of irradiance using the diffuser are more reliable than those made using the reference panel, because calculations with the panel measurements treat all radiance as if it is coming from one direction. However, it was not certain that the diffuser functioned in a cosine corrected manner. In order to verify the validity of the CCHD measurements the following questions were posed:

* What was the nature of the cosine correction; is there a spectral dependency?
* The calibration at the NERC EPFS was performed for a point source of light at 0.5 m distance from the instrument; how does this compare with the circumstances during measurements in the field?
* What is the field of view of the cosine-corrected hemispherical diffuser? It did not appear likely that it measured downwelling irradiance from the whole upper hemisphere of the sky because the diffuser had a domed shape that is recessed below the surrounding rim.

Ideally these questions could be answered by performing a calibration as close as possible to the determination of a BRDF under controlled direct and diffuse illumination conditions. Although this calibration is recommended, it was not feasible in this research.

A.6 Comparison of the reference panel and the CCHD irradiance measurements

If the L_o using a reference panel and the E_{ad} using a CCHD are measured perfectly the ratio of the two measurements should be unity according to:

$$E_{ad} / (L_o \pi) = 1$$

Figure A.1 shows this ratio for 36 measurements performed under the circumstances described in § 4., Table 4.3. It is clear that several types of deviations from unity occur, although the overall average lies close to 1 from 450 to 850 nm. A systematic error is the sharp decline to ratios from 0.8 to 1.2 at 450 nm down to 0.6 to 0.8 at 400 nm. This is caused by either too low CCHD E_{ad} or too high L_o measurements or a combination of both. Possible sources of error for too low CCHD E_{ad} measurements are a spectral effect in the diffuser material or a spectral dependency of the cosine correction. The error does not appear to be a function of the ratio of diffuse to direct solar beam irradiance, for the error also occurs under completely overcast sky conditions. Another possible error source is a spectrally dependent radiometric sensitivity decrease with decreasing wavelength.

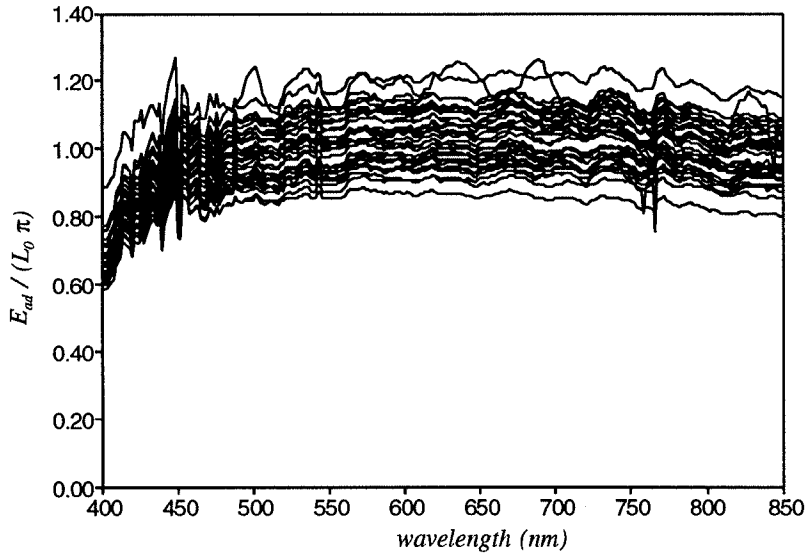

Figure A.1 *The ratio of $E_{ad} / (L_o \pi)$ for 36 measurements performed under varying atmospheric circumstances on five days during the 1990 remote sensing campaign. If the spectroradiometric measurements had been perfect this ratio should have been equal to 1.*

The high frequency noise (in the order of several nm's) in the E_{ad}/L_o ratio is possibly caused by one or more of the following factors:

Errors in both E_{ad} and L_o measurements due to *in situ* effects such as presented by Milton (1987); (see § A.4).
The fluctuation of the intensity of sun and sky light between the two types of measurements.
Errors in the spectral band alignment of the two sensor heads.

Figure A.2. shows the average values and the associated standard deviations of all $E_{ad} / (L_o * \pi)$ spectral ratios; the six spectral ratios taken under clear sky conditions and the 11 spectral ratios taken under completely overcast conditions. Table A.6. presents the values averaged over the wavelength range of 400 - 850 nm and for the spectral range most appropriate for remote sensing of inland waters 500 - 720 nm. The possible relationship between the solar zenith angle and the three groups of ratios was determined by correlation analysis to be $r < 0.10$.

The systematic deviation of the $E_{ad} / (L_o * \pi)$ spectral ratios for clear sky and overcast sky conditions from unity may be partly due to 1) the errors involved in the assumption of the reference panel to be a perfect Lambertian diffuser and 2) the errors involved in the assumption that the CCHD measures the hemispherical irradiance perfectly.

Based on the above criteria it was not possible to recommend one method for measuring the downwelling irradiance for routine operational measurements. Additional calibration measurements of the two methods are required. Special attention should be paid to the reason for the systematic decline in the ratio of E_{ad} to L_o below 450 nm, the exact manner in which the CCHD diffuses irradiance and the exact nature of the cosine correction of the CCHD.

Table A.6 *Average values and standard deviations for all $E_{ad} / (L_o * \pi)$ spectral ratios (All), the six spectral ratios taken under clear sky conditions (Clear) and 11 spectral ratios taken under completely overcast conditions (Overcast).*

		400 - 850 nm $E_{ad} / (L_o * \pi)$		500 - 720 nm $E_{ad} / (L_o * \pi)$	
	N	average	σ	average	σ
All	36	0.99	0.08	1.03	0.08
Clear	6	0.97	0.10	1.01	0.09
Overcast	11	1.04	0.09	1.08	0.05

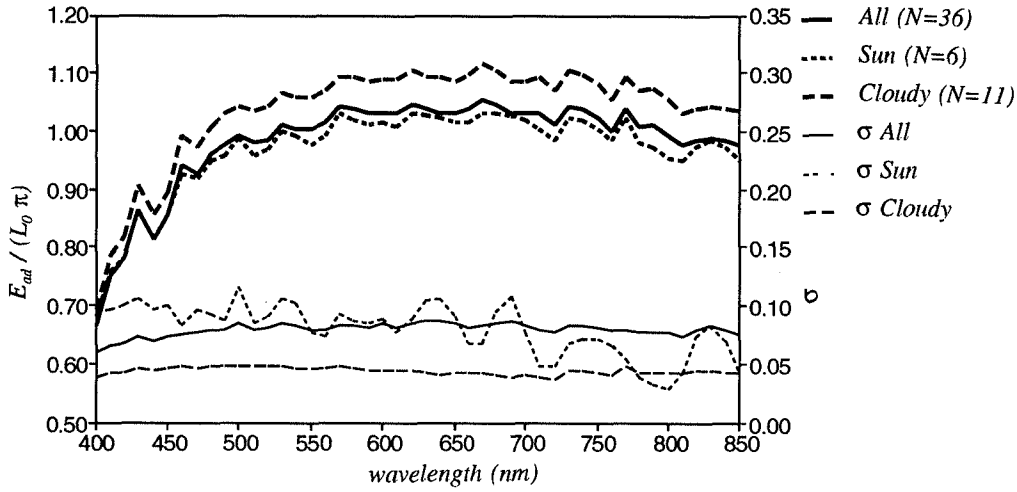

Figure A.2 *The average values and the associated standard deviations of all E_{ad} / (L_o * π) spectral ratios (ALL); the six spectral ratios taken under clear sky conditions (SUN) and the 11 spectral ratios taken under completely overcast conditions (CLOUDY).*

A.7 Conclusions and recommendations

For this research, and for future research using a similar equipment, it is preferred to use the reference panel reflectance measurements based on the criteria of a reduction in the types of measurements required and associated intercalibrations and because the same sensor head and aperture can be used for measuring the subsurface water leaving radiance, the above surface water leaving radiance, the panel reflected irradiance and the diffuse sky radiance. Moreover the error sources for the panel reflectance measurements could be approximated with known error whereas the error sources for the CCHD aperture were less well known. The blue colour of the Spectron sensor heads outer casing could be a possible source of spectral error due to preferential reflectance of blue light. It is advised to paint sensorhead casings as spectrally inert as possible.

In general, it is vital to calibrate the spectral and radiometric characteristics of the instruments as close in time to the *in situ* measurements, under the same illumination conditions. A reference panel should be used that approaches a perfect Lambertian diffuser as close as possible. In order to prevent errors caused by non-linear radiometric effects or caused by changing required integration times a panel reflecting in the same order as the target is preferred. For water applications this would probably be a 10 % reflecting panel.

APPENDIX B TECHNICAL DESCRIPTION OF PORTABLE SPECTRO-RADIOMETERS

B.1 Introduction

In order to correctly interpret the data presented a brief technical description of the spectroradiometers used in this study and their limitations is presented. The Spectron SE590 portable spectroradiometer was used in the 1990 remote sensing campaign. Because measurements of the fraction of diffuse to downwelling irradiance were not performed in 1990, spectroradiometric measurements of downwelling irradiance from the 1992 remote sensing campaign were analysed. A PSII portable spectroradiometer was used in 1992.

B.2 The Spectron SE590 field spectroradiometer

B.2.1 *Introduction*

The Spectron SE590 is a portable spectroradiometer which uses a diffraction grating and a 256 element linear photodiode array detector to measure a target spectrum with a slit band width (half-power) of 8 nm every 2.8 nm over the wavelength range of 400 - 1100 nm. Integration time for one (ir)radiance measurement may be automatically set, ranging from 1/64 to 1 second depending on the absolute amount of radiance at the time of measurement.

In this study the wavelength range from 400-850 nm was used. The instrument used in this research was provided by the University of Nottingham, U.K. and calibrated by the NERC Equipment Pool for Field Spectroradiometry. Two sensorheads may be fitted to the instrument: for this study one sensorhead was fitted with a 15° field of view (FOV) aperture and the other with a cosine corrected hemispherical diffuser. To facilitate subsurface upwelling radiance measurements the 15° FOV aperture was fitted with a 50 cm long and 4 cm diameter perspex tube, coated on the outside with black tape. The sensor heads were attached to a two metre boom enabling upwelling radiance measurements to be made away from the boat to prevent erroneous radiance effects on the measured signal.

B.2.2 *Radiometric calibration*

Calibration of the Spectron SE-590 was carried out in 1991 at the NERC-EPFS at the University of Southampton by Dr T.J. Malthus and Dr E.M. Rollins. The calibration was performed approximately 6 months after the field-based spectroradiometric measurements used in this study; it was impossible to calculate the effect of this time lag on the calibration. The lamp used for calibrating the Spectron with the cosine corrected hemispherical diffuser aperture was calibrated absolutely at the National Physics

Laboratory (NPL), England: Reference No. 128031/CQ5 in 1987; using a 12 V, 100 W, M28, tungsten halogen projector lamp made of fused silica. The lamp had a correlated colour temperature of 3002 °K. The silica envelope was externally grit blasted to provide a diffusing surface. The irradiance measurements were performed at 50 cm distance from the lamp. The calibration values were given in averages over 5 nm bands over 300 - 800 nm. These values were interpolated to Spectron wavelengths using a cubic spline interpolator. The total systematic uncertainty is estimated to be ± 1.5 % relative to the NPL scale of spectral irradiance.

B.2.2.2 *Radiometric calibration for the 1° and the 15° FOV optical heads (the apertured heads)*

The lamp used for the calibration of the Spectron with 1° and the 15° FOV optical heads was a 12 V, 200 W tungsten filament bulb at 8 Amps. The lamp had a correlated colour temperature of 2948 °K. An integrating sphere (type Bentham SRS20, calibrated in 1988) was used, with a diffusing glass plate attached to a 75 mm window. The 1° and the 15° FOV optical heads were positioned against the glass plate. The unit was positioned with the plane of the diffuser in the sphere port.

B.2.2.3 *Spectral (inter)calibration of the two Spectron sensor heads*

For measurements obtained during the 1990 remote sensing campaign a spectral discrepancy between the two sensor heads was evident. Except for this relative shift an absolute shift indicated by the 760 nm oxygen absorption feature in the spectra was established also. Additional measurements were made during the radiometric calibration in Southampton whereby a mercury lamp and a krypton lamp were used for spectral alignment. The 1990 data were partly corrected for this effect. However, spectral alignment differences remained between the sensor heads. Through division of measurements of E_{ad} with the cosine corrected hemispherical diffuser head and the L_o with the 15° FOV aperture, the misalignment is evident as strong deviations within several nanometers from the general trend. This spectral misalignment is probably caused by subtle differences in the diffraction grating, thus causing nonlinear misalignment within a wavelength resolution range. This is a general problem with all Spectron SE590 instruments. Individual wavelength calibrations for each sensor head are required instead of the standard wavelength file supplied with the instrument.

B.3 The Personal Spectrometer II (PS II)

B.3.1 *Introduction*

Similar to the Spectron instrument the PS II portable spectroradiometer uses a diffraction grating and silicon photodiode array detector. Light is guided to the grating and

detector using an optical fibre. It measures the target spectrum with a minimum slit band width (half-power) of 1 nm (at 24°C) every 1.38 - 1.42 nm over the wavelength range of 360 - 1100 nm. In this study only the wavelength range of 400 - 850 nm was used. The system used in this research was provided by the Survey Department, Rijks-Waterstaat Equipment Pool. The optical fibre sensor may be fitted with a range of apertures from 1° to 18° FOV. For measuring upwelling radiance from low reflecting targets such as natural waters, the 18° FOV is used because of the relatively low radiometric sensitivity of the instrument. Integration time for one measurement is between 0.044 and 5.6 seconds depending on the absolute amount of radiance available. Maximum integration times of 5.6 seconds were required over water targets.

Subsurface upwelling radiance measurements were carried out by lowering the aperture into the water. The sensor was attached to a two metre long boom enabling upwelling radiance measurements sufficiently removed from the boat or waterside to prevent erroneous radiance effects on the measured signal.

B.3.2 *Calibration*

A factory based calibration of the PS II was carried out according to traceable NIST, USA, traceable standards. As a light source a NIST traceable quartz halogen light source was used.

Because the PS II showed spectral calibration errors at the time of use in August 1992, a spectral recalibration was carried out using the mercury emission lines of a thermo-luminescent tube as well as the oxygen absorption feature in the solar/sky irradiance spectrum at 761 nm and the water vapour absorption features at +/- 823 and at +/- 900-936 nm. A spectral shift of 15 nm was thus corrected.

APPENDIX C DERIVATION OF THE CONCENTRATION OF CHLOROPHYLL *a* (*C*) FROM $R(0-)_{706} / R(0-)_{676}$

The ratio for subsurface irradiance reflectance can be calculated from the inherent optical properties by:

$$R(0-)_{706} / R(0-)_{676} = r_1 (b_b / (b_b + a(w) + a(ah) + a(t) + a(ph))]_{706} / r_1 (b_b / (b_b + a(w) + a(ah) + a(t) + a(ph))]_{676} \quad [C.1]$$

Because the aim is to extract the concentration of chlorophyll *a*, $a(ph)_{676}$ is expressed as:

$$a(ph)_{676} = a^*_{676} C \quad [C.2]$$

where a^*_{676} is the chlorophyll *a*-specific absorption and *C* is the chlorophyll *a* concentration. Assuming the absorption by chlorophyll *a* to be zero at 706 nm equation C.1 becomes:

$$R(0-)_{706} / R(0-)_{676} = (b_b / (b_b + a(w) + a(ah) + a(t))]_{706} / (b_b / (b_b + a(w) + a(ah) + a(t) + (a^*_{676} C))]_{676} \quad [C.3]$$

Because the absorption by $a(w) + a(ah) + a(t)$ at both wavelengths is not dependent on the chlorophyll *a* absorption, $a(w) + a(ah) + a(t)$ is represented by $a(r)$. Solving equation C.3 for *C*:

$$R(0-)_{706} / R(0-)_{676} = (b_b / (b_b + a(r))]_{706} / (b_b / (b_b + a(r) + (a^*_{676} C))]_{676} \quad [C.4]$$

$$R(0-)_{706} / R(0-)_{676} = (b_b / (b_b + a(r))]_{706} [(b_b + a(r) + (a^*_{676} C) / b_b)]_{676} \quad [C.5]$$

$$R(0-)_{706} b_{b676} / R(0-)_{676} b_{b706} = (1 / (b_b + a(r))_{706}) [(b_b + a(r) + (a^*_{676} C))]_{676} \quad [C.6]$$

Multiplication by $(b_b + a(r))_{706}$:

$$R(0-)_{706} b_{b676} (b_b + a(r))_{706} / (R(0-)_{676} b_{b706}) = [(b_b + a(r) + (a^*_{676} C))]_{676} \quad [C.7]$$

$$R(0-)_{706} b_{b676} (b_b + a(r))_{706} / (R(0-)_{676} b_{b706}-(b_b + a(r))_{676}) = a^*_{676} C \quad [C.8]$$

Thus *C* can be calculated from:

$$C = [R(0-)_{706} b_{b676} (b_b + a(r))_{706}] / [(R(0-)_{676} b_{b706} a^*_{676}-(b_b + a(r))_{676})/(a^*_{676})] \quad [C.9]$$

REFERENCES

Almanza, E. & Melack, J. M., (1985); Chlorophyll differences in Mono Lake (California) observable on Landsat imagery; Hydrobiologia 122:p 13-17.

Austin, R.W., (1974); The remote sensing of spectral radiance from below the ocean surface; Optical Aspects of Oceanography: ed. Jerlov, N.G. & Steeman Nielsen, E., Academic Press, London and New York:p 316-344.

Austin, R.W., (1980); Coastal Zone Colour Scanner radiometry; SPIE Vol. 208 Ocean Optics VI: p 170-177.

Baker, K.S. & Smith, R.C., (1990); Irradiance transmittance through the air/water interface; SPIE Vol. 1302, Ocean Optics X:p 556-565.

Bale, A.J. & Morris, A.W., (1987); In situ measurement of particle size in estuarine waters; Est. Coast. Shelf Sci., 24:p 253-263.

Baret, F. & Andrieu, B., (pers. comm.); Calibration procedure used for the "Frame" measurements during the 1989 Broom's Barn experiment.

Bennett, A. & Bogorad, L., (1973); Complementary chromatic adaptation in a filamentous blue-green alga; J. Cell. Biol., 58:p 410-435.

Biggar, S.F., Labed, J., Santer, R.P., Slater, P.N., Jackson, R.D. & Moran, M.S., (1988); Laboratory calibration of field reflectance panels; in: Recent Advances in Sensors, Radiometry and Data Processing for Remote Sensing, SPIE Vol. 924:p 332-240.

de Boer, T., Kramer, H., Schrotenboer, J. & Voerman, J., (1987a); Hydrologisch, fysisch en chemisch onderzoek in het Tjeukemeer en omgeving; verslag van de resultaten over 1986. Intern verslag Limnologisch Instituut Oosterzee/Nieuwersluis (in Dutch).

de Boer, T., Kramer, H., Schrotenboer, J. & Voerman, J. (1987b); Hydrologisch, fysisch en chemisch onderzoek in twee petgaten in "De Alde Feanen" bij Eernewoude (Friesland); verslag van de resultaten over 1986. Intern verslag Limnologisch Instituut Oosterzee/Nieuwersluis (in Dutch).

Boivin, L.P., Davidson, W.F., Storey, R.S., Sinclair, D. & Earle, E.D., (1986); Determination of the attenuation coefficient of visible and ultraviolet radiation in heavy water; Applied Optics 25; p 877-882.

Bricaud, A., Morel, A & Prieur, L., (1981); Absorption by dissolved organic matter of the sea (yellow substance) in the UV and visible domains; Limnol. Oceanogr., 26(1):p 43-53.

Bricaud, A., Morel, A & Prieur, L., (1983); Optical efficiency factors of some phytoplankters; Limnol. Oceanogr., 28(5):p 816-832.

Bricaud, A., Bedhomme, A-L. & Morel, A., (1988); Optical properties of diverse phytoplanktonic species: experimental results and theoretical interpretation; J. Plankt. Res., 10(5):p 851-873.

Bricaud, A. & Stramsky, D., (1990); Spectral absorption coefficients of living phytoplankton and nonalgal biogenous matter: A comparison between the Peru upwelling area and the Sargasso Sea; Limnol. Oceanogr., 35(3):p 562-582.

Buiteveld, H. & Donze, M., (unpubl.); The optical properties of water.

Bukata, R.P., Jerome, J.H. & Bruton, J., (1988); Particulate concentrations in Lake St. Clair as recorded by a shipborne multispectral optical monitoring system; Rem. Sens. Environ., 25:p 201-299.

Burger-Wiersma, T. & Post, A.F., (1989); Functional analysis of the photosynthetic apparatus of *Prochlorothrix hollandica* (Prochlorales), a chlorophyll *b* containing procaryote; Plant Physiol., 91: p 770-774

Burger-Wiersma, T., Stal, L.J. & Mur, L.R., (1989); *Prochlorothrix hollandica* gen. nov., sp. nov., a filamentous oxygenic photoautotrophic procaryote containing chlorophylls *a* and *b*: assignment to *Prochlorotrichaceae* fam. nov. and order *Prochlorales* Florenzano, Balloni, and Materassi 1986, with emendation of the ordinal description; Intern. J. Systematic Bacteriol., July 1989:p 250-257.

Burger-Wiersma, T., Veenhuis, M., Korthals, H.J., Van de Wiel, C.C.M. & Mur, L.R., (1986); A new procaryote containing chlorophylls a and b; Letters to Nature; Nature 320(20):p 262-264.

Carder, K.L., Hawes, S.K., Baker, K.A., Smith, R.C., Steward, R.G. & Mitchell, B.G., (1991); Reflectance model for quantifying chlorophyll *a* in the presence of productivity degradation products; J. Geoph. Res. 96(C11): p 20.599-20.611.

Carder, K.L.& Steward, R.G., (1985); A remote-sensing reflectance model of a red tide dinoflagellate of west Florida; Limnol. Oceanogr., 30(2):p 286-298.

Carder, K.L., Steward, R.G., Harvey, G.R. & Ortner, P.B., (1989); Marine humic and fulvic acids: Their effects on remote sensing of ocean chlorophyll; Limnol. Oceanogr., 34(2):p 68-81.

Che, N. Jackson, R.D., Philips, A.L., and Slater, P.N., (1985); The use of field radiometers in reflectance factor and atmospheric measurements; SPIE Vol. 499:p 24-33.

Dave, J.V., (1978); Extensive datasets of the diffuse radiation in realistic atmospheric models with aerosols and common absorbing gases; Sol. Energy 21:p 361-369.

Davies-Colley, R.J., Pridmore, R.D. & Hewitt, J.E., (1986); Optical properties of some freshwater phytoplanktonic algae; Hydrobiologia 133:p 165-178.

Davies-Colley, R.J. & Vant, W.N., (1987); Absorption of light by yellow substance in freshwater lakes; Limnol. Oceanogr., 32(2):p 416-425.

Davies-Colley, R.J., Vant, W.N. & Wilcock, R.J., (1988); Lake water colour: comparison of direct observations with underwater spectral irradiance; Water Resources Bulletin, 24(1):p 11-18.

Davies-Colley, R.J., (1983); Optical properties and reflectance spectra of 3 shallow lakes obtained from a spectrophotometric study; New Zealand J. of Mar. & Freshwater Res., 17:p 445-459.

Dekker, A.G. & Peters, S.W.M., (1993); The use of the Thematic Mapper for the analysis of eutrophic lakes: A case study in The Netherlands; Int. J. Remote Sensing 14(5): p 799-822.

Dekker, A.G. & Donze, M., (1992); Imaging spectrometry as a research tool for inland water resources analysis; Lecture Notes at: EUROCOURSE ISE/92: Imaging Spectrometry as a Tool for Environmental Observations, November 23-27,1992: Inland Water Resources Monitoring Friday 27th November 1992; Joint Research Centre(CEC)- I 21020 Ispra(Varese) Italy: p 1-15.(To be published in: EuroCourses, Remote Sensing, Ed. J. Hill, Kluwer AP, Dordrecht, The Netherlands).

Dekker, A.G., Malthus, T.J. & Goddijn, L.M.(1992a); Monitoring cyanobacteria in eutrophic waters using airborne imaging spectroscopy and multispectral remote sensing systems; Proceedings 6th Australasian Remote Sensing Conference, Wellington, New Zealand, 2-6 November 1992; Vol I: p 204-214.

Dekker, A.G., Malthus, T.J. & Wijnen, M.M., (1992b); Spectral band location for remote sensing of turbid and/or eutrophic waters; Proceedings of the First Thematic Conference on Remote Sensing for Marine and Coastal Environments: Needs and Solutions for Pollution Monitoring, Control, and Abatement, New Orleans, Louisiana, USA, 15-17 June 1992, Volume II, SPIE Vol. 1930: p 955-970.

Dekker, A.G., Malthus, T.J. Wijnen, M.M. & Seyhan, E., (1992c); The effect of spectral band width and positioning on the spectral signature analysis of inland waters; Rem. Sens. Environ., 41(2/3): p 211-226.

Dekker, A.G., Malthus, T.J. Wijnen, M.M. & Seyhan, E., (1992d); Remote sensing as a tool for assessing water quality in Loosdrecht lakes; Hydrobiologia 233:p 137-159.

Dekker, A.G., Malthus, T.J. & Seyhan, E., (1991); Quantitative modelling of inland water quality for high resolution MSS-systems; IEEE Trans. on Geosc. and Rem. Sens., 29(1): p 89-95.

Dekker, A.G., Malthus, T.J. & Seyhan, E., (1990); An inland water quality bandset for the CAESAR system based on spectral signature analysis; Proc. Int. Symp. Remote Sensing and Water, Enschede, The Netherlands, August 1990:p 597-606.

Dekker, A.G. & Seyhan, E., (1988); The Remote Sensing Loosdrecht Lakes Project; Int. J. Remote Sensing, 10 & 11(9):p 1761-1773.

Donze, M.(ed), (1989); CAESAR: Performance and first evaluation of application possibilities; Report BCRS-89-06, Final Report TE-1.3, Netherlands Remote Sensing Board, Delft, The Netherlands:pp 101.

Dubelaar, G.B.J., Visser, J.W.M. & Donze, M., (1987); Anomalous behaviour of forward and perpendicular lightscattering of a cyanobacteria owing to intracellular gas vacuoles; Cytometry, 8: p 405-412.

Duggin, M.J. and Cunia, T., (1983); Ground reflectance measurement techniques: a comparison: Applied Optics 23:p 3771-3777.

Epema, G.F., (1992); Spectral reflectance in the Tunisian desert. PhD-Thesis, Landbouwuniversiteit Wageningen, The Netherlands:pp 150.

Ferrari, G.M., (1991); Influence of pH and heavy metals in the determination of yellow substance in estuarine areas; Rem. Sens. Environ. 37:p 89-100.

Ganf, G.G., Oliver, R.L. & Walsby, A.E., (1989); Optical properties of gas-vacuolate cells and colonies of *Microcystis* in relation to light attenuation in a turbid, stratified reservoir (Mount Bold Reservoir, South Australia); Aust. J. Mar. Freshwater Res., 40:p 595-611.

Ghassemi, M. & Christman, R.F., (1968); Properties of the yellow organic acids of natural waters. Limnol. Oceanog., 13:p 583-597

Gitelson, A., (1992); The peak near 700 nm on radiance spectra of algae and water: relationships of its magnitude and position with chlorophyll concentration; Int. J. Remote Sensing, 13(17): p 3367-3373.

Gitelson, A.A., Garbusov, G.P., Lopatshenko, L.L., Mittenzwey, K.H., Makhotenko, A.N., Mudrogelenko, I.V., Penig, J. & Sukhorukov, B.L., (1990); Schnellmethoden zur ermittlung der beschaffenheit von Oberflachen-gewassern mittels Spektrometrie; Acta Hydrochim. Hydrobiol. 18(4):p 397-408.

Gitelson, A.A. & Keydan, G.P., (1990); Remote sensing of inland surface water quality measurements in the visible spectrum; Acta Hydrophys., Berlin 34(1.S):p 5-27.

Gitelson, A.A. & Kondratiev, K.Y., (1991); Optical models of water bodies; Int. J. Remote Sensing (12) :p 373-385.

Gitelson, A.A. & Nikanorov, A.M., (1988); Remote monitoring of ecological condition of aquatic ecosystems; Proc. USA-USSR Symposium, Athens, Georgia, Oct 19-21, 1987; on: Fate and Effects of Pollutants on Aquatic Organisms and Ecosystems:p 166-182.

Gitelson, A.A., Nikanorov, A.M., Szabo, GY. & Szilagyi, F., (1986); Etude de la qualite des eaux de surface par teledetection; Proc. Budapest Symp., July 1986, on: Monitoring to Detect Changes in Water Quality Series: IAHS Publ.no. 157:p 111-121.

Gons, H., Burger-Wiersma, T, Otten, J.H. & Rijkeboer, M., (1992); Coupling of phytoplankton and detritus in a shallow, eutrophic lake (Lake Loosdrecht, The Netherlands); Hydrobiologia 233: p 51-59.

Gons, H.J., Kromkamp, J., Rijkeboer, M. & Schofield, O., (1992); Characterization of the light field in laboratory scale enclosures of eutrophic lake water (Lake Loosdrecht, The Netherlands); Hydrobiologia, 238:p 99-109.

Gons, H., Otten, J. & Rijkeboer, M., (1991); The significance of wind resuspension for the predominance of filamentous cyanobacteria in a shallow, eutrophic lake; Mem. Ist. Ital. Idrobiol., 48:p 233-249.

Gordon, H.G., Brown, O.B. & Jacobs, M.M., (1975); Computed relationships between the inherent and apparent optical properties of a flat homogeneous ocean; Applied Optics, 14(2): p 417-427.

Gordon, H.R. & Morel, A.Y., (1983); Remote assessment of ocean color for interpretation of satellite visible imagery: a review; Lecture Notes on Coastal and Estuarine Studies 4; Springer-Verlag, New York:pp 114.

Gregg, W.W. & Carder, K.L., (1990); A simple spectral solar irradiance model for cloudless maritime atmospheres; Limnol. Oceanogr., 8(35):p 1657-1675.

Grunwald, B., Mauser, W. & Schneider, K., (1988); Data processing for the determination of pigments and suspended solids from Thematic Mapper data; Proc. IGARSS 88 Symposium, Edinburgh, Scotland; ESA Publications:p 1385-1389.

Gulati, R.D., van Liere, L. & Siewertsen, K., (1991); The Loosdrecht lake system: Man's role in its creation, perturbation and rehabilitation; Terrestrial and Aquatic ecosystems:Perturbation and Recovery, Ellis Horwood Ltd. 1991:p 593-606.

de Haan, H., De Boer, T., Kramer, H.A. & Voerman, J., (1982); Applicability of light absorbance as a measure of organic carbon in humic lake water; Water Res., 16:p 1047-1050.

de Haan, H. & De Boer, T., (1986); Geochemical aspects of acqueous iron, phosphorus and dissolved organic carbon in the humic Lake Tjeukemeer, The Netherlands; Freshwater Biology 16: p 661-672.

de Haan, J.F., (1987); Effects of aerosols on the brightness and polarization of cloudless planetary atmospheres; PhD-Thesis, Vrije Universiteit te Amsterdam, The Netherlands;pp 219.

Haardt, H. & Maske, H., (1987); Specific in vivo absorption coefficient at 675 nm; Limnol. Oceanogr., 32(3):p 608-619.

Hilton, J. , (1984); Airborne remote sensing for freshwater and estuarine monitoring; Water Res. 18(10):p 1195-1223.

Hojerslev, N.K., (1988); Natural occurences and optical effects of gelbstoff; Geoph. Inst., Dept. Phys. Ocean., Univ. Copenhagen, Denmark:pp 29.

Jackson, R.D. Slater, P.N., and Moran, M.S., (1988); Accounting for diffuse irradiance on reference reflectance panels, in: Recent Advances in Sensors, Radiometry and Data Processing for Remote Sensing; SPIE Vol. 924:pp 241-248.

Jackson, R.R., Moran, S., Slater, P.N. & Biggar, S.F., (1987); Field calibration of reference reflectance panels; Rem. Sens. Environ. 22:p 145-158.

Jacquet, J.-M. & Zand, B., (1989); Colour analysis of inland waters using Landsat TM data; European Coordinated Effort for Monitoring the Earth's Environment, ESA SP-1102, ESA Publ. Div., ESTEC, Noordwijk, The Netherlands:p 57-70.

Jerlov, N.G. (1968); Optical oceanography; Elsevier Oceanography Series, part 5, Amsterdam, The Netherlands.

Jerlov, N.G., (1976); Marine optics; Elsevier, Amsterdam, The Netherlands.

Kimes, D.S. & Kirchner, J.A., (1982); Irradiance measurement errors due to the assumption of a Lambertian reference panel; Rem. Sens. Environ., 12:p 141-149.

Kirk, J.T.O., (1975a); A theoretical analysis of the contribution of algal cells to the attenuation of light within natural waters. I. General treatment of suspensions of living cells; New Phytol., 75: p 11-20.

Kirk, J.T.O., (1975b); A theoretical analysis of the contribution of algal cells to the attenuation of light within natural waters. II. Spherical cells; New Phytol., 75:p 21-36.

Kirk, J.T.O., (1980); Spectral absorption properties of natural waters: contribution of the soluble and particulate fractions to light absorption in some inland waters of South-eastern Australia; Aust. J. Mar. Freshwater Res., 31:p 287-296.

Kirk, J.T.O., (1981a); Monte Carlo study of the nature of the underwater light field in, and the relationships between optical properties of, turbid yellow waters; Aust. J. Mar. Freshwater Res., 32:p 517-532.

Kirk, J.T.O., (1981b); Estimation of the scattering coefficient of natural waters using underwater irradiance measurements; Aust. J. Mar. Freshwater Res., 32:p 533-539.

Kirk, J.T.O., (1983); Light and photosynthesis in aquatic ecosystems; CSIRO, Canberra, Australia; Cambridge University Press:pp 401.

Kirk, J.T.O., (1984); Dependance of relationship between inherent and apparent optical properties of water on solar altitude; Limnol. Oceanogr., 29(2):p 350-356.

Kirk, J.T.O., (1989); The upwelling light stream in natural waters; Limnol. Oceanogr., 34(8): p 1426-1441.

Kirk, J.T.O., (1991); Volume scattering function, average cosines, and the underwater light field; Limnol. Oceanogr., 36(3):p 455-467.

Klepper, O., Vermij, S.G. & Lingeman, R., (1984); The influence of light scattering on vertical extinction in Lake Maarsseveen; Verh. Int. Ver. Limnol., 22:p 82-86.

Kondratyev, K.Ya., (1969); Radiation in the atmosphere: Department of Atmospheric Physics; Leningrad University; Academic Press, U.S.A.

Kondratyev, K. Ya. & Pozdniakov, D.V., (1990); Passive and active optical remote sensing of the inland water phytoplankton; ISPRS J. of Photogramm. Eng. and Rem. Sensing, 44:p 257-294.

Korthals, H.J. & Steenbergen, C.L.M., (1985); Separation and quantification of pigments from natural phototrophic microbial populations; FEMS Microbiology Ecology, 31:p 177-185.

Krijgsman, J., (in prep); Optical remote sensing of surface water; on the interpretation of reflectance data with high spectral resolution. (PhD-Thesis)

Lathrop, R.G. J. & Lillesand, T.M., (1986); Use of Thematic Mapper data to assess water quality in Green Bay and Central Lake Michigan; Photogramm. Eng. and Rem. Sens., 52(5):p 671-680.

Lathrop, R.G. J. & Lillesand, T.M., (1988); Utility of SPOT-1 data to assess water quality in Southern Bay, Lake Michigan; Technical papers, 1988 ACSM-ASPRS Annual Convention: Image Processing/Remote Sensing, St. Louis, Missouri, March 13-18 1988:p 102-111.

Lathrop, R.G. J. & Lillesand, T.M., (1989); Monitoring water quality and river plume transport in Green Bay, Lake Michigan with SPOT-1 imagery; Photogramm. Eng. and Rem. Sens., 55(3):p 349-354.

Lathrop, R.G. J., Lillesand, T.M. & Yandell, B.S., (1991); Testing the utility of simple multi-date Thematic Mapper calibration algorithms for monitoring turbid inland waters; Int. J. Remote Sensing, 10(12):p 2045-2063.

Lathrop, R.G., (1992); Landsat Thematic Mapper monitoring of turbid inland water quality; Photogramm. Eng. & Rem. Sens., 4(58):p 465-470.

van Liere, L., Breebaart, L. & Dullemont, Y.L., (1989); Determining the relative number of Prochlorophytes in lake phytoplankton using epifluorescence microscopy; Br. phycol. J., 24:p 391 - 394.

Lillesand, T.M. & Kiefer, R.W., (1987); Remote sensing and image interpretation; John Wiley & Sons.

Looyen, W. J. & Dekker, A.G., (1990); CAESAR: an example of a versatile multispectral CCD pushbroom scanner using (non) imaging spectrometry results; EARSeL Advances in Remote Sensing, 1(1):p 101-108.

Maske, H. & Haardt, H., (1987); Quantitative in vivo absorption spectra of phytoplankton: Detrital absorption and comparison with fluorescence excitation spectra; Limnol. Oceanogr., 32(3): p 620-633.

McGarrigle, M.L., (1989); Satellite and low altitude remote sensing of lake chlorophyll in Ireland; Proceedings, SIL 1989 Munchen, FRG.

McGarrigle, M.L., O'Mongain, E., Walsh, J.E., Sommerville, T. & Bree, M., (1990); National survey of lakes by remote sensing: Calibration of a low altitude water quality spectrometry; Environm. Res. Unit, St Martin's House, Waterloo Rd, Dublin, Rep. Ireland:pp 48.

Mie, G. (1908). Beitrage zur Optik truber Medien, speziell kolloidalen Metall-losungen. Ann. Phys, 25:p 377-445.

Milton, E.J., (1987); Review article:Principles of field spectroscopy; Int. J. Remote Sensing, 8(12): p 1807-1827.

Miyazaki, T., Shimizu, H. & Yasuoka, Y., (1987); High-speed spectroradiometer for remote sensing; Applied Optics, 26(22):p 4761-4766.

Moed, J.R. & Hallegraeff, G.M., (1978); Some problems in the estimation of chlorophyll-a and phaeopigments from pre- and post-acidification spectrophotometric measurements. Int. Revue ges. Hydrobiol. 63:p 787-800.

Morel, A., (1987); Chlorophyll-specific scattering coefficient of phytoplankton. A simplified theoretical approach; Deep-Sea Research, 34(7):p 1093-1105.

Morel, A. & Bricaud, A., (1981); theoretical results concerning light absorption in a discrete medium, and application to specific absorption of phytoplankton; Deep-Sea Res., 28:p 1375-1393.

Morel, A. & Bricaud, A., (1986); Inherent optical properties of algal cells including picoplankton: theoretical and experimental results; Can. Bull. of Fish. and Aquat. Sc. 214 : Photosynthetic Pico-plankton; ed: Platt, T.& Li, W.K.W.:p 521-559.

Morel, A. & Gordon, H.R., (1980); Report of the working group on water color; Boundary layer meteorology, 18:p 343-355.

Morel, A. & Prieur, L., (1977); Analysis of variations in ocean colour; Limnol. Oceanogr., 22(4): p 709-722.

Otten, J.H., Gons, H. & Rijkeboer, M., (1992); The dynamics of phytoplankton detritus in a shallow, eutrophic lake (Lake Loosdrecht, The Netherlands); Hydrobiologia 233:p 61-68.

Peacock, T.G., Carder, K.L., Davis, C.O. & Steward, R.G., (1990); Effects of fluorescence and water Raman scattering on models of remote sensing reflectance; SPIE Vol. 1302: Ocean Optics X:p 303-319.

Petzold, T.L., (1972); Volume scattering functions for selected ocean waters; University of California, San Diego: Scripps Inst. Oceanogr. Visibility Lab., Ref.72-78.

Philpot, W.D., (1991); The derivative ratio algorithm: avoiding atmospheric effects in remote sensing; IEEE Trans. on Geosc. and Rem. Sens., 29(3):p 350-357.

Preisendorfer, R.W., (1986); Secchi disk science: visual optics of natural waters; Limnol. Oceanogr., 31(5):p 909-926.

Preisendorfer, R.W., (1976); Hydrologic Optics, Vol 1. Washington, Dep. of Commerce.

Privoznik, K.G., Daniel. K.J. & Incroper, F.P., (1978); Absorption, extinction and phase functions for algal suspensions of *Chlorella pyrenoidosa*; J. Quant. Spectrosc. Radiat. Transfer, 20:p 345-352.

Reardon, B.C. & McGarrigle, M.L., (1989); Utility of Thematic Mapper data for national survey of Irish lakes; European Coordinated Effort for Monitoring the Earth's Environment, ESA SP-1102, ESA Publ. Div, ESTEC, Noordwijk, The Neth.:p 25-31.

Ritchie, J.C., Cooper, C.M. & Schiebe, F.R., (1990); The relationship of MSS and TM digital data with suspended sediments, chlorophyll, and temperature in Moon Lake, Mississippi; Rem. Sens. Environ. 33:p 137-148.

Ritchie, J.C. & Cooper, C.M., (1987); Comparison of Landsat pixel array sizes for estimating water quality; Photogramm. Eng. and Rem. Sens., 53(11):p 1549-1553.

Ritchie, J.C. & Cooper, C.M., (1988); Comparison of measured suspended sediment concentrations with suspended sediment concentrations estimated from Landsat MSS data; Int. J. Remote Sensing, 9(3):p 379-387.

Ritchie, J.C. & Cooper, C.M., (1991); An algorithm for estimating surface suspended sediment concentrations with Landsat MSS digital data; Water Resourc. Bull. 27(3):p 373-379.

Ritchie, J.C., Cooper, C.M. & Yongcoing, J., (1987); Using Landsat multispectral scanner data to estimate suspended sediments in Moon Lake, Mississippi; Rem. Sens. of Environ., 23:p 65-81.

Ritchie, J.C., Schiebe, F.R. & Cooper, C.M., (1983); Spectral measurements of surface suspended matter in an oxbow lake in the Lower Mississippi Valley; J. of Freshw. Ecology, 2(2):p 175-181.

Robinson, B.F. and Biehl L.L., (1979); Calibration procedures for measurement of reflectance factor in remote sensing research; SPIE Vol. 196:p 8-15.

Roesler, C.S. & Perry, M.J., & Carder, K.L., (1989); Modeling in situ phytoplankton absorption from total absorption spectra in productive inland marine waters; Limnol. Oceanogr., 34(8):p 1510-1523.

Seyhan, E., Bunnik, N.J.J., Verhoef, W. & van Kuilenburg, J., (1974); Measurements of spectral signatures for water quality monitoring; NIWARS Publication N0. 24, Delft, The Netherlands;Paper presented at the First General Conference of the Remote Sensing Society, Birmingham, Great Britain, Sept. 1974:pp 29.

Shimoda, H., Etaya, M., Sakata, T., Goda, L. & Stelczer, K., (1986); Water quality monitoring of Lake Balaton using Landsat MSS data; Symp. on Rem. Sens. Res. Developm. & Env. Managem., Enschede, the Netherlands, August 1986:p 765 - 770.

Slater, P.N., (1980); Remote sensing: Optics and optical systems; Addison-Wesley Publ. Comp.

Smith, R.C. & Baker, K.S., (1981); Optical properties of the clearest natural waters (200-800 nm); Applied Optics, 20(2):p 177-184.

Smorenburg, C & Moddemeijer, K., (1991); Final Report Caesar radiance evaluation; TPD-HOI-RPT-91-249, TNO-TPD-TU Delft, The Netherlands (in Dutch):pp 13.

Stavn, R.H., (1992); External factors and water Raman scattering in clear ocean waters: skylight, solar angle, and the air-water interface; SPIE Vol. 1750, Ocean Optics XI:p 138-148.

Stavn, R.H., (1990); Raman scattering effects at the shorter visible wavelength in clear ocean waters; SPIE Vol. 1302-08 Ocean Optics X: p 94-100.

Stavn, R.H. & Weidemann, A.D., (1988); Raman scattering effects in ocean optics; SPIE Proc. 925, Ocean Optics IX:p 131-139.

Tomohiko Oishi (1990); Significant relationship between the backward scattering coefficient of sea water and the scatterance at 120°; Applied Optics 29:p 4658-4665.

Tyler, J.E. (1960); Radiance distribution as a function of depth in an underwater environment; Bull. Scripps Inst. Oceanogr., 7:p 363-411.

van Tongeren, O.F.R., Van Liere, L., Gulati, R.D., Postema, G. & Boesewinkel-de Bruyn, N.(1992); Multivariate analysis of the plankton communities in the Loosdrecht Lakes: relationship with the chemical and physical environment; Hydrobiologia 233:p 105-117.

Vant, W.N. & Davies-Colley, R.J., (1984); Factors affecting clarity of New Zealand lakes; New Zealand J. Mar. & Freshw. Res. 18:p 367-377.

Visser, S.A., (1984); Seasonal changes in the concentration and colour of humic substances in some aquatic environments; Freshwater Biology, 14:p 79-87.

Vos, W.L., Donze, M. & Buiteveld, H., (1986); On the reflectance spectrum of algae in water: the nature of the peak at 700 nm and its shift with varying concentration; Comm. on San. Eng. and Water Management, nr. 7, ISSN-0169-6246, TU Delft, 86-22.

Whitlock, C.H., Poole, L.R., Usry, JW., Houghton, W.M., Witte, W.G., Morris, W.D. & Gurganus, E.A.;, (1981); Comparison of reflectance with backscatter and absorption parameters for turbid waters; Applied Optics, 20 (3):p 517-522.

Witte, W.G., Whitlock, C.H., Harriss, R.C., Usry, J.W., Poole, L.R., Houghton, W.M., Morris, W.D. & Gurganus, E.A., (1982); Influence of dissolved organic materials on turbid water optical properties and remote sensing reflectance; J. of Geophysical Res., C: Oceans and Atmospheres, 87(c1):p 441-446.

Yentsch, C.S. (1962); Measurement of visible light absorption by particulate matter in the ocean; Limnol. Oceanogr.7: p 207-217.

Zepp, R.G. & Schlotzhauer, P.F., (1981); Comparison of photochemical behaviour of various humic substances in water. III Spectroscopic properties of humic substances; Chemosphere 10:p 479-486.

SUMMARY

Introduction

Remote sensing of ocean surface water has contributed greatly to the discovery, mapping and understanding of large scale marine processes. In recent years large increases in spatial resolution of satellite-sensor derived images have become available and increased spectral resolution is now available through instruments flown in aircraft. High spectral resolution is also planned for new satellites in the near future. These developments will make extensive application of passive optical remote sensing to problems in research and management of inland waters attractive in the near future.

Most freshwater systems in the world are affected by nutrients enrichment, leading to undesirable increases in biomass of higher plants and/or planktonic algae. These phenomena often show large local differences and interactions with patterns of water flow. For example, the amount and distribution of nuisance-forming cyanobacteria is of primary concern for water quality management.

Airborne remote sensing offers the possibility of imaging lakes, rivers and canals. Interactions between waterbodies such as inflow and outflow of polluted water and their mixing processes, can be visualised and in part quantified. Thus, remote sensing images can play a role in calibration and validation of two- and three dimensional hydrodynamic and ecological models. Often even a few images are useful as aids to design or improve point sampling monitoring programmes through highlighting the best locations of sampling points.

In the Vecht lakes area a large variation of waters occurs within a small geographical area which can be covered by a few remote sensing flight tracks. This provides an unique opportunity for the development of algorithms valid for a wide range of inland water types. Four main water types are distinguished:

1) The shallow eutrophic to highly eutrophic lakes.
2) The shallow oligotrophic to mesotrophic lakes.
3) The mesotrophic to eutrophic deep lakes.
4) The river and canal waters.

Each of the four water types distinguished has its own characteristic algal type and concentration, contributing to different inherent optical property characteristics. Other parameters also vary along with the four water types. This study aimed to develop and apply remote sensing algorithms to such turbid, mesotrophic to highly eutrophic inland waters. The aim was also to increase understanding of the influence of underwater optical properties on the remotely sensed reflectance signal.

Much of the underwater optical theory stems from research concerning ocean waters. The main difference for the development of a remote sensing method for inland waters

lies in the variation, range and magnitude of the absorption and scattering quantities; in the spectral distribution of these quantities and in changes in the shape of volume scattering functions due to the different nature of the substances in inland waters. The complex, interacting relations between the constituents of water make the often used statistical approach to remote sensing data analysis less desirable. Therefore the main research effort was aimed at developing an analytical model for estimation of optical water quality parameters from remote sensing data.

In order to accomplish the aim of developing multitemporally valid algorithms, it was necessary to apply a suite of laboratory-based, field-based and airborne spectral radiance and irradiance measurements. These data were used to either measure or model the subsurface irradiance reflectance, *R(0-)*. *R(0-)* is the most appropriate parameter of the under water lightfield for use as the independent optical parameter in algorithms for remote sensing, because it is independent of light intensities and only slightly dependent on atmospheric conditions, solar elevation angle and the state of the water surface. It is possible to relate *R(0-)* to the inherent optical properties of absorption and scattering, provided the volume scattering function is known. Once the exact nature of the relationship between the inherent optical properties and the optical water quality parameters is known, it is possible to develop an algorithm for extraction of this property from *R(0-)*. The upwelling radiance signal detected by a remote sensor (L_{rs}) may be recalculated to *R(0-)*. Thus it also becomes possible to estimate the optical water quality parameters from remotely sensed data.

The algorithms developed in this study are intended to be used in further research, where validation, augmentation of the results and possible development of further precision may take place. The strength of this approach also lies in the ability of combining information and results from underwater light climate research as well as *in situ* and remote sensing reflectance measurements.

Contents

After a general introduction to remote sensing of water and to the study area, chapter 1 discusses the place of this research compared to other related remote sensing studies. A brief description of the optical water quality parameters of the study area is given. The chapter ends with a general discussion of the research approach applied.

Chapter 2 discusses the inherent optical properties of absorption and scattering of the inland waters studied and how the optical water quality parameters influence these properties or are influenced by these properties.

Chapter 3 treats the theory and measurement of the upwelling and downwelling light above and below the water surface. The subsurface irradiance reflectance *R(0-)* may be calculated from these properties. *R(0-)* is considered to be the essential parameter for developing models for remote sensing of inland waters, because it is a parameter that is

only minimally influenced by changes in the incoming light. Algorithms with a high multitemporal applicability and validity may be developed on the basis of this *R(0-)*.

Chapter 4 investigates the relationship between *R(0-)* and the inherent optical properties given in chapter 2. A high variability for the water studied was found for this relationship. This led to important conclusions concerning the type of calculations required to estimate water quality parameters from remote sensing. It is preferred to apply combinations of spectral bands whereby the variability in the relationship between *R(0-)* and the inherent optical properties disappears. The most straightforward way of accomplishing this, was dividing two spectral bands. This had the additional effect of being a suitable method for extracting information on several water quality parameters.

in chapter 5 the results from chapters 2, 3 and 4 are combined to develop remote sensing algorithms for estimation of:

1. the primary pigment of most algae: chlorophyll *a*;
2. a pigment typical of (nuisance forming) cyanobacteria: CP-cyanin;
3. a measure of the suspended matter: seston dry weight;
4. a measure of the extinction of light with depth: the vertical attenuation coefficient;
5. a measure of the transparency of water: Secchi depth transparency.

The application of the algorithms developed in chapter 5 to the remote sensing data acquired with the CAESAR multispectral scanner and the CASI imaging spectrometer takes place in chapter 6. The analyses of the data from the two instruments, flown on different days, illustrated the multitemporal validity of the algorithms developed in this study.

Chapter 7 gives the general conclusions, discussion and recommendations for this research.

Conclusions

This research marks a significant change in research methodology pertaining to development and implementation of remote sensing of inland waters. During remote sensing missions it is no longer necessary to gather large quantities of *in situ* samples for statistical analyses in support of the empirical or semi-empirical methods. Research can now focus on increasing understanding of the relationship between water quality parameters and the inherent optical properties, and on the relationship between the inherent optical properties and subsurface irradiance reflectance, *R(0-)*.

It was found that the variability in specific absorption and scattering coefficients within and between the four different water types indicates that the development of remote sensing algorithms for inland water quality analysis must reckon with adjustable parameterisation of absorption and scattering variables for each water type studied.

A decrease in analytical and an increase in semi-empirical elements in the algorithms were required, in successive order, for chlorophyll *a*, CP-cyanin, seston dry weight, vertical attenuation coefficient and Secchi disk transparency. Chlorophyll *a*, CP-cyanin and seston are parameters that influence the optical characteristics of water, whereas K_d and *SD* are a function of the optical properties of the water. This explains the increasing incorporation of semi-empirical techniques from chlorophyll to *SD*: for each parameter in the above sequence, information on the preceding parameter is required in order to develop remote sensing algorithms based on the analytical approach.

It has been demonstrated that two spectral bands centred at 676 and 706 nm are sufficient for estimation of chlorophyll *a*, *DW*, K_d and *SD*. The addition of three spectral bands centred at 600, 624 and 648 nm enables the determination of CP-cyanin. Thus a five spectral band multispectral remote sensing system can remotely sense the optically retrievable parameters discussed in this study. Addition of more appropriately placed spectral bands may enable estimation of other algal light harvesting pigments.

optical water quality parameter detection and estimation techniques require the use of multispectral scanners, but not necessarily the use of imaging spectrometers. Algorithm development and testing, however, does require the use of imaging spectrometers. By virtue of measuring an entire spectrum, data from an imaging spectrometer can also be referred to at any time after the flight for the application or further development of algorithms. Thus imaging spectrometer data probably has more value in the long term. Also newly developed algorithms, for other water quality parameters, using other parts of the optical spectrum, may be applied to previously acquired imaging spectrometer data.

The multitemporal (and multisensor) applicability of the derived algorithms has been demonstrated by the successful application to remote sensing data from two different instruments, flown on two days under different atmospheric conditions and solar zenith angles.

SAMENVATTING

Introductie

Remote sensing van oppervlaktewater vindt zijn oorsprong in het waarnemen, karteren en begrijpen van grootschalige processen in oceanen. Recente ontwikkelingen op het gebied van ruimtelijke resolutie van satellietbeelden en de snel toenemende spectrale resolutie van vliegtuig remote sensing systemen, hebben de mogelijkheden voor remote sensing toepassingen voor binnenwateren aanzienlijk vergroot. Hoge spectrale resolutie sensors zullen in de toekomst beschikbaar komen in satellieten. Deze ontwikkelingen maken het zeer waarschijnlijk dat remote sensing een belangrijke rol gaat spelen op het gebied van integraal waterbeheer van binnenwateren.

Veel zoetwatersystemen worden beïnvloed door nutriëntenverrijking, wat resulteert in sterk toenemende biomassa van waterplanten en/of algen. Deze waterkwaliteitskenmerken tonen vaak sterke lokale variaties en interacties met stroompatronen. Het waarnemen en bepalen van de concentratie en verspreiding van schadelijke cyanobacterieën is een voorbeeld van de toepassingsmogelijkheden van remote sensing.

Vliegtuig remote sensing maakt het mogelijk om meren, rivieren en kanalen waar te nemen. Interacties tussen wateren, zoals in- en uitstroom van vervuild water kunnen worden gevisualiseerd en gedeeltelijk worden gekwantificeerd. Op deze wijze kunnen remote sensing beelden bijdragen aan de calibratie en validatie van twee- en drie dimensionele hydrodynamische en ecologische modellen. Enkele beelden kunnen al voldoende zijn om bijvoorbeeld de positie van bemonsteringspunten van waterkwaliteits meetprogramma's te verbeteren.

In het Vechtplassengebied komen ten minste 18 verschillende wateren voor, welke met een klein aantal vluchtstroken kunnen worden waargenomen. Daarom is dit gebied bij uitstek geschikt voor het ontwikkelen en toepassen van remote sensing modellen. Er is onderscheid gemaakt in vier hoofdwatertypen:

1) eutrofe to zeer eutrofe ondiepe meren.
2) oligotrofe tot mesotrofe ondiepe meren.
3) mesotrofe to eutrofe diepe meren.
4) rivieren en kanalen.

Elk watertype heeft bijvoorbeeld zijn eigen kenmerkende algentypen en -concentraties, die van invloed zijn op de inherent optische eigenschappen. Dit geldt ook voor andere kenmerken zoals doorzicht en zwevende stof gehalte. Doel van dit onderzoek was om remote sensing methoden te ontwikkelen en toe te passen op deze watertypen. Dit vond vooral plaats om inzicht te verkrijgen in de invloed van onderwater optische kenmerken op de waargenomen reflectie van een plas, meer, rivier of kanaal.

Veel van de gebruikte theorie komt voort uit oceaanonderzoek. Een kenmerkend verschil van binnenwater remote sensing onderzoek met het onderzoek van oceaanwateren, is de veel grotere variatie in golflengte afhankelijke absorptie- en verstrooiings-eigenschappen van binnenwateren. Deze grote variatie en de complexe interacties tussen optische eigenschappen zorgen ervoor dat de statistische methode voor remote sensing van binnenwateren minder geschikt is. Hierom werd de aandacht gericht op het ontwikkelen van een analytisch model voor het bepalen van optische waterkwaliteitskenmerken met behulp van remote sensing gegevens.

Teneinde het doel van multitemporeel geldige algoritmen te bereiken, was het noodzakelijk om een uitgebreid meetprogramma uit te voeren in het laboratorium, op het water en vanuit de lucht. Al deze gegevens werden gebruikt om de belangrijkste kenmerk van het onderwater lichtklimaat te bepalen: de onderwater irradiantie reflectie, *R(0-)*. *R(0-)* is slechts in geringe mate afhankelijk van veranderende omstandigheden en daarom zeer geschikt als basis voor het ontwikkelen van algemeen geldende remote sensing algoritmen. *R(0-)* vervult een spilfunctie tussen de inherente optische eigenschappen van absorptie en verstrooiing en het remote sensing signaal. Zowel de inherente optische eigenschappen als het remote sensing signaal kunnen worden omgerekend naar *R(0-)*.

De, in dit onderzoek, ontwikkelde remote sensing algoritmen zijn bedoeld om in toekomstig onderzoek te worden toegepast. De kracht van deze methode ligt erin dat het mogelijk is om zowel laboratorium onderzoek, als veldwaarnemingen en remote sensing metingen met elkaar te combineren.

Inhoud

Hoofdstuk 1 plaatst dit onderzoek in de context van ander remote sensing onderzoek gericht op binnenwateren. Een beknopte beschrijving van het onderzoeksgebied en de optische waterkwaliteitskenmerken wordt gegeven. Het hoofdstuk wordt afgesloten met een algemene inleiding die de gevolgde onderzoeksmethode bespreekt.

In hoofdstuk 2 worden de inherente optische eigenschappen, absorptie en verstrooiing, onderzocht. Tevens wordt bepaald hoe de optische waterkwaliteitskenmerken deze inherente optische eigenschappen beïnvloeden, danwel er zelf door beïnvloed worden.

In hoofdstuk 3 wordt de theorie besproken en worden de metingen gepresenteerd die nodig zijn om het in het water invallende licht en het uit het water omhoog gerichte licht te bepalen. Uit deze metingen kan vervolgens *R(0-)* worden berekend. Op basis van *R(0-)* kunnen remote sensing methoden worden ontwikkeld met algemene geldigheid.

Hoofdstuk 4 behandelt het verband tussen de inherente optische eigenschappen uit hoofdstuk 2 en *R(0-)* uit hoofdstuk 3. Er bleek grote variatie te bestaan in de relatie tussen absorptie en verstrooiing en *R(0-)*. Dit had tot gevolg dat voor informatie

extractie uit remote sensing gegevens de voorkeur wordt gegeven aan methoden die ongevoelig zijn voor deze variabele relatie. Een geschikte methode hiervoor is het op elkaar delen van spectrale banden. Een belangrijk voordeel van deze methode is tevens dat het een zeer geschikte manier is om optische waterkwaliteitskenmerken te bepalen.

In hoofdstuk 5 worden de resultaten van hoofdstukken 2 tot en met 4 geïntegreerd met als doel remote sensing algoritmen te ontwikkelen voor de bepaling van:

1. het primaire pigment van algen: chlorofyl *a*;
2. een kenmerkend pigment voor de (overlast veroorzakende) cyanobacterieën: CP-cyanine;
3. een maat voor het zwevend stof gehalte: seston drooggewicht;
4. een maat voor de verticale uitdoving van licht in de waterkolom: de verticale extinctie coefficiënt;
5. een maat voor het doorzicht: de Secchi doorzicht.

De toepassing van de in hoofdstuk 5 ontwikkelde remote sensing algoritmen op de remote sensing gegevens vindt plaats in hoofdstuk 6. Gegevens verkregen met behulp van twee remote sensing systemen (CAESAR en CASI) op twee afzonderlijke dagen, toonden aan dat de algoritmen inderdaad algemeen toepasbaar zijn.

Hoofdstuk 7 geeft algemene conclusies, aanbevelingen en discussie met betrekking tot remote sensing van binnenwateren.

Conclusies

De resultaten van dit onderzoek markeren een belangrijke verandering in de gebruikte onderzoeksmethode voor de ontwikkeling en toepassing van remote sensing van binnenwateren. Het is niet meer vereist om grote hoeveelheden gegevens *in situ* te verzamelen voor statistische analyse. Nadruk kan voortaan liggen op het vergroten van het inzicht in de relatie tussen de waterkwaliteitskenmerken, de inherente optische eigenschappen, *R(0-)* en het remote sensing signaal.

De variabiliteit in specifieke absorptie en verstrooiing tussen de wateren heeft tot gevolg dat remote sensing algoritmen voor binnenwateren waarschijnlijk zullen moeten worden aangepast aan het type water dat waargenomen wordt.

Een afname in analytische en een toename in semi-empirische elementen in de remote sensing algoritmen bleek noodzakelijk voor de bepaling van chlorofyl *a*, CP-cyanine, seston drooggewicht, de verticale extinctie coefficiënt en het doorzicht. Deze laatste twee kenmerken kunnen alleen analytisch worden bepaald als alle inherente optische eigenschappen bekend zijn.

Het is aangetoond dat twee spectrale banden gecentreerd op 676 nm en 706 nm voldoende zijn om chlorofyl *a*, seston drooggewicht, de vertical extinctie coefficiënt en het

doorzicht te bepalen. Drie spectrale banden op 600, 624 en 648 nm maken het mogelijk om CP-cyanine te bepalen.

Het blijkt dat met vijf spectrale banden alle onderscheiden optische waterkwaliteitskenmerken kunnen worden onderscheiden. Dit houdt in dat een multispectrale scanner geschikt is voor binnenwaterkwaliteitsonderzoek. Een imaging spectrometer heeft echter het voordeel dat continue registratie van een spectrumplaats vindt. Voor onderzoeksdoeleinden wordt hier de voorkeur aan gegeven in verband met de mogelijke ontwikkeling van remote sensing methoden voor andere waterkwaliteitsgegevens.

De multitemporele geldigheid van de hier ontwikkelde methode is aangetoond door het succes van de toepassing van deze algoritmen op data van twee remote sensing systemen, die op twee verschillende dagen opnamen hebben gemaakt.